ISSN 1913-1844 (Print)
ISSN 1913-1852 (Online)

MODERN APPLIED SCIENCE

Vol. 8, No. 3 June 2014

CANADIAN CENTER OF SCIENCE AND EDUCATION

Editorial Board

Contents

Contents

Modern Applied Science; Vol. 8, No. 3; 2014
ISSN 1913-1844 E-ISSN 1913-1852
Published by Canadian Center of Science and Education

Technical and Economic Sustainability of Concrete Pavements

Laura Moretti[1]

[1] Department of Civil, Construction and Environmental Engineering, Sapienza, Università di Roma, Rome, Italy

Correspondence: Laura Moretti, Department of Civil, Constructional and Environmental Engineering, Sapienza, Università di Roma, Rome, Italy. Tel: 39-6-4458-5124. E-mail: laura.moretti@uniroma1.it

Received: January 30, 2014 Accepted: March 13, 2014 Online Published: April 8, 2014

doi:10.5539/mas.v8n3p1 URL: http://dx.doi.org/10.5539/mas.v8n3p1

Abstract

Economic evaluation of road pavements is as important as their technical and structural design: often only initial construction costs are calculated to assess economic project sustainability. Instead, forgetting maintenance costs exposes society to unacceptable risks of expensive and incorrect decisions.

Road pavements design and construction solutions affect maintenance works during service life, which not only entail economical and financial expenditures, but also damage service regularity for users and affect environmental impact. The analysis of pavement distress and the study of its evolution during service life can contribute to find the financially most advantageous solution.

This paper shows a software program developed to analyze structural, functional and financial performances of road concrete pavements both doweled slabs and continuously reinforced.

Keywords: sustainability, concrete pavements, design, maintenance, present value

1. Introduction

In the project phase, it's important to evaluate and guarantee an adequate level of service during the service life. The experience proves that road concrete pavements are durable, so the technicians should consider the structural and functional performance year by year. It affects pavement management system and its social and environmental costs during operation phase (Di Mascio, 2002; D'Andrea et al., 2004). The analysis of road work costs can contribute to finding the most advantageous solution, also considering the functional performances of road pavements (Loprencipe & Cantisani, 2013). In fact, the financial analysis during all service life could modify the stakeholders' choice (Abdullahi et al., 2013) and it could guarantee expenditure programmes under specified budget constraints.

In this paper, the design procedure for Jointed Plain Concrete Pavement (JPCP) is presented. This procedure involves the use of structural models to calculate pavement response and the implementation of distress predictive models to monitor the performance during the evaluation period. Mechanical and functional pavement response, based on critical stresses due to repeated traffic and environmental loading, is evaluated by automatic calculation procedures. A Visual Basic for Application (VBA) code, named ESC (Economic Sustainability of Concrete pavement), has been implemented to analyze input data and give structural and functional solution implementing fatigue and decay curves (Moretti, 2012).

In this model, mechanistic and empirical pavement distress models, proposed by AASHTO Guide 2002 (2008) and Gulen et al. (2001), are used to evaluate pavement condition and define automatically maintenance and repair procedures.

The structural analysis concerns the stresses in concrete at first load and the fatigue damage; the functional analysis concerns the transverse cracking and the International Roughness Index (IRI).

Indeed, structural, material and site-specific environmental data inputs and calculated stresses are used to verify pavement at construction year and to evaluate, year by year, pavement condition during service life. Maintenance plan is derived from international experience (scheduled and preventive maintenance) and effective condition (corrective maintenance).

The tool calculates together the capital resources to be implemented by road operator. The construction costs are calculated considering data listed in the bill of quantities, while maintenance costs are derived from maintenance plan. Given the inflation rate and the discount rate, in this study supposed both constant during all pavement

service life, ESC calculates the Present Value (PV), a synthetic evaluation methodology of economic and financial charges correlated to verified pavement.

2. Software Design Model

Factors influencing pavement design are: traffic, environmental conditions, subgrade bearing capacity and materials characteristics.

ESC consist of default Microsoft Excel® worksheets to input design data. Construction and maintenance costs are derived from project geometrical characteristics, materials, labour, machinery and equipment unit costs. Joints, dowel bars and tie bars amount are automatically calculated by ESC; results have been verified with a finite-element model (Bonin et al., 2007).

The thermal pattern of road concrete pavements generates stresses comparable to stresses related to traffic loads (Chai et al., 2012; Qin & Hiller, 2011; Nishizawa et al., 2009; Faraggi et al., 1987), so in the program has been implemented an innovative verified thermal model to describe temperature in slab thickness and calculate thermal stresses.

2.1 Thermal Model

Pavement thermal pattern of concrete pavements, influenced by air temperature, sun's radiation, wind speed and thermal properties of concrete, is usually described by Barber theory (1957). It defined a sinusoidal function to describe the solution of the one-dimensional problem of heat transfer across a semi-infinite, isotropic, homogeneous solid surface which is in a steady regime, although periodic, with a boundary sinusoidal temperature variation forced in the surface, as in Equation 1:

$$T(z,t) = T_{ag} + \Delta T \cdot \sin\left(2\pi \cdot t/\tau - z\sqrt{\pi/d \cdot \tau}\right) \tag{1}$$

T_{ag} is the average daily air temperature, ΔT is the differential thermal amplitude, t is the time, z is the pavement depth and τ is the period of temperature variation.

Furthermore, for semi-infinite medium, the theoretical phase displacement φ and damping values γ are shown in Equation 2 and Equation 3 respectively:

$$\varphi = \kappa \cdot z \cdot \tau / 2\pi \tag{2}$$

where k is the thermal conductivity of concrete.

$$\gamma = \sqrt{\pi / a \cdot \tau} \tag{3}$$

The Barber formula to evaluate thermal gradients during the day and the night of all seasons is in Equation 4:

$$Tpav(z,t) = T_{ag} + R + \left(\frac{A_g}{2} + 3R\right) \cdot F \cdot \exp(-C \cdot z) \cdot \sin\left(0.262t - C \cdot z - \arctan\frac{C}{H + C}\right) \tag{4}$$

where $Tpav(z,t)$ is the temperature of pavement at depth z at hour h; T_{ag} is the average seasonal daily air temperature; R is the daily solar radiation contribution to air temperature expressed by Equation 5:

$$R = \frac{2 \cdot b \cdot I}{3 \cdot 24 \cdot h} \tag{5}$$

A_g is the daily range in air temperature; b is the surface absorptivity to the total solar radiation; I is the daily solar radiation; h is the heat transfer coefficient, expressed by Equation 6:

$$h = 4.882 \cdot \left(1.3 + 0.4332 \cdot v^{0.75}\right) \tag{6}$$

v is the average wind speed; F is expressed by Equation 7; H is expressed by Equation 8 and C is expressed by Equation 9:

$$F = \frac{H}{\sqrt{(H + C)^2 + C^2}} \tag{7}$$

$$H = \frac{h}{k} \tag{8}$$

where k is thermal conductivity of concrete;

$$C = \frac{0.131 \cdot s \cdot \gamma}{k} \tag{9}$$

where s is specific heat of concrete and γ is density of concrete.

Having the same maximum and minimum temperatures, Barber's model and Thomlinson's model (1940) curves are almost overlapping, but the real development of pavement temperature during a cloudless day is not sinusoidal, because ground solar radiation changes during the daytime (Rao et al., 2001) and is not symmetric with respect to its average value. So, in the thermal model entered in ESC has been implemented the Faraggi, Jofré and Kraemer integrated with Barber's model (Faraggi et al., 1987).

New thermal law (Moretti et al., 2013a) is valid both for flexible and for rigid pavements. It calculates daily temperature range by the Barber's theory, which returns a closed form solution, and defines non symmetric sinusoidal trend of temperatures by Faraggi et al. model. Equation 10 is valid between sunrise and zenith, Equation 11 is valid between zenith and sunrise.

$$T(z,t) = T_{ag} + R + \left(\frac{A_g}{2} + 3R\right) \cdot F \cdot e^{-Cz} \cdot \sin\left(\frac{2t - S_h}{2S_h}\pi - z\sqrt{\frac{\pi \cdot \gamma \cdot c_s}{24 \cdot k}}\right) \tag{10}$$

$$T(z,t) = T_{ag} + R + \left(\frac{A_g}{2} + 3R\right) \cdot F \cdot e^{-Cz} \cdot sen\left(\frac{4(t + S_n) - S_a}{2S_a}\pi - z\sqrt{\frac{\pi \cdot \gamma \cdot c_s}{24 \cdot k}}\right) \tag{11}$$

where T_{sg}, R, A_g, C and F has been described above, S_h is the number of hours between sunrise and zenith and S_n is the number of hours between sunset and the next sunrise. S_h, S_a and S_n values must satisfy the conditions expressed in Equation 12 and Equation 13:

$$2S_h + S_n = 24 \tag{12}$$

$$S_a = 2 \cdot (S_h + S_n) \tag{13}$$

In the thermal curves, t = 0 coincides with the sunrise hour.

Daily thermal gradients derived by the modified Faraggi et al. theory are consistent with measured values: in the night the thermal gradients are next to half of those ones during the day. User inputs thermal seasonal data, so for each 24 hours of the four season the VBA code calculates thermal pavement conditions.

2.2 Technical Analysis

Pavement bearing capacity is defined by modulus of reaction: this parameter depends on thickness and type of subbase layers (granular and/or cement treated subbase) and on modulus of subgrade reaction. The modulus of subbase reaction is automatically provided by ESC code, using Packard charts; maximum permitted modulus of reaction value is 130 MPa/m as recommended in the most of literature references (Domenichini, 1984).

In the computer code, datasheets are provided to input traffic level, establishing average daily heavy vehicles per lane at the road opening year, annual rate of traffic growth, pavement service life, traffic spectrum and hourly distribution per vehicle type. ESC has in its datasheet all traffic spectra defined in the Italian Pavement Design Catalogue (CNR, 1995; Domenichini et al., 1993), but user can defines any other traffic spectrum.

The combination of frequency between thermal gradients and different load configuration during the night and day hours affects the number of repetitions for fatigue calculation. This value has been used also in evaluation of cracking damage (D'Andrea & Fiore, 2003).

Requested data inputs about concrete are: materials amounts and composition of concrete mix (water, cement, aggregates, chemical admixtures); physical and thermal properties of concrete (density, coefficient of absorption of the solar radiation, specific heat, thermal conductivity, Poisson's ratio, cubic characteristic compressive strength of concrete). Elastic modulus is automatically deducted from characteristic cubic compressive strength (R_{ck}).

Depending on the thermal state of the pavement, the calculation model iteratively identifies the structural calculation equation corresponding to the boundary conditions. The theory of Westergaard, the formulas proposed by VENCON-CROW and the analytical solutions of the elastic theory of thin plates are used to obtain stresses by closed form solution, while in Di Mascio et al. (2012) Kenslabs, a finite element software, calculated the stresses in pavement. Results from the proposed model have been validated by the cited structural software. Given the superposition principle, the thermal stresses are derived through an iterative process that modifies the

theory of Eisenmann according to the thermal and structural models above defined.

Fatigue damage is calculated year by year, load by load and hour by hour, with equation of PCA, Bradbury's law, Bennet-Raju's law, Kesler's law, Sawan-Darter's law and equation proposed by MEPDG for JPCP. The maximum calculated value of cumulative fatigue damage index has been used to verify with respect to fatigue the pavement.

The analysis model annually assesses the fatigue level reached and the service level of the designed pavement, planning scheduled or failure maintenance as the status of indicators changes. Strategies of preventive maintenance schedule joint sealing and full depth repair (to restore potholes). Rehabilitation strategies of corrective maintenance schedule diamond grinding to correct roughness and full depth repair to restore slabs cracked (AAVV, 2007; Shahin, 2005).

Distress models used in this analysis are: cracking model by AASHTO Guide 2002 shown in Equation 14 and IRI model by empirical equation proposed by Gulen et al. shown in Equation 15.

$$CRK = \frac{A}{1 + FD \cdot^{-1.68}} \tag{14}$$

where C*RK* is the cracking damage in percent and *FD* is the cumulative fatigue damage.

$$IRI = IRI_0 + C_1 \cdot AGE + C_2 \cdot AADT \tag{15}$$

where *IRI* is the predicted value of *IRI*, IRI_0 is the *IRI* value at the construction year, *AGE* is the year of service life, *AADT* is the annual average daily truck, C_1 and C_2 are corrective coefficients.

2.3 Economic Analysis

The economic impact of the pavement is assessed, as the cost per unit of surface, through the synthetic indicator Present Value. Despite the extreme difficulty of this approach towards a system so vast and multi-sectorial, the indicator calculated by ESC allows more objectively comparisons between design solutions. It takes into account the cash flows generated by the initial cost of construction and maintenance costs discounted at the year of construction. Their sum plus construction costs is the Present Value of project.

The indicator allows not only to assess the proposed solution, but above to compare other concrete pavements also with semi-rigid and flexible pavements. The program also returns a chart of trend of nominal costs incurred during the service life of the pavement (Debroux et al., 2007) or of the railway track (Di Mascio et al., 2014a, 2014b). From this chart is possible to find the year when a solution is more convenient than other compared.

3. Case Study

Three highways Jointed Plain Concrete Pavements listed in the Italian catalogue of road pavements have verified. Each pavement structure consists of a concrete slabs, a subbase, cement-treated layer 15 cm thick, and an unbound granular mix layer 15 cm thick; subgrade resilient modulus is equal to 90 MPa. Slabs are 27, 26 and 24 cm thick for a cumulative heavy traffic respectively equal to 45, 25 and 10 millions of passages.

The R_{ck} of concrete is 55 MPa; the modulus of rupture of concrete (MOR) is calculated with formula proposed in software package VENCON2.0; It's expressed by Equation 16 (Houben, 2009).

$$MOR = 1.3 \cdot [(1600 - h)/1000] \cdot [1.05 + 0.05 \cdot (R_{ck} + 8)]/1.2 \tag{16}$$

where *h* is the thickness of the concrete slab in mm and *MOR* is in MPa.

The annual increase of concrete strength during service life has been considered. Examined concrete slabs were 400 cm long and 380 cm large. Pavement design life is 40 years.

Single (SL) or dual layer (DL) labs with (EAS) or without exposed aggregate surface (NEAS), with metallic or plastic dowel chairs, are examined.

All examined pavements are fatigue tested: fatigue damage (FD) is less than 1 at the end of service life, as represented in Table 1.

Table 1. Fatigue Damage (FD)

Slab thickness (cm)	FD
24	1.80E-01
26	1.30E-01
27	1.49E-01

Threshold values of transverse cracking and IRI are listed in Table 2.

Table 2. Threshold value distresses

Transverse cracking (%)	10
IRI (m/km)	2.5

Corrective maintenance results to be necessary at the years shown is Table 3.

Table 3. Year of service life when threshold limit is achieved

Slab thickness (cm)	Year when threshold limit is achieved (year)	
	Transverse cracking	IRI
24	>40	34
26	>40	34
27	>40	34

During their service life, the examined pavements don't need for the corrective maintenance caused transverse cracking, whereas they need for grinding across the traffic lanes due to roughness progression.

Construction costs are listed in Table 4 and in Table 5.

Table 4. Construction costs (C_C), cases with metallic dowel chairs

Slab thickness (cm)	C_C (€/m^2)			
	EAS+DL	NEAS+DL	EAS+SL	NEAS+SL
24	55.51	51.81	55.10	51.4
26	57.40	53.70	57.08	53.38
27	58.42	54.72	58.08	54.38

Table 5. Construction costs (C_C), cases with plastic dowel chairs

Slab thickness (cm)	C_C (€/m^2)			
	EAS+DL	NEAS+DL	EAS+SL	NEAS+SL
24	52.75	49.05	52.34	48.64
26	54.79	51.09	54.46	50.76
27	55.78	52.08	55.44	51.74

Preventive maintenance strategies defined for these pavements are listed in Table 6, as suggested in literature. Corrective actions are planned according to Table 3.

Table 6. Preventive maintenance

Preventive maintenance work	Year	Quantity	
Joint sealing	10	100%	Total joint length
Full depth patching	10	2%	Total area
Joint sealing	15	60%	Total joint length
Joint sealing	20	60%	Total joint length
Full depth patching	20	2%	Total area
Joint sealing	25	60%	Total joint length
Joint sealing	30	60%	Total joint length
Full depth patching	30	2%	Total area
Joint sealing	35	60%	Total joint length

Nominal maintenance costs are calculated knowing type, extension and timetable of maintenance and rehabilitation works, as expresses by Equation 17.

$$C_x = C_0(1+i)^x \tag{17}$$

where C_x is the maintenance cost incurred in year x; C_0 is the maintenance cost at construction year; i is the annual inflation rate equal to 3%. This supposed value is the average value of the eighteen last years in Italy (Camera di Commercio di Reggio Emilia, 2012); x is the time in the future in years. Figure 1 shows cumulated nominal costs during design life of 24 cm thick EAS+DL pavements with metallic dowel chairs.

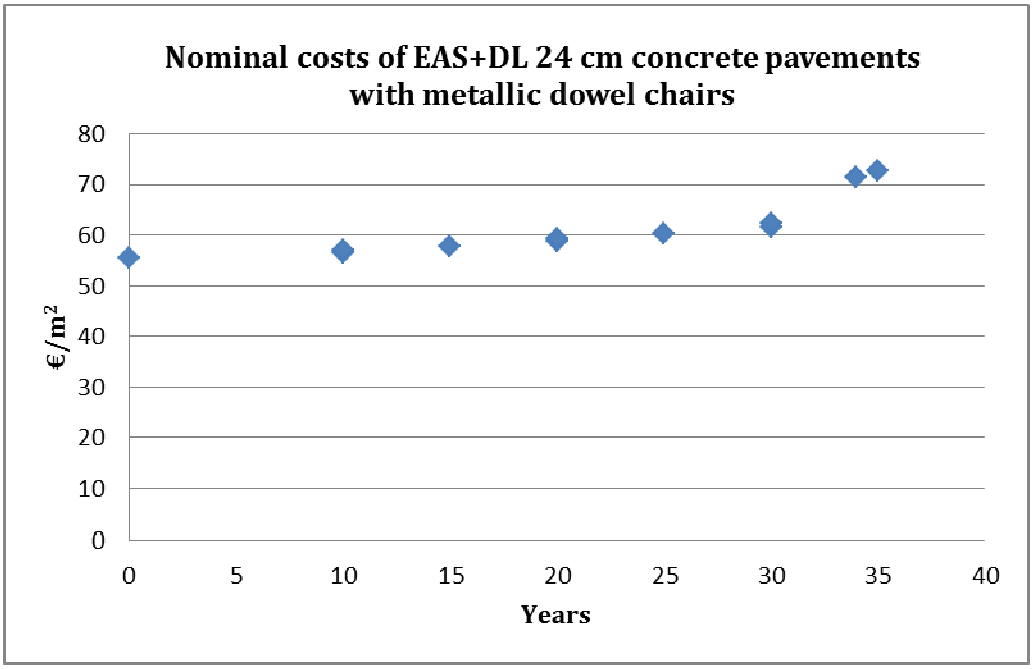

Figure 1. Cumulated nominal costs

Actual maintenance costs are calculated as expressed by Equation 18:

$$C_{A,x} = \frac{C_x}{(1+r)^x} \tag{18}$$

where $C_{A,x}$ is the maintenance cost discounted at construction year x; r is the annual discount rate equal to 4% (the risk premium for the investment is equal to 1%) (Banca d'Italia, 2014; European Central Bank, 2014).

The Present Value of this series of costs is calculated as expressed by Equation 19:

$$PV = C_C + \sum_{x=1}^{N} C_{A,x} \tag{19}$$

where C_C is construction cost incurred in year 0 and N is the number of years in the analysis period.

Table 7 and Table 8 show the obtained PV, respectively for pavements with metallic and plastic dowel chairs, in euro/m^2.

Table 7. PV of pavement investment, cases with metallic dowel chairs

Slab thickness (cm)	PV (€/m^2)			
	EAS+DL	NEAS+DL	EAS+SL	NEAS+SL
24	60.1	62.7	59.7	62.3
26	62.1	64.7	61.7	64.4
27	63.1	65.7	62.8	65.4

Table 8. PV of pavement investment, cases with plastic dowel chairs

Slab thickness (cm)	PV (€/m^2)			
	EAS+DL	NEAS+DL	EAS+SL	NEAS+SL
24	57.3	59.9	56.9	59.5
26	59.5	62.1	59.1	61.8
27	60.5	63.1	60.1	62.8

Results obtained are comparable with values in literature: concrete pavements are more expensive initially, but need limited work maintenance, so are economically competitive versus other common solutions, as bituminous pavements. Indeed, for the examined pavements, the average construction cost is 53.7 €/m^2, but only 7.8 €/m^2 average discounted maintenance cost needs during 40 years of service life.

4. Conclusions

The structural and functional characteristics of concrete pavements have been evaluated by ESC, the proposed automatic procedure in VBA code. The method defines pavement management system during service life and calculates the Present Value (PV) of designed and verified solution. This tool is a quick, simple and user-friendly instrument to estimate total costs in concrete pavements: the procedure is a forward-looking decision framework that assess life time costs in addition to construction costs. The new approach could be used to evaluate economic and technical sustainability of JPCP and to compare different types of both rigid and flexible pavements.

The current study has practical implications as well. The model could be a valid tool for designers and decision-makers. User defines road classes in terms of climatic condition, traffic and subgrade bearing capacity and he designs the structure of pavements and road works: the program calculates the PV needed to implement the solution. The proposed maintenance and rehabilitation policy may be modified to optimize strategies on performance and costs.

The instruments will be integrated in a program written by author to evaluate environmental sustainability of roads (Moretti et al., 2013b). The final software will allow to compare alternative considering not only the construction, maintenance and rehabilitation costs, but also the environmental impacts of examined solution. The multicriteria analysis approach will synthetize the summarizes the complex, often competing, technical and economic aspects (Dano et al., 2011).

References

AASHTO. (2008). *Mechanistic-Empirical Pavement Design Guide - A Manual of Practice*. AASHTO, Washington, DC: USA.

AAVV. (2007). *Long-Life Concrete Pavements in Europe and Canada. U.S. Department of Transportation*

Federal Highway Administration. Report no. FHWA-PL-07-027.

Abdullahi, A. U., Noor Amila Wan, A. Z., Mohd, F. K., & Arazi, I. (2013). Stakeholder Perceptions on Achieved Benefits of PFI Procurement Strategy. *Modern Applied Science, 7*(4), 31-40. http://dx.doi.org/10.5539/mas.v7n4p31

Banca d'Italia. (2014). Retrieved January 28, 2014, from http://www.bancaditalia.it/

Barber, E. S. (1957). *Calculation of maximum pavement temperatures from weather report*. HRB Bulletin 168, National Research Council, Washington, DC: USA.

Bonin, G., Cantisani, G., Loprencipe, G., & Ranzo, A. (2007). Dynamic effects in concrete airport pavement joints. [Effetti dinamici nei giunti delle pavimentazioni aeroportuali in calcestruzzo]. *Industria Italiana Del Cemento, 77*(834), 590-607.

Camera di Commercio di Reggio Emilia. (2012). Retrieved April 12, 2012, from http://www.re.camcom.gov.it/

Chai, G., van Staden, R., Guan, H., & Loo, Y. (2012). Impact of climate related changes in temperature on concrete pavement: a finite element study. Paper presented at the 25th ARRB Conference – Shaping the future: Linking policy, research and outcomes, Perth, Australia 2012.

CNR. (1995). Catalogo delle Pavimentazioni Stradali. B.U. 178.

D'Andrea, A., & Fiore, N. (2003). Fatigue life of asphalt concrete with rubber grains. Paper presented at *the Advances in Damage Mechanics* (pp. 65-74). http://dx.doi.org/10.2495/FDM030071

D'Andrea, A., Bonora, V., & Drago, D. (2004). Asphalt concrete with bottom ash: Environmental aspects. Paper presented at the Proceedings of the International Conference on Restoration, Recycling and Rejuvenation Technology for Engineering and Architecture Application (pp. 56-63).

Dano, U. L., Abdul-Nasir, M., & Abdul-Lateef, B. (2011). A Geographic Information System and Multi-Criteria Decision Analysis in Proposing New Recreational Park Sites in Universiti Teknologi Malaysia. *Modern Applied Science, 5*(3), 39-55.

Debroux, R., Kral, Z., Lemlin, M., Wansart, L., Degraeve, M., Haesen, G., & Di Mascio, P. (2007). Bituminous and continuously reinforced concrete pavements for motorways. An economic comparison (part II). [Pavimentazioni Bituminose ed in Calcestruzzo ad Armatura Continua per Autostrade. un Confronto Economico (II Parte)]. *Industria Italiana Del Cemento, 77*(830), 288-299.

Di Mascio, P. (2002). Concrete pavements and interlocking concrete paving blocks for low-volume roads. [Le pavimentazioni per la viabilità minore in calcestruzzo e in masselli autobloccanti]. *Industria Italiana Del Cemento, 72*(DEC.), 968-991.

Di Mascio, P., Loprencipe, G., & Maggioni, F. (2014a). Modellazione del comportamento visco-elastico degli strati della sede ferroviaria [Visco-elastic modeling for railway track structure layers]. *Ingegneria Ferroviaria, 69*(3), 207-222.

Di Mascio, P., Loprencipe, G., & Moretti, L. (2014b). Competition in rail transport: methodology to evaluate economic impact of new trains on track, 3rd International Conference on Transportation Infrastructure ICTI2014 – Sustainability, Eco-efficiency and Conservation in Transportation Infrastructure Asset Management, Pisa, 22-25 April 2014. (In press).

Di Mascio, P., Moretti, L., & Panunzi, F. (2012). Economic Sustainability of Concrete Pavements. Procedia - Social and Behavioral Sciences, 53, 125-133. *Proceedings, V International SIIV Congress Sustainability of Road Infrastructures*, Rome, Italy, 29th-31st October 2012.

Domenichini, L. (1984). Pavimentazioni stradali in calcestruzzo - Progettazione/esecuzione/manutenzione. A.I.T.E.C.- Associazione Italiana Tecnico Economica del Cemento.

Domenichini, L., Di Mascio, P., Giannattasio, P., Caliendo, C., Festa, B., Marchionna, A., ... Paoloni, G. (1993). Criteri di dimensionamento delle sovrastrutture di Catalogo.

European Central Bank. (2014). Retrieved January 28, 2014, from http://www.ecb.int/home/html/index.en.html

Faraggi, V., Jofré, C., & Kraemer, C. (1987). Combined Effect of Traffic Loads and Thermal Gradients on Concrete Pavement Design. *Transportation Research Record 1136* (pp. 108-118). Pavement Design.

Gulen, S., Zhu, K., Weaver, J., Shan, J., & Flora, W. F. (2001). Development of Improved Pavement Performance Prediction Models for the Indiana Pavement Management System. Publication FHWA/IN/JTRP-2001/17. Joint Transportation Research Program, Indiana Department of Transportation

and Purdue University, West Lafayette, Indiana, 2001. http://dx.doi.org/10.5703/1288284313192

Houben, L. J. M. (2009). The Dutch Structural design Method for Jointed Plain Concrete Pavements. *Workshop Diverse uses of concrete IV, Nairobi, Kenya* (pp. 1-16).

Loprencipe, G., & Cantisani, G. (2013). Unified Analysis of Road Pavement Profiles for Evaluation of Surface Characteristics. *Modern Applied Science, 7*(8), 1-14. http://dx.doi.org/10.5539/mas.v7n8p1

Moretti, L. (2012). Modello di analisi strutturale, funzionale ed economica di pavimentazioni stradali in calcestruzzo. PhD Thesis, Sapienza University of Rome, Italy. Retrieved from http://padis.uniroma1.it/handle/10805/1657

Moretti, L., & Di Mascio, P. (2013a). Model for estimating temperatures in concrete pavements. Model for estimating temperatures in concrete pavements. *Proceedings of the first International Journal of Pavements Conference*, São Paulo, Brazil.

Moretti, L., Di Mascio, P., & D'Andrea, A. (2013b). Environmental Impact Assessment of Road Asphalt Pavements. *Modern Applied Science, 7*(11), 1-11. http://dx.doi.org/10.5539/mas.v7n11p1

Nishizawa, T., Ozeki, T., Katoh, K., & Matsui, K. (2009). Finite Element Model Analysis of Thermal Stresses of Thick Airport Concrete Pavement Slabs. *Transportation Research Record: Journal of the Transportation Research Board, 2095*(1), 3-12.

Qin, Y., & Hiller, J. E. (2011). Modeling the Temperature and Stress Distributions in Rigid Pavements: Impact of Solar Radiation Absorption and Heat History Development. *KSCE Journal of Civil Engineering, 15*(8), 1361-1371. http://dx.doi.org/10.1007/s12205-011-1322-6

Rao, C., Barenberg, E. J., Snyder, M. B., & Schmidt, S. (2001). Effects of Temperature and Moisture on the response on the Jointed Concrete Pavements. *7th International Conference on Concrete Pavements* - Orlando, Florida, USA.

Shahin, M. Y. (2005). *Pavement Management for Airports, Roads, and Parking Lots*. Kluwer Academic Publishers.

Thomlinson, J. (1940). Temperature variations and consequent stresses produced by daily and seasonal temperature cycles in concrete slabs. *Concrete Constructional Engineering, 36*(6), 298-307.

Modern Applied Science; Vol. 8, No. 3; 2014
ISSN 1913-1844 E-ISSN 1913-1852
Published by Canadian Center of Science and Education

Annealing Effect of High Dielectric Material for Low Voltage Electrowetting on Dielectric (EWOD)

Hsiu-Hsiang Chen[1] & Chien-Chung Fu[2]

[1] Industrial Technology Research Institute, Taiwan

[2] Institute of NanoEngineering and Microsystems, National Tsing-Hua University, Taiwan

Correspondence: Hsiu-Hsiang Chen, Industrial Technology Research Institute, Taiwan. E-mail: susanchen@itri.org.tw

Received: February 10, 2014 Accepted: March 18, 2014 Online Published: April 8, 2014

doi:10.5539/mas.v8n3p10 URL: http://dx.doi.org/10.5539/mas.v8n3p10

Abstract

In this paper, the high dielectric constants for Ta_2O_5 (~18.8) and Nb_2O_5 (~25.5) were deposited by a RF reactive magnetron sputtering and respectively annealed at 700 °C and 400 °C O_2 ambiance for 30 min in a conventional furnace. The purpose of this study is to optimize the annealing condition (various temperatures at N_2 or O_2 ambiance) of the high-dielectric-constant Ta_2O_5 and Nb_2O_5 films deposited by RF reactive magnetron sputtering to enhance the dielectric constant of those films to further lower the operating voltage. Based on the results, an electrowetting optical deflector (EOD) filled with the water (1% sodium dodecyl sulfate (SDS)) and dodecane was fabricated and tested, and the contact angle of the inclined liquid surface on the left and right sidewall can be varied about 70° at 9 V operating voltage. This study provides a practical way to fabricate a high dielectric constant layer for low voltage electrowetting on dielectric (EWOD) application.

Keywords: electrowetting optical deflector, anneal, dielectric constant

1. Introduction

Electrowetting phenomenon was first exploited by Lippmann (1875). By varying the voltage between the electrolyte droplet and the substrate, the contact angle of droplet can be modulated. Due to the electrolysis effect, the room to manipulate the contact angle of droplet is very limited. Till Berge (1993) inserted a thin insulating layer between the electrolyte droplet and the electrode to eliminate the electrolysis problem, the contact angle change can be dramatically increased at a large voltage. This improved technology was so called EWOD. Since then, it initiated an explosive growth in electrowetting research, especially in the field of optics (Mugele & Baret, 2005; Kuiper, Hendriks, Hayes, Feenstra, & Baken, 2005; Hou, Zhang, Smith, Yang, & Heikenfeld, 2010; Ceyssensa et al., 2013).

Many studies have used SiO_2 with a low dielectric-constant of about 3.8 as the insulating layer, leading to a large operating voltage of several tens of volts (Smith, Abeysinghe, Haus, & Heikenfeld, 2006; Papathanasiou, Papaioannou, & Boudouvis, 2008; Cho, Fan, Moon, & Kim, 2002; Cho, Moon, & Kim, 2003). The larger operating voltage will cause electrical breakdown and reliability. Thus, in the electrowetting optics application, the low operating voltage is the future trend in order to be compatible with commercial electronic components, reliability and conserve power. Known from Lippmann-Young equation (Mugele & Baret, 2005), decreasing the thickness of the dielectric layer, employing a high dielectric constant material, and minimizing the interfacial surface tension between the electrolyte and the surrounding ambient phase are the three applicable approaches to drop the required operating voltage. However, thinning the dielectric layer tends to induce dielectric breakdown (Berry, Kedzierski, & Abedian, 2006) at high electric field; besides, adding surfactants to the oil-water interface has been proven to slow down the oil-water response time (Roques-Carmes, Palmier, Hayes, & Schlangen, 2005). Therefore, using high dielectric films is the most potential method among the three to achieve the low operating voltage without suffering from other side effects.

A lot of efforts have been dedicated to exploring the deposition of high dielectric constant materials, and promising progress has been reported (Moon, Cho, Garrrell, & Kim, 2002; Li et al., 2008; Chang, Choi, Han, & Pak, 2009; Raj, Dhindsa, Smith, Laughlin, & Heikenfeld, 2009; Lin, Evans, Welch, Hsu, Madison, & Fair, 2010). However, the facilities used in those studies, such as metal-organic chemical vapor deposition (MOCVD) (Moon

et al., 2002) and atomic layer deposition (ALD) (Chang, Choi, Han, & Pak, 2009; Raj, Dhindsa, Smith, Laughlin, & Heikenfeld, 2009), are not widely available. As a consequence, some other cost-saving approaches have been suggested for the material deposition. In the dense wavelength division multiplexing (DWDM) system, it required a high dielectric films (e.g., Ta_2O_5, Nb_2O_5, or TiO_2) to fabricate an interference filter. In general, the most common way to deposit these high dielectric layers is by RF reactive magnetron sputtering, and most of the metal oxides can be deposited by using the metal targets and reaction gas mixtures (e.g., O_2 and Ar).

The purpose of this research was to fabricate a high dielectric constant layer to lower the operating voltage. According to Park's findings (Park, Li, Nam, & Rhee, 1999), a high dielectric constant film can be produced by using sputtering and annealing technologies. The purpose of this study is to optimize the annealing condition of the high-dielectric-constant Ta_2O_5 and Nb_2O_5 films deposited by RF reactive magnetron sputtering (Lin et al., 2011; Zhou, Luo, Li, & Liu, 2009; Coskun & Demirel, 2013; Lai, Lin, Huang, Gai, & Qu, 2006) to enhance the dielectric constant of those films to further lower the operating voltage. The annealing was taken at various temperatures under N_2 or O_2 ambiance in a conventional furnace. The dielectric constant of the resulting films was deduced from capacitance measurement with an inductance capacitance resistance (LCR) meter, and the film surface morphologies were investigated with scanning electron microscope (SEM) and atomic force microscope (AFM). Finally, an electrowetting optical deflector (EOD) device (Chen & Fu, 2011) consisting of a 200-nm Nb_2O_5, layer annealed at 400 °C for 30 min under O_2 ambient was fabricated and tested. The contact angle of the inclined liquid with respective to the EOD sidewalls can be varied up to 70° at the operating voltage of 9 V.

2. Experimental Procedures

The cleaning procedures of the substrate for dielectric film deposition were briefed as follows. First, the p-type (100) silicon wafers were immersed in the piranha solutions for 5 min to remove organic contamination, and then dipped in the buffered oxide etch (BOE) for 30 sec to strip off the native oxide. Next, the wafers were rinsed with deionized (DI) water with resistivity of ~18 MΩ, were dehydrated on a hotplate at 200 °C for at least 20 min, and were cooled to room temperature.

The deposition of dielectric films was carried out in a RF magnetron sputtering system, and the tantalum and niobium targets of 99.99% purity were employed for the Ta_2O_5 and Nb_2O_5 film deposition. To start the sputtering process, the system was first evacuated to a base pressure of 0.67 mPa, followed by the Ar and O_2 gases flow with the rates keeping at 27 sccm and 3 sccm, respectively, corresponding to a total gas pressure of 0.4 Pa. Then, the sputtering power was set to be 300 W, and the substrate temperature was raised to 100 °C. The deposition rates for Ta_2O_5 and Nb_2O_5 were 10 and 2 nm/min, respectively. The dielectric layers with thicknesses of 200 nm were prepared for each material, and the thickness of each coated layer was measured with a surface profile meter (AMBIOS XP-1). Finally, these samples were respectively annealed in a conventional N_2 or O_2 furnace using at temperatures ranging from 400 °C to 1000 °C for 30 min. After annealing procedure, the samples were cooled down to room temperature.

The dielectric constant, surface morphologies, and surface roughness for the resulting dielectric films were respectively analyzed by the LCR (Agilent E4980A) meter, SEM (Hitachi S-4800), and AFM (Veeco) before and after annealing. In order to measure dielectric constants, a metal-insulator-semiconductor (MIS) capacitor with a 500 × 500 μm^2 Al pad was fabricated on top of the dielectric layer using photolithography and lift-off process. The p-type Si substrate was positive biased, and the Al pad was negative biased. The dielectric constant of the resulting films was deduced from capacitance measurement at various frequencies (100 Hz ~100 kHz) and bias (50 mV, 250 mV, and 1 V) with the LCR meter. To calculate the dielectric constant, the post-annealing sample thickness was measured by its cross-sectional SEM image. The surface roughness of dielectric films was analyzed by tapping mode AFM, and the scan area was 1 × 1 μm^2.

An EOD device was fabricated to test the contact angle change of the inclined liquid surface on the sidewalls. The detail fabrication processes have been reported elsewhere (Kuiper et al., 2005; Smith, 2006; Chen et al., 2011). As shown in Figure 1(a), an EOD chamber included two Si sidewalls (coated with a composite dielectric layer) as electrodes, a transparent indium tin oxide (ITO) glass spacer (~3 mm wide) in the bottom, a top glass plate, and two front and back sealing glass plates. The composite dielectric layers was a 200-nm Nb_2O_5 dielectric layer (annealed at 400 °C O_2 ambiance for 30 min) covered by a 100 nm CYTOP® hydrophobic fluoropolymer.

After assembling, the EOD chamber was filled with water (containing 1% SDS) and dodecane, and the liquid-liquid interface formed a convex shape (Figure 1(a)). Figure 1(b) shows the schematic of the voltage connections and liquid incline angle measurement system. The experimental flow chart is shown in Figure 2. The EOD's operation required three electrical terminals: two DC voltage sources (V_L and V_R) attached to the Si

electrodes, and the bottom ITO electrode was electrically grounded. The EOD device was operated in one of the three modes: $V_L = V_R$, $V_L > V_R$, and $V_L < V_R$. The contact angles of the inclined liquid surface on the left and right sidewalls were indicated by θ_L and θ_R, and were measured by a charge coupled device (CCD) image capturing system.

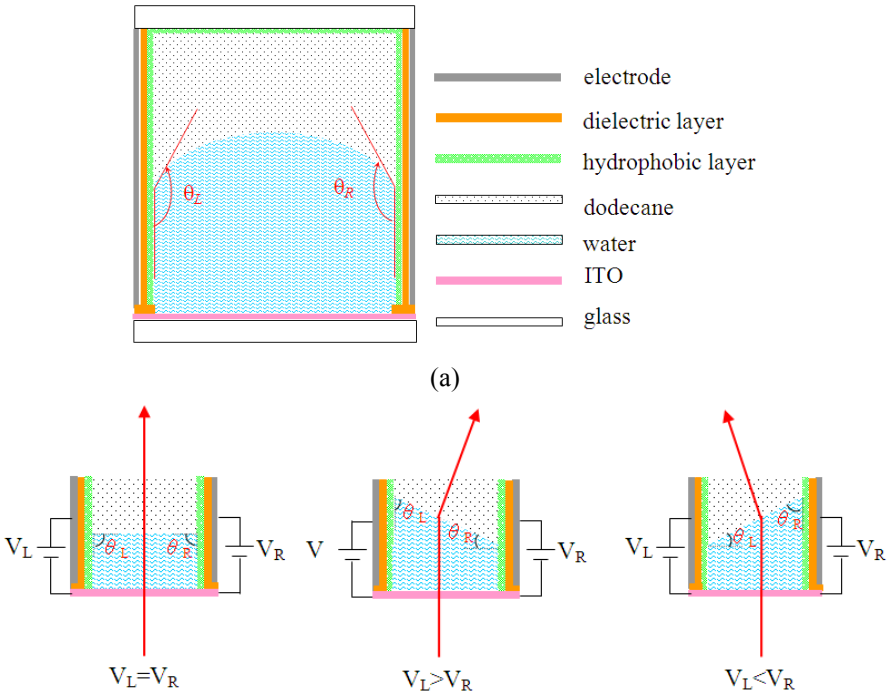

Figure 1. The schematic of (a) a basic EOD device structure; and (b) the three operating modes of an EOD device: $V_L=V_R$, $V_L>V_R$, and $V_L<V_R$ from left to right

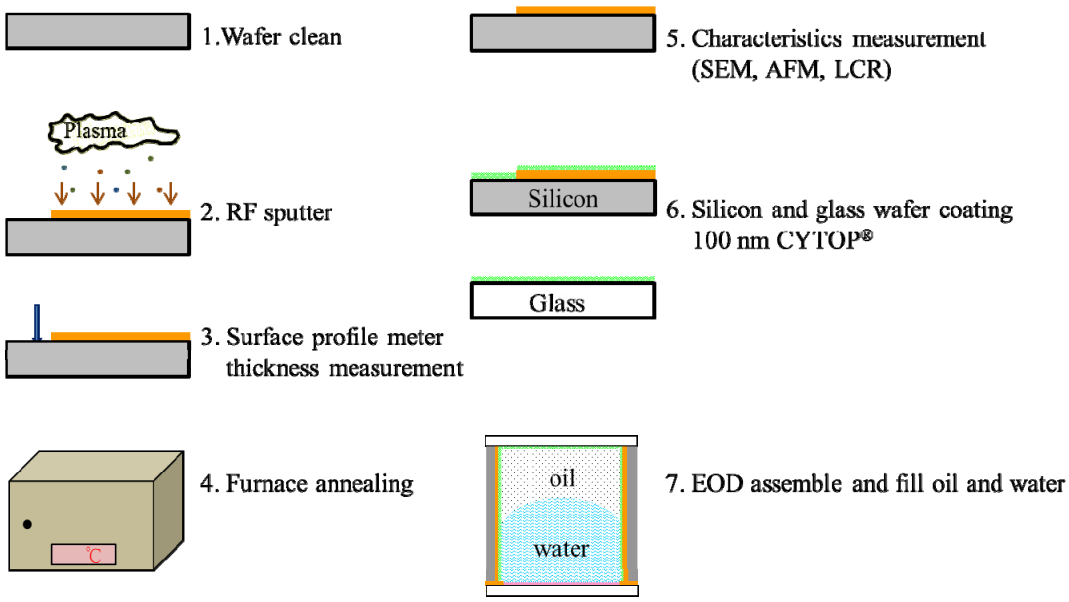

Figure 2. The experimental flow chart

3. Results and Discussion

3.1 Dielectric Constant Characteristics

The thin film deposited by RF reactive magnetron sputtering will form amorphous atoms or ions randomly, and there are dangling bonds and voids. When annealing to certain temperature, the thin film will crystalline and improve crystal imperfections (defect, impurity) to enhance the dielectric constant. To Achieve such a new material could benefit all EWOD devices in terms of lower voltage, east to fabricate and improved reliability.

Figures 3 and 4 illustrate the dielectric constant as a function of various N_2 and O_2 ambient annealing temperatures for Ta_2O_5 and Nb_2O_5. The measuring frequency was fixed at 100 Hz, and measuring voltages were varied from 50 mV to 1 V. The results show that the dielectric constant was found to slightly vary as the measuring voltage increased. This was due to the reason that the MIS capacitance was biased at the accumulation mode voltages.

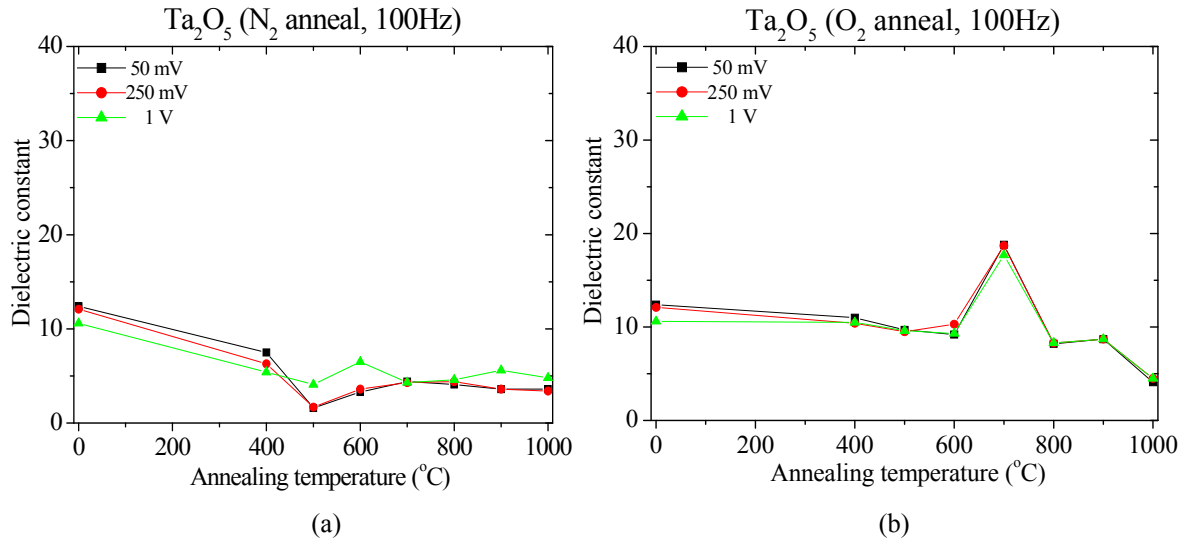

Figure 3. Ta_2O_5 dielectric constant as a function of (a) N_2; and (b) O_2 annealing temperatures. The measuring frequency was fixed at 100 Hz, and measuring voltages were varied from 50 mV to 1 V. The zero annealing temperature indicates the as-deposited samples

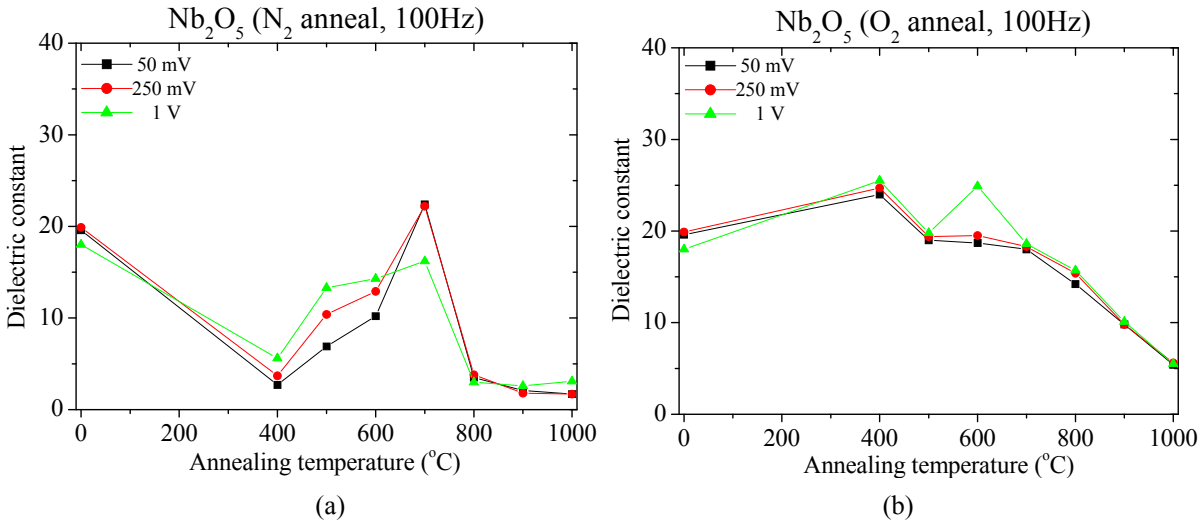

Figure 4. Nb_2O_5 dielectric constant as a function of (a) N_2; and (b) O_2 annealing temperatures. The measuring frequency was fixed at 100 Hz, and measuring voltages were varied from 50 mV to 1 V. The zero annealing temperature indicates the as-deposited samples

Figures 5 and 6 illustrate the dielectric constant as a function of various measuring frequencies (100 Hz ~ 100 kHz) and annealing temperatures (400 °C ~ 1000 °C) for Ta_2O_5 and Nb_2O_5. The measuring voltage was fixed at 1 V, and the dielectric constant was found to decrease as the measuring frequency increased (Joshi & Cole, 1999). Moreover, Figures 5(a) and 6(a) show that annealed in the N_2 temperature did not enhance much the dielectric constants than as-deposited dielectric films, and Figures 5(b) and 6(b) show that annealed in the O_2 temperature can enhance the dielectric constants at certain temperature.

From the Figure 5(b) and 6(b) we selected the best conditioning for Ta_2O_5 (~18.8 at 700 °C) and Nb_2O_5 (~ 25.5 at 400 °C) with O_2 annealing. Figure 7 shows the dielectric constants of the optimized films when the measuring frequencies were varied from 100 Hz to 100 kHz, and measuring voltages were varied from 50 mV to 1 V. The results indicate that the dielectric constant decreased as the measuring frequency increased. These findings were in good agreement with those reported (Joshi et al., 1999; Masse, Szymanowski, Zabeida, Amassian, Klemberg-Sapieha, & Martinu, 2006) for Ta_2O_5 and Nb_2O_5. The literature (Shinriki, Nishioka, Ohji, & Mukai, 1989) shows that Ta_2O_5 and Nb_2O_5 films crystallize at 650 °C and 450 °C to form a hexagonal structure and enhance the dielectric constant.

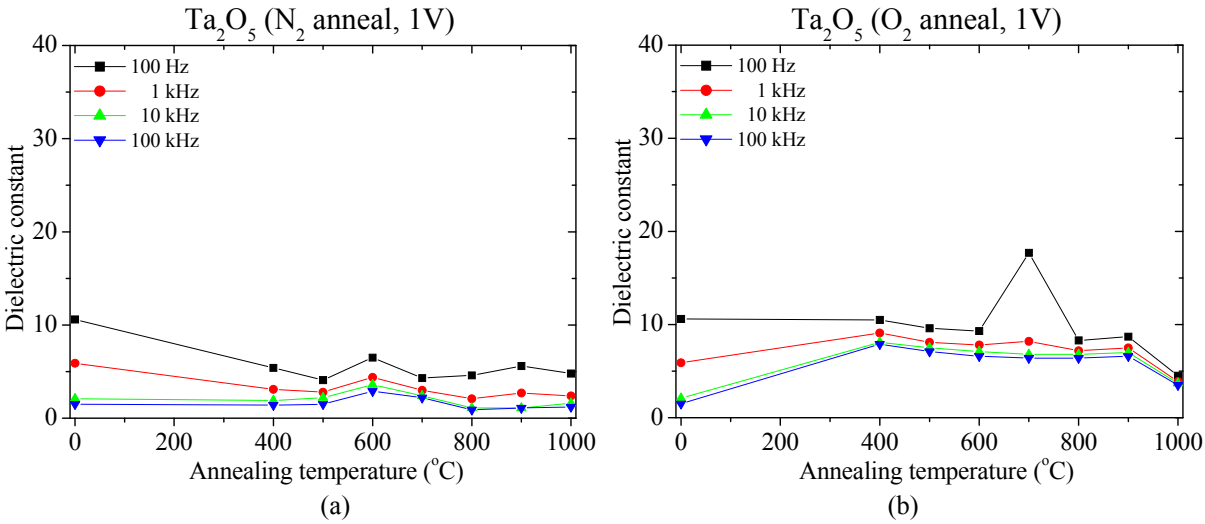

Figure 5. Ta_2O_5 dielectric constant as a function of (a) N_2; and (b) O_2 annealing temperatures. The measuring voltage was fixed at 1 V, and measuring frequencies were varied from 100 Hz to 100 kHz. The zero annealing temperature indicates the as-deposited samples

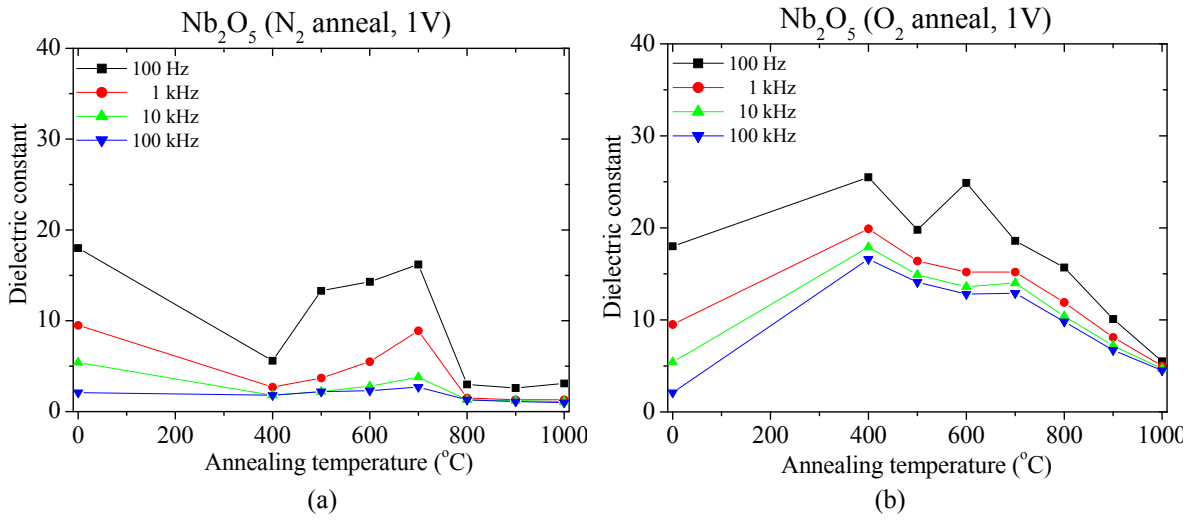

Figure 6. Nb_2O_5 dielectric constant as a function of (a) N_2; and (b) O_2 annealing temperatures. The measuring voltage was fixed at 1 V, and measuring frequencies were varied from 100 Hz to 100 kHz. The zero annealing temperature indicates the as-deposited samples

Besides, in these oxidation processes (annealing temperature ≧900 °C), the dielectric constant was reduced due to the growth of a SiO_2 film, which has a small dielectric constant (3.8), between the dielectric film and the silicon substrate. This can explain the reason that dielectric constant decreased as the annealing temperature increased.

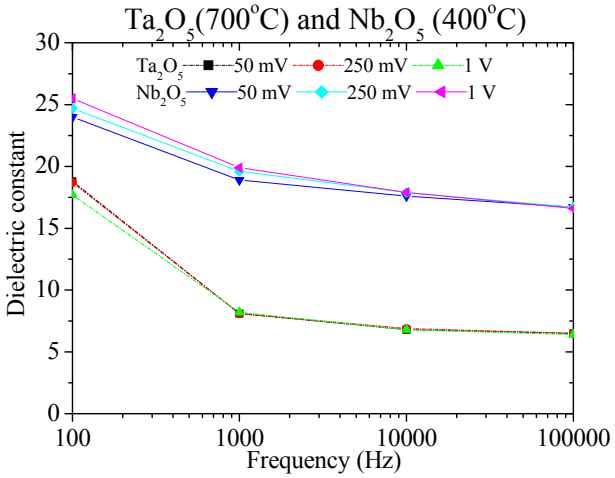

Figure 7. The dielectric constant as a function of measuring frequencies with O_2 annealing temperature at (a) 700 °C Ta_2O_5; and (b) 700 °C Nb_2O_5. The measuring voltages were varied from 50 mV to 1 V

3.2 Surface Morphology Features

Figures 8-11 show the SEM and AFM images of the dielectric film for as deposited and annealed at various temperatures. As shown in Figures 8(a) and 10(a), the surface morphology of the Ta_2O_5 and Nb_2O_5 films was smooth and no defects. Figure 12 displays the average roughness values as a function of N_2 and O_2 annealing temperatures for Ta_2O_5 and Nb_2O_5 dielectric films. The results show that the surface roughness rose as the annealing temperature increased. The surface roughness change for Ta_2O_5 (0.42 nm ~ 1.93 nm) was much smaller than the Nb_2O_5 (0.51 nm ~ 9.06 nm) under various N_2 and O_2 annealing temperatures.

The surface roughness for as deposited Ta_2O_5 and Nb_2O_5 dielectric films was very small (≦0.51 nm); however, when the annealing temperature was gradually increased, the surface of the dielectric layers began to form grain boundary (see Figures 8(b) and 10(b)) and the surface roughness was increased. In the Ta_2O_5 dielectric film, the grain boundary did not form much as the anneal temperatures were below 650 °C; while, when the annealing temperature was above 450 °C, the Nb_2O_5 dielectric film formed a distinct grain boundary (Masse et al., 2006). The surface roughness for the highest dielectric constant conditions of Ta_2O_5 (at 700 °C O_2 annealing) and Nb_2O_5 (at 400 °C O_2 annealing) was 0.65 nm and 1.15 nm, respectively. The surface roughness affects the contact angle and contact angle hysteresis (the difference between forward and backward contact angle). In our case, the low surface roughness is needed to avoid reliability problems.

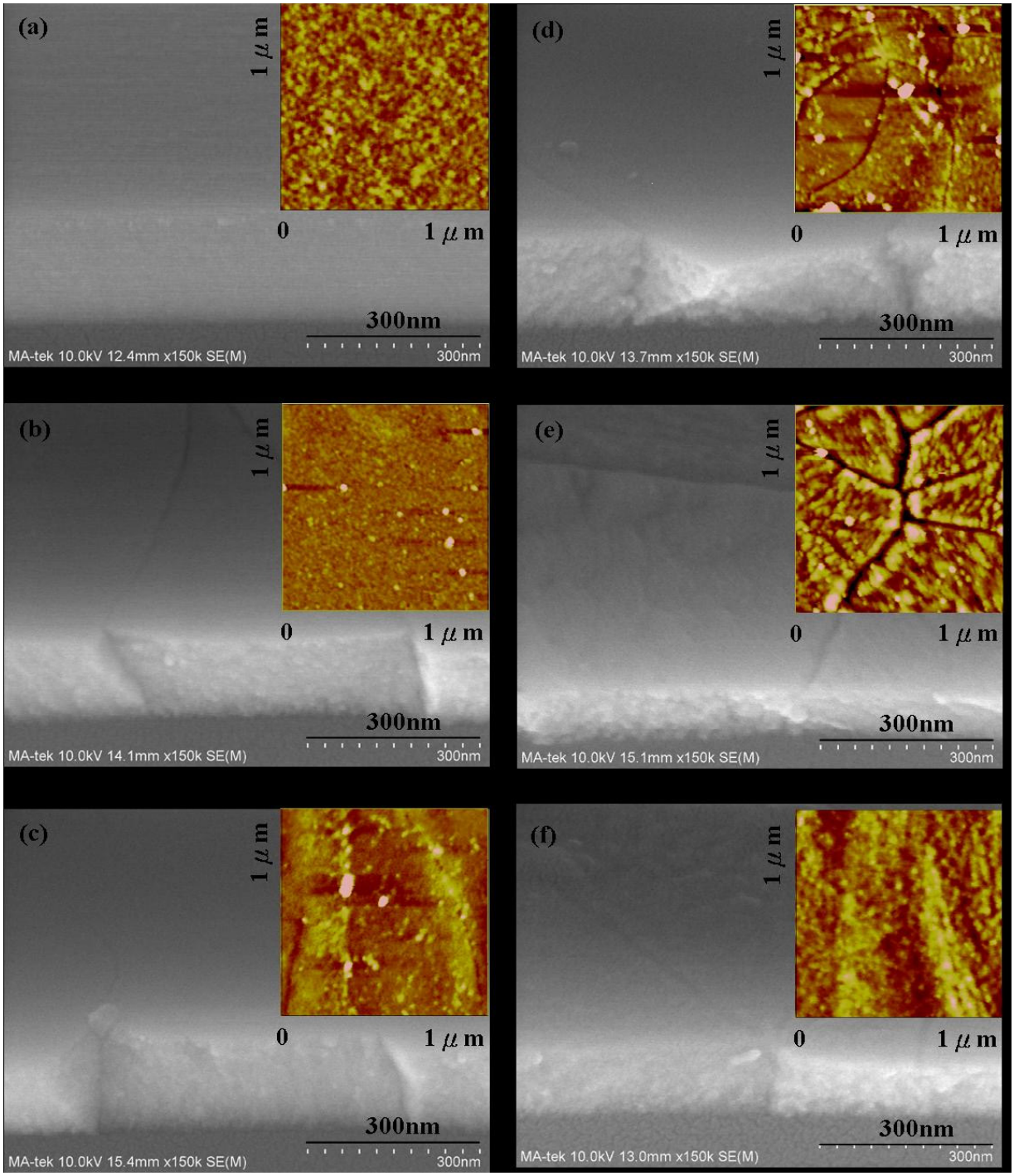

Figure 8. The SEM images show the surface morphology of the Ta_2O_5 film for (a) as deposited, and with N_2 annealing at (b) 400 °C; (c) 600 °C (d) 700 °C; (e) 800 °C; and (f) 1000 °C. The inset picture is the AFM image with 1μm × 1μm area

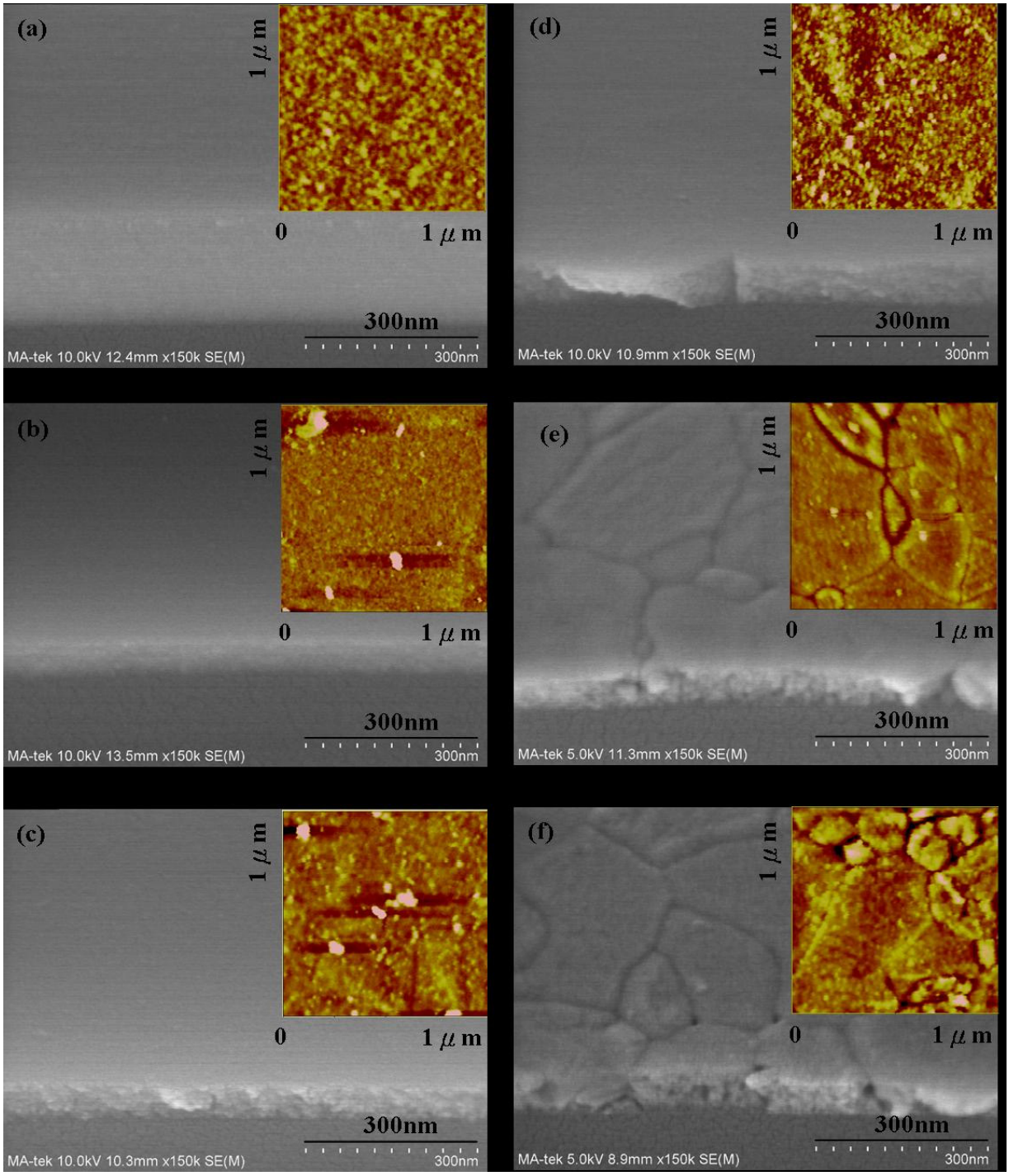

Figure 9. The SEM images show the surface morphology of the Ta_2O_5 film for (a) as deposited, and with O_2 annealing at (b) 400 °C; (c) 600 °C (d) 700 °C; (e) 800 °C; and (f) 1000 °C. The inset picture is the AFM image with 1μm × 1μm area

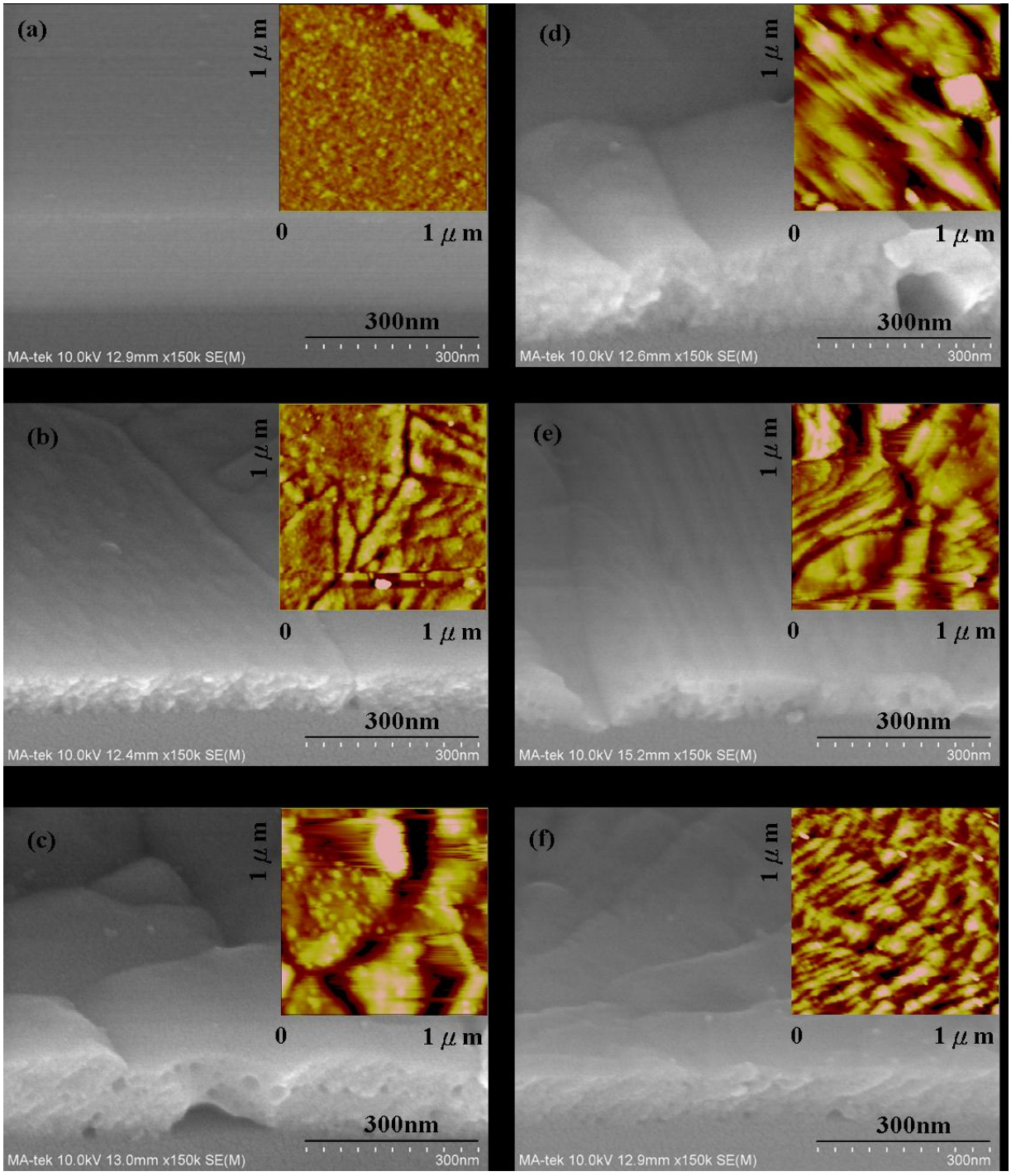

Figure 10. The SEM images show the surface morphology of the Nb_2O_5 film for (a) as deposited, and with N_2 annealing at (b) 400 °C; (c) 600 °C (d) 700 °C; (e) 800 °C; and (f) 1000 °C. The inset picture is the AFM image with 1μm × 1μm area

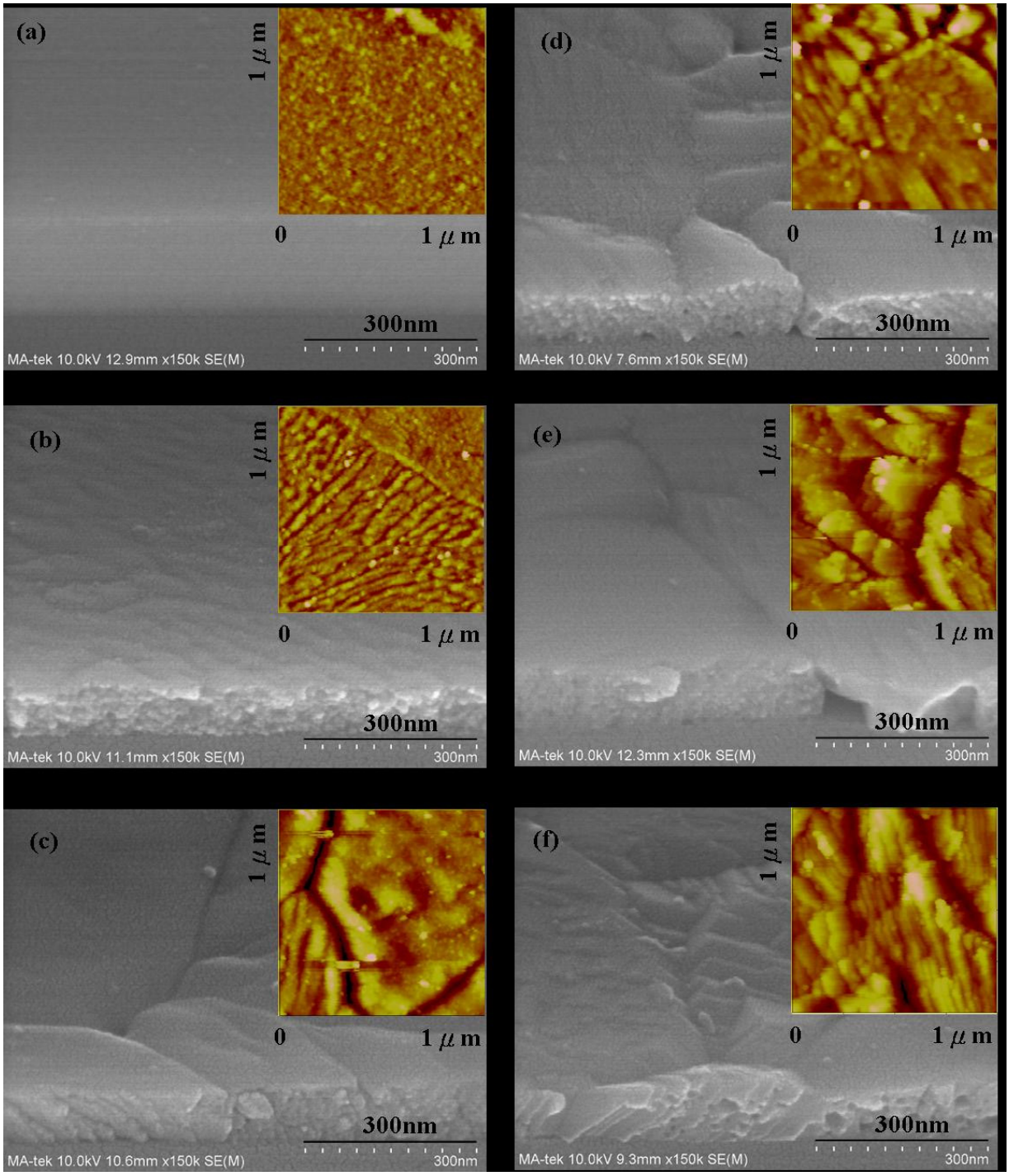

Figure 11. The SEM images show the surface morphology of the Nb_2O_5 film for (a) as deposited, and with O_2 annealing at (b) 400 °C; (c) 600 °C (d) 700 °C; (e) 800 °C; and (f) 1000 °C. The inset picture is the AFM image with 1μm × 1μm area

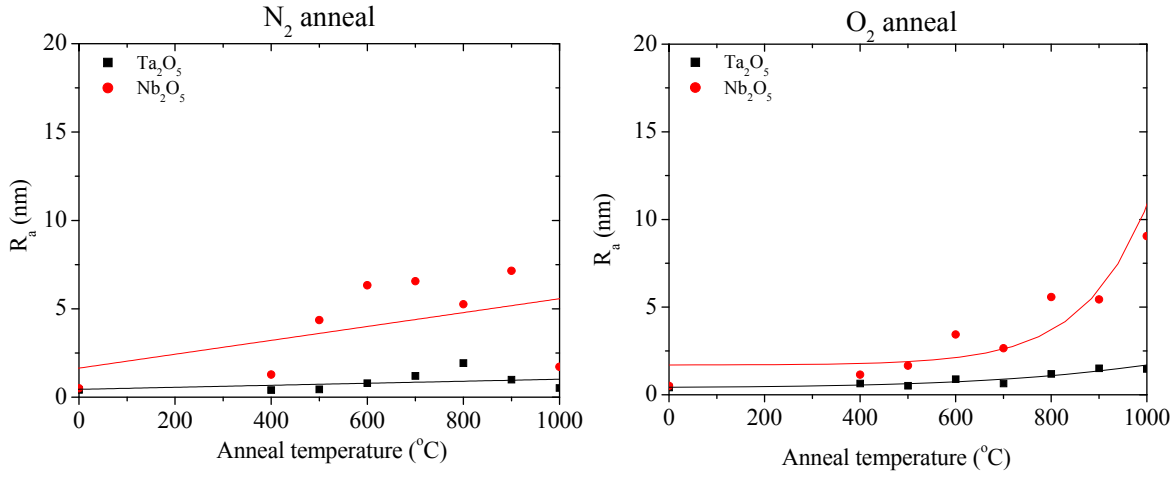

Figure 12. Average roughness as a function of (a) N_2; and (b) O_2 annealed temperatures for Ta_2O_5 and Nb_2O_5 dielectric films (by AFM measurement)

3.3 Demonstration of EOD Deflection

Figure 13 shows the photographs of the EOD device in various operating voltages. When the EOD device was filled inside with the water (1% SDS) and dodecane at zero voltage, the liquid-liquid interface formed a convex shaped meniscus (Figure 13(a)). When the left and right sidewalls biased at 7 V, the liquid-liquid interface become level (Figure 13(b)). In addition, when the V_L = 9 V and V_R = 5 V, the liquid-liquid interface inclined to the upper left corner (Figure 13(c)). Reversing the bias voltage, the liquid-liquid interface inverted to the upper right corner (Figure 13(d)) (Video, 4.11 MB).

Experimental results show that the contact angle of the inclined liquid surface on the two EOD sidewalls can vary about 70° at 9 V operating in a dodecane/water/Cytop®/Nb_2O_5 system, and which was reduced 2 V operating voltage compared to our previous study (Ta_2O_5 without annealing treatment) (Chen et al., 2011).

Due to the contact angle saturation phenomenon, the contact angle of the inclined liquid surface was saturated at 70°. In future work, applying an AC operating voltage (Nanayakkara et al., 2010) and a high quality dielectric film (pinhole free) to avoid charges trapping (Verheijen & Prins, 1999) will reduce contact angle saturation. This paper may provide a good reference for the dielectric constant characteristics in the AC operating voltage.

4. Conclusions

The high dielectric constant layers (Ta_2O_5 and Nb_2O_5) were deposited on the silicon substrate by a RF reactive magnetron sputtering and annealed at various temperatures under N_2 or O_2 ambiance in a conventional furnace. The dielectric constant and surface roughness of the dielectric layers before and after various annealing treatments were studied by an LCR meter, SEM and AFM instruments. The as-deposited dielectric films have an amorphous structure, and the surface roughness is very small (≦0.51 nm). However, when the annealing temperature was gradually increased, the surface of the dielectric layers began to form grain boundary and the surface roughness becomes larger. Experimental results show that annealed in the N_2 ambiance did not enhance the dielectric constant than as-deposited dielectric films, but annealed in the O_2 ambiance can enhance the dielectric constants below certain temperature.

This study gets the high dielectric constants for Ta_2O_5 (~18.8) and Nb_2O_5 (~25.5) deposited by a RF reactive magnetron sputtering and respectively annealed at 700 °C and 400 °C O_2 ambiance for 30 min in a conventional furnace. Moreover, we show that the contact angle of EOD device can change 70° for a dodecane/water/Cytop®/Nb_2O_5/Si system with an applied voltage as low as 9 V.

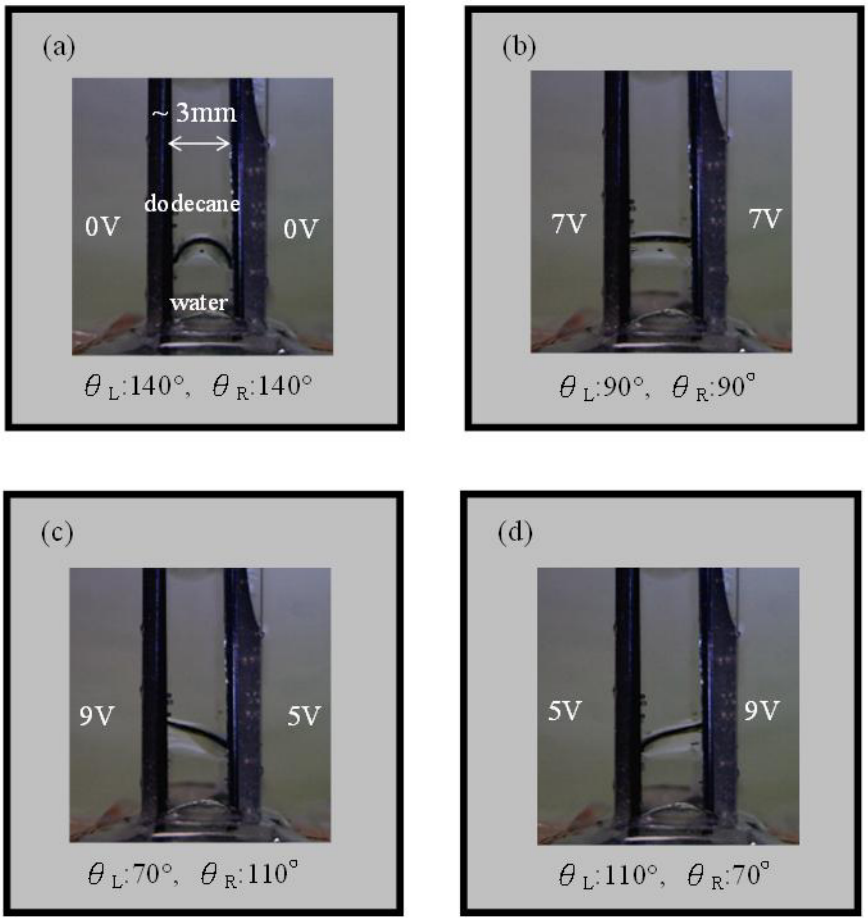

Figure 13. Side view photographs of the EOD device (dodecane and 1%SDS water) with (a) $V_L = V_R = 0$ V; (b) $V_L = V_R = 7$ V; (c) $V_L = 9$ V, $V_R = 5$ V; and (d) $V_L = 5$ V, $V_R = 9$ V. The water is electrically grounded (Video, 4.11 MB)

Acknowledgements

The authors gratefully acknowledge their colleagues Dr. Chiun-Lung Tsai for valuable discussions and comments on the manuscript. Specials thanks are due to Ms. Ming-Fang Hsu for AFM measurement. The research is financially supported mainly by ITRI (Industrial Technology Research Institute, Taiwan).

References

Berge, B. (1993). Electrocapillarity and wetting of insulator films by water. *Comptes Rendus De L Academie Des Sciences Serie II, 317*(2), 157-163.

Berry, S., Kedzierski, J., & Abedian, B. (2006). Low voltage electrowetting using thin fluoroploymer films. *Journal of Colloid and Interface Science, 303*(2), 517-524. http://dx.doi.org/10.1016/j.jcis.2006.08.004

Ceyssens, F., Witters, D., Van Grimbergen, T., Knez, K., Lammertyn, J., & Puers, R. (2013). Integrating optical waveguides in electrowetting-on-dielectric digital microfluidic chips. *Sensors and Actuators B: Chemical, 181*, 166-171. http://dx.doi.org/10.1016/j.snb.2013.01.078

Chang, J. H., Choi, D. Y., Han, S., & Pak, J. J. (2010). Driving characteristics of the electrowetting-on-dielectric device using atomic-layer-deposited aluminum oxide as the dielectric. *Microfluidics and Nanofluidics, 8*(2), 269-273. http://dx.doi.org/10.1007/s10404-009-0511-9

Chen, H. H., & Fu, C. C. (2011). Low Voltage Electrowetting Optical Deflector. *Japanese Journal of Applied Physics, 50*(2011) 037202. http://dx.doi.org/10.1143/JJAP.50.037202

Cho, S. K., Fan, S. K., Moon, H., & Kim, C. J. (2002, January). Towards digital microfluidic circuits: creating, transporting, cutting and merging liquid droplets by electrowetting-based actuation. In *Micro Electro Mechanical Systems, 2002. The Fifteenth IEEE International Conference on* (pp. 32-35). IEEE.

Cho, S. K., Moon, H., & Kim, C. J. (2003). Creating, transporting, cutting, and merging liquid droplets by electrowetting-based actuation for digital microfluidic circuits. *Microelectromechanical Systems, Journal of, 12*(1), 70-80. http://dx.doi.org/10.1109/JMEMS.2002.807467

Coşkun, Ö. D., & Demirela, S. (2013). The optical and structural properties of amorphous Nb2O5 thin filmsprepared by RF magnetron sputtering. *Applied Surface Science, 277*, 35-39. http://dx.doi.org/10.1016/j.apsusc.2013.03.116

Hou, L., Zhang, J., Smith, N., Yang, J., & Heikenfeld, J. (2010). A full description of a scalable microfabrication process for arrayed electrowetting microprisms. *Journal of Micromechanics and Microengineering, 20*(1), 015044. http://dx.doi.org/10.1088/0960-1317/20/1/015044

Joshi, P. C., & Cole, M. W. (1999). Influence of postdeposition annealing on the enhanced structural and electrical properties of amorphous and crystalline Ta_2O_5 thin films for dynamic random access memory applications. *Journal of Applied Physics, 86*(2), 871-880. http://dx.doi.org/10.1063/1.370817

Kuiper, S., Hendriks, B. H. W., Hayes, R. A., Feenstra, B. J., & Baken, J. M. E. (2005, August). Electrowetting-based optics. In *Optics & Photonics 2005* (pp. 59080R-59080R). International Society for Optics and Photonics.

Lai, F., Lin, L., Huang, Z., Gai, R., & Qu, Y. (2006). Effect of thickness on the structure, morphology and optical properties of sputter deposited Nb2O5 films. *Applied Surface Science, 253*(4), 1801-1805. http://dx.doi.org/10.1016/j.apsusc.2006.03.014

Li, Y., Parkes, W., Haworth, L. I., Stokes, A. A., Muir, K. R., Li, P., … Walton, A. J. (2008). Anodic Ta2O5 for CMOS compatible low voltage electrowetting-on-dielectric device fabrication. *Solid State Electronic, 52*(9), 1382-1387. http://dx.doi.org/10.1016/j.sse.2008.04.030

Lin, Y. Y., Evans, R. D., Welch, E., Hsu, B. N., Madison, A. C., & Fair, R. B. (2010). Low voltage electrowetting-on-dielectric platform using multi-layer insulators. *Sensors and Actuators B: Chemical, 150*(1), 465-470. http://dx.doi.org/10.1016/j.snb.2010.06.059

Lin, Y. Y., Evans, R. D., Welch, E., Hsu, B. N., Madison, A. C., & Fair, R. B. (2011). Low Voltage Electrowetting-on-Dielectric Platform using Multi-Layer Insulators. Sens Actuators B Chem. Author manuscript; available in PMC Sep 21, 2011.

Lippmann, G. (1875). *Relations entre les phénomènes électriques et capillaires. Ann. Chim. Phys., 5*, 494.

Masse, J. P., Szymanowski, H., Zabeida, O., Amassian, A., Klemberg-Sapieha, J. E., & Martinu, L. (2006). Stability and effect of annealing on the optical properties of plasma-deposited Ta_2O_5 and Nb_2O_5 films. *Thin Solid Films, 515*(4), 1674-1682. http://dx.doi.org/10.1016/j.tsf.2006.05.047

Moon, H., Cho, S. K., & Garrell, R. L. (2002). Low voltage electrowetting-on-dielectric. *Journal of Applied Physics, 92*(7), 4080-4087. http://dx.doi.org/10.1063/1.1504171

Mugele, F., & Baret, J. C. (2005). Electrowetting: from basics to applications. *Journal of Physics: Condensed Matter, 17*(28), R705. http://dx.doi.org/10.1088/0953-8984/17/28/R01

Nanayakkara, Y. S., Perera, S., Bindiganavale, S., Wanigasekara, E., Moon, H., & Armstrong, D. W. (2010). The effect of AC frequency on the electrowetting behavior of ionic liquids. *Analytical Chemistry, 82*(8), 3146-3154. http://dx.doi.org/10.1021/ac9021852

Papathanasiou, A. G., Papaioannou, A. T., & Boudouvis, A. G. (2008). Illuminating the connection between contact angle saturation and dielectric breakdown in electrowetting through leakage current measurementsa). *Journal of Applied Physics, 103*(3), 034901. http://dx.doi.org/10.1063/1.2837100

Park, Y. B., Li, X., Nam, G. J., & Rhee, S. W. (1999). Effects of annealing in O_2 and N_2 on the microstructure of metal organic chemical vapor deposition Ta_2O_5 film and the interfacial SiO_2 layer. *Journal of Materials Science: Materials in Electronics, 10*(2), 113-119. http://dx.doi.org/10.1023/A:1008960014883

Raj, B., Dhindsa, M., Smith, N. R., Laughlin, R., & Heikenfeld, J. (2009). Ion and liquid dependent dielectric failure in electrowetting systems. *Langmuir, 25*(20), 12387-12392. http://dx.doi.org/10.1021/la9016933

Roques-Carmes, T., Palmier, S., Hayes, R. A., & Schlangen, L. J. (2005). The effect of the oil/water interfacial tension on electrowetting driven fluid motion. *Colloids and Surfaces A: Physicochemical and Engineering Aspects, 267*(1), 56-63. http://dx.doi.org/10.1016/j.colsurfa.2005.06.056

Shinriki, H., Nishioka, Y., Ohji, Y., & Mukai, K. (1989). Oxidized Ta_2O_5/Si_3N_4 dielectric films on poly-crystalline Si for dRAMs. *Electron Devices, IEEE Transactions on, 36*(2), 328-332. http://dx.doi.org/10.1109/16.19933

Smith, N. R., Abeysinghe, D. C., Haus, J. W., & Heikenfeld, J. (2006). Agile wide-angle beam steering with electrowetting microprisms. *Optics Express, 14*(14), 6557-6563. http://dx.doi.org/10.1364/OE.14.006557

Verheijen, H. J. J., & Prins, M. W. J. (1999). Reversible electrowetting and trapping of charge: model and experiments. *Langmuir, 15*(20), 6616-6620. http://dx.doi.org/10.1021/la990548n

Zhou, J. C., Luo, D. T., Li, Y. Z., & Liu, Z. (2009). Effect of sputtering pressure and rapid thermal annealing on optical properties of Ta_2O_5 thin films. *Transactions of Nonferrous Metals Society of China, 19*(2), 359-363. http://dx.doi.org/10.1016/S1003-6326(08)60278-2

Modern Applied Science; Vol. 8, No. 3; 2014
ISSN 1913-1844 E-ISSN 1913-1852
Published by Canadian Center of Science and Education

Aesthetic Curve Design with Linear Gradients of Logarithmic Curvature/Torsion Graphs

R. U. Gobithaasan[1], Kenjiro T. Miura[2], L. P. Yee[1] & A. F. Wahab[1]

[1] School of Informatics & Applied Mathematics, University Malaysia Terengganu, Kuala Terengganu, Malaysia

[2] Graduate School of Science and Technology, Shizuoka University, Shizuoka, Japan

Correspondence: R. U. Gobithaasan, School of Informatics & Applied Mathematics, University Malaysia Terengganu, 21030 Kuala Terengganu, Malaysia. Tel: 60-9-668-3534. E-mail: gr@umt.edu.my

Received: February 27, 2014 Accepted: March 25, 2014 Online Published: April 8, 2014

doi:10.5539/mas.v8n3p24 URL: http://dx.doi.org/10.5539/mas.v8n3p24

Abstract

The quality of a curve for industrial design and computer graphics can be interrogated using Logarithmic Curvature Graph (LCG) and Logarithmic Torsion Graph (LTG). A curve is said to be aesthetic if it depicts linear LCG and LTG function. The Log-aesthetic curve (LAC) was developed bearing this notion and it was later extended to a Generalized Log-aesthetic curve (GLAC) using the κ-shift and ρ-shift approach. This paper reformulates GLAC by representing the Logarithmic Curvature and Torsion graph's gradient function as a nonlinear ordinary differential equation (ODE) with boundary conditions. The outputs of solving the ODEs result in a well defined Cesaro equation in the form of curvature function that is able to produce both planar as well as spatial curves with promising entities for industrial product design, computer graphics and more.

Keywords: visually pleasing curves, fair curves, aesthetic curves, Computer Aided Design

1. Introduction

1.1 The Formulation of Logarithmic Curvature Graph That Leads to Log-Aesthetic Curves

Designing visually pleasing industrial products is crucial since this feature dicates the success of a product (Pugh, 1991). Harada et al. (1999) proposed a novel method to investigate curves used in automobile design called the Logarithmic Distribution Diagram of Curvature (LDDC). They proposed aesthetic curves as curves with a constant LDDC gradient where the gradient is denoted as α. In 2003, Kanaya et al. simplified the formulation of LDDC to a simpler form, hence denoting it as Logarithmic Curvature Graph (LCG). Recently, Gobithaasan and Miura (2014) further proposed on using LCG as a shape interrogation tool for arbitrary curves.

In 2005, Miura derived the fundamentals used to design aesthetic curves and consequently developed a general formula of aesthetic curves called Log-Aesthetic Curves (LAC). Yoshida and Saito (2006) further proposed a method to draw the Log-Aesthetic Curve segment interactively by using two endpoints and their respective tangent vectors, known as the G^1 data. In 2009, Levien and Sequin stated that the Log Aesthetic curve is the most promising curve for aesthetic design. In 2012, Yoshida and Saito further derived a method to render the drawable boundary for Log-Aesthetic Curve segments to indicate whether a segment can be drawn from the given G^1 data or otherwise.

1.2 Generalized Log-Aesthetic Curve

In 2011, Gobithaasan and Miura proposed a planar curve called Generalized Log Aesthetic Curve (GLAC) by extending the formulation of Generalized Cornu Spiral (GCS) (Ali et al., 1999) in a similar manner to Log-Aesthetic Curve. The GLAC comprises of high quality planar spirals such as Generalized Cornu Spiral, Log-Aesthetic Curve, clothoid, Nielsen's spiral, logarithmic spiral, circle involute and etc. It has an additional parameter (denoted as ν) to determine its shape. Compared to the Generalized Cornu Spiral, the Generalized Log Aesthetic Curve segment can be used to satisfy an extra constraint during the design process. To date, it has been further extended to the 3D GLAC called Generalized Log Aesthetic Space Curve (GLASC) (Gobithaasan et al., 2012).

1.3 Recent Advancement of Log Aesthetic Curve

The Log Aesthetic Curve has attracted numerous researchers around the world to investigate its practical applications. Readers are referred to a comprehensive review of these curves by Miura and Gobithaasan (2014) and references therein. In 2013, an article published in Computer Aided Design and Application journal entitled "Designing G^2 Log-Aesthetic Spline" was selected as the best overall paper during the 10th International Conference of Computer Aided Design & Application held in Bergamo, Italy. This paper highlights the readiness of Log Aesthetic Curve for practical Computer Aided Design application pertaining to designing G^2 continuous LAC in automobile design (Miura et al., 2013).

1.4 Research Highlight

In order to indicate its robustness in Computer Aided Design applications, Gobithaasan et al. (2013) showed that the Generalized Log Aesthetic Curve has wider drawable region compared to Log Aesthetic Curve. However, the Logarithmic$_1$ Curvature Graph gradient of GLAC is in the form of a nonlinear function as follows: $\alpha + \nu(\Lambda\alpha s + 1)^{\overline{\alpha}}(1+\alpha)$ whereas LAC has LCG gradient as α. The LCG gradient of GLAC may consist of two segments with opposite sign of LCG gradient, known as the compound rhythm LAC. The highlight of this paper is that we re-formulate the Generalized Log Aesthetic Curve. The final output indicates that the curvature is in a simpler form as compared to the original Generalized Log Aesthetic Curve and the new 2D and 3D GLACs preserve the linearity of Logarithmic Curvature Graph.

2. Logarithmic Curvature and Torsion Graph's Gradient

Gobithaasan et al. (2009) proposed the formula of the Logarithmic Curvature Graph's gradient as follows:

$$\lambda_\kappa(s) = 1 - \frac{\rho(s)\rho''(s)}{\rho'(s)^2} \tag{1}$$

From Equation (1), we know that when the first derivation of the curvature radius equals to zero, hence Equation (1) cannot be determined. For the circle and straight line, only the first derivation of curvature radius equals to zero. A straight line has no radius of curvature hence it does not have both LCGand corresponding gradient. In the case of a circle, the radius of curvature is a constant value and arc length is $2\pi A$, where A is the radius of a circle. Hence, the LCG gradient should be

$$\lambda_\kappa(t) = \frac{\frac{d\log\left[\rho(t)\frac{ds}{d\rho}\right]}{dt}}{\frac{d\log[\rho(t)]}{dt}} = \frac{d\ \mathrm{Log}[A(2\pi)]}{d\ \mathrm{Log[A]}} = 0 \tag{2}$$

Similarly, the Logarithmic Torsion Graph's gradient proposed by Gobithaasan et al. (2012) is

$$\lambda_\tau(s) = 1 - \frac{\mu(s)\mu''(s)}{\mu'(s)^2} \tag{3}$$

Equation (3) is not available for helix due to its constant torsion profile, so the LTG gradient for helix, $\lambda_\tau = 0$.

2.1 Curvature Profile from Linear Logarithmic Curvature Graph's Gradient

Equation (1) can be modified with regards to the curvature function, $\kappa(s)$ as

$$\lambda_\kappa = \frac{\kappa''(s)\kappa(s)}{\kappa'(s)^2} - 1 \tag{4}$$

Therefore, a linear LCG gradient setting is

$$\frac{\kappa''(s)\kappa(s)}{\kappa'(s)^2} - 1 = \gamma s + \alpha \tag{5}$$

where γ represents the gradient in LCG and α is a constant value. Solving the second order nonlinear differential Equation (5) results in

$$\kappa(s) = \begin{cases} c_2 e^{c_1 s} & if\ \alpha = \gamma = 0 \\ c_2(c_1 + s\alpha)^{-1/\alpha} & if\ \gamma = 0 \\ -\dfrac{2\mathrm{ArcTan}\left[\frac{\alpha+s\gamma}{\sqrt{-\alpha^2+2c_1\gamma}}\right]}{\sqrt{-\alpha^2+2c_1\gamma}} & \\ c_2 e & \text{otherwise} \end{cases} \tag{6}$$

where c_1 and c_2 are constants solved from differential equation. Equation (5) is rearranged to become

$$\kappa''(s) = \frac{(1+\alpha+s\gamma)\kappa'(s)^2}{\kappa(s)} \tag{7}$$

where $0 \le s \le S$, S is the total arc length. Let

$$f(s,\kappa,\kappa') = \frac{(1+\alpha+s\gamma)\kappa'(s)^2}{\kappa(s)} \tag{8}$$

for $0 \le s \le S$, with $\kappa(0) = \kappa_a$ and $\kappa(S) = \kappa_b$. $f(s,\kappa,\kappa')$ is continuous on the set $D = \{(s,\kappa,\kappa')|$ for $0 \le s \le S$, with $-\infty < \kappa < \infty$ and $-\infty < \kappa' < \infty\}$. The partial derivatives are $f_\kappa(s,\kappa,\kappa') = -\frac{(1+\alpha+s\gamma)\kappa'(s)^2}{\kappa(s)^2}$ and $f_{\kappa'}(s,\kappa,\kappa') = \frac{2(1+\alpha+s\gamma)\kappa'(s)}{\kappa(s)}$, where both are continuous on D. According to Keller (1968), the first condition for an unique solution to exist is, a constant M must exist so that $|f_{\kappa'}(s,\kappa,\kappa')| = |\frac{2(1+\alpha+s\gamma)\kappa'(s)}{\kappa(s)}| \le M$. The second condition which must be satisfied is $f_\kappa(s,\kappa,\kappa') = -\frac{(1+\alpha+s\gamma)\kappa'(s)^2}{\kappa(s)^2} > 0$ for all $(s,\kappa,\kappa') \in D$. Hence, these conditions can be used as a guide to ensure that Equation (7) has an unique solution based on the selections of $\{\alpha,\gamma\}$. For example, when $\alpha = -1$, the curve becomes clothoid in which a solution always exists when $\gamma < 0$. In general, the inequality $\gamma < (-1-\alpha)/s$ must hold in order to ensure an unique solution always exist. Similar analysis can be carried out for torsion function to cofirm the existence of a solution.

In order to control the curvature's end point, Equation (6) is modified as

$$\kappa(s) = \begin{cases} \left(\frac{\kappa_1}{c_1}\right)^{s/S} c_1 & if\ \alpha = \gamma = 0 \\ \kappa_1(s\alpha + c_1)^{-1/\alpha}(S\alpha + c_1)^{\frac{1}{\alpha}} & if\ \gamma = 0 \\ e^{-\frac{2}{\sqrt{-\alpha^2+2\gamma c_1}}\left(\mathrm{ArcTan}\left[\frac{\alpha+s\gamma}{\sqrt{-\alpha^2+2\gamma c_1}}\right]-\mathrm{ArcTan}\left[\frac{\alpha+S\gamma}{\sqrt{-\alpha^2+2\gamma c_1}}\right]\right)}\kappa_1 & \text{otherwise} \end{cases} \tag{9}$$

where $\kappa_1 = \kappa(S)$. To ensure that Equation (9) is always monotonic, there are constraints that need to be satisfied. These include, when $\gamma = 0$, $\kappa_1 \ne 0$ and has lower bound where $s > -\frac{c_1}{\alpha}$. In the case of $\gamma \ne 0$ and $\alpha \ne 0$, $2c_1\gamma > \alpha^2$ and $\kappa_1 \ne 0$.

2.2 Torsion Profile from Linear Logarithmic Torsion Graph's Gradient

First, change Equation (5) with regards to torsion profile, $\tau(s)$ as

$$\lambda_\tau = \frac{\tau''(s)\tau(s)}{\tau'(s)^2} - 1 \tag{10}$$

Then, to obtain the torsion profile from linear LTG gradient, set

$$\frac{\tau''(s)\tau(s)}{\tau'(s)^2} - 1 = \psi s + \beta \tag{11}$$

where ψ represents the gradient of LTG and β is just an arbitrary constant. Solving the second order nonlinear differential Equation (11) results in

$$\tau = \begin{cases} \mathrm{d}_2 e^{\mathrm{d}_1 s} & if\ \beta = \psi = 0 \\ \mathrm{d}_2(\mathrm{d}_1 + s\beta)^{-1/\beta} & if\ \psi = 0 \\ \mathrm{d}_2 e^{-\frac{2\mathrm{ArcTan}\left[\frac{\beta+s\psi}{\sqrt{-\beta^2+2\mathrm{d}_1\psi}}\right]}{\sqrt{-\beta^2+2\mathrm{d}_1\psi}}} & \text{otherwise} \end{cases} \tag{12}$$

where d_1 and d_2 are constants solved from the differential equation. Similar to the formulation of curvature profile, Equation (12) too has an unique solution. Equation (12) is modified to enable control of the torsion at end point

$$\tau(s) = \begin{cases} \left(\frac{\tau_1}{d_1}\right)^{s/S} d_1 & if\ \beta = \psi = 0 \\ \tau_1(s\beta + d_1)^{-1/\beta}(S\beta + d_1)^{\frac{1}{\beta}} & if\ \psi = 0 \\ e^{-\frac{2}{\sqrt{-\beta^2+2\psi d_1}}\left(\mathrm{ArcTan}\left[\frac{\beta+s\psi}{\sqrt{-\beta^2+2\psi d_1}}\right]-\mathrm{ArcTan}\left[\frac{\beta+S\psi}{\sqrt{-\beta^2+2\psi d_1}}\right]\right)}\tau_1 & \text{otherwise} \end{cases} \tag{13}$$

where $\tau_1 = \tau(S)$. To ensure that Equation (13) is always monotonic, some constraints need to be followed. These conditions are, when $\psi = 0$, $\tau_1 \ne 0$ and has lower bound where $s > -\frac{d_1}{\beta}$. When $\psi \ne 0$ and $\beta \ne 0$,

$2\mathrm{d}_1\,\psi > \beta^2$ and $\tau_1 \neq 0$.

3. The Construction of 2D and 3D Generalized Log Aesthetic Curve

A planar curve is obtained when the curvature profile is solved using the Frenet-Serret equation without the torsion profile (Gray, 1994). For example, when $\kappa_1 = 1, \alpha = 1, \gamma = 1, \mathrm{c}_1 = 1$ with various $S = \{1, 2, 3, 4, 5\}$. These are monotonic decreasing curvature profiles as shown in Figure 1 and thecurves are rendered in Figure 2. On the other hand, when values are changed i.e. $\gamma = -1$ and $\mathrm{c}_1 = -1$, these curvature profiles will increase monotonically and $\kappa_1 = 3$ as shown in Figure 3 and 4. Figure 5 shows the curvature profile with different end of curvature value with the same arc length, 2π and corresponding curves are shown in Figure 6.

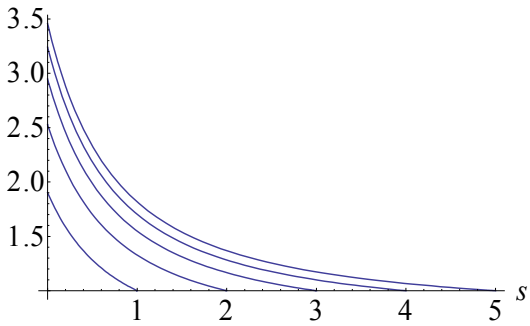

Figure 1. Monotonically decreasing curvature profile with arc length $s = \{1,2,3,4,5\}$

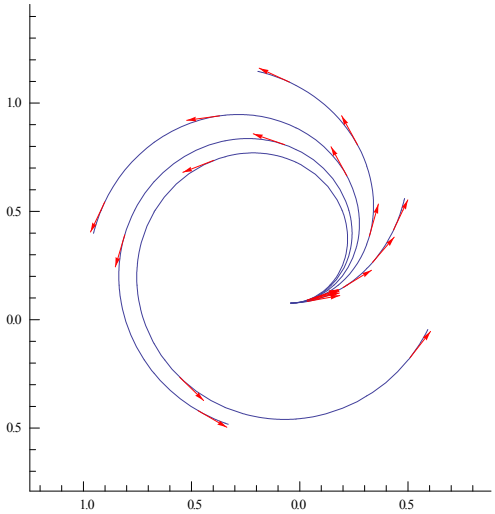

Figure 2. Five examples of planar curves with similar end curvatures and arc length $s = \{1,2,3,4,5\}$

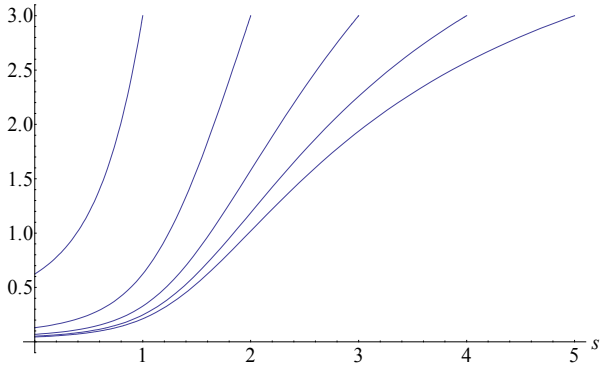

Figure 3. Monotonically increasing curvature profile with arc length $s = \{1,2,3,4,5\}$

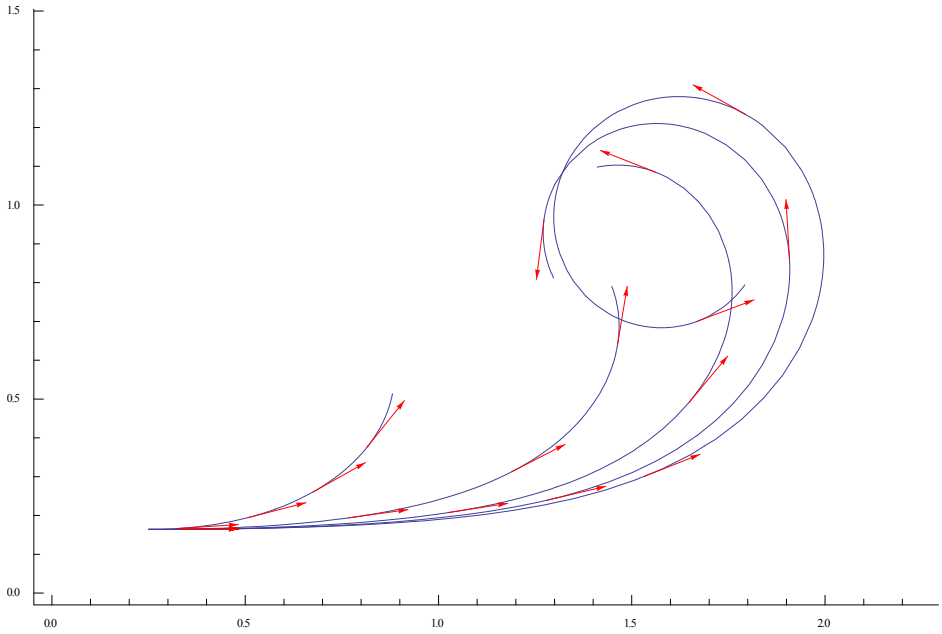

Figure 4. Examples of planar curves with similar curvature at end point with arc length $s = \{1,2,3,4,5\}$

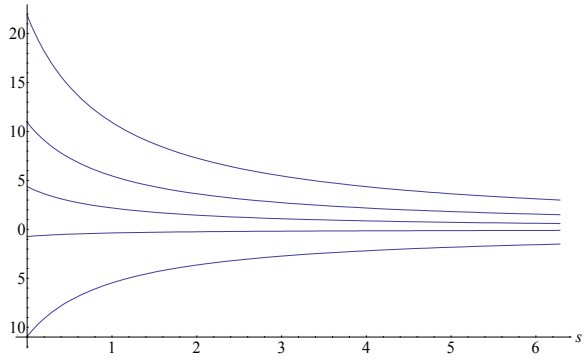

Figure 5. Curvature profile with different end curvatures

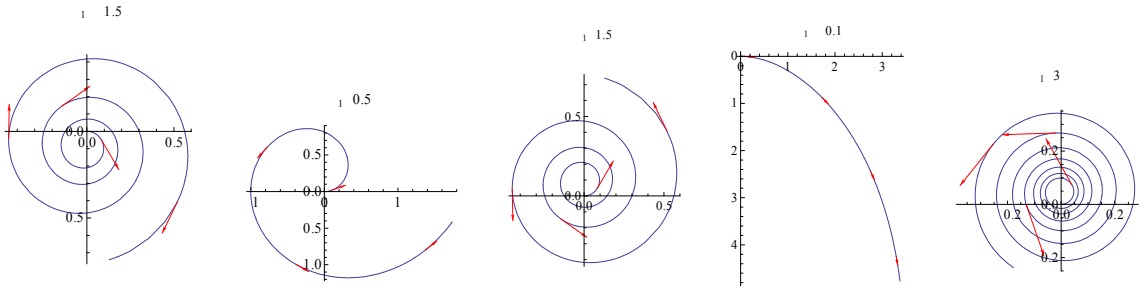

Figure 6. Examples of planar curve with various end curvatures but same arc length

The formulation of the torsion profile is done in the same way as the formulation of curvature profile. Therefore in Figure 7, the pattern of curvature profile of Figure 4 is applied into the torsion profile. Figure 8 depicts the pattern of Figure 6's curvature profile when applied into the torsion profile.

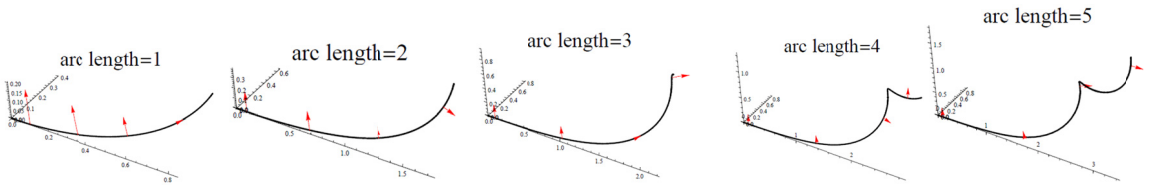

(a) (b) (c) (d) (e)

Figure 7. Planar curves with similar curvatures and torsions at end point with arc length $s = \{1,2,3,4,5\}$

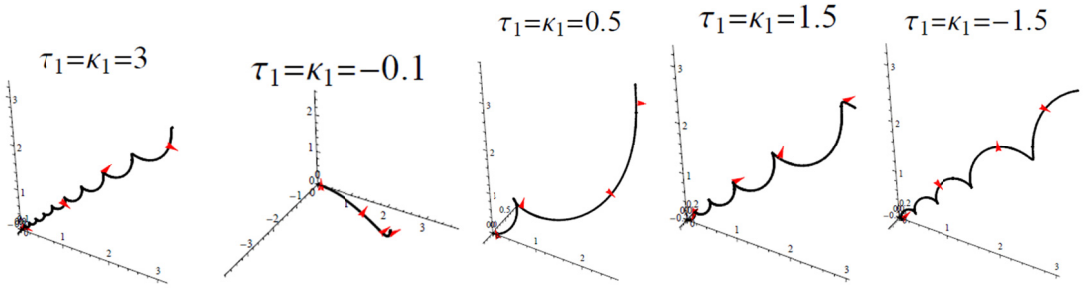

(a) (b) (c) (d) (e)

Figure 8. Space curves with five types of similar curvatures and torsions at end point with the same arc length

4. A Note of Revised Generalized Log Aesthetic Curve

When $c_1 = \kappa_1$ and $\gamma = \alpha = 0$, $\kappa = c_1$ is obtained, which is the constant curvature profile for a circle. When a similar situation occurs to the torsion profile where $d_1 = \tau_1$ and $\psi = \beta = 0$, a helix is obtained. Additionally when $\kappa_1 = 0$ and $\tau_1 = 0$ then $\kappa = \tau = 0$, hence a straight line is obtained.

The Log Aesthetic Curve has a constant value of Logarithmic Curvature Graph's gradient, hence when $\kappa = (c_1 + s\alpha)^{-1/\alpha}(c_1 + S\alpha)^{\frac{\alpha}{\alpha}}\kappa_1$, it becomes the curvature profile for LAC. The parameter α refers to the gradient in LCG as LAC. Due to this, $\tau = (d_1 + s\beta)^{-1/\beta}(d_1 + S\beta)^{\frac{\beta}{\beta}}\tau_1$ is also defined as the torsion profile for Log Aesthetic Space Curve since it has a linear profile of LTG with β as gradient.

In Generalized Log Aesthetic Space Curve, there are some cases when theLCG and LTG gradients are in a linear form. The linear form of LCG and LTG gradient in GLASC are defined as

$$\lambda_\kappa = 1 - s\Lambda + \nu \tag{14}$$

$$\lambda_\tau = \zeta + \frac{1}{\omega} - s\Omega \tag{15}$$

In conclusion, compared to the shape parameters derived, note that when $\gamma = -\Lambda$ and $\alpha = 1 + \nu$ the original Generalized Log Aesthetic Curve is derived, and when $\psi = -\Omega$ and $\beta = \zeta + \frac{1}{\omega}$ the original GLASC is also derived.

5. Conclusion

This paper reformulates Generalized Log Aesthetic Curve with linear Logarithmic Curvature and Torsion Graphs as shown in Equation (5) and (11). The curvature/torsion of revised GLACs is in a simpler form and the end curvatures/torsions can also be controlled to design G^2 continuous spline similar to the works of Ahmad et al. (2007) and Gobithaasan & Ali (2004). Future works include the overall shape analysis and interactive control as conducted by Yoshida and Saito (2006) for practical Computer Aided Design applications.

Acknowledgements

The authors acknowledge University Malaysia Terengganu and Ministry of Education Malaysia (FRGS: 59265) for providing financial aid to carry out this research.

References

Ahmad, A., Gobithasan, R., & Ali, J. Md. (2007). G2 transition curve using quartic Bezier curve, Computer Graphics, Imaging and Visualization: New Advances, CGIV 2007, 223-228. http://dx.doi.org/10.1109/CGIV.2007.44

Ali, J. M., Tookey, R. M., Ball, J. V., & Ball, A. A. (1999). The generalised Cornu spiral and its application to span generation. *Journal of Computational and Applied Mathematics, 102*, 37-47.

Farin, G. E. (1997). *Curves and Surfaces for Computer Aided Geometric Design* (5th ed.). USA: Academic Press.

Gobithasan, R., & Ali, J. M. (2004). Towards G2 curve design with Timmer Parametric Cubic, Int. Conf. on Computer Graphics, Imaging and Visualization, CGIV 2004, 109-114. http://dx.doi.org/10.1109/CGIV.2004.1323969

Gobithaasan, R. U., Karpagavalli, R., & Miura, K. T. (2013). Shape analysis of Generalized Log-Aesthetic curves, Int. Journal of Math. *Analysis, 7*(36), 1751-1759. http://dx.doi.org/10.1155/2013/732457

Gobithaasan, R. U., & Miura, K. T. (2011). Aesthetic Spiral for Design. *Sains Malaysiana, 40*(11), 1301-1305.

Gobithaasan, R. U., & Miura, K. T. (2014). Logarithmic Curvature Graph as a Shape Interrogation Tool. *Applied Mathematical Sciences, 8*(16), 755-765. http://dx.doi.org/10.12988/ams.2014.312709

Gobithaasan, R. U., Miura, K. T., & Ali, J. M. (2009). The Elucidation of Planar Aesthetic Curves. *17th International Conference in Central Europe on Computer Graphics, Visualization and Computer Vision, WSCG'2009 - In Co-operation with EUROGRAPHICS, Full Papers Proceedings* (pp. 183-188).

Gobithaasan, R. U., Yee, L. P., & Miura, K. T. (2012). A Generalized Log Aesthetic Space Curve. *ACM Proceedings of the 2012 Joint Int. Conf. on Human-Centered Computer Environments* (pp. 145-149). http://dx.doi.org/10.1145/2160749.2160780

Gray, A. (1994). *Modern Differential Geometry of Curves and Surfaces*. Boca Raton, FL: CRC Press.

Harada, T., Yoshimoto, F., & Moriyama, M. (1999). An aesthetic curve in the field of industrial design. *Proc. IEEE Symposium on Visual Language, Tokyo* (pp. 38-47).

Kanaya, I., Nakano, Y., & Sato, K. (2003). Simulated designer's eyes: Classification of aesthetic surfaces. *Proc. VSMM* 2003, Montreal (pp. 289-29).

Keller, H. B. (1968). *Numerical methods for two-point boundary-value problems*. Blaisdell, Waltham, Massachusetts.

Miura, K. T., & Gobithaasan, R. U. (2014). Aesthetic curves and surfaces in Computer Aided Geometric Design. Int. *Journal of Automation Technology*, in press.

Miura, K. T., Shibuya, D., Gobithaasan, R. U., & Usuki, S. (2013). Designing Log-aesthetic Splines with G2 Continuity. *Computer-Aided Design and Applications, 10(*6), 1021-1032. http://dx.doi.org/10.3722/cadaps.2013.1021-1032

Miura, K. T. (2005). Derivation of general formula of aesthetic curves. *Proc. of 8th Int. Conf. on Humans & Computers*, Tokyo (pp. 166-171).

Miura, K. T., Shirahata, R., Agari, S., Usuki, S., & Gobithaasan, R. U. (2012). Variational formulation of the log-aesthetic surface and development of discrete surface filters. *Computer-Aided Design and Applications, 9*(6), 901-914. http://dx.doi.org/10.3722/cadaps.2012.901-914

Pugh, S. (1991). *Total Design*. Great Britain: Addison-Wesley Publishing Company.

Yoshida, N., & Saito, T. (2006). Interactive aesthetic curve segments. *Visual Computers, 22*, 896-905.

Modern Applied Science; Vol. 8, No. 3; 2014
ISSN 1913-1844 E-ISSN 1913-1852
Published by Canadian Center of Science and Education

Hamilton-Jacobi Formalism of Singular Lagrangians with Linear Accelerations

Eyad Hasan Hasan[1]

[1] Applied Physics Department, Faculty of Science, Tafila Technical University, Tafila, Jordan

Correspondence: Eyad Hasan Hasan, Applied Physics Department, Faculty of Science, Tafila Technical University, P. O. Box: 179, Tafila 66110, Jordan. E-mail: iyad973@yahoo.com

Received: March 4, 2014 Accepted: April 4, 2014 Online Published: April 8, 2014

doi:10.5539/mas.v8n3p31 URL: http://dx.doi.org/10.5539/mas.v8n3p31

Abstract

This paper examined a new model for solving mechanical problems of second-order linear Lagrangian systems, using the Hamilton-Jacobi formalism. Lagrangians linear in accelerations with coefficients given by functions of coordinates alone yield primary constraints. It is shown that the equations of motion can be obtained from the action integral and these equations are equivalent to the canonical method.

Keywords: Hamilton-Jacobi, linear acceleration, action integral

1. Introduction

The canonical formalism for investigating singular systems has been developed by (Rabei & Guler, 1992; Pimentel & Teixeiria, 1996, 1998). A set of Hamilton-Jacobi partial differential equations was obtained and the equations of motion were written as total differential equations.

The Hamilton-Jacobi treatment has been studied for singular Lagrangians (Rabei et al., 2004). The Hamilton-Jacobi functions in configuration space have been obtained by solving the HJPDEs. This has led to another approach for solving mechanical problems for these singular systems.

Singular Lagrangians with linear velocities have been studied (Rabei et al., 2003) by using the canonical method. In this method, the integrable action was obtained directly without considering the total variation of constraints. In this paper, we wish to extend the model for second-order linear Lagrangian.

More recently, the path integral quantization of Lagrangians with linear accelerations has been investigated (Hasan, 2014) by using the canonical method. It is shown that by calculating the integrable action and constructing the wave function, the quantization has been carried out.

This paper is organized as follow. In Section 2, a new model of singular Lagrangian with linear acceleration is proposed. In Section 3, several illustrative examples are examined. The work closes with some concluding remarks in Section 4.

2. The Model of Hamilton-Jacobi Formalism for Lagrangian with Linear Acceleration

The general form of a second-order linear Lagrangian is

$$L(q_i,\dot{q}_i,\ddot{q}_i)=a_i(q_j,\dot{q}_j)\ddot{q}_i-V(q_j,\dot{q}_j) \tag{2.1}$$

The associated Euler-Lagrange equations

$$\frac{\partial L}{\partial q_i}-\frac{d}{dt}\left(\frac{\partial L}{\partial \dot{q}_i}\right)+\frac{d^2}{dt^2}\left(\frac{\partial L}{\partial \ddot{q}_i}\right)=0 \tag{2.2}$$

Have at most order three. Lagrangians linear in accelerations with coefficients given by functions of coordinates alone yield primary constraints. If $a_i(q,\dot{q})=a_i(q)$, and let $V(q,\dot{q})=V(q)$, then the general form of a second-order linear Lagrangian becomes

$$L(q_i,\dot{q}_i,\ddot{q}_i)=a_i(q_j)\ddot{q}_i-V(q_j) \tag{2.3}$$

The generalized momenta p_i, π_i conjugate to the generalized coordinates q_i, $\dot{q}_i$, respectively:

$$p_i = \frac{\partial L}{\partial \dot{q}_i} - \frac{d}{dt}\left(\frac{\partial L}{\partial \ddot{q}_i}\right);$$

$$p_i = -\frac{da_i}{dt} = b_i(\dot{q}_j) = -H_i^p \tag{2.4}$$

$$\pi_i = \frac{\partial L}{\partial \ddot{q}_i} = a_i(q_j) = -H_i^\pi \tag{2.5}$$

Equations (2.4) and (2.5) become

$$H_i'^{\pi}\left(q_i, \dot{q}_i, p_i, \pi_i\right) = \pi_i + H_i^\pi = 0;$$

$$H_i'^{\pi}\left(q_i, \dot{q}_i, p_i, \pi_i\right) = \pi_i - a_i = 0 \tag{2.6}$$

$$H_i'^{p}\left(q_i, \dot{q}_i, p_i, \pi_i\right) = p_i + H_i^p = 0$$

$$H_i'^{p}\left(q_i, \dot{q}_i, p_i, \pi_i\right) = p_i - b_i = 0 \tag{2.7}$$

Equations (2.6) and (2.7) are called primary constraints (Dirac, 1950).

The canonical Hamiltonian H_0 is given by:

$$H_0 = p_i\dot{q}_i + \pi_i\ddot{q}_i \ - L = b_i(\dot{q}_j)\dot{q}_i + V(q_j) \tag{2.8}$$

The corresponding HJPDEs

$$H_\circ' = \frac{\partial S}{\partial t} + b_i\dot{q}_i + V(q_j) = 0 \tag{2.9a}$$

$$H_\circ'^{\pi} = \frac{\partial S}{\partial \dot{q}} - a_i = 0 \tag{2.9b}$$

$$H_i'^{p} = \frac{\partial S}{\partial q} - b_i = 0 \tag{2.9c}$$

The equations of motion are obtained as total differential equations follows:

$$dq_i = \frac{\partial H_0'}{\partial p_i}dt + \frac{\partial H_j'^{p}}{\partial p_i}dq_j + \frac{\partial H_j'^{\pi}}{\partial p_i}d\dot{q}_j = dq_j \tag{2.10a}$$

$$d\dot{q}_i = \frac{\partial H_0'}{\partial \pi_i}dt + \frac{\partial H_j'^{p}}{\partial \pi_i}dq_j + \frac{\partial H_j'^{\pi}}{\partial \pi_i}d\dot{q}_j = d\dot{q}_j \tag{2.10b}$$

$$dp_i = -\frac{\partial H_0'}{\partial q_i}dt - \frac{\partial H_j'^{p}}{\partial q_i}dq_j - \frac{\partial H_j'^{\pi}}{\partial q_i}d\dot{q}_j = -\frac{\partial V}{\partial q_i}dt + \frac{\partial a_j}{\partial q_i}d\dot{q}_j \tag{2.10c}$$

$$d\pi_i = -\frac{\partial H_0'}{\partial \dot{q}_i}dt - \frac{\partial H_\alpha'^{p}}{\partial \dot{q}_i}dq_\alpha - \frac{\partial H_\alpha'^{\pi}}{\partial \dot{q}_i}d\dot{q}_\alpha = -b_i(\dot{q}_j)dt \tag{2.10d}$$

The set of Equations (2.10) are integrable (Muslih & Guler, 1998), the total variation of Equation (2.6) and Equation (2.7) can be written as:

$$\begin{aligned} dH_i'^{\pi} &= d\pi_i - da_i = 0 \\ &= -b_i(\dot{q}_j)dt - da_i(q_j) \end{aligned} \tag{2.11}$$

$$\begin{aligned} dH_i'^{p} = dp_i - db_i = 0 &= -\frac{\partial V}{\partial q_i}dt + \frac{\partial a_j}{\partial q_i}d\dot{q}_j - db_i(\dot{q}_j) \\ &= -\frac{\partial V}{\partial q_i}dt + \frac{\partial a_j}{\partial q_i}d\dot{q}_j - db_i(\dot{q}_j) \end{aligned} \tag{2.12}$$

So, we have

$$\frac{\partial b_i(\dot{q})}{\partial \dot{q}_j} d\dot{q}_j - \frac{\partial a_j(q)}{\partial q_i} d\dot{q}_j = -\frac{\partial V}{\partial q_i} dt \tag{2.13}$$

which is equivalent to

$$\frac{\partial a_i(q)}{\partial q_j} d\dot{q}_j + \frac{\partial a_j(q)}{\partial q_i} d\dot{q}_j = \frac{\partial V}{\partial q_i} dt \tag{2.14}$$

Or

$$\ddot{q}_j = f_{ij}^{-1} \frac{\partial V(q)}{\partial q_i};$$

Defining the symmetric matrix f_{ij} as

$$f_{ij} = \frac{\partial a_i(q)}{\partial q_j} + \frac{\partial a_j(q)}{\partial q_i} \tag{2.15}$$

If the inverse of the matrix f_{ij} exist, then we can solve all the dynamics q_i, while if the rank of the matrix f_{ij} is n-R, then we can solve the dynamics q_a in terms of independent parameters $(t, q_\alpha, \dot{q}_\alpha)$, $\alpha = 1, 2, ..., R$.

The total derivative of the Hamilton-Jacobi function can be obtained as:

$$dS = \frac{\partial S}{\partial q_i} dq_i + \frac{\partial S}{\partial \dot{q}_i} d\dot{q}_i + \frac{\partial S}{\partial t} dt \tag{2.16}$$

Using the HJPDEs Equations (2.9), we get

$$dS = a_i d\dot{q}_i - V dt \tag{2.17}$$

One can integrate the above Equation (2.17) to give

$$S = \int a_i d\dot{q}_i - \int V dt \tag{2.18}$$

We can use the fact that

$$\int d(a_i \dot{q}_i) = a_i \dot{q}_i = \int a_i d\dot{q}_i + \int \dot{q}_i da_i,$$

Equation (2.18) reduces to

$$S = \frac{1}{2}[a_i \dot{q}_i + \int a_i d\dot{q}_i - \int \dot{q}_j da_j] - \int V dt \tag{2.19}$$

By some rearragment, Equation (2.19) becomes

$$S = \frac{1}{2} a_i \dot{q}_i - \frac{1}{2} \int [\dot{q}_j da_j - a_i d\dot{q}_i + 2V dt] \tag{2.20}$$

And using the fact that

$$\frac{d}{dt}(q_j da_j) = -q_j db_j + \dot{q}_j da_j,$$

$$S = \frac{1}{2} a_i \dot{q}_i - \frac{1}{2} \int \frac{d}{dt}(q_j da_j) - \frac{1}{2} \int [q_j db_j - a_i d\dot{q}_i + 2V dt]$$

$$S = \frac{1}{2} a_i \dot{q}_i - \frac{1}{2} \frac{d}{dt} \int q_j da_j - \frac{1}{2} \int [q_j db_j - a_i d\dot{q}_i + 2V dt] \tag{2.21}$$

Assuming that the function $a_i(q)$ and $V(q)$ satisfy the following conditions

$$q_j \frac{\partial a_i}{\partial q_j} = a_i, \quad \frac{\partial V}{\partial q_j} q_j = 2V$$

Equation (2.21) becomes

$$S = \frac{1}{2} a_i \dot{q}_i - \frac{1}{2} \frac{d}{dt} \int q_j da_j - \frac{1}{2} \int q_j [db_j - \frac{\partial a_i}{\partial q_j} d\dot{q}_i + \frac{\partial V}{\partial q_j} dt] \tag{2.22}$$

The action S to be an integrable function, the terms in the brackets must be zero, i.e.

$$db_j - \frac{\partial a_i}{\partial q_j} d\dot{q}_i + \frac{\partial V}{\partial q_j} dt = 0 \tag{2.23}$$

Equation (2.23) gives the equation of motion for the coordinates q_j .

3. Examples

3.1 The First Example

Consider the following singular Lagrangian:

$$L = -q_1\ddot{q}_1 + q_2\ddot{q}_2 - \frac{1}{2}(q_2^2 + q_2^2) \tag{3.1}$$

The potential of this Lagrangian is given by

$$V = \frac{1}{2}(q_1^2 + q_2^2)$$

and the coefficients a_1 and a_2 are

$$a_1 = -q_1, \quad a_2 = q_2$$

The generalized momenta by using Equation (2.4) and Equation (2.5) are:

$$p_1 = \frac{\partial L}{\partial \dot{q}_1} - \frac{d}{dt}\left(\frac{\partial L}{\partial \ddot{q}_1}\right) = \dot{q}_1 = -H_1^p; \tag{3.2a}$$

$$p_2 = \frac{\partial L}{\partial \dot{q}_2} - \frac{d}{dt}\left(\frac{\partial L}{\partial \ddot{q}_2}\right) = -\dot{q}_2 = -H_2^p; \tag{3.2b}$$

$$\pi_1 = \frac{\partial L}{\partial \ddot{q}_1} = -q_1 = -H_1^\pi; \tag{3.2c}$$

$$\pi_2 = \frac{\partial L}{\partial \ddot{q}_2} = q_2 = -H_2^\pi . \tag{3.2d}$$

From Equation (2.6) and Equation (2.7) the primary constraints are given as

$$H_1'^\pi = \pi_1 + q_1; \tag{3.3a}$$

$$H_2'^\pi = \pi_2 - q_2; \tag{3.3b}$$

$$H_1'^p = p_1 - \dot{q}_1; \tag{3.3c}$$

$$H_2'^p = p_2 + \dot{q}_2 . \tag{3.3d}$$

The canonical Hamiltonian H_0 is given by

$$H_\circ = \dot{q}_1^2 - \dot{q}_2^2 + \frac{1}{2}(q_1^2 + q_2^2) . \tag{3.4}$$

Making use of (2.23), we can obtain the equation of motion for q_1 and q_2

$$d\dot{q}_1 + q_1 dt + d\dot{q}_1 = 0, \tag{3.5a}$$

$$-d\dot{q}_2 + q_2 dt - d\dot{q}_2 = 0 . \tag{3.5b}$$

These equations are given by

$$2\ddot{q}_1 + q_1 = 0; \tag{3.6a}$$

$$2\ddot{q}_2 - q_2 = 0 . \tag{3.6b}$$

Equations (3.6) have the following solutions

$$q_1 = A\cos\frac{t}{\sqrt{2}} + B\sin\frac{t}{\sqrt{2}}; \tag{3.7a}$$

$$q_2 = Ae^{t/\sqrt{2}} + Be^{-t/\sqrt{2}} . \tag{3.7b}$$

3.2 The Second Example

Let consider the singular Lagrangian:

$$L = q_2\ddot{q}_1 - q_1\ddot{q}_2 - q_3\ddot{q}_3 - \frac{1}{2}(q_1^2 + q_2^2 + q_3^2)\cdot \tag{3.8}$$

The potential of this Lagrangian is given by

$$V = \frac{1}{2}(q_1^2 + q_2^2 + q_3^3), \tag{3.9}$$

and the coefficients a_1, a_2 and a_3 are

$$a_1 = q_2, \quad a_2 = -q_1, \quad a_3 = -q_3$$

The generalized momenta by using Equation (2.4) and Equation (2.5) are:

$$p_1 = \frac{\partial L}{\partial \dot{q}_1} - \frac{d}{dt}\left(\frac{\partial L}{\partial \ddot{q}_1}\right) = -\dot{q}_2 = -H_1^p; \tag{3.10a}$$

$$p_2 = \frac{\partial L}{\partial \dot{q}_2} - \frac{d}{dt}\left(\frac{\partial L}{\partial \ddot{q}_2}\right) = \dot{q}_1 = -H_2^p; \tag{3.10b}$$

$$p_3 = \frac{\partial L}{\partial \dot{q}_3} - \frac{d}{dt}\left(\frac{\partial L}{\partial \ddot{q}_3}\right) = \dot{q}_3 = -H_3^p; \tag{3.10c}$$

$$\pi_1 = \frac{\partial L}{\partial \ddot{q}_1} = q_2 = -H_1^\pi; \tag{3.10d}$$

$$\pi_2 = \frac{\partial L}{\partial \ddot{q}_2} = -q_1 = -H_2^\pi; \tag{3.10e}$$

$$\pi_3 = \frac{\partial L}{\partial \ddot{q}_3} = -q_3 = -H_3^\pi\cdot \tag{3.10f}$$

By Equation (2.6) and Equation (2.7) the primary constraints are given as

$$H_1'^\pi = \pi_1 - q_2; \tag{3.11a}$$

$$H_2'^\pi = \pi_2 + q_1; \tag{3.11b}$$

$$H_3'^\pi = \pi_3 + q_3; \tag{3.11c}$$

$$H_1'^p = p_1 + \dot{q}_2; \tag{3.11d}$$

$$H_2'^p = p_2 - \dot{q}_1; \tag{3.11e}$$

$$H_3'^p = p_3 - \dot{q}_3\cdot \tag{3.11f}$$

The canonical Hamiltonian H_0 is given by

$$H_\circ = \dot{q}_3^2 + \frac{1}{2}(q_1^2 + q_2^2 + q_3^2)\cdot \tag{3.12}$$

Making use of (2.23), we can obtain the equation of motion for q_3

$$d\dot{q}_3 + q_3 dt + d\dot{q}_3 = 0\cdot \tag{3.13}$$

This equation can be written as

$$2\ddot{q}_3 + q_3 = 0, \tag{3.14}$$

Which have the following solution

$$q_3 = A\cos\frac{t}{\sqrt{2}} + B\sin\frac{t}{\sqrt{2}}\cdot \tag{3.15}$$

4. Conclusion

This paper investigated the Hamilton-Jacobi formalism for singular Lagrangian with linear acceleration. Lagrangians linear in accelerations with coefficients given by functions of coordinates alone yield primary constraints. It is proven that the total derivative of the Hamilton-Jacobi function has been constructed using the HJPDEs and Hamilton-Jacobi function is integrable. It is shown that both the equations of motion and the integrable action are obtained from the integrability conditions and the number of independent parameters are determined from the rank of matrix f_{ij} .

References

Dirac, P. A. M. (1950). Generalized Hamiltonian Dynamics. *Canadian Journal of Mathematical Physics, 2*, 129-148. http://dx.doi.org/10.4153/CJM-1950-012-1

Hasan, E, H. (2014). Path Integral Quantization of Lagrangians with Linear Accelerations. *European Scientific Journal, 10*(3), 331-345.

Muslih, S. I., & Guler, Y. (1998). Is gauge fixing of constrained systems necessary. *Il Nuovo Cimento B, 113*, 277-290.

Pimentel, R. G., & Teixeira, R. G. (1996). Hamilton-Jacobi Formulation for Singular Systems with Second-Order Lagrangians. *Il Nuovo Ciemento B, 111*, 841-854. http://dx.doi.org/10.1007/BF02749015

Pimentel, R. G., & Teixeira, R. G. (1998). Generalization of the Hamilton-Jacobi Approach for Higher-Order Singular Systems. *Il Nuovo Ciemento B, 113*, 805-820.

Rabei, E. M., & Guler, Y. (1992). Hamilton-Jacobi Treatment of Second-Class Constraints. *Physical Review A, 46*(6), 3513-3515. http://dx.doi.org/10.1103/PhysRevA.46.3513

Rabei, E. M., Hasan, E. H., & Ghassib, H. B. (2004). Hamilton-Jacobi Treatment of Constrained Systems with Second-Order Lagrangians. *International Journal of Theoretical Physics, 43*(4), 1073-1096. http://dx.doi.org/10.1023/B:IJTP.0000048601.92005.fe

Rabei, E. M., Nawafleh K. I., Abdelrahman, Y. S., & Omari, H. Y. R. (2003). Hamilton-Jacobi treatment of lagrangians with linear velocities. *Modern Physics Letters A, 18*(23), 1591-1596. http://dx.doi.org/10.1142/S0217732303011277

Rabei, E. M., Nawafleh K. I., & Ghassib, H. B. (2004). Hamilton-Jacobi Treatment of Constrained Systems. *International Journal of Modern Physics A, 19*, 347-354. http://dx.doi.org/10.1142/S0217751X04017719

Copyrights

Modern Applied Science; Vol. 8, No. 3; 2014
ISSN 1913-1844 E-ISSN 1913-1852
Published by Canadian Center of Science and Education

Modified Suspender Force Calculation Method of Suspension Bridge

Li Dongdong[1] & Liao Xiaofang[1]

[1] Department of Civil engineering, Chongqing Jiaotong University, Chongqing, China

Correspondence: Li Dongdong, Department of Civil Engineering, Chongqing Jiaotong University, Chongqing 400074, China. Tel: 86-150-8673-9828. E-mail: 616234757@qq.com

Received: February 13, 2014 Accepted: March 10, 2014 Online Published: April 8, 2014

doi:10.5539/mas.v8n3p37 URL: http://dx.doi.org/10.5539/mas.v8n3p37

Abstract

Through the mechanical analysis of the suspenders of suspension bridge , the suspender is assumed to be a tensional beam pined at one end and elastically supported at the other end, basing on which the vibration shape function for axial tension beam is established and corresponding formulas to calculate the cable force are obtained. The relationship between the elastic support stiffness and the transverse difference between two ends is obtained according to numerous analyses on a suspension bridge. The suspender forces of Qingcaobei Yangtze River Bridge are respectively calculated using traditional method and the method in this paper. Comparisons between two calculation results are then conducted which proves that the method in this paper can meet the precision of suspenders with different lengths, especially to the short suspenders, whose calculation deviation can be controlled in the engineering allowance.

Keywords: suspension bridge, suspender force, calculation method

1. Introduction

The cable force tester is usually used for measuring the suspension bridge cable force in engineering. In the testing theory, the suspender is assumed to be a chord whose transverse stiffness can be neglected and then the cable force can be calculated according to the conversion relation between the frequency and the chord tension. Above calculation method is relative accurate for long suspender but it can't serve for short suspender whose transverse stiffness can't be neglected. Much work has been done to solve this problem, such as simplifying the short suspender to be a beam consolidated in both ends, which can be used for the cable force calculation of the cable stayed bridge with the cable consolidated in the intersection between the main beam and cable tower. However, when it comes to the suspension bridge, this simplification can't meet the factual suspender boundary condition any more. Hence, a modified simplification is correspondingly made to specially calculate the tension force of the suspension bridge's short suspender shown in Figure 1 where Δ stands for the displacement difference between each ends of the suspender (Figure 1(b)), k stands for the elastic supported stiffness of the suspender (Figure 1(c)).

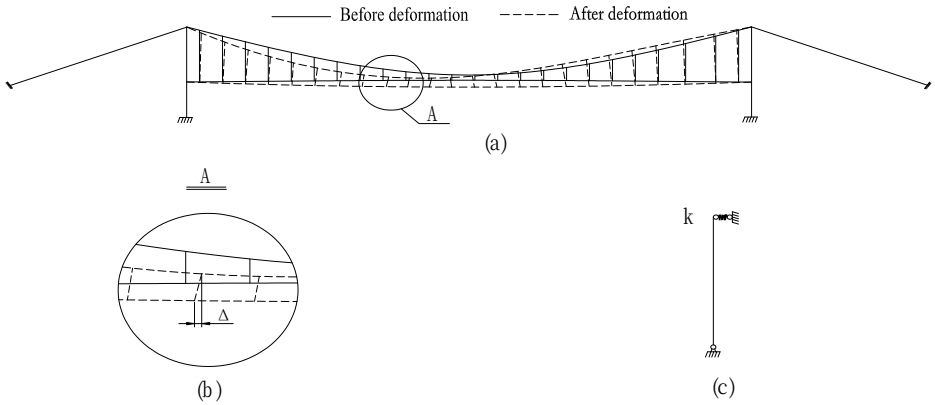

Figure 1. Simplification of suspension bridge suspender

2. The Calculation Principle

Three assumptions are made to the calculating model as follows:

a) The elastically supported beam always works in elastic stage.

b) The section is constant along beam length and the material is homogeneous, isotropic.

c) The vibration of the beam is tiny.

2.1 Establishment of the Shape Function

Research have proved that the shape function of the uniform simply supported beam can be expressed through the sine function

$$\psi_0(x) = \sin(\frac{\pi x}{l})$$

In this equation, l stands for the calculating length of the simply supported beam. Define the point at the left end as the original point and the beam axis direction as X-axis of the coordinate system (Figure 2).

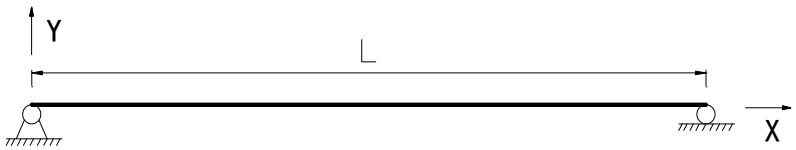

Figure 2. Simply supported beam

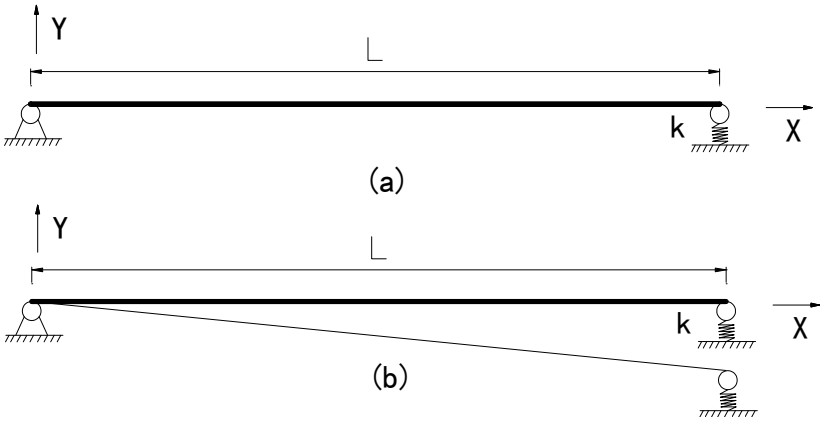

Figure 3. Elastically supported beam

As to the elastically supported beam (Figure 3(a)), its shape function must be firstly determined before calculating the natural frequency when using Rayleigh method. Principally, the beam shape function can be arbitrarily selected once the geometrical boundary conditions can be satisfied. It has been proved that the engineering accuracy can be basically approved taking the deformed shape under self-weight as the shape function to calculate the natural frequency. And when the beam is rigid, the vertical displacement of the elastically supported beam is

$$\psi_1(x) = \frac{mg}{2kl}x$$

Where l stands for the length of the calculating length of the simply supported beam; m is the beam mass; g is gravity acceleration; k is the stiffness of the elastic support.

According to the superposition principle of linear elastic body, the shape function of the elastically supported beam can be assumed as follows

$$\psi(x) = \psi_0(x) + \psi_1(x) = \sin(\frac{n\pi x}{l}) + \frac{mg}{2kl}x \tag{1}$$

In which n stands for the order of the shape function and the other symbols represent the same meanings as mentioned above.

It can be derived that when $x=0$, $\psi(0)=0$ and when $x=l$, $\psi(l)=\frac{mg}{2k}$ which satisfy the geometrical boundary condition of the beam. Therefore, Equation (1) can be taken as the shape function of the elastically supported beam.

2.2 Deduction of Relationship between Frequency and Axial Force

The location of elastically supported beam in global coordinate system at any time can be determined as

$$v(x,t)=\psi(x)\cdot Z(t)=\psi(x)\cdot Z_0\sin(\omega t), x\in[0,l]$$

Here *t* and *w* respectively mean the time and circular frequency, and basing on which the bending strain energy can be obtained:

$$V_B=\frac{1}{2}\int_0^l EI\cdot(\frac{\partial^2 v}{\partial x^2})^2\cdot dx=\frac{1}{2}{Z_0}^2\sin^2(\omega t)\cdot\int_0^l EI\cdot[\psi''(x)]^2\cdot dx$$

Where *EI* stands for the transverse bending stiffness.

And the maximum bending strain energy

$$V_{B\max}=\frac{1}{2}{Z_0}^2\cdot\int_0^l EI\cdot[\psi''(x)]^2\cdot dx$$

The axial tensile strain energy

$$V_t=\frac{1}{2}\int_0^l T\cdot(\frac{\partial v}{\partial x})^2\cdot dx=\frac{1}{2}{Z_0}^2\sin^2(\omega t)\cdot\int_0^l T\cdot[\psi'(x)]^2\cdot dx$$

The maximum axial tensile strain energy

$$V_{t\max}=\frac{1}{2}{Z_0}^2\cdot\int_0^l T\cdot[\psi'(x)]^2\cdot dx$$

Kinetic energy of the elastically supported beam

$$W=\frac{1}{2}\int_0^l m\cdot(\frac{\partial v}{\partial t})^2 dx=\frac{1}{2}Z_0\omega^2\sin^2(\omega t)\cdot\int_0^l m\cdot[(\psi(x)]^2 dx$$

The maximum kinetic energy of the elastically supported beam

$$W=\frac{1}{2}Z_0\omega^2\cdot\int_0^l m\cdot[(\psi(x)]^2 dx$$

The maximum kinetic energy is equal to the maximum strain energy

$$W=V_{B\max}+V_{t\max}$$

Then, the relationship between the frequency and axial force can be expressed as follows

$$\omega^2=\frac{\int_0^l EI\cdot[\psi''(x)]^2 dx+\int_0^l T\cdot[\psi'(x)]^2 dx}{\int_0^l m\cdot[\psi(x)]^2 dx}$$

$$\omega=2\pi f$$

Or

$$T=\frac{4\alpha\pi^2 f^2\int_0^l m\cdot[\psi(x)]^2 dx-\int_0^l EI\cdot[\psi''(x)]^2 dx}{\int_0^l[\psi'(x)]^2 dx} \quad (2)$$

Where *f* stand for engineering frequency, α stands for the correction coefficient of suspender force and can be obtained from the following equation

$$\alpha = \begin{cases} 0.75 & 0m \le l \le 20m \\ 0.90 & 0m \le l \le 20m \\ 1.0 & l \ge 20m \end{cases} \tag{3}$$

2.3 Discussion on the Stiffness of the Elastic Support

Factually, the elastic support stiffness changes nonlinearly with the difference between the transverse displacements at each end of suspender and is influenced by many factors such as the main cable stiffness, the tower stiffness and external loads. Therefore, numerical analysis is made on a suspension bridge with MIDAS/CIVIL to explore how k (the elastic support stiffness) changes with different Δ (transverse displacement difference) and the k-Δ curve of its suspenders is obtained. As is shown in Figure 4, k increases gradually with the increase of Δ but the increase speed turns to slow down, that is, the k-Δ curve is a conic curve.

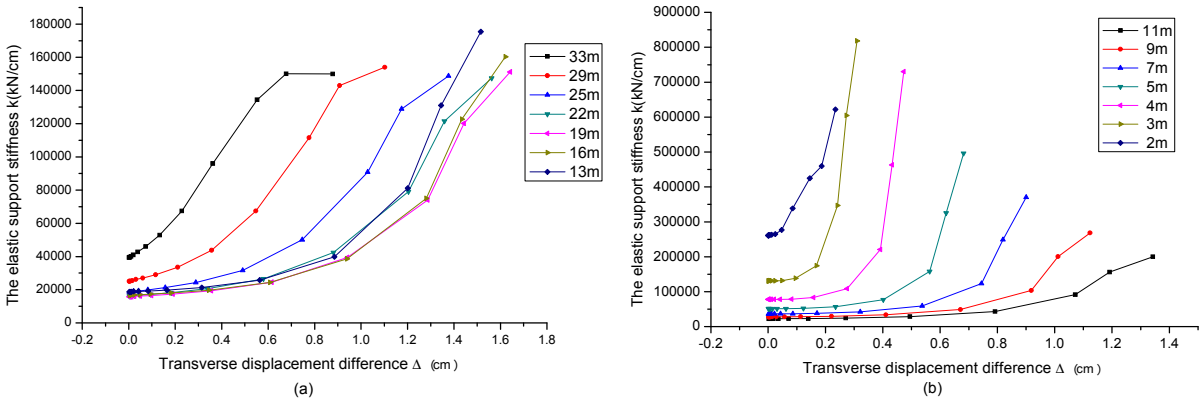

Figure 4. Variation curve of elastic support stiffness k with Δ

On the basis of the analysis above, the relationship between k (elastic support stiffness) and Δ (transverse displacement difference) can be approximately expressed as a conic curve. Obviously, matters will become complex if a conic curve is used to describe the relationship of k-Δ in engineering. Considering that k locates at the denominator of Equation (1) and the increase of k has tiny impact on $\psi(x)$, the initial tangent stiffness k_0 can be used to replace the real k. In some other words, k can be approximately taken as a constant (Figure 5) that the calculation process can be simplified and meanwhile the calculation accuracy can be guaranteed.

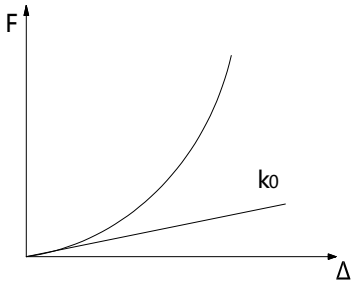

Figure 5. Initial tangent stiffness k_0

3. Engineering Example

Qingcaobei Yangtze river bridge, a suspension bridge with a main span of 245 + 788 +245 m, is a controlling engineering as a part of the expressway from Nanchuan to Fuling and ground anchors are adapted at each bank (Figure 6). It has two main cables which consist of 88 galvanized steel wires and the sag span ratio of the main cable is about 1/10. Orthotropic plate streamlined steel box girder is chose as the stiffening girder which is 30.7 m in width and 3.5 m in height. Flexible suspenders are adopted in this bridge, pinned at main cable and stiffening girder.

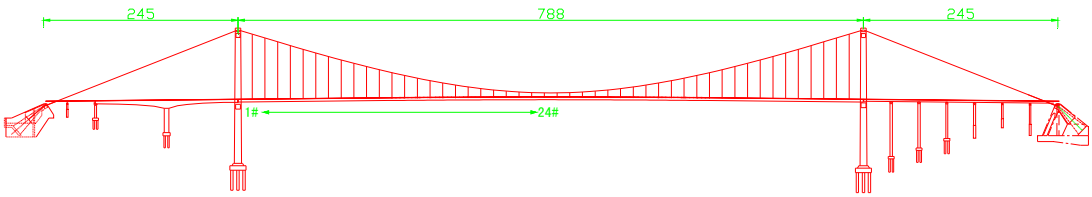

Figure 6. General arrangement diagram of Qingcaobei Yangtze river bridge (Unit: m)

Depending on the elastic support stiffness obtained from the numerical analysis of Qingcaobei Yangtze River Bridge using MIDAS/CIVIL, the suspender forces T_2 are calculated by the method proposed in this paper and the traditional calculation method of cable force T_1 that can express as the following

$$T_1 = 4\pi^2 f^2 - EI \cdot \pi^2 / l^2$$

Here, the meanings of symbols are the same to the above.

Comparisons between theoretical suspender force and the suspender force calculated by different methods is shown in Table 1 and Figure 7.The suspenders are numbered from 1# to 24# as shown in Figure 6.

Table 1. Comparison of theoretical suspender force with the suspender force calculated by different methods

Suspender number	Theoretical suspender force T0(kN)	Engineering frequency (Hz)	Initial tangent stiffness k0 (N/m)	Length of suspender (m)	Mass of suspender (kg)	Calculating suspender force T1(kN)	(T1-T0)/ T0x100%	Calculating suspender force T2(kN)	(T2-T0)/ T0x100%
1#	2553.80	0.1802	1203048	81.1351	2925.888	2501.27	2.1%	2542	-0.5%
4#	1520.00	0.2022	543183.1	63.5735	2292.582	1514.52	0.4%	1556.3	2.4%
7#	1541.30	0.3001	450653.4	48.4044	1745.551	1471.95	4.5%	1509.3	-2.1%
10#	1556.90	0.5096	527983.1	35.6266	1284.765	1691.41	8.6%	1546.8	-0.6%
13#	1565.00	0.8579	772200.8	25.2517	910.6255	1704.45	8.9%	1546.4	-1.2%
16#	1562.20	1.6717	1402525	17.2821	623.2265	2070.08	32.5%	1556.7	-0.4%
19#	1557.00	3.2131	3484321	11.7144	422.4439	2082.03	33.7%	1558.5	0.1%
22#	1552.90	4.9789	19955654	8.5369	307.8571	2181.08	40.5%	1626.7	4.8%
23#	1553.20	5.2364	92783505	8.0075	288.7653	1981.18	27.6%	1475	-5.0%
24#	1551.30	5.5643	142857100	7.7427	279.2173	2019.99	30.2%	1503.3	-3.1%

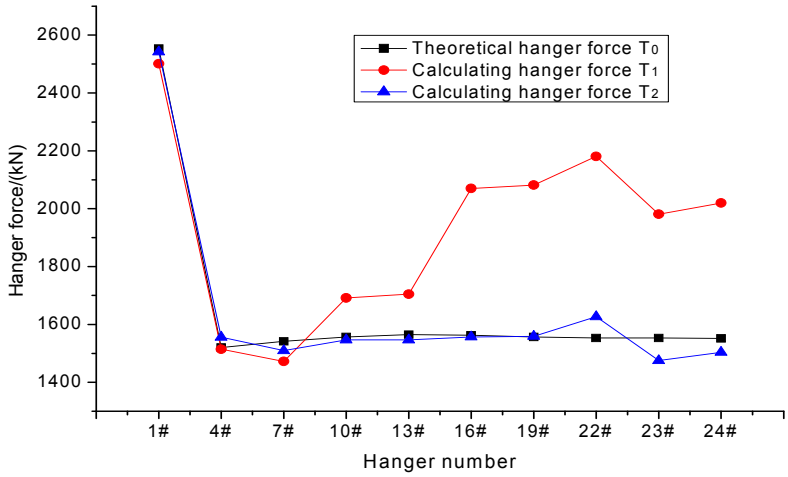

Figure 7. Comparison of theoretical suspender force with the suspender force calculated by different methods

As is shown in Table 1, the calculating suspender force basing on traditional calculation method of cable force has high precision when the suspender is long enough. However, the deviation of suspender force gets greater

with the decrease of suspender length, which even reached 40.5% and the results in this case can't be applied in engineering. In this case, traditional calculation method can't be used anymore and the data proves that the method proposed in this paper can meet the precision of suspenders with different lengths and the deviation can be controlled in the engineering allowance.

4. Conclusions

On the computation and analysis above, the following conclusion can be drawn.

(1) The model regarding the suspenders as a tensioned beam pinned at one end and elastically supported at the other end fits the real stress states well.

(2) According to the analysis above, it can be obtained that the k-Δ curve is a conic curve, in which the elastic support stiffness k increase faster than Δ. The elastic support stiffness k can be approximately taken as a constant（the initial value of k-Δ curve）to simplify the calculation process and guarantee the computational accuracy.

(3) The method proposed in this paper can meet the precision of suspenders with different lengths, especially to the short suspenders, whose calculation deviation can be controlled in the engineering allowance.

References

Clough, R. W., & Penzien, J. (1993). *Dynamics of structures* (pp. 90-95). New York: McGraw-Hill.

Li, G. H. (1992). *Stability and vibration of the bridge structure* (pp. 367-396). Beijing: China railway Press.

Li, T. B. (2007). The *Research and Practical Application of Frequency Method of Cable Force Measurement* (pp. 59-68).

Ren, W., & Chen, G. (2005). Practical formulas to determine cable tension by using cable fundamental frequency. *China Civil Engineering Journal, 38*(11), 26-31.

Wang, R. H., Zheng, K. Z., & Liu, C. H. (2009). Practical Formulas for Estimation of Short Cable Tension by Vibration Method. *Science Technology and Engineering, 9*(11), 2988-2991.

Wang, X. Q. (2010). *Nonlinear and reliability analysis of cable-stayed bridge* (pp. 2-32). Beijing: China Communications Press.

Copyrights

Modern Applied Science; Vol. 8, No. 3; 2014
ISSN 1913-1844 E-ISSN 1913-1852
Published by Canadian Center of Science and Education

A Novel Electric Power Plants Performance Assessment Technique Based on Genetic Programming Approach

Ahmad Attari Ghomi[1], Ayyub Ansarinejad[2], Hamid Razaghi[1], Davood Hafezi[1] & Morteza Barazande[1]

[1] Qom Province Electricity Distribution Company, Qom, Iran

[2] Department of Industrial Engineering, University of Tehran, Tehran, Iran

Correspondence: Ayyub Ansarinejad, Department of Industrial Engineering, University of Tehran, Tehran, Iran. E-mail: ansarinejad@outlook.com

Received: January 26, 2014 Accepted: March 13, 2014 Online Published: April 8, 2014

doi:10.5539/mas.v8n3p43 URL: http://dx.doi.org/10.5539/mas.v8n3p43

Abstract

This paper presents a novel nonparametric efficiency analysis technique based on the Genetic Programming (GP) in order to measure efficiency of Iran electric power plants. GP model was used to predict the output of power plants with respect to input data. The method, we presented here, is capable of finding a best performance among power plant based on the set of input data, GP predicted results and real outputs. The advantage of using GP over traditional statistical methods is that in prediction with GP, the researcher doesn't need to assume the data characteristic of the dependent variable or output and the independent variable or input. In this proposed methodology to calculate the efficiency scores, a novel algorithm was introduced which worked on the basis of predicted and real output values. To validate our model, the results of proposed algorithm for calculating efficiency rank of power plants were compared to traditional method. Real data was presented for illustrative our proposed methodology. Results showed that by utilizing the capability of input-output pattern recognition of GP, this method provides more realistic results and outperform in identification of efficient units than the conventional methods.

Keywords: electric power plants, performance evaluation, genetic programming

1. Introduction and Background

The most significant issues developing countries are facing with, is finding the appropriate way of operating and managing their power industries (Yunos & Hawdon, 1997). Electricity is extremely important in the economic development of every society (Liu et al., 2010). In 2007, Iran generated about 190 billion kilowatt-hours (Bkwh) electricity and consumed 153 Bkwh. Iran heavily relies on conventional fossil fuel power plants (especially natural gas generator). Iran's nominal electrical production capacity is about 49,000 Megawatts (MW). Nominal capacity of some power plants is under 10%. Most power plants in Iran are old, and can't work under nominal capacity. On the other hand, Iran needs to increase its power plants generate capacity around 10% annually, to fulfill the 7-9 percent annual demand growth (http://www.eia.doe.gov).

The expenses of constructing electricity power plants and producing electricity are relatively high. In addition, the environmental damage and its consequent costs of burning fossil fuels for electricity generation is remarkable. Hence, performance assessment and efficiency evaluation of a group of selected homogenous thermal electricity power plants or in performance evaluation literature, decision-making units (DMUs) to reduce such costs seem necessary. In 2007, 25.6 percent of the whole amount of electricity produced came from gas turbines; 2.2 from hydroelectric plants; 45.4 from steam power plants; and 26.6 from combined cycle power plants. The rest of it was produced by diesel generators. Figure 1 shows the electricity generated by each of different types of power plants in Iran (http://www.tavanir.org.ir).

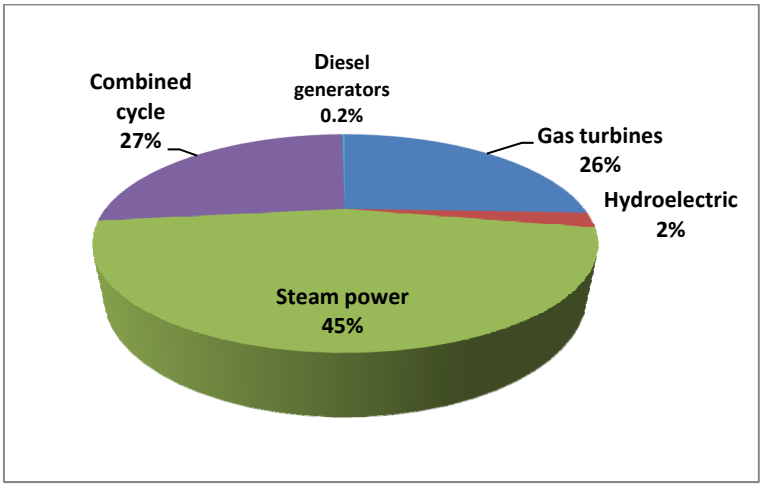

Figure 1. Electricity generation by different types of power plants

One of the benchmarking methods in performance evaluation is frontier benchmarking method. This method has a stronger concentration on performance differences among DMUs than other methods. This approach can be most suitable when the main goal is to reduce the performance space among the DMUs (Jamasb & Pollitt, 2004). In the field of efficiency frontier analysis, several approaches and methodologies are applied in the past thirty years, like performance indicators. There are different types of parametric econometric methods such as ordinary least square (OLS), Stochastic frontier approach (SFA), thick frontier approach (TFA) and distribution-free approach (DFA). Data Envelopment Analysis (DEA) and Free Disposal Hull are two widely used and well known nonparametric methods which are based on a mathematical programming (Tyagi et al., 2009; Bauer et al., 1998). These parametric and non-parametric methodologies are applied to many cases in electrical field (Azadeh et al., 2009; Iglesias et al., 2010; Park & Lesourd, 2000; Yunos & Hawdon, 1997; Pérez-Reyes & Tovar, 2010; Sueyoshi et al., 2010). Among the efficiency frontier analyses, DEA is more widely applied in many fields. Park and Lesourd (2000) presented an application of DEA-BCC (Banker, Charnes and Cooper) and SFA for measuring of South Korea, 64 conventional fuel power plants efficiencies. To improve the statistical explanation of data, they export the DEA-BCC efficiency results into an econometric estimate of a standard production function. They further perform a statistical analysis of the DEA results and compared the results with results obtained by the previous stochastic-frontier method (Park & Lesourd, 2000). During the period 2001–2004, Iglesias et al. (2010) applied DEA and SFA methods, to measure the relative efficiency of a set of wind farms. They debated that the results can provide, an important pre efficiency measure, plus economic impact aspects of relevance for wind farm development companies (developers), technology suppliers and operators (Iglesias et al., 2010). During 2004–2006, Liu et al. (2010) evaluate the power-generation efficiency of main thermal power plants in Taiwan using DEA. In the mentioned study to verify the stability of the DEA model a stability test was performed. The results show that all power plants achieved acceptable overall operational efficiencies. Combined cycle power plants were the most efficient plants (Liu et al., 2010).

Pombo and Taborda (2006) assessed Colombia's power distribution utilities performance before and after the regulatory reform in 1994. They measured the DEA technical efficiencies and showed that econometric tests on DEA efficiency scores show a positive effect of regulatory reform. Sueyoshi and Goto (2001) applied the slack-adjusted DEA (SA-DEA) model to examine the performance of Japanese electric power generation companies from 1984 to 1993. It is clear that by applying different methods and considering the variety of assumptions in different methods, Inconsistency of conclusions for DMUs efficiency are often happened (Azadeh et al., 2010). Each of the parametric and non-parametric methods has its strengths and weaknesses. The parametric methods require assumption about the data characteristic structure. Despite the fact that the non-parametric methods do not require any assumption for data structure, therefore if the data has statistical noise the calculated efficiencies, e.g. by DEA, may be distorted (Tyagi et al., 2009; Bauer, 1990). Azadeh et al. (2007) mentioned the fact that DEA is barely capable to estimate the DMUs performance. They showed that artificial neural networks (ANNs) can be used to overcome this issue. ANNs are the widely accepted pattern recognition approach. The ANN mechanism is motivated by the animal central nervous systems. It has been proven that ANNs are efficient in estimating the production function behavior and then in measuring the efficiency considering non linear condition (Azadeh et al., 2007). Despite having a very good performance,

ANNs is not capable of extracting interpolation equations. The ANN implementation is needed to be done by a computer program. The new hybrid approach combining DEA and ANNs (Athanassopoulos & Curram, 1996) has been applied in many fields (Mostafa, 2009; Pendharka, 2010; Çelebi & Bayraktar, 2008; Wu, 2009; Wu et al., 2006; Wang et al., 2009). Wu et al. (2006) integrated DEA and ANNs to calculate the relative efficiency of a big Canadian bank branches. In this study in first stage a CCR model of DEA and in the next stage NN model was used to measure the relative efficiencies. By better estimation of performance pattern this approach can identify efficient units robustly. In the field of vendor evaluation and selection, Wu (2009) presented a DEA, decision trees and NNs hybrid model to evaluate performance of suppliers. The mentioned hybrid model can perform as a classification and a regression model simultaneously. The model consists of two modules: Module 1 calculate DEA efficiencies and Module 2 utilizes efficiencies data to train Decision Tree, NNs model and applies the DT-NN model to new suppliers. In this paper Genetic programming (GP) is applied as a novel approach for evaluating performance of power generation industry. GP is a machine learning method that can be used to find the best fitness function. The results of GP are represented as hierarchy structures and show the steps to obtain the fitness function. The main advantage of GP over ANN and traditional statistical methods is its ability to generate simplified estimation equations without considering any assumption about data relationship and structure of data. GP is applied in several fields (Kaboudan, 2003) such as forecasting electricity demand (Lee et al., 1997); forecasting long term energy consumption (Karabulut et al., 2008) in real-time runoff (Khu et al., 2001); predicting financial data (Iba & Sasaki, 2002); predicting stock prices (Kaboudan, 2000) in fault analysis of the diesel engine fuel (Sun et al., 2004); prediction of ski-jump bucket spillway scour (Azamathulla et al., 2008); river pipeline scour (Azamathulla & Ghani, 2010) and longitudinal dispersion coefficients in streams (Azamathulla & Ghani, 2011) and etc. This study presents a genetic programming procedure for performance evaluating of a set of homogeneous steam power plants and benchmarking. By considering a set of power plants of same types to apply the presented model, more accurate and reliable results are guaranteed.

2. Genetic Programming

Genetic programming (GP) as an extension of the genetic algorithms was firstly presented by Koza (1992). GP is an area of evolutionary computation methods that creates computer programs.

The computer programs generated by GP are presented as tree structures and expressed in the functional programming language (LISP) (Koza, 1992). The classical GP technique is also called “tree-based GP” (Koza, 1992). The main differences between GP and GA are (Willis et al., 1997):

- GP creates solutions or chromosomes as a tree structured in the variable length; while GA’s generally make use of chromosomes of fixed length and structure.
- GP typically integrate syntax with a specific domain that regulates meaningful arrangements of information on the chromosome. For GAs, the chromosomes are typically syntax-free.
- GP maintain the syntax of its tree-structured chromosomes in ‘reproduction’ step, by using the genetic operators.
- GP solutions are often coded in the way that let the chromosomes to be executed directly. GA’s are rarely coded in this form.

GP is able to automatically predict the generation of mathematical expressions or programs (Tsakonas, 2006). Like many other areas of computer sciences, GP has been widely utilized in the real world condition. GP creates numerous random populations in the large space of possible solutions (computer programs) to avoid the likelihood of stopping in a “local optimum” (Muttil & Lee, 2005). The functions or programs are called organisms or chromosomes. During the evolution process to find best solution, the size and form of the populations dynamically change (Brezocnik & Balic, 2001). From a set of function and terminal genes, possible solutions in GP can be formed in a recursive manner.

In GP, function set (F) is consisting of all mathematical functions (the basic mathematics operations (+, -, ×, /, etc.), Boolean logic functions (AND, OR, NOT, etc.) or …).

The terminal set T contains the arguments for the functions and can consist of numerical constants, logical constants, variables, etc. In Figure 2 a simple tree structure of a GP model is shown. GP Tree structure has a root node with links went out from each function and end to a terminal.

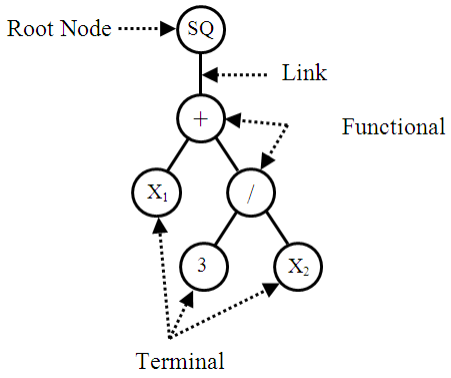

Figure 2. The tree structure of a GP model $(X_1 + 3/X_2)^2$ (Gandomi et al., 2010)

After several random populations of random parse trees has been produced, the GP algorithm calculates their fitness and selects the better parse trees for generates new individuals by reproduction, crossover, and mutation, in all iterations, GP creates the new generation (Koza, 1992). This three process (selection, reproduction and variation) will be go on until the specific stopping criterion (such as specific MSE) is satisfied. During the crossover procedure, a point on a branch of each pair of chosen parent is selected randomly and then the set of terminals and/or functions from that point exchanged to obtain two new programs. To ensure the exchange of genetic material among the evolved programs the crossover operation is required. Figure 3 shows a typical crossover operation of two computer programs. From two parental computer programs (Parent I, Parent II) two new child computer programs (Child I, Child II) are generated. The randomly generated Childs by crossover can be seen in Figure 3. Both child programs include the genetic material from their parents. Preserve syntactical structure of the computer programs during the crossover process is very important (Kovacic et al., 2004).

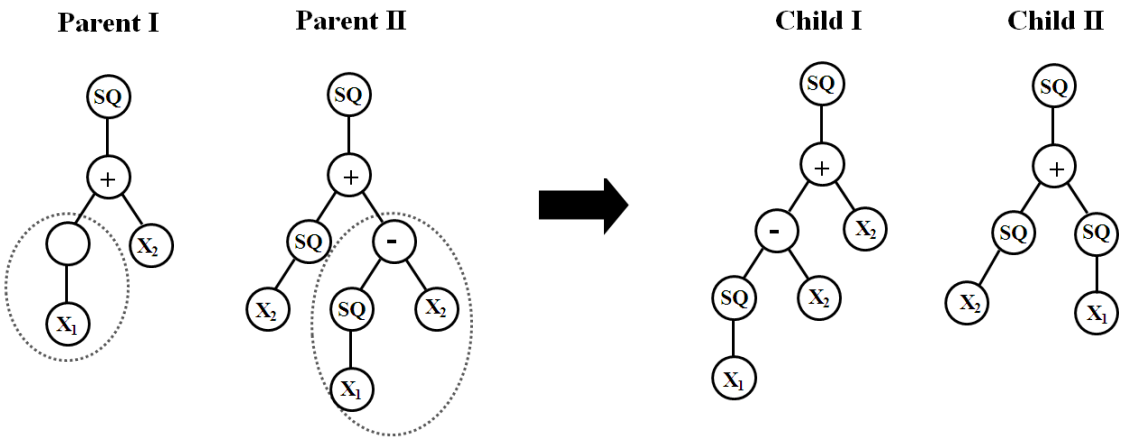

Figure 3. Typical crossover operation in GP (Gandomi et al., 2010)

Crossover is responsible for improvements in fitness, and mutation takes a secondary role responsible for reintroducing random population that have been missed from the population. In the mutation operation, the GP algorithm selects a function or terminal randomly and mutates it. Both of a function node or a terminal node can be exchanged during mutation. A node in the tree is chosen at random. If it's a terminal node it is simply replaced by another terminal and if it is a function node in the point mutation application, it is replaced by a new function with the same equality. In the tree mutation application, a new function node (not necessarily with the same parity) is chosen, and the original node together with its relative sub-tree is substituted by a new randomly generated sub-tree (Li et al., 2007). Figure 4 shows a typical mutation operation in GP. Generally mutation doesn't play a major role in GP (Koza, 1992).

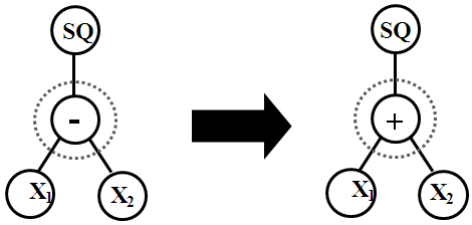

Figure 4. Typical mutation operation in GP

Here are the steps the GP algorithm follows to generate a computer programs (see Figure 5):

(1) Creation an initial population by producing of random compositions of the functions and terminals (computer programs).

(2) Execution of the programs in the population separately and calculate fitness values of each programs to find out how well they solve the problem.

(3) Creation of a new population of programs.

- Copying the best existing programs (reproduction).
- Creating new computer programs by the crossover and mutation operations.

(4) The best program that can be found in any generation defines the output of the GP algorithm (Koza, 1992).

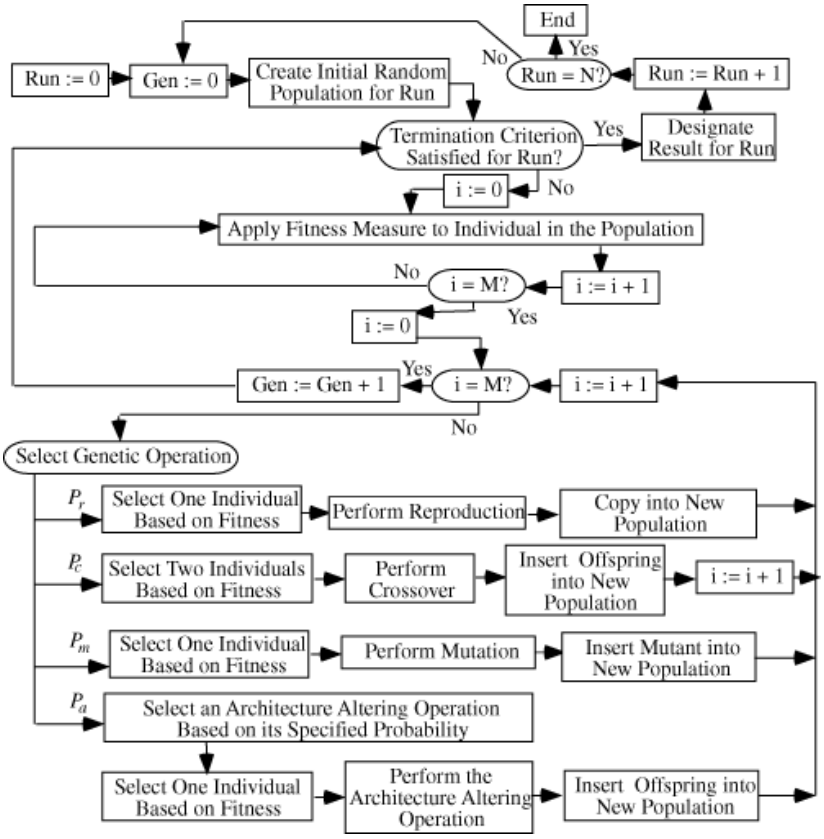

Figure 5. Flowchart of genetic programming (Koza, 1992)

2.1 Unique Aspects of GP

The main benefit of GP in over the other artificial intelligence and traditional approaches (such as NN and Regression), is that GP does not need any definition of functional form of solutions to start optimization. GP creates many randomly functions and selects the one with the best fitness value. The benefit of GP over the

conventional regression methods is that conventional regression need to specify the model structure in advance, which is mostly suboptimal. ANNS require the identification of the network structure and then the coefficients (weights) are calculated during the learning process. In GP, the terminal and function sets are defined initially, and then both the optimal form of the model and the coefficients are calculated by GP algorithm (Muttil & Lee, 2005). The GP models can provide additional information about the problem by finding the best fit analytic function. In contrast, ANNs can't provide any analytical function besides the interpretation of the network weights is not generally possible. Opposing to ANNS, GP have a good ability to distinguish among the effective input data and inputs that have no effect on a solution. Therefore, GP can reduce the dimension of the model, and better model interpretation will be achieved (Muttil & Lee, 2005).

3. Methodology

In the present study, a GP-based algorithm is introduced to measure Iran's main electricity power plants efficiency during a specific period. The presented model is input oriented because of the selected power plants have particular demand to fulfill. Thus, the input quantities are the main decision parameters. By finding cost function instead of production function the GP method can be extend as an output oriented model. In this study one output is considered for simplicity. The proposed algorithm is as follows:

(1) Divide the data to input (S) and output (P) sets. Assume that "n" power plants have to be assessed.

(2) Form S as inputs contain all data from input variables of the previous periods.

(3) Divide S to two sub sets: learning ($S_{Learning}$) and validation ($S_{validation}$) sets.

The learning data are used for learning process. A validation data are also used to test the capability of the model on new data. During the learning process the performance of the evolved models on the validation set is monitored.

The learning and validation data sets used to select the best evolved models and included in the training process. Since better extrapolate of GP is preferred the validation data are chosen from closer data periods $S_{Testing}$.

(4) Use GP method to find best program function.

(A) Choose training variables.

(B) Train GP using the learning data ($S_{Learning}$).

(C) Evaluate the model using the validation data $S_{Validation}$.

Calculate the GP best fit function with the desired precision on the validation data.

(5) Calculate fitness value for $S_{Testing}$ using the GP best fit function.

(6) Calculate the absolute error between the real output ($P_{real}(i)$) and GP best fit function ($P_{GP}(i)$) in the current period:

$$D_i = |P_{real_{(i)}} - P_{GP_{(i)}}|,\ i = 1,2,\dots,n \tag{1}$$

(7) Calculate the error weight for each predicted value of power plants ($E_{weight_{(i)}}$):

$$E_{weight_{(i)}} = \frac{D_i}{\sum_{i=1}^{n} D_i},\ i = 1,2,\dots,n \tag{2}$$

(8) Calculate Raw Efficiency Scores: For obtaining Raw Efficiency Scores real value is divided to the summation of effects of the each absolute error ratio ($E_{weight_{(i)}}$) and predicted value.

$$RE_{score_{(i)}} = \frac{P_{real_{(i)}}}{P_{GP_{(i)}} + E_{weight_{(i)}}},\ i = 1,2,\dots,n \tag{3}$$

(9) Final efficiency scores calculation. The efficiency scores are between 0 and 1. The power pant with maximum score takes the highest rank.

$$E_{score_{(i)}} = \frac{RE_{score_{(i)}}}{Max\,(RE_{score_{(i)}})} \times 100,\ i = 1,2,\dots,n \tag{4}$$

The steps of proposed algorithm are illustrated in Figure 6.

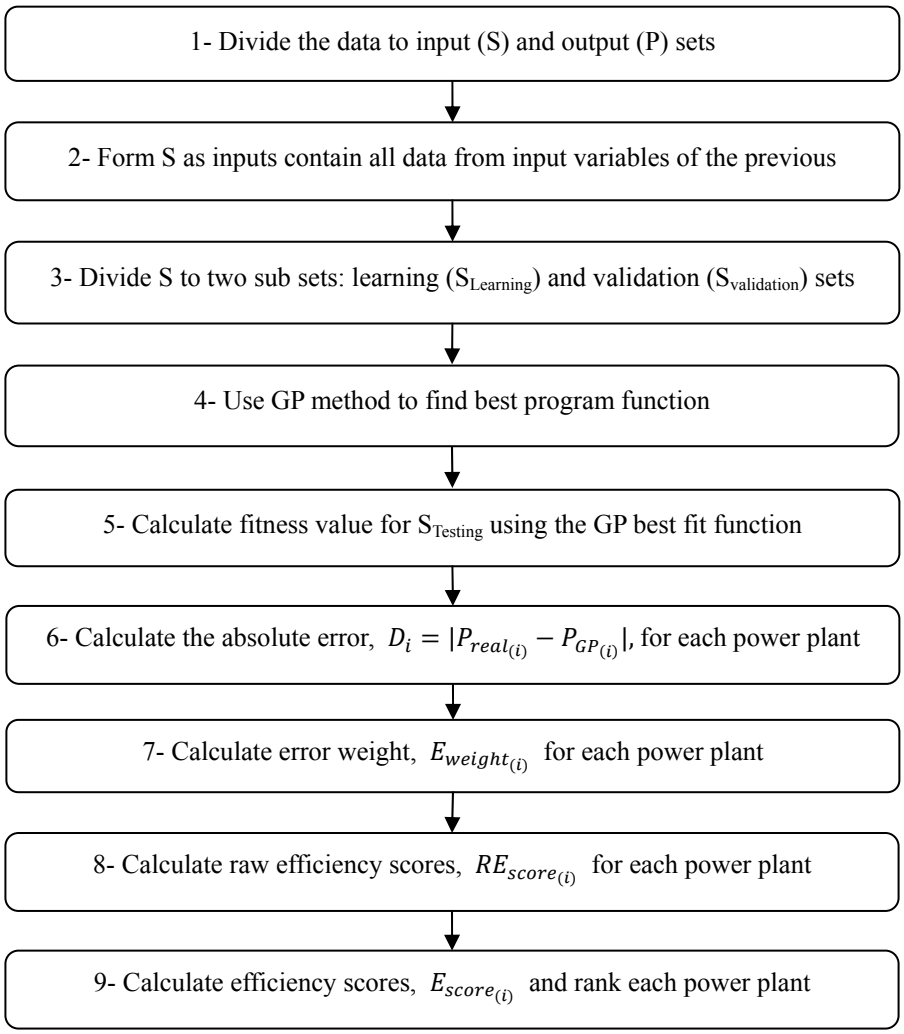

Figure 6. Steps of proposed methodology

4. Case Study

The conventional thermal steam-electric production plan is defined by engineering framework. In such framework, appropriate input parameters are the consumed fuel quantity and installed power. The installed power is the maximum nominal power for that the plants are originally designed. Labor input variables are for controlling and maintenance services, which also require funds (Azadeh et al., 2007). Electrical energy production is the output. According to some researches on the performance evaluation of Iran's thermal power plants (e.g., Emami Meibodi, 1998), labor is not a major factor. Consequently, GP-based formulation of the electric power (MWh) generated from thermal power plants in each power plants (P) is considered to be as follows:

$$P = f(IC, IP, FC) \tag{5}$$

Where,

IC (MW): Capital (install capacity)

IP (MWh): Internal power (Internal consumption)

FC (TJ): Fuel consumption

IC is measured in terms of installed thermal generating capacity (Hawdon, 1997; Fare et al., 1983). IP is the energy consumption of plant (e.g. powered equipments, etc.). Various fossil fuels such as natural gas, gasoline and mazut have been used as fuel in the production procedure. The type of fuel is depended on availability; cost and environmental issues (Azadeh et al., 2010). FC measurement scale is Tera Joule (TJ). One hundred forty-eight data sets collected from 1997 to 2004 by Azadeh et al. (2010) were used for applying the proposed

performance evaluation and estimation model. The basic descriptive statistics of model parameters is calculated in Table 1. For more detailed information about Iran's thermal power plants, such as total output, generation capacity and fuel consumption can be found in TAVANIR management organization (1997–2004). To start analysis, the main data sets in several periods were separated to training and testing subsets. The training data were used for the learning process and the testing data were employed to evaluate the capability of the model on data sets that were not included in the analysis.

For analysis data sets from 1997 to 2002, 117 sets were used as the training data (100 sets for learning and 17 sets for validation). Also, 31 data sets from 2003 to 2004 were taken for the testing of the models.

Table 1. The basic descriptive statistics of model parameters

Parameter	IC (MW)	IP (MWh)	FC (TJ)	P (MWh)
Mean	731.4	273767.8142	1084398.382	4148901.203
Standard Deviation	557.4	200881.381	832885.7401	3282302.083
Sample Variance	310687.2	4.0E+10	6.9E+11	1.1E+13
Minimum	50	3215	22023	56254
Maximum	1890	823033	3298201	11640505
Confidence Level (95.0%)	90.5	32632.3	135298.4	533194.8

In the computerized GP predictive algorithm several parameters should be considered. These parameters should be set properly in order to get the best GP prediction model for the Electricity production in steam power plants. Table 2 shows the GP model parameters. Four basic mathematics operators were sets in the procedure in order to maintain the simplicity of the model. Population size sets the number of programs in the population that GP will evolve. The generation number sets the number of levels the algorithm will use before the run terminates. Based on the complexity of model the appropriate values of these parameters should be selected. Herein, a reasonably large value of initial population and generations were tested to find production function with minimum inaccuracy. The rates of the mutation and crossover operations for the optimal models were 50%. The maximum tree depth was also set to an optimal value of 12.

The other values of effective parameters are selected based on trial and error experiments (Gandomi et al., 2010). In this study tree-based GP software, GPLAB (Silva, 2007) in addition with subroutines coded in MATLAB was used.

Table 2. The GP parameter settings

Parameter	Settings
Function set	+, -, ×, /
Population size	100-1000
Maximum tree depth	12
Total generations	4000
Initial population	Ramped half-and-half
Sampling	Tournament
Expected no. of offspring method	Rank 89
Fitness function error type	linear error function
Termination	Generation 40
Minimum probability of crossover	0.1
Minimum probability of mutation	0.1
Real max level	30
Survival mechanism	Keep best

4.1 Performance Measures

Correlation coefficient (R) and mean absolute percent error (MAPE) were used to evaluate the performance of the GP models. R and MAPE are calculated using the following relations:

$$R = \frac{\sum_{i=1}^{n}(h_i-\bar{h}_i)(t_i-\bar{t}_i)}{\sqrt{\sum_{i=1}^{n}(h_i-\bar{h}_i)^2 \sum_{i=1}^{n}(t_i-\bar{t}_i)^2}} \quad (6)$$

$$MAPE = \frac{1}{n}\sum_{i=1}^{n}\left|\frac{h_i-t_i}{h_i}\right| \times 100 \quad (7)$$

where h_i and t_i are respectively the actual and predicted output values for the i^{th} output, $\bar{h}_i$ is the average of the actual outputs, and n is the number of sample.

4.2 GP-Based Formulation of Electricity Production and Analysis

The GP-based formulation of the electric power generated from thermal power plants (P) is as given below:

$$P\ (MWh) = \left(\mathrm{IP} + 3\mathrm{FC} - \frac{(9+\mathrm{IC})\left(\mathrm{IC}\left(\frac{\mathrm{FC}}{\mathrm{IC}}+\mathrm{IP}\right)+1377\mathrm{IC}^2\right)}{\mathrm{IP}-\mathrm{IC}-\mathrm{FC}-\mathrm{IC}^2}\right) \quad (8)$$

Comparisons of the measured versus predicted P values using GP are shown in Figure 7. As it is seen, the prediction accuracy of the GP model is very good for both of the training and testing data sets. The contribution of each input parameter in the model was evaluated through a sensitivity analysis. For this purpose, frequency values of the variables were obtained. A frequency value equal to 1.00 for an input indicates that this variable was appeared in 100% of the best thirty programs evolved by GP. This methodology is a common approach for the GP-based sensitivity analysis (Alavi et al., 2010). The frequency values of the variables are shown in Figure 8. As can be seen in this figure, the electricity production significantly influenced by all the parameters. However, the results indicate that it is more sensitive to the fuel consumption (FC) and install capacity (IC) than the internal consumption (IP).

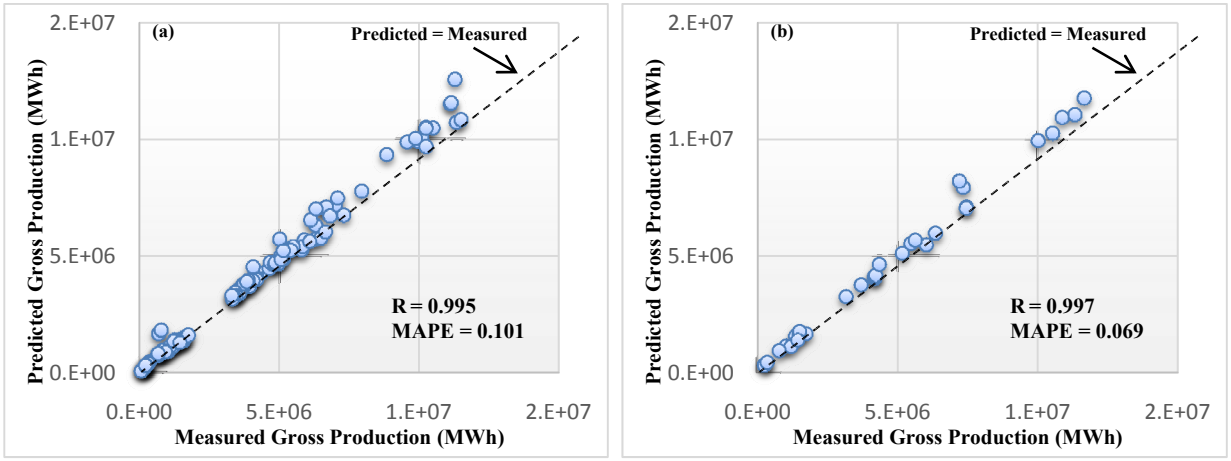

Figure 7. Measured versus predicted electricity production using GP: (a) training data, (b) testing data

To further verification of the model, a parametric study was performed in this study. The main goal is to find the effect of each parameter on the electricity production. The methodology is based on the change of one predictor variable at a time while the other predictor variables are kept constant at the average values of their entire data sets. Figure 9 presents the predicted values of the electricity production as a function of IC, FC, and IP. The results of parametric analysis indicate that the electricity production continuously increases due to increasing IC and IP.As shown in Figure 9(c), the electricity production initially decreases with increasing FC up to about 5.4E+05TJ, and afterwards it starts increasing.

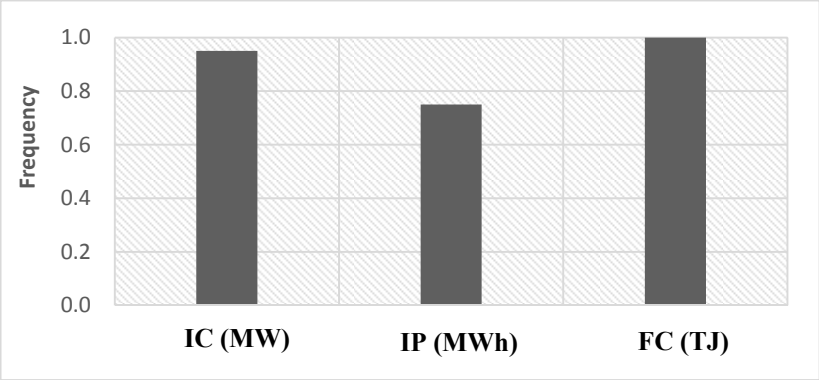

Figure 8. Sensitivity analysis of the predictor variables in the GP model

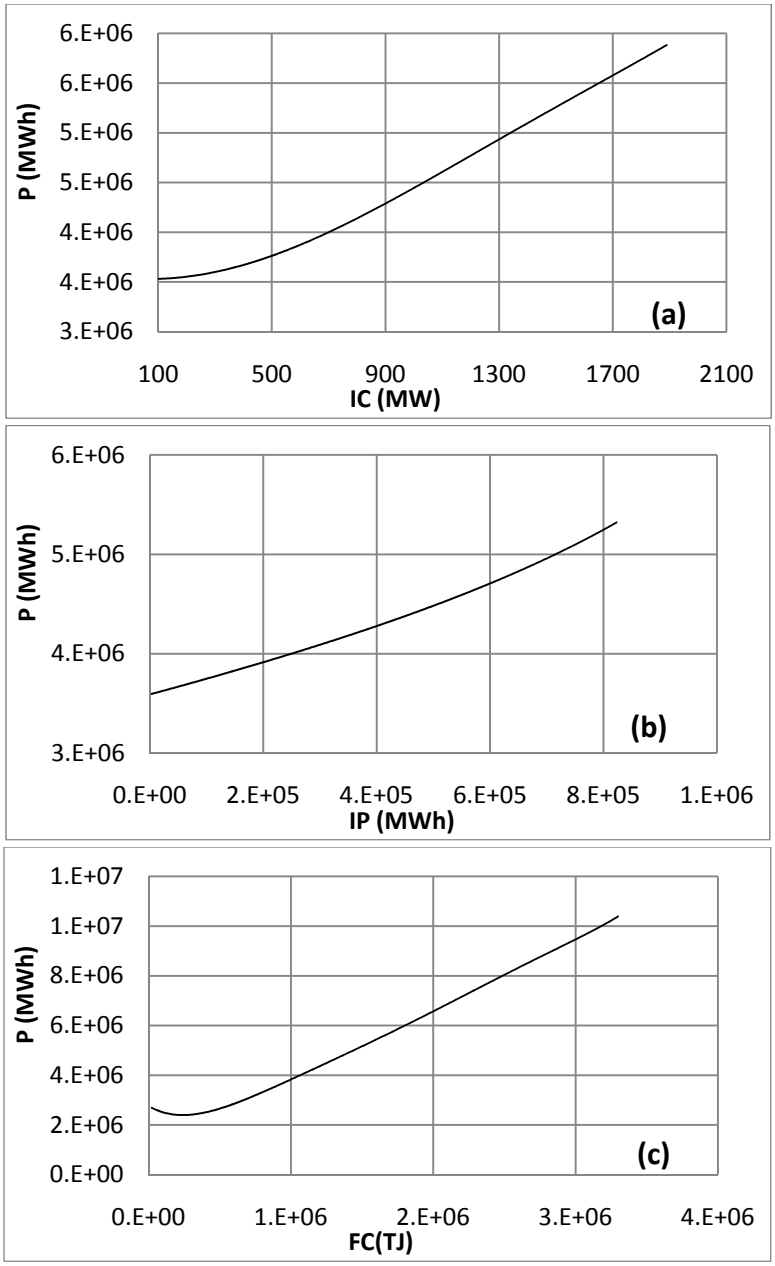

Figure 9. Parametric analysis of the electricity production in the GP model

5. Validity Verification

Based on the estimated results for outputs of power plants calculated by the GP model, the plant efficiencies are quantified. The results are shown in Table 3 through Table 5. In Table 3 the rankings of the power plants based on Athanassopoulos and Curram (1996) study which is called ‘‘standardized efficiency’’ is shown (Costa & Markellos, 1997; Delgado, 2005; Azadeh et al., 2007). Also Table 4 shows the calculation results according to Azadeh et al. (2007) approach. Finally Table 5 summarized the main results of efficiency scores based on the proposed GP estimation model, which can be seen in Figure 6.

Table 3. Efficiency scores estimation by the standardized efficiency algorithm

Power Plants	$P_{Real(i)}$	$P_{GP(i)}$	$Ei = P_{Real(i)} - P_{GP(i)}$	$Fi = 100 \times (P_{Real(i)} / (P_{ANN(i)} + \max E_i \mid E_i \geq 0))$	Rank
Montazerghaem	3297100	3335966.289	-38866.289	89.21	10
Besat	1500253	1682872.54	-182619.536	73.45	15
Firoozi	212403	310681.88	-98278.884	31.68	19
Salimi	11310817	11000250.67	310566.328	99.57	2
Shazand	7438002	7128665.43	309336.573	99.33	3
Rajaei	6342203	5982403.61	359799.388	100	1
Beheshti	1435991	1366089.86	69901.139	83.2	13
Tabriz	4341330	4594212.58	-252882.575	87.63	11
Mofatteh	5134547	5314179.90	-179632.900	90.49	9
Bistoon	4210280	4095904.47	114375.526	94.49	6
Ramin	10861867	10764449.95	97417.052	97.64	4
Madhaj	922587	944762.00	-22175.003	70.72	16
Bandarabbas	7196540	8144942.68	-948402.683	84.62	12
Zarand	341402	407945.86	-66543.857	44.47	18
Esfahan	5621431	5600168.68	21262.323	94.32	7
Montazeri	11137177	11283224.42	-146047.415	95.66	5
Toos	3831065	3851999.95	-20934.945	90.96	8
Mashhad	665887	770047.05	-104160.047	58.94	17
Iranshahr	1492847	1591231.36	-98384.360	76.52	14

Table 4. Estimation of efficiency scores by the Azadeh et al. (2007) algorithm

Power Plants	$P_{Real(i)}$	$P_{GP(i)}$	E_i	E_i'	Sh_i	Fi	Rank
Montazerghaem	3297100	3628549.66	-331449.66	-0.0913	1390450.97	65.69	12
Besat	1500253	2053443.7	-553190.7	-0.2694	786,874.38	52.82	14
Firoozi	212403	782995.79	-570592.79	-0.7287	300,041.99	19.61	19
Salimi	$1.1*10^7$	8177297.48	3133519.52	0.3832	3133519.52	100	1
Shazand	7438002	7164642.93	273359.07	0.0382	2745472.89	75.05	6
Rajaei	6342203	5701384.48	640818.52	0.1124	2184755.98	80.42	4
Beheshti	1435991	1757228.32	-321237.32	-0.1828	673365.41	59.08	13
Tabriz	4341330	4617026.03	-275696.03	-0.0597	1769232.59	67.98	11
Mofatteh	5134547	5378608.18	-244061.18	-0.0454	2061068.93	69.02	10
Bistoon	4210280	4249969.03	-39689.03	-0.0093	1628577.29	71.62	8
Ramin	$1.1*10^7$	9195861.73	1666005.27	0.1812	3523830.75	85.39	3
Madhaj	922587	1685681.91	-763094.91	-0.4527	645949.01	39.57	16

Bandarabbas	7196540	7340823.66	-144283.66	-0.0197	2812984.89	70.88	9
Zarand	341402	891289.53	-549887.53	-0.617	341539.87	27.69	18
Esfahan	5621431	5310960.15	310470.85	0.0585	2035146.38	76.52	5
Montazeri	$1.1*10^7$	9370519.03	1766657.97	0.1885	3590758.98	85.93	2
Toos	3831065	3858784.97	-27719.97	-0.0072	1478676.55	71.78	7
Mashhad	665887	1245295.4	-579408.4	-0.4653	477194.02	38.66	17
Iranshahr	1492847	2043592.09	-550745.09	-0.2695	783099.28	52.81	15

Table 5. Efficiency scores estimation based on the proposed approach

Power Plants	P_{Real}	P_{GP}	D_i	$E_{Weight(i)}$	$RE_{Score(i)}$	$E_{score(i)}$	Rank
Montazerghaem	3297100	3335966.289	38866.28949	0.0113	0.98835	93.23	9
Besat	1500253	1682872.54	182619.5355	0.0531	0.89148	84.09	15
Firoozi	212403	310681.88	98278.88412	0.0286	0.68367	64.49	19
Salimi	11310817	11000250.67	310566.3283	0.0902	1.02823	96.99	4
Shazand	7438002	7128665.43	309336.573	0.0899	1.04339	98.42	3
Rajaei	6342203	5982403.61	359799.3877	0.1045	1.06014	100	1
Beheshti	1435991	1366089.86	69901.13884	0.0203	1.05117	99.15	2
Tabriz	4341330	4594212.58	252882.5752	0.0735	0.94496	89.14	13
Mofatteh	5134547	5314179.90	179632.9004	0.0522	0.9662	91.14	12
Bistoon	4210280	4095904.47	114375.5264	0.0332	1.02792	96.96	5
Ramin	10861867	10764449.95	97417.05159	0.0283	1.00905	95.18	6
Madhaj	922587	944762.00	22175.00268	0.0064	0.97653	92.11	11
Bandarabbas	7196540	8144942.68	948402.6831	0.2756	0.88356	83.34	16
Zarand	341402	407945.86	66543.85697	0.0193	0.83688	78.94	18
Esfahan	5621431	5600168.68	21262.32276	0.0062	1.0038	94.69	7
Montazeri	11137177	11283224.42	146047.4151	0.0424	0.98706	93.11	10
Toos	3831065	3851999.95	20934.94534	0.0061	0.99457	93.81	8
Mashhad	665887	770047.05	104160.0469	0.0303	0.86474	81.57	17
Iranshahr	1492847	1591231.36	98384.36003	0.0286	0.93817	88.49	14

To compare results and check the accuracy of the proposed method, a non-parametric inference method- Spearman rank correlation test- is used. To be more specific for each Power Plant, the statistical significances of the difference between the ranking obtained by proposed methodology, conventional and Azadeh et al. (2007) algorithm are determined using Spearman's rank correlation test. Spearman test evaluates the similarity of the rankings of the different DMUs. In the Spearman test, to examine the null hypothesis a test statistic, Z, is calculated using Equations (9) and (10) and compared with a pre-determined level of significance, α value. The null hypothesis is "The rankings of two methods are not similar". By considering level of significance α equal to 0.05, critical Z value will be 1.645. If the test statistic computed by Equation (10) exceeds 1.645, the null hypothesis is rejected and we can conclude that alternate hypothesis which is "The two rankings are similar" is true (IC &Yurdakul, 2010).

$$r_s = 1 - \left[\frac{6\sum_{j=1}^{k}(d_j)^2}{K(K^2-1)}\right] \tag{9}$$

$$Z = r_s\sqrt{(K-1)} \tag{10}$$

In Equation (9), d_j is the ranking difference of Power Plants j in different methods and K is the number of Power Plants. r_s represents the Spearman rank correlation coefficient. Table 6 shows the calculated values of d_j, r_s and Z.

Table 6. Determination of the significance of the difference between the proposed method and conventional methods

Power Plants	Efficiency ranking of proposed method	Efficiency ranking of conventional method	Efficiency ranking of Azadeh et al. (2007) method	d_j (proposed vs. conventional method)	d_j (proposed vs. Azadeh et al. (2007) method)
Montazerghaem	9	10	12	-1	1
Besat	15	15	14	0	0
Firoozi	19	19	19	0	3
Salimi	4	2	1	2	-3
Shazand	3	3	6	0	-3
Rajaei	1	1	4	0	-11
Beheshti	2	13	13	-11	2
Tabriz	13	11	11	2	2
Mofatteh	12	9	10	3	-3
Bistoon	5	6	8	-1	3
Ramin	6	4	3	2	-5
Madhaj	11	16	16	-5	7
Bandarabbas	16	12	9	4	0
Zarand	18	18	18	0	2
Esfahan	7	7	5	0	8
Montazeri	10	5	2	5	1
Toos	8	8	7	0	0
Mashhad	17	17	17	0	-1
Iranshahr	14	14	15	0	1
	proposed vs. conventional method	$r_s = 0.8158$		proposed vs. Azadeh et al. (2007) method	$r_s = 0.7123$
		$Z = 3.4611$			$Z = 3.022$

The calculated Z-values, 3.4611 and 3.022, are higher than 1.645, which indicates that the difference in ranking results of the proposed vs. conventional method and the proposed vs. Azadeh et al. (2007) method, by considering level of significance α equal to 0.05 is statistically insignificant. Based on the test results, it can be concluded that the ranking of Power Plants, obtained by proposed method is reliable.

Table 7 shows the summarized main results in presenting the efficiency scores of the conventional and proposed algorithm and PCA (ZPCA). Based on the results in Table 7, it can be seen that the mean efficiency scores of the conventional algorithm is smaller than mean technical efficiency for the Power Plants based on the proposed algorithm. Statistical t-test has been conducted In order to test significantly difference of the two technical efficiencies obtained from the two algorithms.

Table 7. Efficiency scores results

Power Plants	Efficiency scores by the proposed algorithm	Efficiency scores by Azadeh et al. (2007) algorithm
Bandarabbas	93.23	65.69
Beheshti	84.09	52.82
Besat	64.49	19.61
Bistoon	96.99	100
Esfahan	98.42	75.05
Firoozi	100	80.42
Iranshahr	99.15	59.08
Madhaj	89.14	67.98
Mashhad	91.14	69.02
Mofatteh	96.96	71.62
Montazerghaem	95.18	85.39
Montazeri	92.11	39.57
Rajaei	83.34	70.88
Ramin	78.94	27.69
Salimi	94.69	76.52
Shazand	93.11	85.93
Tabriz	93.81	71.78
Toos	81.57	38.66
Zarand	88.49	52.81
Mean	90.255	63.711

The results of t-test are illustrated in Table 8.

Table 8. Hypothesis testing of the mean efficiencies (**μ**E) of the proposed and Azadeh et al. (2007) algorithms

Hypothesis	
H_0	μ_E(proposed algorithm) - μ_E (Azadeh et al. (2007) > 25
H_1	μ_E (proposed algorithm) - μ_E (Azadeh et al. (2007) algorithm) <25
Calculated t-statistic	0.30
P-Value	0.616
Decision	Since the p-value is greater than α-level (0.01), there is no evidence to Reject H_0.

Base on Table 8 The null hypothesis cannot be rejected, that means technical efficiencies of the proposed algorithm is 25 percent larger than mean technical efficiencies of the Azadeh et al (2007) algorithm at the 1% level of significance.

6. Conclusion

In this paper a nine-step algorithm was proposed to measure and rank the efficiency of electricity production units (Power Plants) in Iran. The unique feature of proposed algorithm is using the result of GP model to calculate efficiency. Using GP can help to better estimate the performance patterns of Power Plants. GP doesn't require explicit assumption about the function structure of the dependent (output) and independent (input) variables and this can lead to better estimation and results than conventional method such as regression or neural

network. The proposed algorithm was applied to a set of steam power plants in 2004. The efficiency results and rankings were compared with the two other methods, conventional and Azadeh et al. (2007) approach. To validate our proposed algorithm and ensure that the proposed algorithm calculates the efficiency scores statistically similar to conventional method the Spearman rank correlation test is used. The results indicate that the efficiency scores are closer to the ideal efficiency with considering the fact that the rankings of Power Plants statistically remain the same. Because of better performance patterns recognition of GP method, the proposed algorithm calculates more precise and realistic results than the conventional approach. When the production function is unknown, The GP based algorithm for measuring technical efficiency can lead to better results than other techniques.

Because of lack of both theoretical and empirical works in efficiency analysis more research in this field is needed. For the future studies, utilization of other prediction techniques such as neural network in combination of GP method to better pattern recognition of production function is advised. Also to obtain more realistic results and to reduce the estimation error of results considering more output and input indicators is useful.

References

Alavi, A. H., Gandomi, A. H., Sahab, M. G., & Gandomi, M. (2010). Multi expression programming: a new approach to formulation of soil classification. *Engineering with Computers, 26*(2), 111-118. http://dx.doi.org/10.1007/s00366-009-0140-7

Athanassopoulos, A. D., & Curram, S. P. (1996). A comparison of data envelopment analysis and artificial neural networks as tools for assessing the efficiency of decision making units. *Journal of the Operational Research Society*, 1000-1016.

Azadeh, A., Ghaderi, S. F., Anvari, M., & Saberi, M. (2007). Performance assessment of electric power generations using an adaptive neural network algorithm. *Energy Policy, 35*(6), 3155-3166. http://dx.doi.org/10.1016/j.enpol.2006.11.012

Azadeh, A., Ghaderi, S. F., Omrani, H., & Eivazy, H. (2009). An integrated DEA-COLS-SFA algorithm for optimization and policy making of electricity distribution units. *Energy Policy, 37*(7), 2605-2618. http://dx.doi.org/10.1016/j.enpol.2009.02.021

Azadeh, A., Saberi, M., & Anvari, M. (2010). An integrated artificial neural network algorithm for performance assessment and optimization of decision making units. *Expert Systems with Applications, 37*(8), 5688-5697. http://dx.doi.org/10.1016/j.eswa.2010.02.041

Azamathulla, H. M., & Ghani, A. A. (2010). Genetic programming to predict river pipeline scour. *Journal of Pipeline Systems Engineering and Practice, 1*(3), 127-132. http://dx.doi.org/10.1061/(ASCE)PS.1949-1204.0000060

Azamathulla, H. M., & Ghani, A. A. (2011). Genetic programming for predicting longitudinal dispersion coefficients in streams. *Water Resources Management, 25*(6), 1537-1544. http://dx.doi.org/10.1007/s11269-010-9759-9

Azamathulla, H. M., AB GHANI, A., Zakaria, N. A., Lai, S. H., Chang, C. K., Leow, C. S., & Abuhasan, Z. (2008). Genetic programming to predict ski-jump bucket spill-way scour. *Journal of Hydrodynamics, Ser. B, 20*(4), 477-484. http://dx.doi.org/10.1016/S1001-6058(08)60083-9

Bauer, P. W. (1990). Recent developments in the econometric estimation of frontiers. *Journal of econometrics, 46*(1-2), 39-56. http://dx.doi.org/10.1016/0304-4076(90)90046-V

Bauer, P. W., Berger, A. N., Ferrier, G. D., & Humphrey, D. B. (1998). Consistency conditions for regulatory analysis of financial institutions: a comparison of frontier efficiency methods. *Journal of Economics and Business, 50*(2), 85-114. http://dx.doi.org/10.1016/S0148-6195(97)00072-6

Brezocnik, M., & Balic, J. (2001). A genetic-based approach to simulation of self-organizing assembly. *Robotics and Computer-Integrated Manufacturing, 17*(1-2), 113-120. http://dx.doi.org/10.1016/S0736-5845(00)00044-2

Çelebi, D., & Bayraktar, D. (2008). An integrated neural network and data envelopment analysis for supplier evaluation under incomplete information. *Expert Systems with Applications, 35*(4), 1698-1710. http://dx.doi.org/10.1016/j.eswa.2007.08.107

Costa, A., & Markellos, R. N. (1997). Evaluating public transport efficiency with neural network models. *Transportation Research Part C: Emerging Technologies, 5*(5), 301-312.

http://dx.doi.org/10.1016/S0968-090X(97)00017-X

Delgado, F. J. (2005). Measuring efficiency with neural networks. An application to the public sector. *Economics Bulletin, 3*(15), 1-10.

EIA. (n.d.). Energy Information Administration - Official Energy Statistics from the U.S. Government. Retrieved from http://www.eia.doe.gov/

Emami, M. A. (1998). *Efficiency considerations in the electricity supply industry: the case of Iran*. A thesis submitted to university of Surrey for the degree of Doctor of Philosophy.

Fare, R., Grosskopf, S., & Lovell, C. A. K. (1985). *The measurement of efficiency of production*. Springer. http://dx.doi.org/10.1007/978-94-015-7721-2

Gandomi, A.H., Alavi, A.H., Arjmandi, P., Vesali, M. (2010). Modeling of Compressive Strength of HPCMixes Using a Combined Algorithm of Genetic Programming and Orthogonal Least Squares. *Journal of Mechanics of Materials and Structures*, in press. http://dx.doi.org/10.2140/jomms.2010.5.735

Hawdon, D. (1998). Improving the performance of electricity industries in developing countries: Is World Bank policy on deregulation the way forward. *Deregulation of Electric Utilities*, 203-27. http://dx.doi.org/10.1007/978-1-4615-5729-6_9

Iba, H., & Sasaki, T. (2002). Using genetic programming to predict financial data. Evolutionary Computation, 1999. CEC 99. *Proceedings of the 1999 Congress on* (Vol. 1).

IC, Y. T., & Yurdakul, M. (2010). Development of a quick credibility scoring decision support system using fuzzy TOPSIS. *Expert Systems with Applications, 37*(1), 567-574. http://dx.doi.org/10.1016/j.eswa.2009.05.038

Iglesias, G., Castellanos, P., & Seijas, A. (2010). Measurement of productive efficiency with frontier methods: A case study for wind farms. *Energy Economics, 32*(5), 1199-1208. http://dx.doi.org/10.1016/j.eneco.2010.03.004

Jamasb, T., & Pollitt, M. G. (2004). Benchmarking and regulation of electricity transmission and distribution utilities: lessons from international experience.

Kaboudan, M. A. (2000). Genetic programming prediction of stock prices. *Computational Economics, 16*(3), 207-236. http://dx.doi.org/10.1023/A:1008768404046

Kaboudan, M. A. (2003). Forecasting with computer-evolved model specifications: a genetic programming application. *Computers & Operations Research, 30*(11), 1661-1681. http://dx.doi.org/10.1016/S0305-0548(02)00098-9

Karabulut, K., Alkan, A., & Yilmaz, A. S. (2008). Long term energy consumption forecasting using genetic programming. *Mathematical and Computational Applications, 13*(2), 71.

Khu, S. T., Liong, S. Y., Babovic, V., Madsen, H., & Muttil, N. (2001). Genetic Programming and Its Application in Real-Time Runoff Forecasting. *Journal of the American Water Resources Association, 37*(2), 439-451. http://dx.doi.org/10.1111/j.1752-1688.2001.tb00980.x

Kovacic, M., Balic, J., & Brezocnik, M. (2004). Evolutionary approach for cutting forces prediction in milling. *Journal of Materials Processing Technology, 155-156*, 1647-1652. http://dx.doi.org/10.1016/j.jmatprotec.2004.04.318

Koza, J. R. (1992). *Genetic programming: on the programming of computers by means of natural selection*. The MIT press.

Lee, D. G., Lee, B. W., & Chang, S. H. (1997). Genetic programming model for long-term forecasting of electric power demand. *Electric Power Systems Research, 40*(1), 17-22. http://dx.doi.org/10.1016/S0378-7796(96)01125-X

Li, W. X., Dai, L. F., Hou, X. B., & Lei, W. (2007). Fuzzy genetic programming method for analysis of ground movements due to underground mining. *International Journal of Rock Mechanics and Mining Sciences, 44*(6), 954-961. http://dx.doi.org/10.1016/j.ijrmms.2007.02.003

Liu, C. H., Lin, S. J., & Lewis, C. (2010). Evaluation of thermal power plant operational performance in Taiwan by data envelopment analysis. *Energy Policy, 38*(2), 1049-1058. http://dx.doi.org/10.1016/j.enpol.2009.10.057

Mostafa, M. M. (2009). Modeling the efficiency of top Arab banks: A DEA-neural network approach. *Expert*

Systems with Applications, 36(1), 309-320. http://dx.doi.org/10.1016/j.eswa.2007.09.001

Muttil, N., & Lee, J. H. W. (2005). Genetic programming for analysis and real-time prediction of coastal algal blooms. *Ecological Modelling, 189*(3-4), 363-376. http://dx.doi.org/10.1016/j.ecolmodel.2005.03.018

Park, S. U., & Lesourd, J. B. (2000). The efficiency of conventional fuel power plants in South Korea: A comparison of parametric and non-parametric approaches. *International Journal of Production Economics, 63*(1), 59-67. http://dx.doi.org/10.1016/S0925-5273(98)00252-7

Pendharkar, P. C. (2011). A hybrid radial basis function and data envelopment analysis neural network for classification. *Computers & Operations Research, 38*(1), 256-266. http://dx.doi.org/10.1016/j.cor.2010.05.001

Pérez-Reyes, R., & Tovar, B. (2010). Explaining the inefficiency of electrical distribution companies: Peruvian firms. *Energy Economics, 32*(5), 1175-1181. http://dx.doi.org/10.1016/j.eneco.2010.02.002

Pombo, C., & Taborda, R. (2006). Performance and efficiency in Colombia's power distribution system: Effects of the 1994 reform. *Energy Economics, 28*(3), 339-369. http://dx.doi.org/10.1016/j.eneco.2005.08.001

Silva, S. (2007). *GPLAB, a genetic programming toolbox for MATLAB*. Retrieved from http://gplab.sourceforge.net

Sueyoshi, T., & Goto, M. (2001). Slack-adjusted DEA for time series analysis: Performance measurement of Japanese electric power generation industry in 1984-1993. *European Journal of Operational Research, 133*(2), 232-259. http://dx.doi.org/10.1016/S0377-2217(00)00295-2

Sueyoshi, T., Goto, M., & Ueno, T. (2010). Performance analysis of US coal-fired power plants by measuring three DEA efficiencies. *Energy Policy, 38*(4), 1675-1688. http://dx.doi.org/10.1016/j.enpol.2009.11.017

Sun, R., Tsung, F., & Qu, L. (2004). Combining bootstrap and genetic programming for feature discovery in diesel engine diagnosis. *International Journal of Industrial Engineering, 11*(3), 273-281.

TAVANIR management organization. (1997–2004). Electric Power Industryin Iran 1997–2004, TAVANIR management organization. Retrieved from http://www.tavanir.org.ir

Tsakonas, A. (2006). A comparison of classification accuracy of four genetic programming-evolved intelligent structures. *Information Sciences, 176*(6), 691-724. http://dx.doi.org/10.1016/j.ins.2005.03.012

Tyagi, P., Yadav, S. P., & Singh, S. (2009). Relative performance of academic departments using DEA with sensitivity analysis. *Evaluation and Program Planning, 32*(2), 168-177. http://dx.doi.org/10.1016/j.evalprogplan.2008.10.002

Wang, C. H., Chuang, C. C., & Tsai, C. C. (2009). A fuzzy DEA-Neural approach to measuring design service performance in PCM projects. *Automation in Construction, 18*(5), 702-713. http://dx.doi.org/10.1016/j.autcon.2009.02.005

Willis, M. J., Hiden, H. G., McKay, B., Montague, G. A., & Marenbach, P. (1997). Genetic programming: An introduction and survey of applications. *IEE Conference Publications* (pp. 314-319).

Wu, D. (2009). Supplier selection: A hybrid model using DEA, decision tree and neural network. *Expert Systems with Applications, 36*(5), 9105–9112. http://dx.doi.org/10.1016/j.eswa.2008.12.039

Wu, D. D., Yang, Z., & Liang, L. (2006). Using DEA-neural network approach to evaluate branch efficiency of a large Canadian bank. *Expert Systems with Applications, 31*(1), 108-115. http://dx.doi.org/10.1016/j.eswa.2005.09.034

Yunos, J. M., & Hawdon, D. (1997). The efficiency of the national electricity board in Malaysia: An intercountry comparison using DEA. *Energy Economics, 19*(2), 255-269. http://dx.doi.org/10.1016/S0140-9883(96)01018-3

Modern Applied Science; Vol. 8, No. 3; 2014
ISSN 1913-1844 E-ISSN 1913-1852
Published by Canadian Center of Science and Education

Modelling of Particle Dispersion in Mechanically Ventilated Space

Ismail Abdul Rahman[1], Jouvan Chandra Pratama Putra[1] & Ade Asmi[2]

[1] Faculty of Civil and Environmental Engineering, Universiti Tun Hussein Onn Malaysia (UTHM), Malaysia

[2] Faculty of Civil Engineering, Bakrie University, Indonesia

Correspondence: Jouvan Chandra Pratama Putra, Faculty of Civil and Environmental Engineering, Universiti Tun Hussein Onn Malaysia (UTHM), Malaysia. E-mail: jouvanchandra@gmail.com

Received: October 10, 2013 Accepted: February 10, 2014 Online Published: April 8, 2014

doi:10.5539/mas.v8n3p60 URL: http://dx.doi.org/10.5539/mas.v8n3p60

Abstract

This study presents simulation works carried out regarding to the airflow movement and particle dispersion in mechanically ventilated laboratory space at Faculty of Civil and Environmental Engineering of Universiti Tun Hussein Onn Malaysia. The measurement of air velocity was taken using Anemometer kit 4 in 1 while the particle dispersion was measured using Met-One Particle Counter GT-521 and measured at random points. The measured air velocity and particle dispersion are then used as input in simulation work using Comsol Multiphysics software. The simulation results are validated with the measured value and found that the percentage differences are within 6 – 10 % which is accepted by many researchers.This study found that the amount of particle dispersion increased toward the corner of the space and concurrently with the airflow movement. This is indicates that the particle dispersion depends on the airflow movement.

Keywords: Comsol Multiphysics, particle dispersion, airflow movement

1. Introduction

Modeling is process of emulating a real system (Robinson, 2007), while simulation is the process of manipulating of the model for the purpose of understanding the behavior of the system or for evaluating various strategies for the operation of the system (Shannon, 1975). The advantage of modeling is that it able to combine several physic phenomena into a single entity (COMSOL, 2007). Modelling also able to carried out analysis using several approaches for getting appropriate solution(Pryor, 2011).

Malaysia, as a country which has a hot and humid climate (Yau, Chew, & Saifullah, 2012) is essential to provide thermal comfort during office hours. Air-conditioning is one of mechanical ventilation system that widely used to provide it (Ismail et al., 2009). However, mechanical ventilation system is could be associated with IAQ problems such high levels of air contaminants due to the insufficient of airflow (Meckler, 1991). For IAQ assessment, modeling and simulation of indoor particle dispersion is important to assess for better prediction of human exposure to particle pollutants (Abadie & Limam, 2007). Indoor particle concentration is affected by the inhomogeneous of airflow that generated through ventilation system and effected to the health of people (Mendonça, Abadie, & Blondeau, 2012).

Previously, there are several studies on particle dispersion in mechanically ventilated space using modelling and simulation software (Cheong et al., 2003; Chung, 1995; Tian, Tu, Yeoh, & Yuen, 2006). Cheong et al. (2003) used Computational Fluid Dynamic (CFD) software to simulate particle dispersion in air-conditioned room by adopting the Re-Normalization Group (RNG) as k-ε turbulence model. The simulation results indicated that the patern of particle dispersionis highly dependent on the air velocity flow. Chung (1995) investigated the air movement and particle transport in partitioned enclosure by using EXACT3 software. The software using k-ε model to simulate the airflow, while Brownian-motion is adopted for simulates particle dispersion. The results indicated that the path of particle depends greatly on the region of room where it originates. Besides, it is also found that particle dispersion in the range of 0.1 – 1.0 μm were not affected by their different diameters.Tian et al. (2006), numerically investigated particle dispersion indoor through FLUENT software. To simulate the indoor airflow they used three basic turbulence models such as: standard k-ε, RNG k-ε, and RNG based on LES (Large Eddy Simulation), while the particle distribution was simulated using the Lagrangian particle-tracking model. The results indicated that the RNG based LES model provided the best agreement for Low-Reynolds-Number (LRN) turbulence indoor airflow, while the Lagrangian particle-tracking model for particle distribution indoor.

2. Measurement of Particle

This study was carried out on mechanically ventilated laboratory at Faculty of Civil and Environmental Engineering of Universiti Tun Hussein Onn Malaysia (UTHM). Measurement of particles dispersion and air velocity were conducted for eight hours duration for one day. The number of samples in this laboratory is 20 as respect to the Equation 1.

$$N_L=\sqrt{A} \quad (1)$$

Where;

N_L: The minimum number of sampling locations.

A: The area or zone in square meter (m^2).

Measurement of samples was carried out using two types of equipment. For particle dispersion, equipment used is Met One Particle GT-521 which is used to measure Particulate Matter (PM) ≥ 0.3 μm, while Anemometer kit 4 in 1 to measure the air velocity. Prior to the measurement, all the equipments are calibrated according to GT-521-9800 Rev D standard (Met One Instruments Inc., 2001) for accurate measurement.

Figure 1. Met one particle counter GT-521

Figure 2. Anemometer kit 4 in 1

3. Modelling of Particle Distribution

Modelling process involved several steps which include selecting application mode, assigning constant parameters, creating geometry, meshing, and selecting solver parameter and running the simulation. For this study, the selected module is k-ε analysis in application mode of chemical engineering of Comsol Multiphysics software. This module adopted Navier-Stokes equation which is characterized by density of air, dynamic viscosity, velocity of air, pressure, and gravity as in Equation 2.

$$\rho\frac{du}{dt} - \nabla.[\eta(\nabla u+(\nabla u)^T)] + \rho(u.\nabla)u + \nabla p = F \quad (2)$$

Where;

- η is the dynamic viscosity (kg/m.s).
- u is the velocity (m/s).
- ρ is the density (kg/m^3).
- p is the pressure (Pa).
- F is a volume force such as gravity (m/s^2).

For modelling particle dispersion, mass transportation module with Lagrangian analysis in application mode of chemical engineering in Comsol Multiphysics software was selected. This module used diffusion equation which is characterized by mass concentration, diffusion coefficient, and reaction rate as formulated in Equation 3.

$$\partial\frac{\partial c}{\partial t} + \partial(-D\partial c) = R \quad (3)$$

Where;

- C is the mass concentration (mol/m^3).
- D is the diffusion coefficient (m^2/s).
- R is the reaction rate (mol/m^3).

Once the parameters in Navier-Stokes and diffusion equation were filled, then meshing was carried out to divide the geometry model into smaller shape or area. To solve mesh problem, solver parameter is needed and for this study Direct (Pardiso) linear system solver was used. This solver was selected because it is more efficient in memory storage for 2D analysis as compared to other solver parameters in 2D such as Direct (UMFPACK) and Direct (SPOOLES).

3.1 Air Movement

Modelling process of air movement involved 778 elements with 7,091 degree of freedom solved within 32.503 sec as shown in Figure 3. The simulation result shows that, the maximum of air velocity in this laboratory is 1.272 m/s, while the air velocity at the occupant's location is in the range of 0.005 m/s to 0.43 m/s. For airflow estimation, the air velocity at the occupant's location is multiplied with its area. Thus, the estimated airflow for this laboratory is in the range of 6.05 m^3/s to 52.03 m^3/s. The airflow movement is originated through inject airflow from air-conditioning system and distributed to the laboratory space where the airflow movement was mostly distributed to the corner as depicted in Figure 4. The rate of ventilation is calculated by dividing estimated airflow with the number of occupant. Hence, for this laboratory the rate of ventilation calculated is in the range of 302.5 l/s/p to 2,601.5 l/s/p.

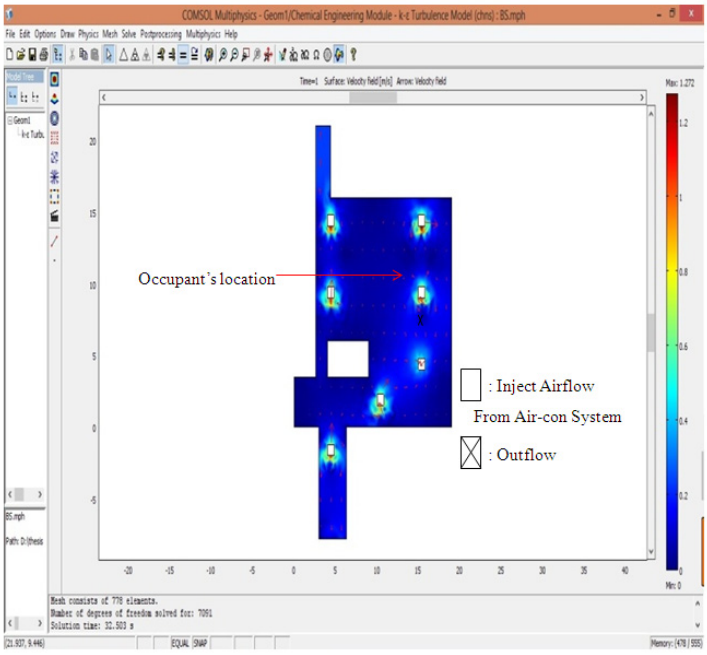

Figure 3. Air velocity distribution

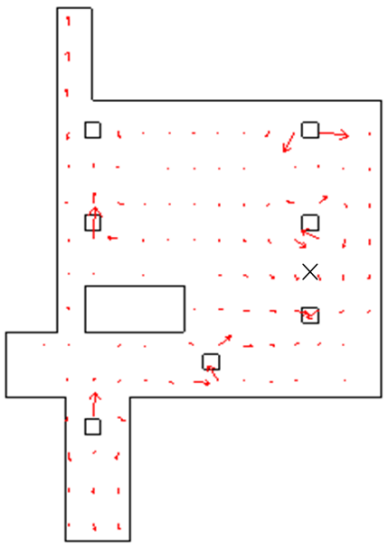

Figure 4. Airflow movement

Average hourly data of air velocity distribution generated from the simulation was compared with the measured average hourly data for validation purpose. The comparison of the average hourly data for duration of eight hours is as shown in Figure 5. The measured value is below than the simulated value with percentage difference range from 6 % to 9 % as in Table 1.

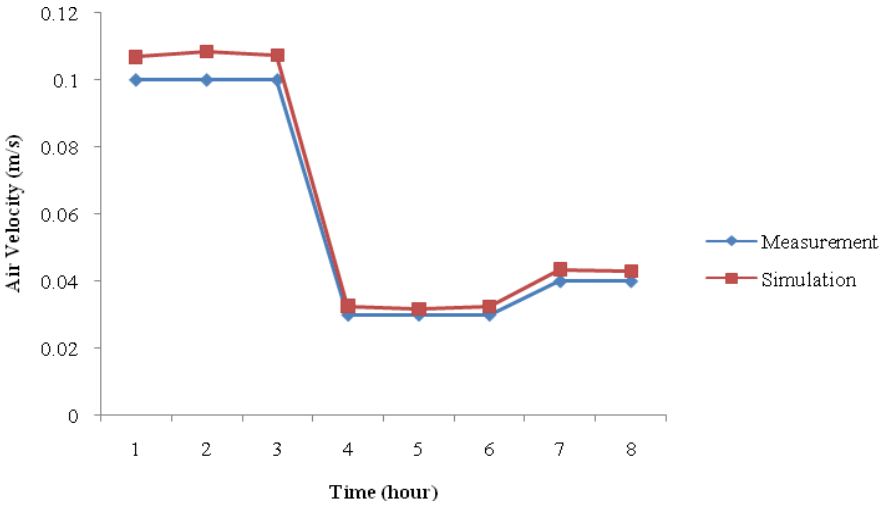

Figure 5. Measured vs. simulated of air velocity

Table 1. Percentage difference between measurement and simulation results

Hours	Air Velocity (m/s)		PD (%)
	Measurement	Simulation	
1	0.1	0.107	7
2	0.1	0.1085	8.5
3	0.1	0.1075	7.5
4	0.03	0.0327	9
5	0.03	0.0318	6
6	0.03	0.0324	8
7	0.04	0.0436	9
8	0.04	0.043	7.5

3.2 Particle Dispersion

For particle dispersion with size ≥ 0.3 µm, the modelling process involved 778 elements with 1,663 degree of freedom solved within 27.5 sec as in Figure 6. The figure shows dispersion of the particle in the laboratory where the maximum value of particle dispersion is $4.532.10^{-16}$ mol/m^3 which is equal with 272,826,400 particle/m^3, while the minimum value of particle dispersion is $1.483.10^{-16}$ mol/m^3 which is equal with 89,276,600 particle/m^3. The dispersion of particle is increasing in the corner of this laboratory as shown in Figure 7, where it location is quite far from air-conditioning system.

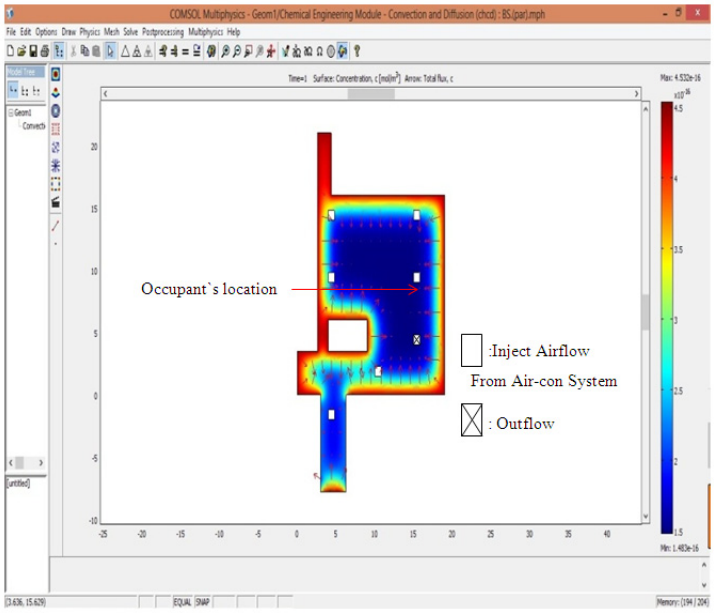

Figure 6. Particle dispersion

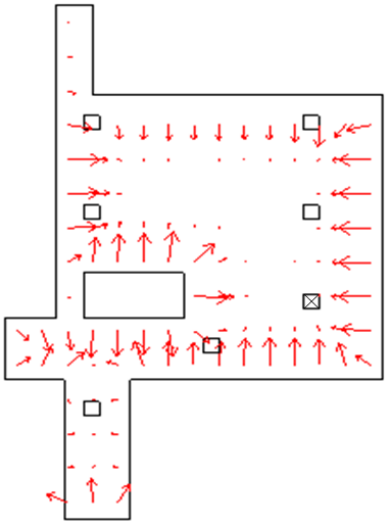

Figure 7. Path of particle dispersion

Beside air velocity, the comparison is also on particle dispersion. The average hourly data for particle dispersion simulated and measured within duration of eight hours are as shown in Figure 8. Differences of the values are in the range of 6.7 % to 10 % as in Table 2.

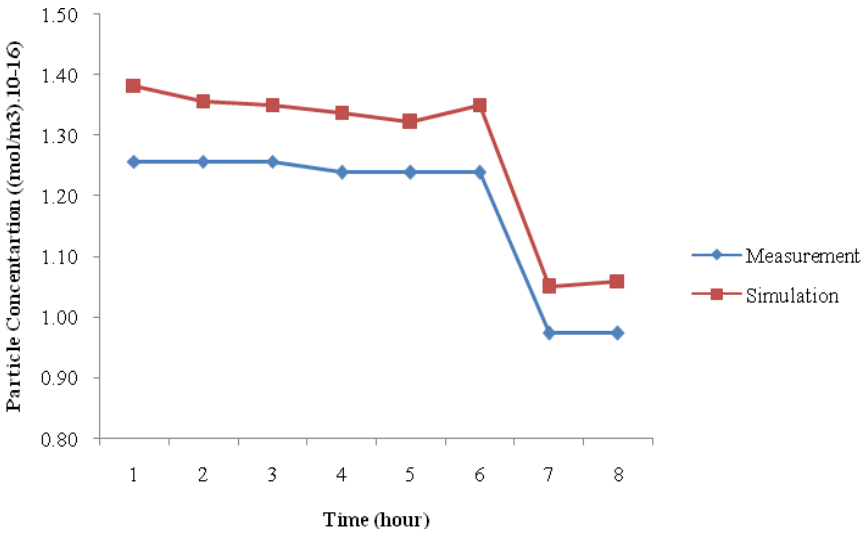

Figure 8. Measured vs. simulated of particle dispersion

Table 2. Percentage difference between measurement and simulation results

Hours	Particle Distribution (mol/m^3)		PD (%)
	Measurement	Simulation	
1	1.2569E-16	1.383E-16	10
2	1.2569E-16	1.357E-16	8
3	1.2569E-16	1.351E-16	7.5
4	1.23924E-16	1.338E-16	8
5	1.23924E-16	1.322E-16	6.7
6	1.23924E-16	1.351E-16	9
7	9.74E-17	1.05E-16	7.8
8	9.74E-17	1.06E-16	8.8

According to Chowdhury et al. (2008), and Judkoff et al. (2008), tolerable percentage difference is in the range of 6 – 10 %. Hence, this is within the suggested tolerance. The discrepancy of air velocity and particle dispersion maybe due to the dissimiliarities of air density, dynamic viscosity, diffusion coefficient, and reaction rate applied in Comsol Multiphysics model.

From the simulation results, particle dispersion is influenced by airflow movement of the space. The dispersion is lesser at the centre of the space due to presence of diffuser which discharges the airflow and causing the particle spreading to the corner of the space. The result of this simulation works found that the ventilation rate of the space is in the range of 302.5 l/s/p – 2,601 l/s/p and this meet with ASHRAE standard of minimum ventilation rate for indoor space which is 10 l/s/p.

4. Conclusions

This study demonstrates the simulation works regarding the airflow movement and particle dispersion using Comsol Multiphysics software. It is to assess the influence of air movement towards particle dispersion in a well ventilated space. The simulated results are validated with the measured value and found that the percentage differences are within 6 – 10 % which is accepted by many researchers. This study found that the amount of particle dispersion increased toward the corner of the space and concurrently with the airflow movement which is similar with finding from (Cheong et al., 2003). This is indicates that the particle dispersion depends on the airflow movement.

Acknowledgements

Thanks and gratitude to Ministry of Higher Education Malaysia and Research and Innovation Centre of Universiti Tun Hussein Onn Malaysia for funding this paper under Short Term Grant (STG) vote 1073.

References

Abadie, M. O., & Limam, K. (2007). Numerical evaluation of the particle pollutant homogeneity and mixing time in a ventilated room. *Building and Environment, 42*(11), 3848-3854. http://dx.doi.org/10.1016/j.buildenv.2006.11.010

Bambang, B. P. (2008). *Analysis of Natural Ventilation at Meeting Room of Physics Engineering and Residential House*. Bandung Institute of Technology.

Cheong, K. W. D., Djunaedy, E., Poh, T. K., Tham, K. W., Sekhar, S. C., Wong, N. H., & Ullah, M. B. (2003). Measurements and computations of contaminant' s distribution in an office environment. *Building and Environment, 38*, 135-145. http://dx.doi.org/10.1016/S0360-1323(02)00031-8

Chowdhury, A. A., Rasul, M. G., & Khan, M. M. K. (2008). Thermal-comfort analysis and simulation for various low-energy cooling-technologies applied to an office building in a subtropical climate. *Applied Energy, 85*(6), 449-462. http://dx.doi.org/10.1016/j.apenergy.2007.10.001

Chung, K. C. (1995). Three dimensional analysis of airflow and contaminant particle transport in a partitioned enclosure. *Building and Environment, 34*, 7-17. http://dx.doi.org/10.1016/S0360-1323(97)00073-5

COMSOL. (2007). COMSOL Multiphysics Quick Start and Quick Reference V.3.4. In *Comsol Multiphysics*. COMSOL AB.

Ismail, A. R., Jusoh, N., Zulkifli, R., Sopian, K., & Deros, B. M. (2009). Thermal Comfort Assessment : A Case Study at Malaysian Automotive Industry. *American Journal of Applied Sciences, 6*(8), 1495-1501.

Judkoff, R., Wortman, D., Doherty, B. O., & Burch, J. (2008). *A Methodology for Validating Building Energy Analysis Simulations*.

Meckler, M. (1991). *Indoor Air Quality Design Guidebooks*. Lilburn, GA, USA: Fairmoont Press.

Mendonça, K. C., Abadie, M. O., & Blondeau, P. (2012). Modeling Particle Distribution Using The Zonal Approach: Case Study of a Hospital Room. In *Ventilation 2012* (pp. 1-6).

Met One Instruments Inc. (2001). *MODEL GT-521 PARTICLE COUNTER OPERATION MANUAL - GT-521-9800 Rev. D*. NW Washington Blvd. Grant Pass, Oregon 97526.

Paul, T., Sree, D., & Aglan, H. (2010). Effect of mechanically induced ventilation on the indoor air quality of building envelopes. *Energy and Buildings, 42*(3), 326-332. http://dx.doi.org/10.1016/j.enbuild.2009.09.010

Pryor, R. W. (2011). *Multiphysics Modeling Using COMSOL: A First Principles Approach*. Sudbury, Massachusetts: JONES and BARTLETT.

Robinson, S. (2007). Conceptual modelling for simulation Part I: definition and requirements. *Journal of the Operational Research Society, 59*(3), 278-290. http://dx.doi.org/10.1057/palgrave.jors.2602368

Rouaud, O., & Havet, M. (2002). Computation of the airflow in a pilot scale clean room using K- “turbulence models ` les de turbulence K-” pour le calcul de Utilisation de mode ´ coulement d ’ air dans une salle blanche a l ’ e ´ chelle pilote l ’ e. *International Journal of Refrigeration, 25*, 351-361.

Shannon, R. E. (1975). *Systems Simulation - The Art and Science*. *BBAA VI International Colloqium on: Bluff Bodies Aerodynamics & Applications*. NJ: Prentice- Hall.

Tian, Z. F., Tu, J. Y., Yeoh, G. H., & Yuen, R. K. K. (2006). On the numerical study of contaminant particle concentration in indoor airflow. *Building and Environment, 41*, 1504-1514. http://dx.doi.org/10.1016/j.buildenv.2005.06.006

Wong, N. H., & Huang, B. (2004). Comparative study of the indoor air quality of naturally ventilated and air-conditioned bedrooms of residential buildings in Singapore. *Building and Environment, 39*, 1115-1123. http://dx.doi.org/10.1016/j.buildenv.2004.01.024

Yau, Y. H., Chew, B. T., & Saifullah, A. Z. a. (2012). Studies on the indoor air quality of Pharmaceutical Laboratories in Malaysia. *International Journal of Sustainable Built Environment, 1*(1), 110-124. http://dx.doi.org/10.1016/j.ijsbe.2012.07.005

Yu, B. F., Hu, Z. B., Liu, M., Yang, H. L., Kong, Q. X., & Liu, Y. H. (2009). Review of research on air-conditioning systems and indoor air quality control for human health. *International Journal of Refrigeration, 32*(1), 3-20. http://dx.doi.org/10.1016/j.ijrefrig.2008.05.004

Modern Applied Science; Vol. 8, No. 3; 2014
ISSN 1913-1844 E-ISSN 1913-1852
Published by Canadian Center of Science and Education

Study on Migration from IPv4 to IPv6 of a Large Scale Network

Muhammad Yeasir Arafat[1], M Abdus Sobhan[1] & Feroz Ahmed[1]

[1] Department of Electrical and Electronic Engineering, School of Engineering and Computer Science, Independent University, Bangladesh

Correspondence: Muhammad Yeasir Arafat, School of Engineering and Computer Science, Independent University, Bangladesh. Tel: 88-017-1930-1525. E-mail: yeasir08@yahoo.com

Received: February 11, 2014 Accepted: April 1, 2014 Online Published: April 8, 2014

doi:10.5539/mas.v8n3p67 URL: http://dx.doi.org/10.5539/mas.v8n3p67

Abstract

This work mainly addresses the design a large scale network using dual stack mechanisms. We concentrated on the most imperative theoretical notions of the IPv6 protocol, such as IP addressing, address allocation, routing with the OSPF and BGP protocols and routing protocols performance in dual stack network using GNS3 simulations and Wireshark Network protocol analyzer. It is evaluate a real large-scale network environment utilizing accessible end-to-end estimation methods that focuses on a large-scale IPv4 and IPv6 backbone and made performance the IPv4 and IPv6 network. In this paper, we compiled IPv6 address planning in a large scale network, performance metrics of each network in terms of time sequence graph, round trip time, TCP throughput, TCP connection time and the number of TCP connections per second that a client can establish with a remote server. It is found that, a minor degradation in the throughput of the TCP, TCP response time and a lower packet loss rate are arise in a real large scale dual stack network. We also showed a concise case study on relationship between RTT and network topology, which is cooperative to develop the performance of IPv6 networks. The result shows the proposed scheme for network migration from IPv4 to IPv6 is more reliable than other existing schemes.

Keywords: IPv6, IPv4, double stack, simulators, performance measurement, BGPv4, OSPFv3, migration, ISP

1. Introduction

Currently, the Internet consists of native IPv4, native IPv6, and IPv4/IPv6 dual stack networks. Unfortunately, IPv4 and IPv6 are unsuited protocols. When both IP versions are available and the users of Internet desire to connect without any limitations, a transition mechanism is mandatory. During the occasion of migration from IPv4 to IPv6 networks, a number of transition mechanisms have been suggested by IETF to ensure smooth, stepwise and independent changeover. The conception of transiting from IPv4 mesh to IPv6 mesh is being processed strongly. The transition between IPv4 internet and IPv6 will be a long procedure as they are two completely separate protocols. IPv6 is not backward well-suited with IPv4, and IPv4 hosts and routers will not be adept to deal directly with IPv6 traffic and vice-versa. As IPv4 and IPv6 will co-exist for a long time, this wants the transition and inter-operation mechanism. Due to this cause several transitions mechanisms have been developed that can be used to build the transition to IPv6 efficiently. Most of the applications today support IPv4 and therefore there is a need to run these applications on IPv6 access network, especially to persons who are generally on mobile and they want to securely connect to their home network so as to reach IPv4 services. IPv6 is developed as a network layer protocol, overcoming the problems in IPv4. Its 128-bit address format considerably enlarges the address space and will gratify the address demands for a fairly long time. Although, IPv6 has no built-in backwards compatibility with IPv4, which means IPv6 networks cannot correspond with IPv4 in environment. Competently IPv6 has considered a parallel, independent network that coexists with its support IPv4. IPv6-supported applications and IPv6-accessible contents are still the marginal; the majority of network resources, services and applications still remain in IPv4. A number of transition techniques are existing to maintain the connectivity of both IPv4 and IPv6, to accomplish inter connection between IPv4 and IPv6, and also support the adoption process of IPv6. Vendors expect to invest on implementing well-developed transition techniques, so that their products can have good capability and bring high profits. As for internet service providers (ISP), they require to find a way to provide the existing services for both IPv4 and IPv6 users, and organize their services with an expected deployment of transition techniques on the Internet.

In this paper first, present an IP address planning and network design for dual stack network which encompass

IPv4 and IPv6 address simultaneously. A large scale network implemented with help of advance dynamic routing protocols. Second, investigate the different behaviors of IPv6 performance on a path-by-path basis over time performance. In this paper a virtual study of the performance of IPv4-only network with that of dual stack transition mechanism (DSTM) under various types of traffic patterns is accepted out. In the proposed DSTM enabled network architecture, the hosts in IPv4 network commences connection with hosts in the IPv4 network over an integrated IPv4/IPv6 network. The analysis makes use of Wireshark graphing capabilities to showed round trip time for ACKs overt time known as a round trip time graph, transmission throughput using TCP sequence numbers called throughput graph, sequence number versus time graphs that help to see if traffic is moving along without interruption, packet loss, or long delays called as time sequence graph Stevens and tcptrace.

2. Transition Method

Since there is such a large difference between IPv4 and IPv6, they cannot communicate directly with each other. A system that is capable of handling IPv6 traffic can be made backward compatible, but an already deployed system that handles only IPv4 is not able to handle IPv6 datagram. This means that a major upgrade process would need to take place, involving hundreds of millions of machines, in order to make a complete transition to IPv6. This way is too expensive and time consuming and in any case will not happen overnight. The network world will most likely see a gradual transition to IPv6, where IPv6 will be integrated into the IPv4 world that exists today. There are different kinds of technologies which can be applied such as dual stack, tunnelling, and translation. At present, three transition mechanisms, dual stack, tunneling, and translation, are proposed to solve the problems due to the co-existence of IPv6 and IPv4. Over several transition techniques have been used and tested for the communications between different networks to ensure IPv4 and IPv6 interoperability. Therefore, to make decision on the best suited transition methods, it is really important to have an overview of the current IPv4 networks. In addition, enterprises must analyze needed functionalities, scalability, and securities in the corporation.

2.1 Dual Stack

The Dual Stack technique is entitled as native dual stack or dual IP layer. Both protocols IPv4 and IPv6 run parallel on the similar network infrastructure which does not necessitate encapsulation of IPv6 interior IPv4 and vice versa. A common dual-stack migration approach as shown in Figure 1 makes a transition from the core to the edge. This includes enabling two TCP/IP protocol stacks on the WAN core routers. In a common dual stack migration firstly the edge routers, and firewalls, then the server-farm switches and finally the desktop access routers. Once the network supports IPv6 and IPv4 protocols, the process will enable dual protocol stacks on the servers and then the edge entities. The dual stack doubles the communication requirements, which in turn causes performance degradation. The dual stack method is literally to use two IPv4 and IPv6 stacks for operating simultaneously, which enables apparatus to run on either protocol, according to accessible services, network availability, and administrative policies. This can be accomplished in both end systems and network devices. As a result, IPv4 enabled programs use IPv4 stack and this goes the identical for IPv6.

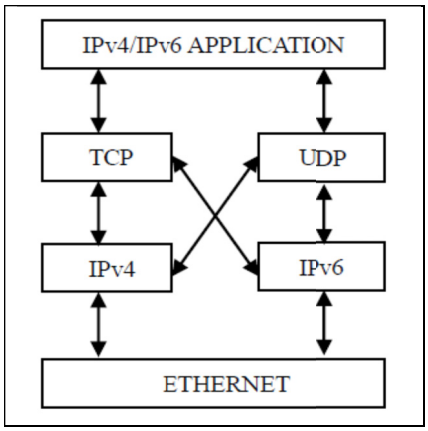

Figure 1. Dual stack mechanism

The IP header version field would play an important role in receiving and sending packets. In other words, this kind of IPv6 transition is the encapsulation of IPv6 within IPv4. The complete transition can be managed by domain name system (DNS).

2.2 Tunnelling

Tunnelling, from the insight of transitioning, enables unsuited networks to be bridged and it is usually applied in a point-to-point or sequential manner of a network. Three mechanisms of tunnelling are offered: IPv6 over IPv4, IPv6 to IPv4 automatic tunnelling and tunnel broker. Tunnelling IPv6 traffic over an IPv4 network is another possibility. This approach allows the IPv6 traffic to be encapsulated in an IPv4 packet and forwarded, creating an IPv6 tunnel over the IPv4 infrastructure. A tunnel can be created as a solution for transporting IPv6 traffic, from IPv6 node to the destination IPv6 node, over the IPv4-only network. A "virtual link" is created and, from the perspective of the two establishing IPv6 nodes, this appears as a point-to-point link. The different types of tunnelling techniques can be categorized into two types: manually configured and automatic tunnelling. A point-to-point link has to be manually configured, as the name suggests. For automatic tunnelling, an IPv6 node can dynamically tunnel packets by using a 6 to 4 address. This is used to transfer data between compatible networking nodes over incompatible networks. There are two ordinary scenarios to apply tunnelling: the allowance of end systems to apply off link transition devices in a distributed network and the act of enabling edge devices in networks to inter-connect over incompatible networks.

2.3 Translation

The meaning of translation is to convert directly protocols from IPv4 to IPv6 or vice versa, which might result in transforming those two protocol headers and payload. This mechanism can be established at layers in protocol stack, consisting of network, transport, and application layers. The translation method has many mechanisms, which can be either stateless or stateful. While stateless means that the translator can perform every conversion separately with no reference to previous packets, stateful is the vice versa, which maintains some form of state in regard to previous packets. The translation process can be conducted in either end systems or network devices. The fundamental part of translation mechanism in transition process is the conversion of IP and ICMP packets. All translation methods, which are used to establish communication between IPv6-only and IPv4-only hosts, for instance, NAT-PT or BIS, apply an algorithm known as stateless IP/ICMP translator (SIIT).

3. Design a Large Scale Network in Dual Stack

In this paper, a large scale network is design based on dual stack network. This dual stack network is designed for a nationwide ISP. Design considerations are given below:

3.1 Topology Design

In this paper our designed ISP has 4 main operating area or region. Each region has 2 small POP. Each region network has one data centre to host content. Regional network are inter-connected with multiple link.

(i) *Regional Network*

Each regional network has three routers. One core and two edge routers, point of presence (POP) for every region. POP will use a router to terminate customer network, i.e. edge router. Each POP is an aggregation point of ISP customer.

(ii) *Design Consideration*

Each regional network should have address summarization capability for customer block and CS link WAN. Prefix planning should have scalability option for next couple of years for both customer block and infrastructure. No Summarization require for infrastructure WAN and loopback address. All WAN links should be ICMP reachable for link monitoring purpose. Conservation will get high preference for IPv4 address planning and aggregation will get high preference for IPv6 address planning. OSPF is running in ISP network to carry infrastructure IP prefix. Each region is a separate open shortest path first (OSPF) area. Transport core is in OSPF area 0. Customer will connect on either static or external border gateway protocol (eBGP). Internal border gateway protocol (iBGP) will carry external prefix within ISP core IP network.

(iii) *IPv6 Address Plan Consideration*

Big IPv6 address space can cause very large routing table size. Most transit service provider apply IPv6 aggregation prefix filter (i.e. anything other than /48 &<=/32 prefix size. Prefix announcement need to send to internet should be either /32 or /48 bit boundary IPv6 address plan consideration (RFC3177). WAN link can be used on /64 bit boundary. End site/customer sub allocation can be made between /48~/64 bit boundary. APNIC utilization/HD ratio will be calculated based on /56 end site assignment/sub-allocation.

(iv) *Addressing Plans – ISP Infrastructure*

• *Point-to-Point links:* Protocol design expectation is that /64 is used (/127 now recommended/standardized (rfc6164)). (Reserve /64 for the link, but address it as a /127).

• *Other options:* A /126s are being used (mirrors IPv4 /30). A /112s are being used. For node ID we have leaves free final 16 bits. There are some discussion about /80s, /96s and /120s.

• *ISPs should receive /32 from their RIR:* Normally address block for router loop-back interfaces a number all loopbacks out of one /48 address. We have used /128 IP address for loopback. Address block for infrastructure /48 network block allow 65k subnets. A /48 network address per region, this is for the largest international networks. A /48 network address for whole backbone. Customers get one /48 block network address. Unless they have more than 65k subnets inwhich case they get a second /48 (and so on). In typical deployments today Several ISPs give small customers a /56 or single LAN end-sites a /64, e.g.: /64 if end-site will only ever be a LAN. A /56 block network for medium end-sites (e.g. small business) and a /48 network block for large end-sites. Registries will regularly assign the next block to be contiguous with the first allocation, minimum allocation is /32. Very expected that subsequent allocation block will make this up to a /31.

• IPv6 Allocation Form registry is: 2406:6400::/32.

• IPv4 Allocation From registry is: 172.16.0.0/19.

3.2 Address Plan for IPv6

For the address planning we followed RFC 3849, which is IPv6 address prefix reserved for documentation. Details IP address plan for IPv6 is given below (Tables 1 to 8):

Table 1. Top level distribution infrastructure and customers

Block	Prefix	Description
1	2406:6400::/32	Parent Block
2	2406:6400:0000:0000::/36	Infrastructure
	2406:6400:1000:0000::/36	
	2406:6400:2000:0000::/36	
	2406:6400:3000:0000::/36	
	2406:6400:4000:0000::/36	
	2406:6400:5000:0000::/36	
	2406:6400:6000:0000::/36	
	2406:6400:7000:0000::/36	
3	2406:6400:8000:0000::/36	Customer network Region 1
	2406:6400:9000:0000::/36	
4	2406:6400:a000:0000::/36	Customer network Region 2
	2406:6400:b000:0000::/36	
5	2406:6400:c000:0000::/36	Customer network Region 3
	2406:6400:d000:0000::/36	
6	2406:6400:e000:0000::/36	Customer network Region 4
	2406:6400:f000:0000::/36	

Table 2. Summarization option infrastructure and customers

Block	Prefix	Description
7	2406:6400:8000:0000::/35	CS net summery region1 [R2]
8	2406:6400:a000:0000::/35	CS net summery region2 [R5]
9	2406:6400:c000:0000::/35	CS net summery region3 [R8]
10	2406:6400:e000:0000::/35	CS net summery region4 [R11]

Table 3. Details distribution infrastructure

Block	Prefix	Description
2	2406:6400:0000:0000::/36	Infrastructure
11	2406:6400:0000:0000::/40	Loopback, Transport & WAN
	2406:6400:0100:0000::/40	
	2406:6400:0200:0000::/40	
	2406:6400:0300:0000::/40	
	2406:6400:0400:0000::/40	
	2406:6400:0500:0000::/40	
	2406:6400:0600:0000::/40	
	2406:6400:0700:0000::/40	
16	2406:6400:0800:0000::/40	R2 DC
	2406:6400:0900:0000::/40	
17	2406:6400:0a00:0000::/40	R5 DC
	2406:6400:0b00:0000::/40	
18	2406:6400:0c00:0000::/40	R8 DC
	2406:6400:0d00:0000::/40	
19	2406:6400:0e00:0000::/40	R11 DC
	2406:6400:0f00:0000::/40	

Table 4. Details loopback address

Block	Prefix	Description
20	2406:6400:0000:0000::/48	Loopback
43	2406:6400:0000:0000::1/128	R1 loopback 0
44	2406:6400:0000:0000::2/128	R2 loopback 0
45	2406:6400:0000:0000::3/128	R3 loopback 0
46	2406:6400:0000:0000::4/128	R4 loopback 0
47	2406:6400:0000:0000::5/128	R5 loopback 0
48	2406:6400:0000:0000::6/128	R6 loopback 0
49	2406:6400:0000:0000::7/128	R7 loopback 0
50	2406:6400:0000:0000::8/128	R8 loopback 0
51	2406:6400:0000:0000::9/128	R9 loopback 0
52	2406:6400:0000:0000::10/128	R10 loopback 0
53	2406:6400:0000:0000::11/128	R11 loopback 0
54	2406:6400:0000:0000::12/128	R12 loopback 0

Table 5. Summarization customers block region 1

Block	Prefix	Description
	2406:6400:8000:0000::/35	Customer block region 1 [R2]
	2406:6400:8000:0000::/37	Customer block POP1 [R1]
	2406:6400:8800:0000::/37	Customer block future use/POP
	2406:6400:9000:0000::/37	Customer block future use/POP
	2406:6400:9800:0000::/37	Customer block POP2 [R3]

Table 6. Summarization customers block region 2

Block	Prefix	Description
	2406:6400:A000:0000::/35	Customer block region 2 [R5]
	2406:6400:A000:0000::/37	Customer block POP1 [R4]
	2406:6400:A800:0000::/37	Customer block future use/POP
	2406:6400:B000:0000::/37	Customer block future use/POP
	2406:6400:B800:0000::/37	Customer block POP2 [R6]

Table 7. Summarization customers block region 3

Block	Prefix	Description
	2406:6400:c000:0000::/35	Customer block region 3 [R8]
	2406:6400:C000:0000::/37	Customer block POP1 [R7]
	2406:6400:C800:0000::/37	Customer block future use/POP
	2406:6400:C000:0000::/37	Customer block future use/POP
	2406:6400:C800:0000::/37	Customer block POP2 [R9]

Table 8. Summarization customers block region 4

Block	Prefix	Description
	2406:6400:e000:0000::/35	Customer block region 4 [R11]
	2406:6400:E000:0000::/37	Customer block POP1 [R10]
	2406:6400:E800:0000::/37	Customer block future use/POP
	2406:6400:E000:0000::/37	Customer block future use/POP
	2406:6400:E800:0000::/37	Customer block POP2 [R12]

3.3 Address Plan for IPv4

IP address Plan for IPv4 is given below (Table 9 to 12):

Table 9. Parent block IPv4

Block	Prefix	Size	Description
1	172.16.0.0	/19	Parent Block
2	172.16.0.0	/20	Infrastructure
3	172.16.16.0	/20	Customer Network

Table 10. Details infrastructure WAN block IPv4

Block	Prefix	Size	Description
12	172.16.10.0	/24	WAN Prefix
13	172.16.10.0	/30	Router 2-1 WAN
14	172.16.10.4	/30	Router 2-3 WAN
15	172.16.10.8	/30	Router 1-3 WAN
16	172.16.10.24	/30	Router 5-4 WAN
17	172.16.10.28	/30	Router 5-6 WAN
18	172.16.10.32	/30	Router 4-6 WAN
19	172.16.10.48	/30	Router 8-7 WAN
20	172.16.10.52	/30	Router 8-9 WAN
21	172.16.10.56	/30	Router 7-9 WAN
22	172.16.10.72	/30	Router 11-10 WAN
23	172.16.10.76	/30	Router 11-12 WAN
24	172.16.10.80	/30	Router 10-12 WAN

Table 11. Details infrastructure block transport & loopback IPv4

Block	Prefix	Size	Description
25	172.16.12.0	/24	Transport link
26	172.16.13.0	/24	Transport link
27	172.16.15.0	/24	Loopback

Table 12. Details customer IPv4 block

Block	Prefix	Size	Description
28	172.16.6.0	/20	Customer network
29	172.16.16.0	/22	Router 2 summary net
30	172.16.16.0	/23	Router 1 CS network
31	172.16.18.0	/23	Router 3 CS network
32	172.16.20.0	/22	Router 5 summary net
33	172.16.20.0	/23	Router 4 CS network
34	172.16.22.0	/23	Router 6 CS network
35	172.16.24.0	/22	Router 8 summary net
36	172.16.24.0	/23	Router 7 CS network
37	172.16.26.0	/23	Router 9 CS network
38	172.16.28.0	/22	Router 11 summary net
39	172.16.28.0	/23	Router 10 CS network
40	172.16.30.0	/23	Router 12 CS network

4. Simulation and Analysis

Simulations are performed using GNS3. For the simulation we used Cisco 7200 series router. A server contain core i7 processor with 8GB RAM used for run the simulation.

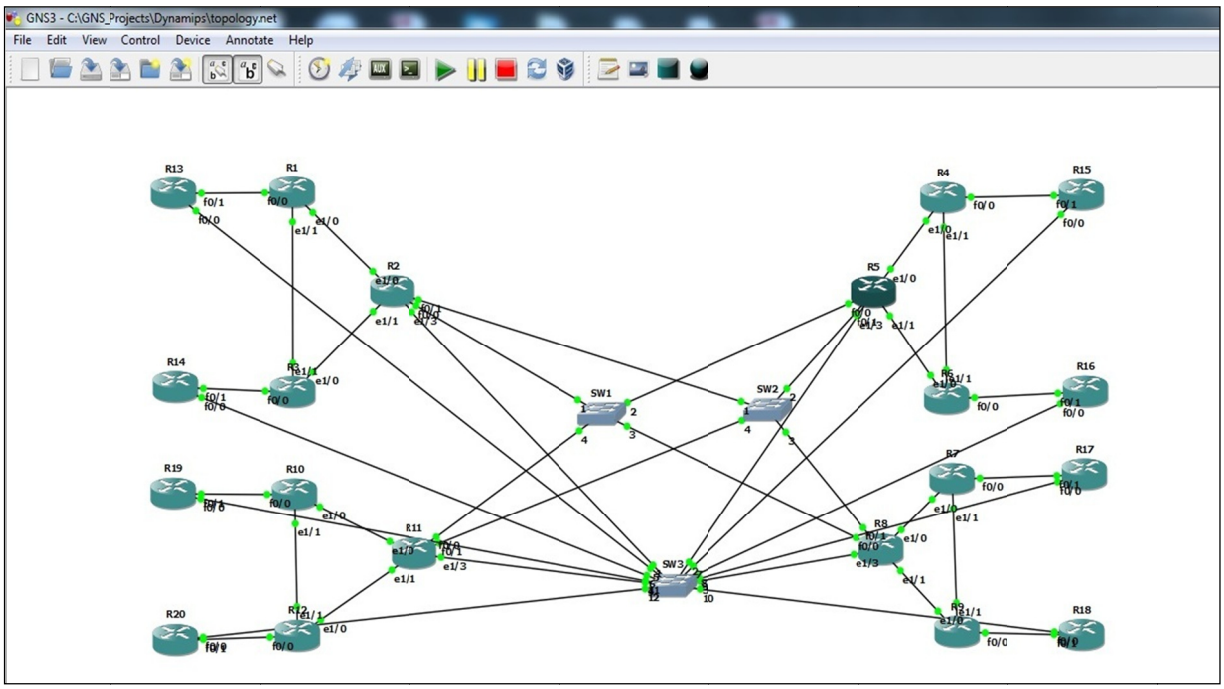

(a)

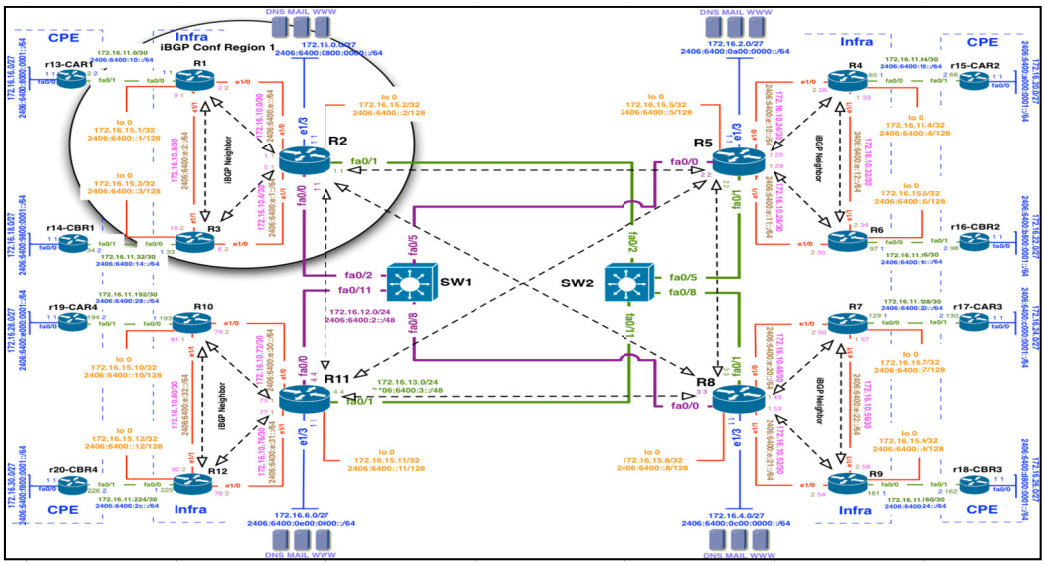

(b)

Figure 2. (a) Simulation network in GNS 3 (b) iBGP peering For Region 1 simulation Network in GNS 3

In the test bed dual stack network, an ISP has 4 main operating area or region. Each region has 2 small POP. POP will use a router to terminate customer network. GNS 3 topology is given in Figure 2(a).

4.1 Network Connection Pattern

Before enabling OSPF3 on an Interface, the following steps must be done on a Router. Enable IPv6 unicast routing and enable IPv6 CEF. In region 1 router R1, R2, R3 have iBGP peering with other networks showed in Figure 2(b).

In the same way R5, R4, R6 have iBGP peering with others in region 2. R8, R7, R9 have iBGP peering with others in region 3. R11, R10, R12 have iBGP peering with others in region 4.

4.2 Output and Analysis

For analysis routing protocols we used Wireshark. This paper contains details analysis of wireshark traces for investigating the behaviors of TCP congestions control mechanism. Packets are captured from the routers interface. It is discussed some measurement from the topology with necessary figures. The papers will analysis the following facets:

• Basic slow start and avoidance mechanisms in IP network.

• Variation of the TCP slow starts mechanism that uses fast retransmit followed by congestion avoidance.

• Receiver-advertised flow control mechanisms

• Round trip time and Throughput of the connections.

4.2.1 OSPFv3 Packet Analysis

There are two types of changes which may occur in the topology: link status changes and link weight changes. The OSPF protocol detects link status changes via the HELLO protocol. The Hello packet encloses no address information at all. Rather, it contains an Interface ID that the originating router has allottedto uniquely identify (among its own interfaces) its interface to the link. This Interface ID will be used as the network-LSA's link state ID if the router becomes the designated router on the link. The OSPF packet header now embraces an "Instance ID" that permits multiple OSPF protocol illustrations to be run on a single link. The neighbour arrangement performs the same function in both IPv6 and IPv4. Specifically, it collects all information mandatory to form an adjacency between two routers when such an adjacency becomes essential. When the OSPF protocol detects a change in the topology, it creates new LSAs appropriate for the cause and floods them throughout the OSPF domain. As the new LSAs are flooded they are accounted for in the "OSPF caused OSPF updates" statistic.

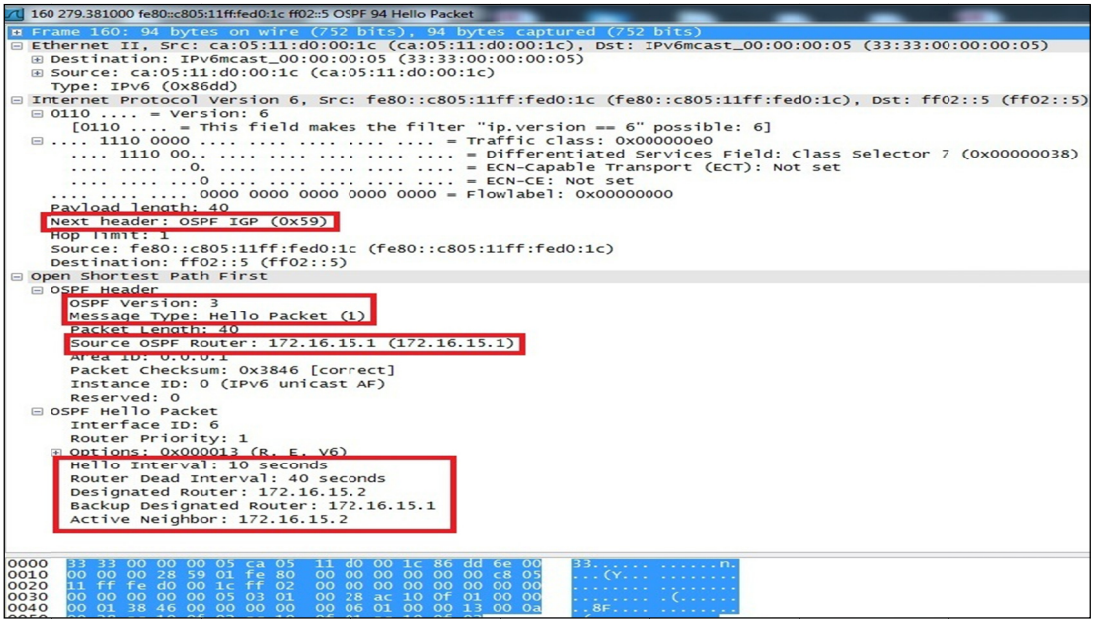

Figure 3. OSPF Hello packet

Each neighbor arrangement is hop to a single OSPF interface. The Interface ID that the neighbor advertises in its Hello packets should be traced in the neighbor structure. The router will include the neighbor's Interface ID in the router's router-LSA when either a) advertising a point-to-point or point-to-multipoint link to the neighbor or b) advertising a link to a network where the neighbor has become the designated router. In IPv6 OSPF sprints directly over IPv6's network layer. When, it is encapsulated in one or more IPv6 headers with the Next Header field of the immediately encapsulating IPv6 header set to the value 89. In Figure 3 we have shown OSPF v3 hello packet which source OSPF route from 172.16.15.1. This designated route from 172.16.15.2 and backup designated route from 172.16.15. This is OSPF hello packet, which next header is OSPF IGP. Hello packet

interval time duration is 10s. OSPF caused BGP updates are measured when the connection between two iBGPpeers changes. This signals a change in the underlying OSPF network between the peers, and so the cause of the subsequent updates is attributed to the OSPF protocol. All routing protocols create overhead when performing routing; often this is routing traffic overhead when exchanging information with other routers, this routing traffic is necessary for protocol operation. However in certain situations such as a rapidly changing network this traffic can come to consume large amounts of available bandwidth and be detrimental to the network throughput. Link state protocols such as OSPF are more complicated than distance vector protocols and create extra overhead in the form of bandwidth, memory and CPU usage in order to calculate and store the routing tables, in smaller networks this leads to EIGRP being more efficient. When used in larger networks. OSPFs hierarchical nature gives an advantage over EIGRP when used with properly configured areas in order to limit routing overhead. Simulations performed by found that IGP has better bandwidth utilization and lower protocol traffic than OSPF.

OSPFv3 packets are transmitted in IPv4 datagram's with a protocol identifier equals to 89. That is, OSPF does not use TCP or UDP in the transport layer. OSPF packets have a common header plus a specific part, resulting in five different types of packets: Hello (Type-1), Database Description (Type-2), Link-State Request (Type-3), Link-State Update (Type-4), and Link-State Acknowledgment (Type-5).

4.2.2 BGP Packet Analysis

BGP is the path-vector protocol that is work on exchanging external AS routing information and operates level of address blocks or AS prefixes. BGP routers exchange routing information using open, update, notification and keepalive message.A snippet of captured date showing update and keepalive message is shown in Figure 4 captured BGP traffic is from the TCP port 179. Figure 4 illustrates frame number 138 and the number of bytes captured on this frame. As messages originate from multiple protocols, the frame shows Ethernet protocol source and destination address, the source and destination addresses of IP, source and destinations port numbers for TCP and details of BGP. In Figure 4 we have shown BGP keep alive message from 2406:6400::1 to 2406:6400::2.

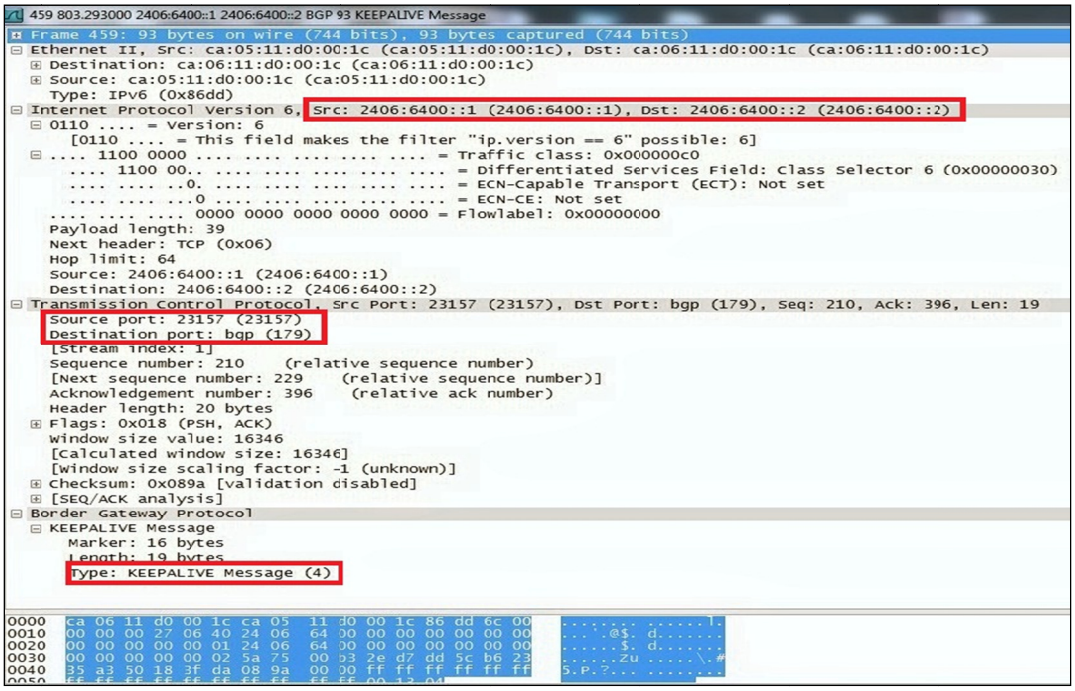

Figure 4. BGP Packet analysis

BGP operates over a Transmission Control Protocol (TCP) as a transport protocol (port number 179). TCP has an advantage over User Datagram Protocol (UDP) connections: BGP does not need to implement fragmentation, retransmission, acknowledgment, and sequencing. BGP has the capability to support Classless Inter-Domain Routing (CIDR) in order to reduce the size of the Internet routing tables. CIDR allows routers to group routes

together in order to minimize the number of routing information carried by the core routers, which makes it a dominant Internet routing protocol and allows the aggregation of routers. Internet Protocol version 6 (IPv6) uses CIDR routing technology and CIDR notation in the same way as Internet Protocol version 4 (IPv4). IPv6 was designed for fully classless addressing. In CIDR, all Internet blocks can be of random size and classless addressing uses a variable number of bits for the network and host portions of the address. A view of the traffic collected using Wireshark is shown in Figure 4. It illustrates the protocol structure for a randomly selected BGP update message, which contains path attributes for the advertised Network Layer reach ability Information (NLRI). It opens and saves captured packet data, imports and exports packet data from and to other capture programs, filters and searches packets based on various criteria, colorizes packet display based on filters, and creates various statistics.As messages originate from multiple protocols, the frame shows Ethernet protocol source and destination address, the source and destination addresses of IP, source and destinations port numbers for TCP, and details of BGP. The update message has a marker of 16 bytes and length of 19 bytes. There are four types of message like type 1 indicates open message, Type 2 indicates that this message is an update message, type 3 indicates notification message, and type 4 indicates keepalive message. IGP is assigned to the origin attribute, AS path attribute has a length of 19 bytes, maximum hop limit 64, and payload length 39 bytes.

4.2.3 TCP Operations

The TCP operation is defined in RFC1323 are no operation (for padding), maximum window size (SYN), window scale (SYN), SACK permitted (SYN), SACK option (Acknowledges), time stamp (SYN & Acknowledges). The usage of the TCP SACK option is negotiated during the 3-Way hand shake. The Selective acknowledgement (SACK) option can be activated from one or both sides. Without SACK option, only the last received segment of a contiguous series can be acknowledged. The SACK Option allows acknowledging non-contiguous segments of a series and can request for specific segments. The SACK Option can improve the throughput of LFN's significantly. Acknowledges (ACK) is used to point whether the acknowledgment field is valid. PSH is place when the sender requests the remote application to push this data to the remote application. RST is used to reset the connection. SYN (for synchronize) is used inside the connection start up phase, and FIN (for finish) is used to close the connection in an arranged mode. Information gathered during the handshake consists of the sender and receiver advertised window Sizes (rwnd), maximum segment size (MSS), whether a window scale option (WS) is being used, and if the sender and receiver support selective acknowledgement (SACK) options. The TCP checksum is applied to a synthesized header that contains the source and destination addresses from the external IP datagram. The first stage of a TCP session is establishment of the connection. This requires a three-way handshake, ensuring that both sides of the connection have an explicit understanding of the sequence number space of the remote side for this session.

The performance insinuation of this protocol exchange is that it takes one and a half round-trip times (RTTs) for the two schemes to synchronize status before any data can be sent. Once the connection is established, TCP starts slowly to determine the bandwidth of the connection and to avoid overflowing the receiving host and other devices or links in the path. After the connection has been established, the TCP protocol manages the consistent exchange of data between the two systems. The traffic service reply time is explicit as the time between a request and the corresponding response. A single packet of length 19 is sent with the PSH flag set. The PSH flag indicates to the receiver that the contents of the receive buffer should be immediately passed to the application layer. Another data packet of size 19 is sent. At this point there are 20 bytes of in flight or unacknowledged data on the wire.

Figure 5. TCP connection handshake

The sequence number of the TCP SYN segment that is used to initiate the TCP connection between the router to router. The flow graph shows the BGP peers participating in the traffic exchange. At time 16.146 s, an update message is sent from source address 172.16.15.1 to the destination address 172.16.15.2, port 179 and the destination sends an acknowledgement back to the source implying that it is ready for traffic exchange. An exchange of data happens between only two BGP peers at a time.When the addresses 172.16.15.1 and 172.16.15.2 exchange data among themselves, there is no data exchanged between 2406:6400::1 and 2406:6400::2.

The receiver acknowledges (ACK) data sent by the sender. A window size (rwnd) of 16346 is also advertised by the receiver with this ACK. When the connection was established, a congestion window (cwnd) of size 1 MSS (size 1460 bytes) is initialized. Each time an ACK is received this congestion window is increased by 1 MSS. With ACK sent with, the congestion window size is increased by 1, like, cwnd = cwnd + 1 MSS, or 2 MSS = 2920 bytes. This pattern of sending data and receiving ACKs between the sender and receiver continues. When congestion is encountered, as indicated in the trace by a fast retransmission, a congestion avoidance algorithm is used to reduce the sender's window size, and to grow it back towards the receiver's advertised window size. Congestion avoidance requires that another variable be maintained called the slow start threshold or sshtresh. The flow graph of the captured IPv4 and IPv6 traffic is shown in Figure 5. It includes the source address, destination address, TCP port number, TCP message (ACK).The flow graph has shown the IPv4 and IPv6 BGP peers participating in the traffic exchange. At time 17.738 s, an ACK message is sent from source address 172.16.15.2 to the destination address 172.16.15.1 and the destination sends an acknowledgement back to the source implying that it is ready for traffic exchange. An exchange of data happens between only two BGP peers at a time. At time 55.521 s, an ACK message is sent from source address 2406.6400::2 to the destination address 2406.6400::1 and the destination sends an acknowledgement back to the source implying that it is ready for traffic exchange. An exchange of data happens between only two BGP peers at a time. When the destination address receives the acknowledgement, it knows that the link is active and it resumes the data exchange again. The Wireshark System recognizes many abnormalities or errors and creates a list sorted by severities likes: segment lost, duplicate ACK, retransmissions, fast Retransmissions, zero window and window full.

4.2.4 Time Sequence Graph

Time sequences show the general activity and events that occur during the lifetime connection. The X-axis represents time, and Y-axis represents sequence number space. TCP Stream Graph allows recognizing all the

following abnormalities:

• *Lost Frames*

• Duplicate Frames

• Out of order Frames

• TCP Sequence number and Segment Sizes

• Acknowledges, Delayed Acknowledges

• Duplicate and Selective Acknowledges

• Retransmissions and Fast Retransmissions

• Windows Sizes, sliding Window, exceeded und frozen Windows Size

• Window Scaling, Zero Window and Window Full Situation

• Slow Start, full Flow rate and Flow throttling

A graph of TCP sequence numbers versus time is given in Figure 6. When an ACK is obtained, it contains the sequence number relating to the following byte to be received. By default, Wireshark convert all sequence numbers into relative numbers to facilitate comprehension and tracking of the loads engaged in a TCP session. This means that the sequence number corresponding to the first packet in a TCP connection always begins with 0 and not from a random value 0 - (2^32)-1) generated by the TCP/IP stack of the operating system. By under perfect situation, the representation of connection will show a line growing over time showing the effective performance of TCP connection. A time sequence graph is shown in Figure 6. Using the Time-Sequence-Graph (Stevens) of this trace, all sequence numbers from the source (2406:6400::5) to the destination (2406:6400::4) are increasing monotonically with respect to time. If there is a retransmitted segment, the sequence number of this retransmitted segment should be smaller than those of its neighboring segments. When ACKs are delayed, such as when an ACK is produced for every other packet, the growth is still approximately linear but somewhat slower. Due to occasion's gaps and jumps that interrupts the continuity of the line. This is normally due to a resend of data as a consequence of lost segments, ACK duplications, expired timeouts, etc.

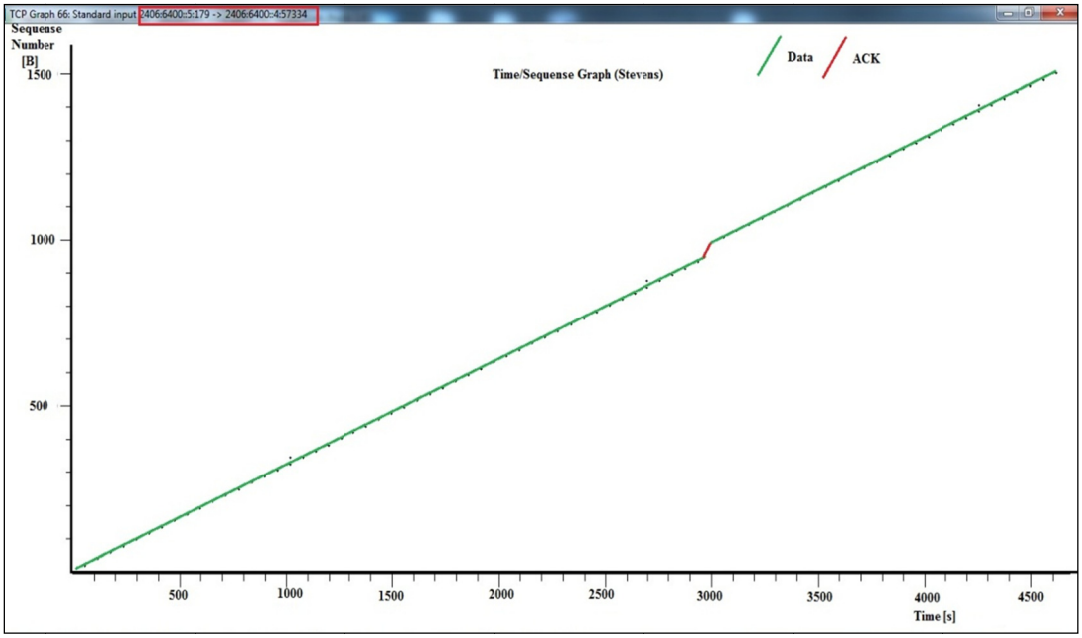

Figure 6. Time sequence graph

The time-sequence graph for the same period mentions there are gaps (showed in red) between sequence numbers, this indicating congestion in the network. These gaps also concur with the fast retransmission and retransmission events in the trace. The round trip time graph for ACK indicates some dots that are gather closer towards the x-axis indicating a consistent response time but there are a quit a few dots that are sharply climbing

towards the top. The dots in red color are during the time the fast retransmits arise and shown the maximum length in RTT. This graph gives a very valuable source of information to notice anomalies in the behavior of certain connections. The given time-sequence graph for the connections shows a reasonable slope, equal to the maximum bandwidth from end-to-end.

In Figure 7 we have shown time sequence graph in TCP trace from 2406:6400::9:179 to 2406:6400::8:50475. The *y*-axis of Figure 7 represents the relative TCP sequence number. Each small tick mark represents 5,000 sequence numbers. The *x*-axis is time, in seconds. The solid line comprises many smaller *I*-shaped line segments, each of which represents the range of sequence numbers contained in a TCP segment. The height of the *I* indicates the user-data payload size, in bytes. The slope of the "line" formed by these I-shaped characters is the data rate achieved by the connection. Any movement to the lower right indicates a retransmission.

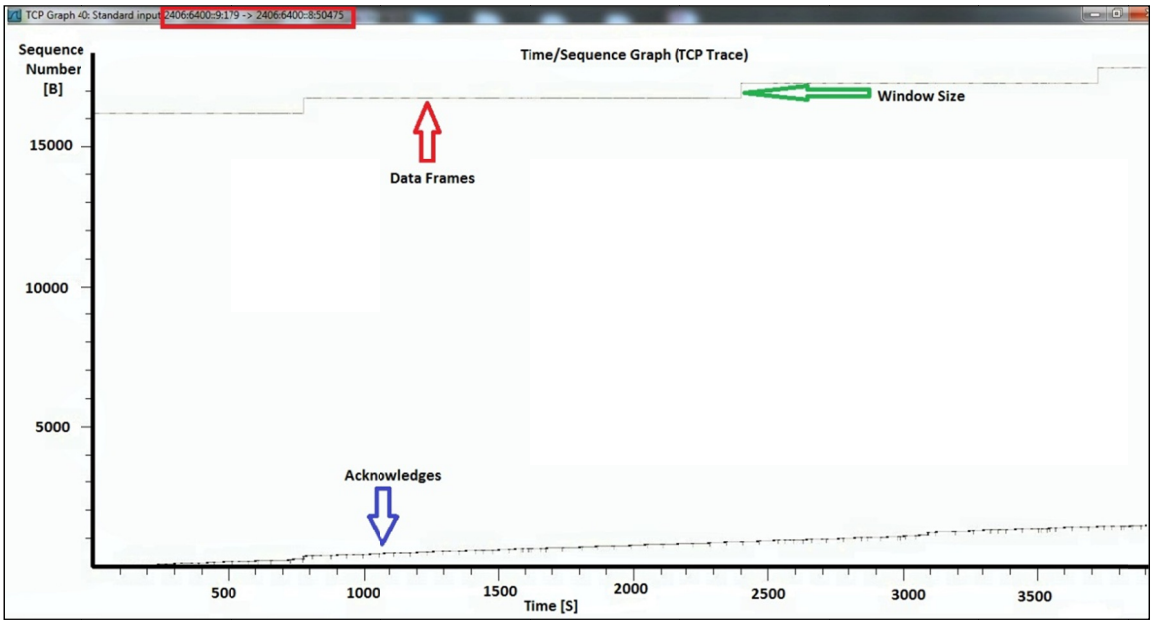

Figure 7. Time sequence graph (TCP trace)

The slope of the line for any given time range provides the average throughput over that time. As we can see, the highest sequence number sent was about 17000 at time 3500, which provides for a rough average good put rate of 4.85 bytes/s.

The bottom line represents the highest ACK number received at the sender so far. As discussed previously, TCP searches for additional bandwidth while it operates, by increasing its congestion window. It does not violate the receiver's advertised window. We see this in operation in this graph as the upper line moves from the lower line toward the upper line over time. If the upper line is never reached, either the sender or the usable network capacity is the limiting factor for the throughput of the connection. If the upper line is always reached, the receiver's window is the likely limiting factor.From the figure it shown increase of time sequence of Byte are increase accordingly. Here data frame are beginning from 16000 Bytes.

4.2.5 RTT Measurements

Round-trip time (RTT) is the duration of time it takes for a signal to be sent plus the length of durations it takes for an acknowledgment of that signal to be received. This time delay consequently comprisesof the transmission time spanbetween the two points of a signal. In the context of computer networks, the signal is generally a data packet, and the RTT is also known as the ping time. The RTT was originally estimated in TCP which can be found reference number: RTT = (α · Old RTT) + ((1 − α) · New round trip sample), Where α is constant weighting factor ($0 \leq \alpha < 1$). Choosing a value α close to 1 makes the weighted average resistant to changes that last a short time. Choosing a value for α close to 0 makes the weighted average respond to changes in delay very quickly. In a network, particularly a wide-area network or the Internet, RTT is one of several factors affecting latency, which is the time between a request for data and the complete return or display of that data. RTT evaluation is one of the most important performance parameters in a TCP exchange, particularly in the case of a

large file transfer. All TCP implementations eventually drop packets and retransmit them, no matter how good the quality of the link. If the RTT estimate is too low, packets are retransmitted unnecessarily; if it is too high, the connection may sit idle while the host waits for a timeout.

One simple way to find the RTT for such a flow is to find the time between the syn-ack and the data packet. The response flows take a little different information. When a host transmits a TCP packet to its peer, it ought to wait a certain time for an acknowledgment. If the reply does not reach within the expected period, the packet is implicit to have been lost and the data are retransmitted again. If the traffic flows over the wide-area Internet, a second or two seconds are reasonable during peak operation times. Network traffic for transmission control protocol RTT is shown in Figures (8, 9). If the RTT guess is too low, packets are retransmitted gratuitously; if it is too high, the connection may sit inactive while the host waits for a timeout.

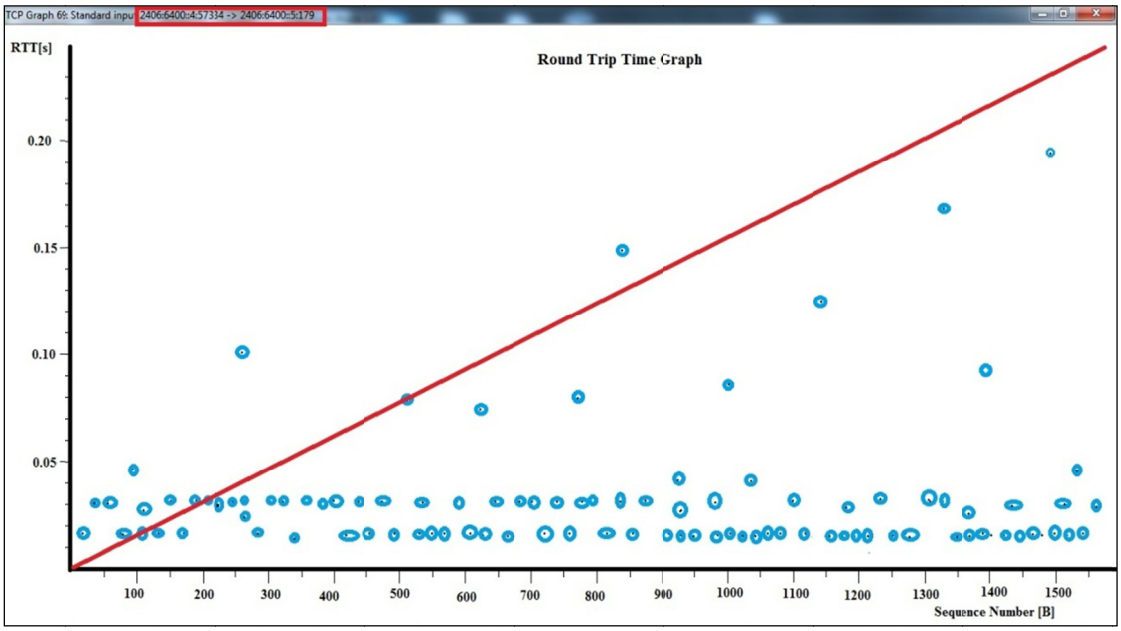

Figure 8. RTT graph for IPv6 connection

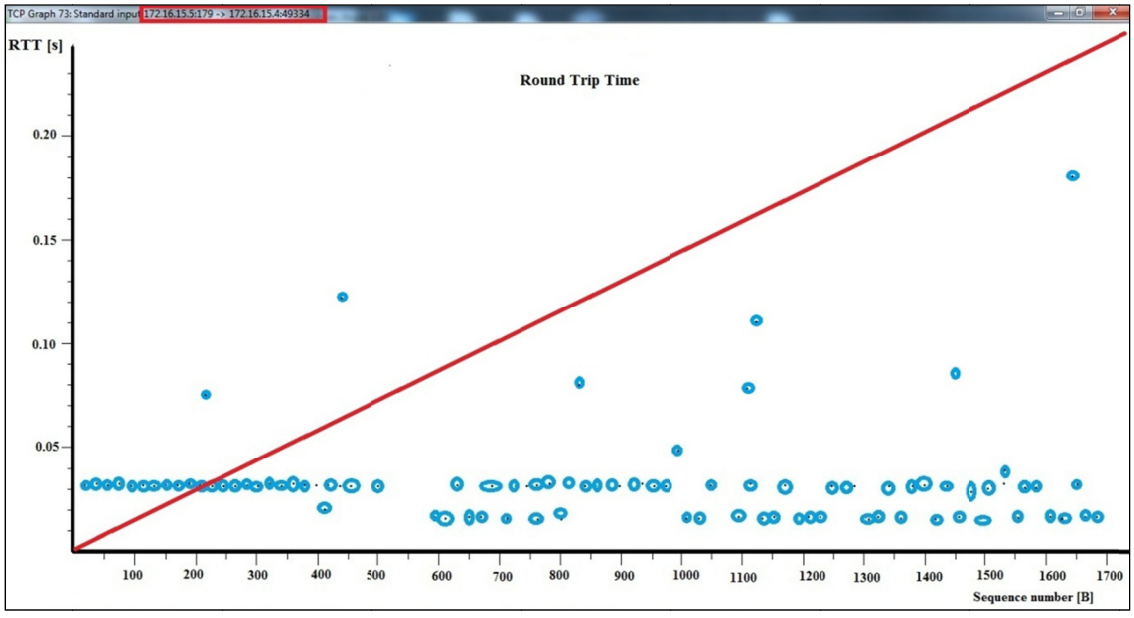

Figure 9. RTT graph for IPv4 connection

From the Figure 8 average RTT for IPv6 address 2406:6400::4 to 2406:6400::5 are below 0.05 s. Sometimes we got higher RTT when router working process becomes high. In the Figure 9 shows RTT for IPv4 address 172.16.15.5 to 172.16.15.4. In Figures 8 and 9 shown for IPv4 and IPv6 average RTT are below 0.05 s. The differences in round trip time on IPv4 and IPv6connection do not show significant difference.

4.2.6 TCP CUBIC

TCP CUBIC is an achievement of TCP that has an optimized congestion control algorithm for networks with large bandwidth delay product (BDP). The key aspect of CUBIC is that its window enlargement function is defined in real time so that its increase will be independent of RTT. Instead, window development depends only on the time between two successive congestion events. This property of CUBIC makes it friendly and fair to other flows in heterogeneous network. Congestion window of CUBIC is determined by the following function: $Wcubic = C(t-K)^3 + Wmax$, where C is a scaling factor, t is the elapsed time from the lastwindow reduction, $Wmax$is the window dimensions just before the last window reduction and $K=\sqrt[3]{Wmax\beta/C}$, where$K$ is theestimated time period that would take to reach $Wmax$. Disregarding further packet loss, K is computed as follows: $Wmin$ is the reduced window size just after the last congestion event. Congestion window after congestion event is in steady state where it grows concavely up to $Wmax$, after which it enters probing state and grows convexly until next congestion event. ß is a constant multiplicative decrease factor applied to window reduction at the time of loss event. As per the Figure 8 exposed, the minimum RTT was around 0.03 sec and maximum RTT was around 0.18. The congestion C=0.5, t=0.18, K=3, β=0.8

$$K=\sqrt[3]{65535*0.8/0.5}= 47.1553$$

$Wcubic = 0.5(0.18-47.1553)^3 + 65535 = 13705.3004$ or 13705 approx. In this Graph we study that, CUBIC set up snooping for bandwidth in which the window grows step-by-step at the start, accelerating its development as it proceeds away from $Wmax$. This assessed development $Wmax$ improves the constancy of the protocol and increase the consumption of the network while the fast growth left from $Wmax$ ensures the scalability of the protocol.

4.2.7 Throughput

Throughput is imperative to understanding end-to-end performance. In Figure 10 shows the TCP throughput outcomes of a perfect form and a real IPv6 backbone for different packet sizes. From the TCP throughput outcomes we discerned the very close throughputs for both IPv4 and IPv6 networks in terms of small message sizes. From the TCP throughput results, we furthermore discoveredthat throughputs for both IPv4 and IPv6 networks in any message size are very similar. In a real large dual stack network, the throughputs of the IPv6 augment rapidly in small message sizes of 256 bytes. Then the throughput becomes level until the 768-byte message size range. Conversely, the throughputs decreased a little bit up to the 1408-byte message size range. In a real large-scale network, we attained a minor degradation for IPv6 compared to IPv4 networks because the overhead of the IPv6 address size is more significant. TCP reflect on two most important factors: TCP window size and the round trip latency to transfer data. If the TCP window size and the round trip latency are known, the maximum possible throughput of a data transfer between two hosts may be calculated in spite of of the bandwidth using the expression: TCP-Window-Size-in-bits / Latency-in-seconds = Bits-per-second throughput. Instantaneous throughput is the rate (bps) at which a host receives the packets.

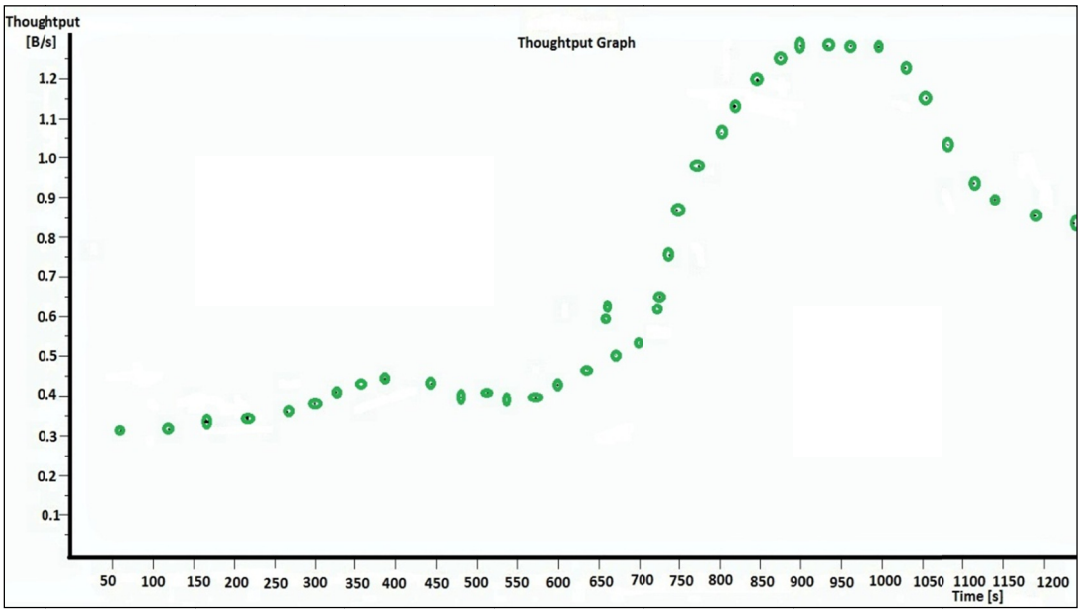

Figure 10. Throughput graph

If the packets consist of *F* bits and the transfer takes *T* seconds for the host to receive all F bits, then the average throughput of the packets transfer is *F/T* bps. In the figure we have shown throughput [Byte/second] increasing over increase of time. At 950 s throughput becomes maximum 1.2 B/s. After a certain times throughput becomes stable. We can calculate throughput two ways. Throughput without window scaling depends on TCP window size and round trip time.Maximum throughput = TCP Window Size / Round-trip time.Throughput with widow scaling depends on bandwidth, round trip time and TCP window size.Throughput with window scaling calculate by given formula Scaling factor calculation = Bandwidth x Round trip Time /TCP window Size. For 10Mbit/second scaling factor is = 10Mbit/s x 200ms/ 500000bits = Factor 4. We analysis the throughput, when error rate is 0, we reached maximum throughput. When router process increases rapidly congestion occurred due to RTT loss in router interface. We determined whether window is put reasonable is the most precise. If the window is put unreasonable, the throughout produced by congestion vary significantly. Suppose that each link is 10 Mbits / s, RTT is around 2-8 ms from the router interface, the length of each TCP data segment is 64 to 1000 bytes, the value of the receiving window of the receiver is rwnd = 32 to 64 bytes, window size is 16346, maximum hop limit 64 andthe simulation step size is 50 ms.

5. Conclusion

In this paper we have focused network migration from IPv4 to IPv6 in a large scale network. Dual stack network permits hosts to simultaneously reach IPv4 and IPv6 content making it a flexible coexistence approach.In the tunnelling concept we cannot move fully in IPv6. There are also other problems like TCP migration from IPv4 to IPv6 increase protocol overhead that increase latency and packet delay, each and every router need to configure tunnel for IPv6, which gives more overhead. It is also difficult to maintain the network as a Service Provider.In this paper, we conducted IPv6 address planning, an end-to-end performance assessment on a real large-scale network backbone. In order to build a dual stack network, it is necessary devices and network infrastructures that have supported IPv6 connections. The whole system of dual stack must be IPv6 compatible from source address to destination address. The following shows our investigative findings are explored on end-to-end user application performance using metrics such as: round trip time, time sequence, TCP throughputs, the IPv6 network does as well as the IPv4 network in terms of end-to-end performance. In dual stack network round trip time on IPv6 and IPv4 connection do not show significant difference. In a real large dual stack network situation, the throughput of the IPv6 expanded rapidly in small message sizes of 256 bytes, and, it leveled out before 768-byte message size range. In dual stack network we found same TCP throughput for IPv6 and IPv4 network. Our estimation outcomes show that the dual stack network is adept to provide stable network connectivity for IPv4 and IPv6 end-hosts.

Acknowledgements

The authors would like to thanks Department of Electrical and Electronic Engineering, School of Engineering

and Computer Science, Independent University, Bangladesh.

References

Arafat, M. Y., Ahmed, F., & Sobhan, M. A. (2014). On the Migration of a Large Scale Network from IPv4 to IPv6 Environment. *International Journal of Computer Networks & Communications (IJCNC), 6*(2), 111-126. http://dx.doi.org/10.5121/ijcnc.2014.6210

Aziz, M. T., Islam, M. S., & Khan, M. N. I. (2012). Throughput Performance Evaluation of Video/Voice Traffic in IPv4/IPv6 Networks. *International Journal of Computer Applications, 35*(2), 6-12.

Bates, T., Chandra, R., Katz, D., & Rekhter, Y. (2007). Multiprotocol Extensions for BGP-4. *Internet Request for Comments, RFC 4760, Jan. 2007*.

Ciflikli, C., Gezer, A., & Ozsahin, A. T. (2012). Packet traffic features of IPv6 and IPv4 protocol traffic. *Turk J. Elec. Eng. & Comp. Science, 20*(5), 727-749.

Fall, K. R., & Stevens, W. R. (2012). TCP/IP Illustrated. *Addison-wisely professional computer series, Pearson Education,* 2012, vol. 1.

Fatah, F. N., Suhendra, A., Marwan, M. A., & Firdaus, H. (2013). Performance Measurements Analysis of Dual Stack IPv4-IPv6. *Second Intl. Conference on Advances in Information Technology — AIT, 2013*.

Hinds, A., Atojoko, A., & Zhu, S. Y. (2013). Evaluation of OSPF and EIGRP Routing Protocols for IPv6. *International Journal of Future Computer and Communication, 2*(4), 287-291. http://dx.doi.org/10.7763/IJFCC.2013.V2.169

Internet Engineering Task Force (IETF) RFC 6052, 3513. (n.d.). Retrieved from http://tools.ietf.org/html/rfc6052,3513

Internet Engineering Task Force (IETF) RFC. (n.d.). Retrieved from http://tools.ietf.org/html/rfc3849, 4291, 6104

Lefty, V. R., Lizzie, N. D., Cinhtia, G. S., & Victor, C. P. (2012). Design and Simulation of an IPv6 Network Using Two Transition Mechanisms. *IJCSI International Journal of Computer Science Issues, 9*(6), 60-65.

Marrone, I. L., Barbieri, L. A., & Robles, M. M. (2013). TCP Performance - CUBIC, Vegas & Reno. *Journal of Computer Science & Technology, 13*(1), 1-8.

Rekhter, Y., Li, T., & Hares, S. (2006). A Border Gateway Protocol 4 (BGP 4). *Internet Request for Comments, vol. RFC 4271*, Jan. 2006.

Rhee, I., & Xu, L. (2008). CUBIC: A New TCP-Friendly High-Speed TCP Variant (2008). *ACM SIGOPS Operating Systems Review, 42*(5), 64-74. http://dx.doi.org/10.1145/1400097.1400105

Tahir, A., Shahbaz, N., & Afzaal, H. (2013). Network Migration and Performance Analysis of IPv4 and IPv6. *European Scientific Journal, 8*(5), 72-84.

Wang, Y., Ye, S., & Li, X. (2005), Understanding Current IPv6 Performance: A Measurement Study. *10th IEEE Symposium on Computer Communications,* June 2005. http://dx.doi.org/10.1109/ISCC.2005.151

Copyrights

Modern Applied Science; Vol. 8, No. 3; 2014
ISSN 1913-1844 E-ISSN 1913-1852
Published by Canadian Center of Science and Education

Geographically Weighted Regression Modeling for Analyzing Spatial Heterogeneity on Relationship between Dengue Hemorrhagic Fever Incidence and Rainfall in Surabaya, Indonesia

Baharuddin[1,2], Suhariningsih[1] & Brodjol Sutijo Suprih Ulama[3]

[1] Faculty of Science and Technology, Airlangga University, Surabaya, Indonesia

[2] Department of Mathematics, Haluoleo University, Kendari, Indonesia

[3] Department of Statistics, Institut Teknologi Sepuluh Nopember, Surabaya, Indonesia

Correspondence: Baharuddin, Department of Mathematics, Faculty of Mathematics and Natural Sciences, Haluoleo University, Kendari 93232, Indonesia. E-mail: baharuddinsaid@yahoo.com

Received: February 20, 2014 Accepted: March 25, 2014 Online Published: April 8, 2014

doi:10.5539/mas.v8n3p85 URL: http://dx.doi.org/10.5539/mas.v8n3p85

Abstract

Geographically weighted regression (GWR) modeling has been extended to evaluate spatial heterogeneity on the relationship between dengue hemorrhagic fever (DHF) incidence and rainfall in Surabaya, Indonesia. We employed monthly data in 2010 as repeated observation for each subdistrict in Surabaya, subdistrict was then considered as spatial unit. Problem of temporally correlated errors in this modeling was solved by means of data transformation. The GWR model was compared with global regression model using some statistical criteria. The GWR model reveals that the relationship between the DHF incidence and the rainfall is significantly varied in every subdistrict. The influence of the rainfall on the DHF incidence was greater over southeastern subdistricts than other subdistricts in Surabaya. This result holds an important consequence on policy making for regulation in preventing DHF infection according to local characteristic climate in a certain region.

Keywords: geographically weighted regression, dengue, incidence, rainfall, correlated error

1. Introduction

Dengue hemorrhagic fever (DHF) which is defined as a disease caused by infection of dengue virus, has become a serious health problem for societies in many tropical and sub tropical countries. Approximately 50 millions people are infected by the dengue virus in almost 100 countries every year (World Health Organization [WHO], 2009). In Indonesia, the desease that is transmitted by *Aedes aegypti* mosquito was firstly discovered in Surabaya and Jakarta in 1968 (Aiken & Leigh, 1978). During last decade, Surabaya is claimed as the DHF endemic region in Indonesia (Mulyatno, Yamanaka, Yotopranoto, & Konishi, 2012). Various programs have been accomplished to prevent and control the desease, however the DHF incidence in Surabaya remains relatively high. The high of the DHF case requires a serious effort to block the spread of DHF epidemic desease by means of analyzing risk factor which is associated with dengue virus infection.

Some studies concerning risk factors of dengue virus infections on DHF infected societies have been broadly conducted. Phuong et al. (2008) reported that job and surrounding environment were the two main factors affecting DHF incidence. Meanwhile, Allwinn (2011) found that visiting to DHF endemic region would make one infected by the virus. Other risk factors discovered by the reports were presence of mosquito nest, condition of water container, and inhabitant mobility (Soghaier et al., 2013). However, the studies merely to the point or limit of exploring risk factors according to global viewpoint, in which the inter-variable relationship is assumed to be spatially constant for all regions. Consequently, the conclusion does not describe any local characteristic.

Further study based on spatial consideration is originated by the presence of confusing results about DHF transmission. A study in South Thailand revealed negative correlation between DHF incidence and rainfall (Thammapalo, Chongsuwiwatwong, McNeil, & Geater, 2005), meanwhile a study in Central Thailand showed positive correlation between them (Wiwanitkit, 2005). But, Picardal and Elnar (2012) performed a study in Central Visayas (Philippines) did not show any correlation between the two variables. According to these findings, we hypothesize that the relationship between DHF incidence and rainfall in a certain region is spatially

different.

One of new relatively methods to examine spatial risk factor is geographically weighted regression (GWR). This statistical method adjusts frame of global to local regression model, which enables regression parameter estimation for every single point of the spatial unit (Fotheringham, Brunsdon, & Charlton, 2002). Relationship between independent variable (*X*) and dependent variable (*Y*) in GWR model is different for all regions (Leung, Mei, & Zhang, 2000). The GWR method has been employed by Lin and Wen (2011), Hsueh, Lee, and Beltz (2012), and Khormi and Kumar (2011) in analyzing DHF case. Those studies engaged spatial data at a certain time (cross-sectional data) in GWR modeling.

The objective of this study is to extend the frame of GWR modeling in analyzing spatial heterogeneity that is correlated with DHF incidence in Surabaya by three ways. First, we combined both spatial and temporal data in the modeling. In this case, we employed monthly data as repeated observation for each spatial unit. Second, we solved problem of temporally correlated error which may occur during the modeling. Third, we evaluated spatial heterogeneity from the relationship between the DHF incidence and the rainfall in Surabaya. The acquired GWR model was compared with global regression model by means of some statistical tests. The result of this study will be practically useful for authorities in regulating program to prevent the DHF infection based on local characteristic climate in a certain region.

2. Materials and Methods

2.1 Study Area

The study was conducted in Surabaya, the capital city of East Java province in Indonesia. During last decade, Surabaya is one of the highly risk of the DHF endemic cities in Indonesia (Health Office of Surabaya City, 2011, unpublished). Surabaya locates in northeast Java island around 7°11'–7°21' south latitude and 112°36'–112°54' east longitude with area of 326.36 km^2 (Statistics of Surabaya City, 2011). Surabaya is the second biggest city in Indonesia having population of 2.6 millions on 2010 cencus. As a region with tropical climate, Surabaya has high atmospheric temperature, and different rainfall as well as atmospheric pressure along the year.

The subdistrict, the 'kecamatan' in Indonesian, was used as the spatial unit in this study. 16 of 31 subdistricts in Surabaya were chosen for modeling. In general, those subdistricts lie on low continental with high about 3–6 m over the sea surface, except in south region, the high of the subdistricts may reach about 25–50 m over the sea surface (Statistics of Surabaya City, 2011).

2.2 Data Collection

Data for number of DHF sufferers in every subdistric every month during 2010 was booked from Health Office of Surabaya City. These monthly data were considered as repeated observation for each subdistrict, one subdistrict is defined as one spatial unit. We also obtained data for number of population in every subdistrict from Statistics of Surabaya City. The DHF incidence in every subdistrict each month was attained by dividing the number of the DHF sufferers by the number of the population for every certain subdistrict, and multiplying it by 100,000. The DHF incidence was chosen as dependent variable (*Y*) in the regression modeling.

Climate factor, in this study is the rainfall, was chosen as the independent variable (*X*). This climate factor was taken from three meteorological stations, i.e. Maritim Perak I, Maritim Perak II, and Juanda International Airport meteorological stations. The number of data for every variable was $n = 192$ (16 subdistricts times 12 months).

2.3 Statistical Methods

Relationship between DHF incidence and rainfall can be analyzed by comparing the results of global regression and GWR modelings. If the GWR model is more reliable than the global regression model then relationship between the two variables is spatially different for each subdistrict. On the other side, the global regression model describes constant relationship for all study regions.

The regression modeling was firstly executed by ordinary least squares (OLS) method in examining the global relationship between DHF incidence (*Y*) and rainfall (*X*). The regression model is defined by including subdistric indices and time of occurrences:

$$Y_{i;t} = \beta_0 + \beta_1 X_{i;t} + \xi_{i;t}, \qquad \xi_{i;t} = \rho \xi_{i;t-1} + \varepsilon_{i;t} \tag{1}$$

where $Y_{i;t}$ is DHF incidence in subdistrict i ($i = 1,2,\cdots,16$) during t^{th} month ($t = 1,2,\cdots,12$); $X_{i;t}$ is rainfall in subdistrict i in t^{th} month; β_0 is OLS intercept coefficient; β_1 is OLS slope coefficient; $\xi_{i;t}$ is correlated error; ρ is the autocorrelation with $|\rho| < 1$; and $\varepsilon_{i;t}$ is error assumed to be normal distribution with zero mean and known standard deviation. Estimation of autocorrelation ($\hat{\rho}$) was extracted from OLS

regression modeling through the origin:

$$\xi_{i;t} = \rho\xi_{i;t-1} + \varepsilon_{i;t} \tag{2}$$

(Myers, 1990). To solve problem of correlated error in ξ, a data transformation was performed:

$$Y^*_{i;t} = Y_{i;t} - \rho Y_{i;t-1}, \qquad X^*_{i;t} = X_{i;t} - \rho X_{i;t-1} \tag{3}$$

for $t = 1,2,\cdots,12$ in every single subdistrict i (we defined $t = 0$ for December 2009). Further regression was conducted on the transformed data. As regression modeling for time series data, an initial diagnosis was done to examine the autocorrelation by means of Durbin-Watson *d*-statistic. If the value of *d* is less than lower bound d_L, then autocorrelation is present. If the value of *d* is higher than upper bound d_U, then there will be no autocorrelation. If $d_L \le d \le d_U$ then decision is inconclusive (Myers, 1990). Significance of the OLS regression model is expressed by *t*-statistic, sum of squared errors (*SSE*), Akaike information criterion (*AIC*), and coefficient of determination (R^2) (Myers, 1990; Fotheringham et al., 2002).

The spatial heterogeneity from the relationship between DHF incidence (*Y*) and rainfall (*X*) will be analyzed by GWR model. Unlike the OLS regression model, the GWR model enables regression parameter estimation in different subdistricts (Fotheringham et al., 2002). The GWR model we employed was the model which contained temporally correlated error:

$$Y_{i;t} = \beta_0(u_i, v_i) + \beta_1(u_i, v_i)X_{i;t} + \xi_{i;t}, \qquad \xi_{i;t} = \rho\xi_{i;t-1} + \varepsilon_{i;t} \tag{4}$$

where $\beta_0(u_i, v_i)$ and $\beta_1(u_i, v_i)$ are GWR coefficients in subdistrict i; location point of subdistrict i is defined by latitude and longitude coordinates (u_i, v_i); and $\varepsilon_{i;t}$ is error which is assumed having normal distribution with zero mean and known standard deviation. Resolving correlated error problem on ξ can be done by transforming the data as expressed in Equation (3) and autocorrelation ρ is refined with the OLS regression model to compare the two models.

The first step in the GWR modeling is defining the latitude and longitude coordinates (u_i, v_i) for each subdistrict. These geographycal coordinates was used to specify Euclidean distance between observed data in subdistrict i in t^{th} month and observed data in subdistrict j in l^{th} month:

$$d_{i;t(j;l)} = \sqrt{(u_i - u_j)^2 + (v_i - v_j)^2} \tag{5}$$

Month indices t and l in Equation (5) do not influence the distance between subdistricts. The distance in Equation (5) is termed as fundamental background in weighting the data to estimate the parameter of the GWR model. The closer the distance between the estimated point to subdistrict, the larger the weight of the data during the parameter estimation. In this study, the weighting of data was conducted by means of Gaussian function:

$$\psi_{i;t(j;l)} = \exp\left(-d^2_{i;t(j;l)} \big/ 2b^2\right) \tag{6}$$

where $b > 0$ is bandwidth constant in which its designating was done by cross-validation method (Fotheringham et al., 2002). Gaussian function is an exponential function that gives weight 1 for data where the parameter of subdistrict is being estimated and weight with undeviating decrease value for data in other subdistricts, the weight continues to reduce as the distances among subdistricts increases. Gaussian function was employed in forming weighted matrix:

$$\mathbf{W}(u_i, v_i)_t = \operatorname{diag}\left(\psi_{i;t(1;1)}, \psi_{i;t(1;2)}, \cdots, \psi_{i;t(1;q)}, \cdots, \psi_{i;t(m;1)}, \psi_{i;t(m;2)}, \cdots, \psi_{i;t(m;q)}\right) \tag{7}$$

where $0 \le \psi_{i;t(j;l)} \le 1$ is weight data for subdistrict j in l^{th} month to estimate the parameter in subdistrict i in t^{th} month. Every observed data has one weighted matrix $\mathbf{W}(u_i, v_i)_t$ in estimating the parameter. By algebraic matrix approach, the estimation of the parameter $\hat{\beta}(u_i, v_i) = (\beta_0(u_i, v_i), \beta_1(u_i, v_i))^T$ in subdistrict i by means of weighted least squares (WLS) method is expressed in:

$$\hat{\beta}(u_i, v_i) = \left[\mathbf{X}^T\mathbf{W}(u_i, v_i)_t\,\mathbf{X}\right]^{-1}\mathbf{X}^T\mathbf{W}(u_i, v_i)_t\,\underset{\sim}{\mathrm{Y}} \tag{8}$$

(Fotheringham et al., 2002). All observed data in a certain subdistrict has the same estimated parameter. It is due to the reality that the data weighting only engage the distances among the subdistricts. Meanwhile the monthly data is defined as the repeated observation in a subdistrict.

The GWR modeling was firstly conducted on the untransformed data. As we have discussed, the GWR model was calibrated to monthly data, and the initial diagnosis was done to examine the autocorrelation by means of Durbin-Watson statistic. If autocorrelation is present in the error then the further GWR model was fitted on the

transformed data. Significance test of the GWR model was conducted by hypothesis test which proposed by Brunsdon, Fotheringham, and Charlton (1999). The null hypothesis in this test represents $\beta_k(u,v)$ function which is unchanged in all coordinates (u,v) in the study area for $k=0$ and $k=1$. If there is no proof to reject the null hypothesis, then the OLS global regression model will be acceptable enough to describe the data. In the meantime, the test for variation of each set of β_k across the study area will be completed by F_3-statistic that was initiated by Leung et al. (2000). The significance of the GWR model is also represented by sum of squared errors (*SSE*) and coefficient of determination (R^2). Comparison of the GWR model and global regression model will be conducted by Akaike information criterion (AIC). According to this criterion, the regression model which posses the smallest AIC value is then defined as the best one (Fotheringham et al., 2002).

3. Results

3.1 Result of OLS Regression

The regression modeling using OLS method on the untransformed data gives Durbin-Watson statistic with d = 0.690 in which the value is less than the lower bound d_L = 1.758 (α = 0.05). The result shows that autocorrelation is present in the error. Estimation of autocorrelation by applying Equation (2) provides $\hat{\rho}=0.652$. The OLS estimation on the transformed data by employing Equation (3) presents global regression model as follows Equation (1):

$$Y = 8.394 + 0.012X \tag{9}$$

where Y is the DHF incidence and X is the rainfall. The regression model is globally suitable for all study regions. Diagnosis on the error of this model provides statistic d = 1.940, for which the value is higher than the upper bound d_U = 1.778 (α = 0.05). This is indicating that there is no autocorrelation in the error. All P-values of the regression coefficient in the model were smaller than 0.05 (see Table 1). Hence, the rainfall influences the DHF incidence in Surabaya.

Table 1. Test of global regression coefficient

Variable	Coefficient	Standard error of coefficient	*t*-statistic	*P*-value
Intercept	8.394	1.471	5.71	0.000
Rainfall	0.012	0.004	3.24	0.001

The model has $SSE = 7371.81$, $AIC = 1247.27$, and $R^2 = 42.93\%$. Further analysis on the model reveals that the error approaches normal distribution.

3.2 Result of GWR Model

The GWR estimation on the untransformed data provides Durbin-Watson statistic with d = 0.900 in which the value is less than the lower bound d_L = 1.758 (α = 0.05). This result reveals that the model has correlated errors, so we need data transformation. To compare the global regression and the GWR models, the further modeling employed $\hat{\rho}=0.652$. Based on the cross-validation criteria (see Fotheringham et al., 2002), the GWR modeling on the transformed data provides optimum bandwidth b = 0.053. Thus, Gaussian function is expressed as:

$$\psi_{i;t(j;l)} = \exp\left(-d^2_{i;t(j;l)} \big/ 2(0.053)^2\right) \tag{10}$$

Table 2 represents the summary of estimated parameter (regression coefficient) for the obtained GWR model. All the coefficient values of the global regression lies in interval for coefficient of the GWR model.

Table 2. Summary for coefficient of GWR model

Coefficient	Minimum	1st Quartile	Median	3st Quartile	Maximum	Global
$\hat{\beta}_0$	8.107	8.147	8.265	8.449	8.802	8.394
$\hat{\beta}_1$	0.006	0.008	0.009	0.012	0.019	0.012

Diagnosis on the error of this GWR model provides Durbin-Watson statistic d = 1.913 in which the value is higher than the upper bound d_U = 1.778 (α = 0.05). It is then indicated that there is no autocorrelation in the error.

Further evaluation on the model reveals that the error approaches normal distribution.

The GWR model has sum of squared errors $SSE = 7120.25$, which is smaller than the global regression. It clearly shows that the GWR model has estimation $\hat{Y}$ closer Y compared to the global regression. The coefficient of determination from the GWR model ($R^2 = 44.88\%$) also increases slightly higher than the OLS regression model.

Table 3 represents summary of calculation *F*-statistic which was employed to examine the significance of the GWR model (see Brunsdon et al., 1999). The smaller of the *P*-value from 0.05 reveals that the GWR model is more reliable than the global regression model. It also means that the relationship between the DHF incidence and the rainfall in Surabaya is influenced by a geographical factor.

Table 3. Comparison of GWR and OLS global regression models

Source of variation	Sum of squares	Denominator	Mean square	*F*-statistic	*P*-value
OLS error	7371.810				
GWR improvement	251.560	2.652	94.866		
GWR error	7120.250	187.348	38.005	2.496	0.000

The value of Akaike information criterion that was obtained from the GWR model is $AIC = 1242.19$. This value is again smaller than the global regression model. It indicates that the GWR model is more relevant in describing the data than the OLS regression model. Further examination shows that the parameter $\hat{\beta}_1$ varied significantly in every subdistrict (see Table 4). This can be seen from the *P*-value of the coefficient $\hat{\beta}_1$ with value smaller than 0.05. Meanwhile, the coefficient $\hat{\beta}_0$ remains constant for all study regions.

Table 4. Significance test for variation of each set of $\hat{\beta}_0$ and $\hat{\beta}_1$ across the study area

Coefficient	Numerator degree of freedom	Denominator degree of freedoms	F_3-statistic	*P*-value
$\hat{\beta}_0$	67.106	188.8	0.074	1.000
$\hat{\beta}_1$	54.393	188.8	4.627	0.000

4. Discussion

This study reveals that the DHF incidence in Surabaya has a correlation with the rainfall. The higher the rainfall, the more the risk of the spreading DHF. The result strengthen the previous studies that the rainfall is concluded as a risk factor in the spread of the dengue (Aiken & Leigh, 1978; Wiwanitkit, 2005; Hii, Zhu, N. Ng, L. Ng, & Rocklöv, 2012). In principal, rainfall creates the area or nest of the dengue vector mosquito wider and wider. Rainfall alters numerous artificial containers into habitats for the mosquito. Breeding habitats of *Aedes aegypti* mosquito usually take place in unclosed water container, flower vase, tin can, or tire around the citizen environment (WHO, 2009). The mosquito prefers to lay its egg on the wall of the water container slightly over the water surface. In a favourable environment, the egg can survive desiccation in several months (Hopp & Foley, 2001). The egg will become a mosquito larva after immersing in water for couple of days. Therefore, the rainfall can increase rapidly the population density of *Aedes aegypti* mosquitoes.

The GWR modeling indicates that the relationship between the DHF incidence and the rainfall in Surabaya is spatially different. It implies that in some subdistricts higher DHF incidence is associated with higher rainfall, whereas in some subdistricts DHF incidence has little correlation with rainfall. After grouping subdistricts by region, the influence of the rainfall on the DHF incidence in subdistricts near southeastern of Surabaya is larger than other subdistricts (Figure 1). Since the rainfalls were different from one subdistrict to another (Kane & Yusof, 2013), an understanding about spatial varying relationship is very useful in policy making for preventing the DHF infection.

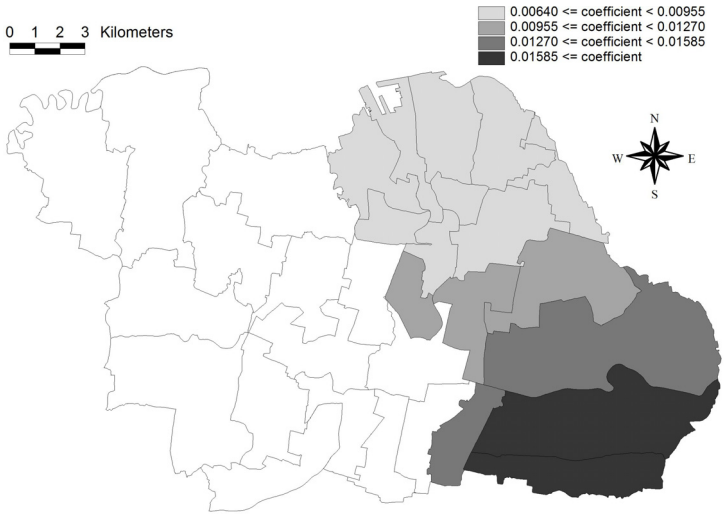

Figure 1. Spatial map of GWR coefficient of the rainfall influence on DHF incidence in Surabaya, Indonesia. Subdistricts given by white color are not included in modeling because of incomplete data

One of the statistical criteria which is employed in regression modeling is coefficient of determination (R^2). The coefficient represents the percentage of variation in the DHF incidence (Y) that is explained by the rainfall (X) in the model. Both GWR and OLS regression models provides low R^2. It fairly indicates that there exists other factors affecting the DHF incidence in Surabaya, like environment (Phuong et al., 2008; Khormi & Kumar, 2011), citizen mobility (Allwinn, 2011), human density and mosquito abundance (Lin & Wen, 2011), social and economical dynamics (Khormi & Kumar, 2011), transportation (Hsueh et al. 2012), and the condition of the water container (Soghaier et al., 2013).

5. Conclusion

The rainfall is correlated with the DHF incidence in Surabaya, Indonesia. The relationship between the DHF incidence and the rainfall varies in each subdistrict. The citizen who lives in southeastern of Surabaya takes higher risk of dengue infection when the rainfall is relatively high.

Acknowledgements

We thank to Directorate General of Higher Education, Ministry of Education and Culture of the Republic of Indonesia to provide funding. Acknowledgement also goes to Health Office of Surabaya City, Statistics of Surabaya City, and Maritim Perak I, Maritim Perak II, and Juanda International Airport meteorological stations for supporting data.

References

Aiken, S. R., & Leigh, C. H. (1978). Dengue haemorrhagic fever in South-east Asia. *Transactions of the Institute of British Geographers, New Series, 3*(4), 476-497.

Allwinn, R. (2011). Significant increase in travel-associated dengue fever in Germany. *Medical Microbiology and Immunology, 200*, 155-159. http://dx.doi.org/10.1007/s00430-011-0185-2

Brunsdon, C., Fotheringham, A. S., & Charlton, M. (1999). Some notes on parametric significance tests for geographically weighted regression. *Journal of Regional Science, 39*(3), 497-524. Retrieved from http://www.researchgate.net/profile/Martin_Charlton/publication/228605522_Some_notes_on_parametric_significance_tests_for_geographically_weighted_regression/file/5046351b8225eb8bfe.pdf

Fotheringham, A. S., Brunsdon, C., & Charlton, M. (2002). *Geographically weighted regression: The analysis of spatially varying relationships*. Chichester: Wiley.

Hii, Y. L., Zhu, H., Ng, N., Ng, L. C., & Rocklöv, J. (2012). Forecast of dengue incidence using temperature and rainfall. *PLoS Neglected Tropical Diseases, 6*(11), e1908. http://dx.doi.org/10.1371/journal.pntd.0001908

Hopp, M. J., & Foley, J. A. (2001). Global-scale relationships between climate and the dengue fever vector, *Aedes aegypti*. *Climatic Change, 48*, 441-463.

Hsueh, Y. H., Lee, J., & Beltz, L. (2012). Spatio-temporal patterns of dengue fever cases in Kaoshiung City,

Taiwan, 2003-2008. *Applied Geography, 34*, 587-594. http://dx.doi.org/10.1016/j.apgeog.2012.03.003

Kane, I. L., & Yusof, F. (2013). Assessment of risk of rainfall events with a hybrid of ARFIMA-GARCH. *Modern Applied Science, 7*(12), 78-89. http://dx.doi.org/10.5539/mas.v7n12p78

Khormi, H. M., & Kumar, L. (2011). Modeling dengue fever risk based on socioeconomic parameters, nationality, and age groups: GIS and remote sensing based case study. *Science of the Total Environment, 409*, 4713-4719. http://dx.doi.org/10.1016/j.scitotenv.2011.08.028

Leung, Y., Mei, C. L., & Zhang, W. X. (2000). Statistical tests for spatial nonstationarity based on the geographically weighted regression model. *Environment and Planning A, 32*, 9-32. http://dx.doi.org/10.1068/a3162

Lin, C. H., & Wen, T. H. (2011). Using geographically weighted regression (GWR) to explore spatial varying relationships of immature mosquitoes and human densities with the incidence of dengue. *International Journal of Environmental Research and Public Health, 8*, 2798-2815. http://dx.doi.org/10.3390/ijerph8072798

Mulyatno, K. C., Yamanaka, A., Yotopranoto, S., & Konishi, E. (2012). Vertical transmission of dengue virus in *Aedes aegypti* collected in Surabaya, Indonesia, during 2008-2011. *Japanese Journal of Infectious Diseases, 65*, 274-276. http://www.ncbi.nlm.nih.gov/pubmed/22627316

Myers, R. H. (1990). *Classical and modern regression with applications*. Boston: PWS-KENT.

Phuong, H. L., de Vries, P. J., Boonshuyar, C., Binh, T. Q., Nam, N. V., & Kager, P. A. (2008). Dengue risk factors and community participation in Binh Thuan Province, Vietnam, a household survey. *The Southeast Asian Journal of Tropical Medicine and Public Health, 39*(1), 79-89.

Picardal, J. P., & Elnar, A. R. R. (2012). Rainfall, temperature and the incidence of dengue in Central Visayas, Philippines are not correlated. *CNU Journal of Higher Education, 6*.

Soghaier, M. A., Mahmood, S. F., Pasha, O., Azam, S. I., Karsani, M. M., Elmangory, M. M., … Eltigai, E. (2013). Factors associated with dengue fever IgG sero-prevalence in South Kordofan State, Sudan, in 2012: Reporting prevalence ratios. *Journal of Infection and Public Health*. http://dx.doi.org/10.1016/j.jiph.2013.07.008

Statistics of Surabaya City. (2011). *Surabaya in figures 2011*. Surabaya: Statistics of Surabaya City.

Thammapalo, S., Chongsuwiwatwong, V., McNeil, D., & Geater, A. (2005). The climatic factors influencing the occurrence of dengue hemorrhagic fever in Thailand. *The Southeast Asian Journal of Tropical Medicine and Public Health, 36*(1), 191-196. http://www.ncbi.nlm.nih.gov/pubmed/15906666

Wiwanitkit, V. (2005). Strong correlation between rainfall and the prevalence of dengue in central region of Thailand in 2004. *Journal of Rural and Tropical Public Health, 4*, 41-42.

World Health Organization. (2009). *Dengue: Guidelines for diagnosis, treatment, prevention and control* (New ed.). Geneva: WHO Press.

Modern Applied Science; Vol. 8, No. 3; 2014
ISSN 1913-1844 E-ISSN 1913-1852
Published by Canadian Center of Science and Education

Investigation of the Relationship of Brand Personality, Subjective Norm and Perceived Control on Consumers' Purchase Intention of Organic Fast Food

Charraz Othman[1] & Muhammad Sabbir Rahman[2]

[1] Graduate School of Management, Multimedia University, Cyberjaya, Malaysia

[2] Faculty of Languages and management, International Islamic University Malaysia, Jalan Gombak, Selangor Darul Ehsan, Kuala Lumpur, Malaysia

Correspondence: Charraz Othman, Graduate School of Management, Multimedia University, Cyberjaya, Malaysia. E-mail: charraz2012@yahoo.com

Received: February 21, 2014 Accepted: March 20, 2014 Online Published: April 16, 2014

doi:10.5539/mas.v8n3p92 URL: http://dx.doi.org/10.5539/mas.v8n3p92

Abstract

Organic fast food among the Malaysian consumers is an emerging theme of discourse. As more people are eating foods bought from fast food restaurants, this eating out lifestyle further heightened the problems of unhealthy eating and unbalanced diets (Azlina et al., 2011). So, to help consumers improve their personal wellness, fast food restaurants should consider various organic meals into their extended services. Indeed, this work intends to weigh into the proposed factor (TPB constructs; subjective norm and perceived dominance and brand personality dimensions; sincerity, excitement, competence, sophistication and ruggedness) towards purchase intention of organic fast food in Malaysian perspective. The outcomes distinguish that three of the factors have a significant positive association with organic fast food intention to purchase normally, sincerity, competence and sophistication. Hence, the outcome proposed that the strongest ingredients in this relation are sincerity. Therefore, the researchers agreed that fast food operators may successfully incorporate brand personality variables such as sincerity, competence and sophistication to influence on the formation of customers' intention of organic fast food. Hence, this study successfully develop theoretical and pragmatic aspects to discover the purchase intention of organic fast food on the perspective of Malaysian consumers'.

Keywords: organic food, fast food, brand personality, green purchase intention, subjective norm, perceived behavioural control, theory of planned behaviour (TPB)

1. Introduction

Nowadays, a hundred millions of people without giving a much thought of their purchases bought a fast food every day (Janet, 2008). Jill (2004) stated, fast foods as a broad term used for a limited menu of foods that provide themselves to production-line techniques and products such as burgers, pizzas, chicken or sandwiches tend to specialize by suppliers. Meanwhile, Ehsan (2012) defined the fast food market as the sale of food and drinks for immediate consumption either on the premises or in designated eating areas shared with other food service operators or for consumption elsewhere. Mashhadi (2012) indicated that the fast food is low price, fast service and suitable places for eating. Hence, fast food consumption is getting popular, especially with younger people (Ehsan, 2012). Nonetheless, when fast food is growing, diet food consumption also growing in popularity through rising health awareness among consumers (Chang & Roth, 2001) thereby, the phenomenon of consuming organic food has emerged since people are starting to be cognizant of the importance of eating a healthy food in their daily life (Follows, 2000).

Asian eating habits are changing to emulate those of the West since the coming of globalization and this is why the use of fast food is likewise on the rise (SMEDA, 2006). Healthy lifestyle highlighted the slogan; "back to nature" that has become a cause for universal order. This tie is based that everything coming from nature is good and advantageous and also ensures an existence of equilibrium between human and nature (Chang & Roth, 2001). According to Budi Suprapto (2012), organic food has been accepted in Malay since around year 1992. National Organic Standards Board of the U.S. Department of Agriculture (USDA, 2000) concluded that the organic food is a variety of agricultural products that can produced organically, including produce of grains, meat, poultry,

eggs, dairy products and processed food products as it must be produced without the use of modern synthetic inputs such as sewer-sludge fertilizers, more synthetic fertilizers and pesticides, genetic industrial (biotechnology), hormones growth, antibiotics and are not processed using irradiation, industrial solvents, or chemical food additives (Justin, 2012). Kihlberg and Risvik (2007) found, the organic food tastes better than conventional by the bulk of organic consumers. Moreover, Chen (2009) stated that the organic foods usually contain less harmful additives and more nutrients than conventional foods and they hold no other danger of food intoxication. Hence, additives in organic food products are firmly controlled and restricted since it represents the difference between organic and non-organic food (Heaton, 2002).

The worldwide marketplace for organic food reaches US$69.2 billion, compared to the previous year, which is up US$4 billion in 2011 as stated by Research Institute of Organic Agriculture (FiBL, 2012) while in Malaysia organic market is comparatively young. Nevertheless, the need for organic food is dramatically increased in Malaysia since the changes in consumers' lifestyle and eating pattern to choose the intellectual nourishment that is healthy, eco-friendly and concerns towards food consumption and environmental issues (Zeinab, 2012). Consumers in Malaysia become more health conscious of their foods in daily life (Jane, 2012) since they have found out some lack in the conventional food safety (Shaharudin, Pani, & Suhardi, 2010).

Thus, this study describes and reviews the TPB model (Theory of Planned Behaviour) in predicting individual' intention to execute a particular behaviour. Furthermore, as a means to expand the original TPB model, we investigated the added amount of brand personality into the TPB construct to measure the intention to purchase of organic fast food by Malaysian consumers. The brand personality is considered to be an indispensable piece of fast-food restaurant business that defined as a "branded convenience food" (Suvenus, 2009). The brand personality theory is founded on the idea that in guild to render substance to the product, people attaches human characteristics to a brand, thereby providing managers anticipate on this feeling by giving these human characteristics to their ware in their merchandising schemes. Above all this research investigated the impact of subjective norm, perceived control, sincerity, excitement, competence, sophistication, ruggedness and purchase intention on organic fast food that is put on to flourish in the Malaysian market.

2. Theoretical Background and Hypothesis Development

Purchase intention as point out by Shaw and Constanzo (1983), is a good predictor for behaviour (Aertsens, Verbeke, & Huylenbroeck, 2011) while Ajzen and Madden (1986) stated that intention variable plays an crucial role toward behaviour because intention is considered as a mediator of motivational factors that have an impact on a behavior (Ajzen, 1991). As Organic food production and buying (behaviour) interest has increased in recent years among the consumers , therefore, several empirical studies on this market have been tackled since the organic food market has set about growing trend (Anssi, 2005).

As Ferber and Priskie (1965) point out, the intention-purchase relationship has attracted many of empirical studies highlighting significant inconsistencies between purchase intention and purchase behavior (Tirtiroglu & Elberk, 2008). Moreover, Chong (2013) found that organic purchase intention is conceptualized as the possibility and willingness of an individual to give preference to products that having eco-friendly type over other conventional products in their buying consideration. Organic purchasing is defined as purchasing goods and services which have less harmful for environmental and human health (Lee, 2009) while as stated by (Mostafa, 2007), organic purchase behaviour relates to the use of the products and services which are useful to the environment, recyclable and responsive to ecological concerns. Sheppard (1988) point out that the relation between intentions and activities has been composed with respect to many different types of behaviours as cited in (Anssi, 2005). Thus, the intentions to purchase organic fast food are significant predictors of actual behaviour in this study.

Fisbein and Ajzen (1975) asserts, using planned behaviour theory, the word of intention can be explained which assumes that humans always have a purpose in acting. Thus, since the purchase intention helps most organic food producers to key out the behaviour of customers and their perceptions into the merchandise then it is something crucial to concentrate on (Magistris, 2008) since intention shows how tough a person is to make some attempts. Studies (Anssi, 2005) have demonstrated that the intentions of buying organic food to the behaviour is positive and has been proven that the efficacy of the TPB of organic food consumption. In addition, TPB more recently often been applied in the range of food choice and to model organic food selection (Magistris, 2008). While Chen (2007) studied that subjective norm and perceived control significantly boost the consumer's intention to buy organic foods.

While brand personality is an attractive and appealing concept in the market today that described it as one of the core dimensions of the brand identity and perhaps as the closest variable to the consumers' decision making

process of buying and it also refers to the thought that relationships are imperative in community life (Rajagopal, 2006). Otherwise, Aaker (1997) defined Brand personality as "the circle of human characteristic associated with a trade name" and it's conceived to be an important element for the success of the trade name in terms of taste and choice (Rajagopal, 2006). Hence, customers' attitudes and behaviours towards the stigma will reflect on brand, personality which may regard on the consumer tendency in connection with the brand and ultimately affect purchase likelihood (Aaker, 1996). So, the factors that contribute to describe the purchase behaviour of environment-friendly merchandise, especially organic food, still need to be further explored. Figure 1 presents the theoretical framework of the study.

2.1 Subjective Norm

Subjective norms on customer intention are understood as the external factors' effects and refers to the "an important individuals or groups referent that likelihood given either approve or disapprove to performing a behaviour" (Ajzen, 1991). Taylor (1999) reported that a subjective norm is a proficient interpreter of behaviour when an individual's actions affect some other person's benefit. Conversely, Lapinski, Rimal, DeVries and Lee (2007) establish that the issue of subjective norms is insignificant when only one individual affected in the arriving at a selection. Withal, the subjective norms' role was obscure in a previous survey of purchase design and behaviour of organic food, especially regards to forming the behaviour (Ajzen, 1991). Recent surveys also point to the impact of "subjective norm" on the attitude towards buying organic food (Aertsens, Mondelaers, & Van Huylenbroeck, 2009). According to Eagly et al. (1993) subjective norm perform a behaviour with a consumer's motivation to construct the first moments of an important person such as family, friends and significant others (Yangui, Font, & Gil, 2013). Rather, consumers will have more intention on purchasing organic foods if the significant people of them think organic foods are safe. Conversely, they will have poorer intention if those people important for they believe organic foods are unfit. Therefore, the consumers' intention to purchase organic fast food will increase when the intention of important person surrounding them rises since the organic foods are supposed as healthier and environmentally friendly rather than conventional foods (Chong, 2013).

According to Ajzen (2006), subjective norm is a person's social pressure to engage in behaviour and it is said to be decided by the full set of reachable normative beliefs regarding the potentials of individual referents (e.g. Family or friends). Chen (2007) point out; applied to organic food consumption; it is positively related between the consumers' intention of organic food and their subjective norm. Conversely, Anssi Tarkiainen (2005) stated, subjective norm and intention to buy organic has no direct way. While, Christopher Armitage (2001) explained that subjective norm have no direct effect on intention after checking on attitude and PBC (Bamberg & Moser, 2007). However, Bamberg and Moser (2007) discover that subjective norm has no direct link with intention in a situation of pro-green behaviour. The first hypothesis of the research model is proposed as follows:

H1: Subjective norm has a positive impact on organic fast food purchase intention in Malaysia

2.2 Perceived Control

Perceived behavioural control (PBC) is the point of perceiving one's his ability to handle given situations towards successfully (Ajzen, 1991). Meanwhile, Bandura (1986) point out that it is concerned and judgments of what an individual can manage with anything skills one possesses not the skills an individual has since it is highly shown an individual necessary the confidence in their ability to be successful on perform the behaviour since it is determined an individual's behaviour (Swann, Chang-Schneider, & Larsen McClarty, 2007). Other that, perceived controllable deals with the consumers' actual possibilities, i.e. external control to buy organic food while the perceived self-efficacy deals with consumers' internal control for purchasing organic food as cited in Anssi Tarkiainen (2005). Consequently, the level of PBC should raise as the individual has both access that tools is required also an information, accomplishments and opportunities to effectively utilize them.

In addition, Chong (2013) point out that the consumers' perceived difficulty and their designs to purchase organic foods related positively each other when personality behaviour becomes more potent. Therefore, according to several empirical studies Aertsens et al. (2009), income (PBC) appears to act as a significant positive role in clarifying organic food purchasing in Europe. Nevertheless, in several studies of USA, they did not find this relation to be significant as cited by (Gracia & Magistris, 2007) while studies in Canada (Aertsens et al., 2009) set forth a positive connection between income and willingness to buy organic products, upward to a given degree of income. Lockie, Lyons and Lawrence (2002) studied, the proportion of Australians consuming organic food stands up when income upturns and the changes in organic food utilization also get up to changes in the condition of income (Riefer & Hamm, 2008).

Meanwhile, Aertsens et al. (2009) observe a positive effect from PBC on the buying intention on organic apples,

while this it was not significant for organic pizza. The past research of organic consumption has demonstrated that the most important causes for not buying the organic food or the lack of availability as a difficulty and organic food's relatively higher cost compared to formal ones as cited by (Aertsens et al., 2009). It is clearly not under consumers' control. Overall, intentions to purchase organic food significantly related to a combination of the attitude, (personal and subjective) subjective norms and (perceived) behavioural control while Aertsens et al. (2009) stated TPB model possibly will help explain organic food purchase intention. Therefore, the second hypothesis is determined as follows:

H2: Perceived control influences positively the intention to purchase organic fast food in Malaysia.

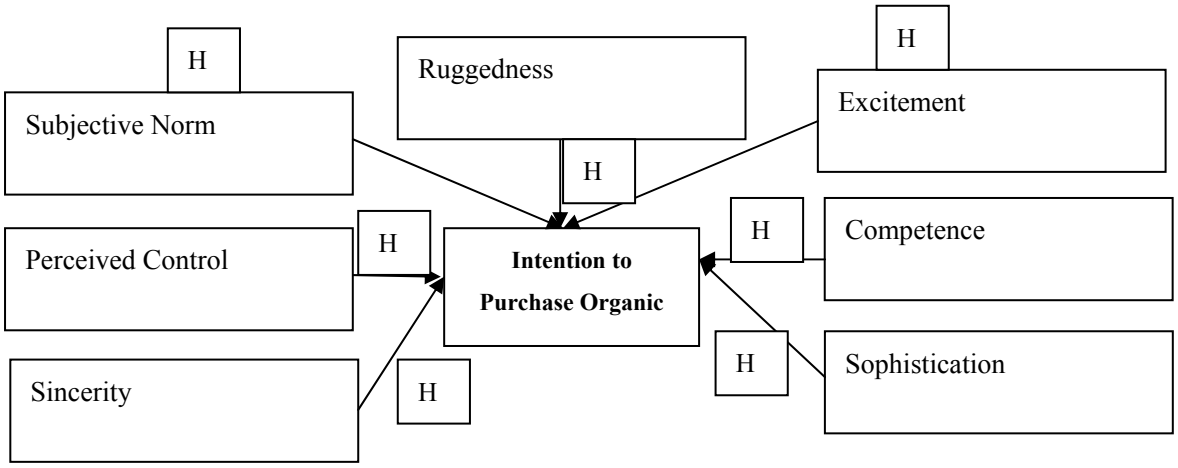

Figure 1. Research framework for organic fast food purchase intentions

2.3 Sincerity

According to Maehle, Otnes and Supphellen (2011), sincere brands considered a high moral while exciting brands present a chance to occurrence feelings of excitement. Therefore, a brand with sincere personality, character can make a much positive relationship than a brand with an exciting personality (Maehle et al., 2011). Brands that are presented as sincere would concern to customers in many demographics who are in search of a down-to-earth approach to the product they are purchasing.

Sincerity is a dimension that connected to concepts as warmth and acceptance which there are four different facets that have been known for sincerity: down-to-earth, honest, wholesome and cheerful (Aaker, 1997), real and sincere (Aaker, 2001).

In the other hand, sincerity also presents in agreeableness which indicates strong social orientations, cooperation and harmony seeking person as cited by Hasliza (2012) and according to Aaker (1997), nurturance, warmth, family orientation and traditionalism also are characteristics of sincere of brand personalities. Succeeding, the third hypothesis as follows:

H3: Sincerity has a positive impact on the organic fast food purchase intention in Malaysia.

2.4 Excitement

Excitement is defined as "the degree of talkativeness, freedom, happiness and energy shown in a brands' personality trait (Lin, 2010). Hence, it takes a sense of adventure to customers' lives, especially those who already live exciting and adventuresome lives (Jennifer, 2011). Therefore, the traits such as daring, spirited, imaginative and up-to-date may show the excitement, personality of the customer who a young and adventurous person.

Gil and Hellgren (2011) point out; an excitement is seen encapsulates concepts such as sociability, energy and activity also this dimension has four facets which are: daring, spirited, imaginative and up-to-date. It is capturing the energy and activity elements of extraversion as well as exciting and contemporary (Aaker, 2001) that represent the "tendency towards change, visionary orientations, strong intuition, creative imagination and inherent enthusiasm as cited by Hasliza (2012). Further, exciting of brand personalities convey vitality, uncommon and independence (Lin, 2010). And so, the fourth hypothesis of the research model as follows:

H4: Excitement has a positive impact on the organic fast food purchase intention in Malaysia.

2.5 Competence

Aaker (1997) defines competence as the level of responsibility, purpose and patience in a brands' personality trait. Therefore, it conveys the features of dependability, intelligence, and achiever. In addition, competitive companies are trying to win with competitors for their excitement personality. For example, industries like automotive and information technology such as Apple which competes for the excitement and competency based on purchase at the same time.

Competence is a dimension connected to concepts as duty, security, dependability and achievement which similar to conscientiousness (Aaker, 2001). It delivers three different facets: reliable, intelligent and successful that are more on, task-oriented, structured and logical and enables an individual to concentrate on certain facets of acting, learning and changing behaviour as well as personality related capacities as Hasliza (2012) concluded. Then, the fifth hypothesis of the research model is defined as follows:

H5: Competence has a positive impact on the organic fast food purchase intention in Malaysia.

2.6 Sophistication

As point out by Aaker (1997), sophistication is the degree of elegance and style in a brand personality attribute which presents the characteristics of upper class and charm. Instantly, customers may classify the brands and products in this brand dimension such as luxury items that are in higher categories.

Sophistication is a dimension that includes traits as aspiration, glamour and sexiness and has two facets: upper class and charming as found by Aaker (2001) as well as romantic that indicate the trend of strong emotion and sensitivity of a person (Hasliza, 2012). Thus, Sophistication is ones of the ways to segment and target markets for different consumer will react differently towards a special view. The sixth hypothesis of the proposed model is defined as follows:

H6: Sophistication has a positive impact on the organic fast food purchase intention in Malaysia.

2.7 Ruggedness

As stated by Jennifer (2011), ruggedness brand personality is associated with camping equipment and vehicles which suitable for carrying livestock and farm equipment. So, the characteristic of hardness such as outdoorsy, tough, strong and rugged like to purchase goods marketed with ruggedness.

According to Gil and Hellgren (2011), ruggedness in whatever manner is regarded as strength, masculinity and is presenting a glamorized view of ideals that there are two different facets for this dimension: outdoorsy lifestyle and tough also masculine and western (Aaker, 2001) that indicate a reliable, strict and structured individual (Hasliza, 2012). All the same, this dimension is suitable for an American to look into brand personality dimensions according to suitable culture.

In other hand, in certain community market (Aaker, 2001) since it seems to be more suited for the Malaysian community which is perceived as westernized from the findings in several literature reviews thus the original brand personality dimensions is starting to be applied in this conceptual research (Hasliza Hassan, 2012). Lastly, the hypothesis of the proposed model is defined as follows:

H7: Ruggedness has a positive impact on the organic fast food purchase intention in Malaysia.

2.8 Theory of Planned Behaviour (TPB) Model Brand Personality Model

In this work, we applied Theory of Planned Behaviour (TPB) as our theoretical contribution to understand and predict fast food consumption behaviour (Ajzen, 1991). To predict the intention to purchase organic fast food among Malaysian consumers' this research applied three primary antecedents namely, subjective norm (perceived social pressure from one's immediate environment to perform or not perform the behaviour) (Ajzen & Fishbein, 1980) and perceived control(ability)that states the people's perceptions of their skill to accomplish a given behaviour) (Ajzen, 2006; Anssi, 2005).

In summation, the scale of brand personality (1997) is employed as the framework to explain the variables of personality that will be applied to define the personality towards an organic fast food eatery. Therefore, the theoretical framework has been widely employed by other researchers and Aaker (1997) which her goals were to produce a theoretical framework of dimensions that could be able to measure brand personality while being honest, valid and useful when making generalizations across product classes. The five dimensions identified in the survey were: Sincerity, Excitement, Competence, Sophistication and Ruggedness.

3. Methods

3.1 Data Collections and Sample

This research gathered data from 169 Malaysian consumers (63 males and 106 females), which were contributed a response rate of 56.0 percentage (300 questionnaire was distributed). Under the racial perspective majority number of respondents grouped under (58.6%) of Malay. Roughly 20.0 percent of the respondents were Chinese followed by Indians. Meanwhile, the majority (around 80%) of the respondents was aged between 25 to 44 years while the respondents above 45 years old, around (3%). However, more than (80%) of the respondents were employed, full-time (60.9%), part-time (7.7%) and self-employed (17.8%). It was found that the bulk of the respondent's income were between RM3001 to RM4000 (52.1%). Thus, based on the respondent's answers, consumers moderately agreed that the organic fast food has the characteristics of sincerity.

Table 1. Demographic profiles

Respondents	Frequency *(n)*	Percentage *(%)*
Gender		
Male	63	37.3
Female	106	62.7
Ethnicity		
Malay	99	58.6
Chinese	33	19.5
Indian	26	15.4
Sabahan	7	4.1
Sarawakian	4	2.4
Age		
18 to 24	21	12.4
25 to 34	83	49.1
35 to 44	58	34.3
45 to 54	4	2.4
Above 55	3	1.8
Income		
Less than RM1000	23	13.6
RM1001 to RM2000	13	7.7
RM2001 to RM3000	36	21.3
RM3001 to RM4000	88	52.1
RM4001 to RM5000	6	3.6
Over RM5001	3	1.8

3.2 Instrument Development and Data Analysis

For raising the appropriate result, the questionnaire was designed in three sections: section A, B and C. The source section (Section A) contained questions about demographics and socioeconomic (e.g., age, gender, race, marital status, employment status and income) and the second section (Section B) contained questions about consumers' knowledge of organic merchandise. Final part (Section C) gauges the variety, namely; subjective norm, perceived control, brand personality dimensions, namely; sincerity, excitement, competence, sophistication and ruggedness as well as an intentions which each variable was assessed along a five-point scale Likert style. The questionnaires adapted from several of previous study.The questionnaire was adapted from Aaker (1997) and the Theory of Planned Behaviour (TPB) by Ajzen (1991) and modified based on the position of Malaysian environment. The statements for subjective norm and perceived control were adapted from the

existing TPB construct scales (Kim & Han, 2010) and have been evolved based on the model questionnaire proposed by Ajzen (Ajzen & Fishbein, 1980). All responses were completed on a five-point Likert scale. In addition, the brand personality scale was adapted from the previous research (Lee, 2009; Aaker, 1997). However, several of the items excluded from this study since there are irrelevant for this current research. Thereof, 27 points would be utilised to measure brand personality in this workplace. Intention to purchase was adapted from existing scales developed by Kim and Han (2010). The detail items of construct are provided in the Appendix. To test the above mentioned hypothesis this research applied multiple regression to examine the influence of the independent variables that bear on the metric of the dependent variable as stated by Sekaran and Bougie (2010). In this study, multiple regression analysis was applied to analyse the effect of subjective norm, perceived control, sincerity, excitement, competence, sophistication and ruggedness towards the intention to purchase organic fast food. The result from the multiple regression output revealed that three variables are significant to the purchase intention organic fast food while four was not significant. Therefore, the hypothesis result shows that all the variables are not significantly supported except for sincerity, competence and sophistication which are 0.00, 0.05 and 0.04 respectively. The multiple regression analysis based on the linear relationship between independent variables and a dependent variable. Thus, the correlation analysis for autonomous and dependent variable of hypothesis shows there is a high significant correlation between sincerity (0.78), competence (0.76) and excitement (0.73) while perceived control (0.42), subjective norm and ruggedness (0.56) induce a lower correlation on organic fast food intention.

Table 2. The result of the main effects in the proposed model

Variables	TPB constructs & Brand Personality Dimensions—Purchase Intention	
	B	***P***
Subjective norm	0.124	0.172
Perceived control	0.040	0.567
Sincerity	0.340	0.004
Excitement	0.221	0.169
Competence	0.262	0.045
Sophistication	0.262	0.038
Ruggedness	-0.300	0.056
Adjusted *R*-Squared = 0.646		

a. Dependent Variable: Purchase intention.

Table 2 depicts the result of regressions among seven variables against the dependent variable. Grounded on the data presented above, the b value shows the kinship between the predictor and the final result. Therefore, the regression equation can be formalised as follows:

$$Y = a + b1X1 + b2X2 + b3X3 + b4X4 + b5X5 + b6X6 + b7X7 + e$$

All the result extracted from Table 2 indicates that the positive relationship between independent variables and purchase intention of consumers on purchasing organic fast food. However, Ruggedness was found less influence towards intention to purchase organic fast food.

Meanwhile, Sincerity was found most influence when purchase organic fast food in Malaysia that (34%) in aggregate. Furthermore, the p-values for the all predictors are more than 0.05, except for sincerity (0.00), Competence (0.05) and Sophistication (0.04). Based on the result above the subjective norm, perceived control, excitement and ruggedness are not significantly predicting the variability of organic purchase intention in Malaysia. Whereas, Sincerity variable ($\beta = 0.340$) attained the highest effects on organic fast food purchase intention followed by competence and sophistication ($\beta = 0.262$).

4. Managerial Implication

The prediction of organic fast food purchase intention from TPB variables was similar to the levels of prediction obtained from other behavioural research (Armitage, Norman, & Conner, 2002). Thus, the results revealed that perceived control remained weaker predictor of purchase intentions. From the research the perceived control variable found no significant positive influence on purchase intention of organic fast food (Christopher, 2001),

subjective norm often as the weakest component among the TPB constituents that answerable for the described variations in pattern.

As, for instance, Thompson, Haziris and Alekos (1994) found that subjective norm is a poor predictor of behavioural intention in food choice. Therefore, in order to draw the consumers to purchase organic fast food, the perceptions of the people who are vital to them must be influenced. In this case, sellers of organic food should keenly find techniques to raise environmental alarms (e.g., promoting pro-organic campaigns and pro-healthy fast food). Moreover, intentions to purchase organic fast food, mostly are found out by the positive approach in which referents as family, kin or friends that considered on intention to purchase organic fast food. Thus, in lodge to improve the influence such referents, the vendors should find ways to provide the certain organic features of their products and service to the residential area.

It can be caused from various information sources like television, website, magazines, brochures and etc. into organic fast food perceptions. Moreover, this study also recommends that several of the brand personality constructs such as sincerity, competence and sophistication are sufficient for explaining intentions to purchase organic fast food.

Therefore, brand personality variables apparently can provide significant force for consumer purchase intention formation on organic fast food perspectives. Well, in order to draw the consumers to purchase organic fast food based on the perceptions of the masses who are significant to them, managers and vendors should look for ways to determine the reference group of the consumers such as promoting pro-healthy fast food through advertising endorser. Thus, fast food companies may recommend and promote products, namely organic fast food in order to make a differential product image and influence on consumer purchase behaviour because it can produce a recommendation and endorsement effect and build customers' reliability on organic fast food purchase intention.

5. Conclusion and Further Research

In Malaysia, the organic fast food is weighed at the introductory level where not many people are concerned about. The interest to conduct this study is to possess a better understanding of Malaysian consumers' purchase intention in organic fast food purchasing context.

Overall, in society to encourage consumers' willingness to purchase organic fast food, a several useful strategy for marketing communication campaigns must be designed with concern as there are no scientific facts that organic food products are healthier or more nutritious than conventional food (Magistris, 2008). In Malaysia the industry of organic fast food, perhaps too young since there are only a few restaurants employed this concept of the eatery.

Hence, the industry of organic fast food needs more brand exposures in order to create the brand awareness in consumer minds. The exposures can be managed by focusing in marketing programs to increase customer awareness in the surrounding residential areas. Further enquiries are needed to substantiate the significance of the societal force and groups of reference on purchase intention of organic fast food in the restaurant setting. This study successfully incorporates brand personality variables such as sincerity, competence and sophistication to determine the purchase intention of the organic fast food.

References

Aaker, J. L. (1997). Dimensions of Brand Personality. *Journal of Marketing Research, XXXIV*, 347-356. http://dx.doi.org/10.2307/3151897

Aertsens, J., Verbeke, W., Mondelaers, K., & Van Huylenbroeck, G. (2009). Personal determinants of organic food consumption: a review. *British Food Journal, 111*(10), 1140-1167. http://dx.doi.org/10.1108/00070700910992961

Ahmad, S. N. B., & Juhdi, N. (2010). Organic Food: A Study on Demographic Characteristics and Factors Influencing Purchase Intention Among Consumers in Klang Valley Malaysia. *International Journal of Business and Management, 5*(2), 1-14.

Ajzen, I. (1991). The Theory of Planned Behavior. *Organizational Behavior and Human Decision Processes, 50*, 179-211. http://dx.doi.org/10.1016/0749-5978(91)90020-T

Armitage, C., Norman, P., & Conner, M. (2002). Can the theory of planned behaviour mediate the effects of age, gender and multidimensional health locus of control? *British Journal of Health Psychology, 7*, 299-316. http://dx.doi.org/10.1348/135910702760213698

AzlanAmran, G. Y. (2012). Determinants of Behavioral Intention on Sustainable Food Consumption Among Consumers' of Low Income Group: Empirical Evidence From Malaysia. *WEI International European Academic Conference Proceedings* (pp. 84-93).

Bamberg, S., & Moser, G. (2007). Twenty years after Hines, Hungerford, and Tomera: A new meta-analysis of psycho-social determinants of pro-environmental behaviour. *Journal of Environmental Psychology, 27*, 14-25. http://dx.doi.org/10.1016/j.jenvp.2006.12.002

Biemans, S. Z. (2009). Factors underlying consumption of organic food in the opinion of Polish consumers. *Agronomy Research, 7*(2), 768-774.

Chakrabarti, S. (2010). Factors influencing organic food purchase in India – expert survey insights. *British Food Journal, 112*(8), 902-915. http://dx.doi.org/10.1108/00070701011067497

Chang, G., & Roth, C. B. (2001). Structure of MsbA from E. coli: A homolog of the multidrug resistance ATP binding cassette (ABC) transporters. *Science, 293*(5536), 1793-800. http://dx.doi.org/10.1126/science.293.5536.1793

Chen, M. F. (2007). Consumer attitudes and purchase intentions in relation to organic foods in Taiwan: Moderating effects of food-related personality traits. *Food Quality and Preference, 18*, 1008-1021. http://dx.doi.org/10.1016/j.foodqual.2007.04.004

Chen, M. F. (2009). Attitude toward Organic Food Among Taiwanese as related to Health Consciousness, Environmental Attitudes and the Mediating Effects of a Healthy Lifestyle. *British Food Journal, 111*(2), 165-178. http://dx.doi.org/10.1108/00070700910931986

Chong, C. W. (2013). Factors Influencing on Purchasing Behaviour of Organic Foods. *Human and Social Science Research, 1*(2), 93-104.

Christopher, J., & Armitage, M. C. (2001). Efficacy of the Theory of Planned Behaviour: A meta-analytic review. *British Journal of Social Psychology*, 471-499.

Cuza, A. I. (2012). Factors Influencing Consumption of Organic Food in Romania. *The USV Annals of Economics and Public Administration, 12*(1), 15.

Danseh, S. Y. S., Hashemnia, S., & Sefidmazgi, M. R. (2012). Evaluating effective factors on customers' attitude to by green products (Case study: consumers of products with A and Benergy labels in Rasht). *International Research Journal of Applied and Basic Sciences, 3*(11), 2316-2322.

Dardak, R. A., Abidin, A. Z. Z., & Ali, A. K. (2009). Consumers' perception, consumption and preference on organic product: Malaysian Perspective. *Economic and Technology Management Review*, 95-107.

de Magistris, T., & Gracia, A. (2008). The decision to buy organic food products in Southern Italy. *British Food Journal, 110*(9), 929-947. http://dx.doi.org/10.1108/00070700810900620

DellaVigna, S., Moretti, E., & Pathania, V. (December 2008). *The Effect of Fast Food Restaurants on Obesity*.

Dolatabadi, H. R., Kazemi, A., & Rad, N. S. (November 2012). The Impact of Brand Personality on Product Sale through Brand Equity (Case Study: Cosmetic Products Retailers). *International Journal of Academic Research in Business and Social Sciences, 2*(11).

Ehsan, U. (2012). Factors important for the selection of fast food restaurants: an empirical study across three cities of Pakistan. *British Food Journal, 114*(9), 1251-1264. http://dx.doi.org/10.1108/00070701211258808

Essoussi, L. H., & Zahaf, M. (2008). Decision making process of community organic food consumers: an exploratory study. *Journal of Consumer Marketing, 25*(2), 95-104. http://dx.doi.org/10.1108/07363760810858837

Follows, S. B., & Jobber, D. (2000). Environmentally responsible purchase behaviour: A test of a consumer model. *European Journal of Marketing, 34*(5/6), 723-746. http://dx.doi.org/10.1108/03090560010322009

Frank, B. (2012). The formation of consumer attitudes and intentions towards fast food restaurants: How do teenagers differ from adults? *Managing Service Quality, 22*(3), 260-280. http://dx.doi.org/10.1108/09604521211230987

French, D. P., Sutton, S., Hennings, S. J., Mitchell, J., Wareham, N. J., Griffin, S., ... Kinmonth, A. L. (2005). The Importance of Affective Beliefs and Attitudes in the Theory of Planned Behavior: Predicting Intention to Increase Physical Activity. *Journal of Applied Social Psychology, 35*(9), 1824-1848. http://dx.doi.org/10.1111/j.1559-1816.2005.tb02197.x

Gotschi, E., Vogel, S., & Lindenthal, T. (2007). High school students' attitudes and behaviour towards organic products: survey results from Vienna. *Department of Economics and Social Sciences*, 2-18.

Gracia, A., & Magistris, T. De. (2007). Organic food product purchase behaviour: A pilot study for urban consumers in the South of Italy. *Spanish Journal of Agricultural Research, 5*(4), 439-451. http://dx.doi.org/10.5424/sjar/2007054-5356

Gracia, A., T. D. (2007). Organic Food Product Purchase Behaviour: A pilot study for urban consumers in the South of Italy. *Spanish Journal of Agricultural Research, 5*(4), 439-451. http://dx.doi.org/10.5424/sjar/2007054-5356

Haghiria, M., Hobbs, J. E., & McNamara, M. L. (2009). Assessing Consumer Preferences for Organically Grown Fresh Fruit and Vegetables in Eastern New Brunswick. *International Food and Agribusiness Management Review, 12*(4).

Hair Jr, J. F., Barry, J., & Babin, R. E. (2009). *Multivariate Data Analysis* (7th ed.). Prentice Hall.

Hassan, H., & Rahman, M. S. (June 2012). The Impact of Hypermarket Corporate Brand Extensions on Brand Personality: A Conceptual Analysis of Malaysian Market. *International Journal of Business and Management, 7*(12).

Heaton, S. (2002). *Organic Food and Health: The Evidence. Compass Internet Ltd*. Retrieved from The Positive Health Online website: http://www.positivehealth.com

Hoogendam, J. B. (2011). The role of social identity and attitudes toward sustainability brands in buying behaviors for organic products. *Journal of Brand Management, 18*(9), 697-708. http://dx.doi.org/10.1057/bm.2011.3

Jill Davies, G. J. L. (2004). Fast food: dietary perspectives. *Nutrition & Food Science, 34*(2), 80-82. http://dx.doi.org/10.1108/00346650410529050

Khare, A., & Handa, M. (2009). Role of individual self-concept and brand personality congruence in determining brand choice. *Innovative Marketing, 5*(4), 63-71.

Kihlberg, I., & Risvik, E. (2007). Consumers of organic foods – value segments and liking of bread. *Food Quality and Preference, 18*(3), 471-481. http://dx.doi.org/10.1016/j.foodqual.2006.03.023

Kim, Y. J., & David Njite, M. H. (2012). The Role of Emotion in Consumers' Intentions to Select Eco-Friendly Restaurants: Broadening and Deepening the Theory of Planned Behaviour (pp. 4-36).

Kuhar, A., & Juvancic, L. (2010). Determinants of purchasing behaviour for organic and integrated fruits and vegetables in Slovenia. *Agricultural Economic Review, 11*(2), 70-83.

Kumar, B. (2012). Theory of Planned Behaviour Approach to Understand the Purchasing Behaviour for Environmentally Sustainable Products. *Indian Institute of Management*, 2-43.

Kumar, R. (2011). *Research Methodology: A step-by-step guide for beginners.* London: SAGE Publications.

Lapinski, M. K., Rimal, R. N., DeVries, R., & Lee, E. L. (2007). The Role of Group Orientation and Descriptive Norms on Water Conservation Attitudes and Behaviors. *Health Communication, 22*(2), 133-142. http://dx.doi.org/10.1080/10410230701454049

Lea, E., & Worsley, T. (2005). Australians' organic food beliefs, demographics and values. *British Food Journal, 107*(11), 855-869. http://dx.doi.org/10.1108/00070700510629797

Lee, J. W. (2009). Relationship Between Consumer Personality and Brand Personality as self-Concept: From the Case of Korean Automobile Brands. *Academy of Marketing Studies Journal, 13*(1).

Lin, L. (2010). The relationship of consumer personality trait, brand personality and brand loyalty: An empirical study of toys and video games buyers. *Journal of Product & Brand Management, 19*(1), 4-17. http://dx.doi.org/10.1108/10610421011018347

Lockie, S., Lyons, K., & Lawrence, G. (January 2002). Eating 'Green': Motivations Behind Organic Food Consumption in Australia. *European Society for Rural Sociology, 42*(1), 24-40.

Lončarić, R., Lončarić, Z., & Zmaić, K. (2009). Computer model for predicting organic food consumer behavior in Croatia. *4th Aspects and Visions of Applied Economics and Informatics*, 419-426.

Lückerath, B. (October 2010). How Brands become People-A Study on the Impact of Brand Personality on Brand Value. *Copenhagen Business School, 75*, 170-819.

Maehle, N., Otnes, C., & Supphellen, M. (2011). Consumers' Perceptions of the Dimensions of Brand Personality. *Journal of Consumer Behaviour, 10*(5), 290-303. http://dx.doi.org/10.1002/cb.355

Malik, M. E., & Naeem, B. (2012). Aaker's Brand Personality Framework: A Critical Commentary. *Journal of Basic and Applied Scientific Research*, 11992-11996.

Mashhadi, A. H. (2012). Impact of External Environment on the Performance of the Fast Food Industry. *International Journal of Management, Economics and Social Sciences, 1*(1), 19-25.

Mohd Rizaimy Shaharudin, J. J., & Suhardi Wan Mansor, S. J. (2010). Purchase Intention of Organic Food; Perceived Value Overview. *Canadian Social Science, 6*(1), 70-79.

Mondelaers, K., Verbeke, W., & Van Huylenbroeck, G. (2009). Importance of health and Environment as Quality Traits in the Buying Decision of Organic Products. *British Food Journal, 111*(10). http://dx.doi.org/10.1108/00070700910992952

Morgan, G. A., Leech, N. L., Gloeckner, G. W., & Barrett, K. C. (July 12, 2012). *IBM SPSS for Introductory Statistics: Use and Interpretation.* Routledge.

Mostafa, M. M. (2007). Gender differences in Egyptian consumers' green purchase be-haviour: The effects of environmental knowledge, concern and attitude. *International Journal of Consumer Studies, 31*(3), 220-9. http://dx.doi.org/10.1111/j.1470-6431.2006.00523.x

Mulyanegara, R. C., Tsarenko, Y., & Anderson, A. (Jan–Feb 2009). The Big Five and brand personality: Investigating the impact of consumer personality on preferences towards particular brand personality. *Journal of Brand Management, 16*(4), 234-247. http://dx.doi.org/10.1057/palgrave.bm.2550093

Niessen, J. H. (June 16-20, 2008). Identifying the gap between stated and actual buying behaviour on organic products based on consumer panel data. *16th IFOAM Organic World Congress, Modena, Italy*, 346-349.

Nishimura, J. S., & Tristán, O. M. (2011). Using the theory of planned behavior to predict nascent entrepreneurship. *Academia, Revista Latinoamericana de Administración, 46*, 55-71.

Olsen, S. O., & Grunert, K. G. (2010). The role of satisfaction, norms and conflict in families' eating behaviour. *European Journal of Marketing, 44*(7/8), 1165-1181. http://dx.doi.org/10.1108/03090561011047571

Opoku, R. A., Abratt, R., Bendixen, M., & Pitt, L. (2007). Communicating brand personality: Are the web sites doing the talking for food SMEs? *Qualitative Market Research: An International Journal, 10*(4), 362-374. http://dx.doi.org/10.1108/13522750710819702

Pal Kraft, J. R. (2005). Perceived difficulty in the theory of planned behaviour: Perceived behavioural control or affective attitude? *British Journal of Social Psychology, 44*, 479-496. http://dx.doi.org/10.1348/014466604X17533

Paul, J., & Rana, J. (2012). Consumer behavior and purchase intention for organic food. *Journal of Consumer Marketing, 29*(6), 412-422. http://dx.doi.org/10.1108/07363761211259223

Pearson, D., Henryks, J., & Jones, H. (2010). Organic food: What we know (and do not know) about consumers. *Renewable Agriculture and Food Systems, 26*(2), 1-7.

Peter Midmore, S. N., Anne-Marie Sherwood, D. V., & Mette Wier, R. Z. (2005). Consumer Attitudes to Quality and Safety of Organic and Low Input Foods: A review. *Quality Low Input Food*, 5-67.

Phuah, K. T., Rezai, G., Mohamed, Z., & Shamsudin, M. N. (2012). Consumers' awareness and consumption intention towards green foods. *African Journal of Business Management, 6*(12), 4496-4503. http://dx.doi.org/10.5897/AJBM11.1414

Pino, G., Peluso, A. M., & Guido, G. (2012). Determinants of Regular and Occasional Consumers' Intentions to Buy Organic Food. *The Journal of Consumer Affairs, Spring, 46*(1), 157-169. http://dx.doi.org/10.1111/j.1745-6606.2012.01223.x

Purkayastha, S. (2009). Brand Personality: An Empirical Study of Four Brands in India. *The Icfaian Journal of Management Research, 8*(4).

Radman, M. (2005). Consumer consumption and perception of organic products in Croatia. *British Food Journal, 107*(4), 263-273. http://dx.doi.org/10.1108/00070700510589530

Raj Arora, C. S. (2009). A mixed method approach to understanding brand personality. *Journal of Product & Brand Management, 18*(4), 272-283. http://dx.doi.org/10.1108/10610420910972792

Rajagopal. (2006). Insights from research Brand excellence: measuring the impact of advertising and brand personality on buying decisions. *Emerald Group Publishing Limited, 10*(3), 56-65.

Rajagopal. (2007). Buying decisions towards organic products: an analysis of customer value and brand drivers. *International Journal of Emerging Markets, 2*(3), 236-251.

Research Institute of Organic Agriculture (FiBL). (February 22, 2012). *Organic World: Global Organic Farming Statistics and News*. Retrieved from http://www.organic-world.net

Rezai, G., Mohamed, Z., & Shamsudin, M. N. (2011). Malaysian Consumer's Perceptive Towards Purchasing Organically Produce Vegetable. *International Conference on Business and Economic Research*, 3-10.

Richard Shepherd, M. M. (Jun 2005). Determinants of Consumer Behaviour Related to Organic Food. *Proquest Central, 34*(4-5), 352.

Riefer, A., & Hamm, U. (2008). Changes in Families' Organic Food Consumption. *12th Congress of the European Association of Agricultural Economists – EAAE 2008*. Ghent; Belgium.

Robert East, M. W. (2013). Consumer Behaviour: Applications in Marketing. *California: SAGE* .

Robyn, E., & Goodwin, B. A. (2008). Using knowledge, attitudes, social norms, past behaviour and perceptions of control to predict undergraduates‟ intention to incorporate glycaemic index into dietary behaviour. *Nutrition and dietetics, 66*(1), 54-59. http://dx.doi.org/10.1111/j.1747-0080.2008.01318.x

Rutherford, L. G., & DeVaney, S. A. (2009). Utilizing the Theory of Planned Behavior to Understand Convenience Use of Credit Cards. *Association for Financial Counseling and Planning Education*, 488-6687.

Sabiha Kilic, H. C. (December 2011). Consumers' "Brand Personality" Perception of Global Brands in Informational Technology: An Ampirical Research on Hitit University Students. *International Journal of Business and Social Science, 2*(22).

Salleh, M. M., Ali, S. M., Harun, E. H., Jalil, M. A., & Shaharudin, M. R. (2010). Consumer's Perception and Purchase Intentions Towards Organic Food Products: Exploring Attitude Among Academician. *Canadian Social Science, 6*(6), 119-129.

Samsudin, A., Jusoff, K., Zaini, Z. M. M., Musa, M., Khalid, K., Ngali, N., ... Hamid, M. (2011). Customer's Perception Towards Mcdonald's Icon-Based Nutritional Labels. *World Applied Sciences Journal 12 (Special Issue On Service Sector Transforms the Economy)*, 1-07.

Sangkumchaliang, P., & Huang, W. (2012). Consumers' Perceptions and Attitudes of Organic Food Products in Northern Thailand. *International Food and Agribusiness Management Review, 15*(1).

Ščasný, M., Urban, J., & Zvěřinová, I. (2012). What Motivates Czech Consumers to Buy Organic Food? *Czech Sociological Review, 48*(3), 709-736.

Scott Wysong, S. B. (2012). The Influence of Situational Variables on Brand Personality Choice. *International Journal of Marketing Studies, 4*(6).

Sekaran, U., & Bougie, R. (2010). *Research Methods for Business: A Skill Building Approach* (5th ed.). West Sussex, UK: John Wiley & Sons Ltd.

Shabnam, S. (July 2013). Proposed Model for Predicting Environmental Purchase Behavior of Consumers. *European Academic Research, I*(4), 444-466.

Shaharudin, M. R., Pani, J. J., & Suhardi Wan Mansor, S. J. (2010). Factors Affecting Purchase Intention of Organic Food in Malaysia's Kedah State. *Cross-cultural Communication, 6*(2), 105-116.

Shaharudin, M. R., Pani, J. J., Mansor, S. W., Elias, S. J., & Sadek, D. M. (May 2010). Purchase Intention of Organic Food in Kedah, Malaysia: A Religious Overview. *International Journal of Marketing Studies, 2*(1).

SMEDA. (2006, Dec). *Fast Food Restaurant*. Retrieved from http://www.smeda.org/

Sophonsiri, S., & Polyorat, K. (2009). The Impact of Brand Personality Dimensions on Brans Association and Brand Attractiveness: The Case Study of KFC in Thailand. *Journal of Global Business & Technology, 5*(2).

Suprapto, B., & Wijaya, T. (2012). Model of Consumer's Buying Intention towards Organic Food: A Study among Mothers in Indonesian. *International Conference on Economics, Business and Marketing Management, 29*, 1-8.

Swann Jr, W. B., Chang-Schneider, C., & Larsen McClarty, K. (2007). Do People's Self-Views Matter? Self-Concept and Self-Esteem in Everyday Life. *American Psychological Association, 62*(2), 84-94. http://dx.doi.org/10.1037/0003-066X.62.2.84

Tarkiainen, A., & Sundqvist, S. (2005). Subjective norms, attitudes and intentions of Finnish consumers in buying organic food. *British Food Journal, 107*(11), 808-822. http://dx.doi.org/10.1108/00070700510629760

Thompson, K. E., Haziris, N., & Alekos, P. J. (1994). Attitudes and Food Choice Behaviour. *British Food Journal, 96*(11), 9-13. http://dx.doi.org/10.1108/00070709410074632

Tirtiroglu, E., & Elbeck, M. (2008). Qualifying Purchase Intentions Using Queueing Theory. *Journal of Applied Quantitative Methods, 3*(2), 167-168.

Traci, H., & Freling, L. P. (2005). An Empirical Analysis of the Brand Personality Effect. *The Journal of Product and Brand Management, 14*(7), 404-413. http://dx.doi.org/10.1108/10610420510633350

Tsakiridou, E., Boutsouki, C., Zotos, Y., & Mattas, K. (2008). Attitudes and behaviour towards organic products: An exploratory study. *International Journal of Retail & Distribution Management, 36*(2), 158-175. http://dx.doi.org/10.1108/09590550810853093

Tung, S. J., Shih, C. C., Wei, S., & Chen, Y. H. (2012). Attitudinal inconsistency toward organic food in relation to purchasing intention and behavior: An illustration of Taiwan consumers. *British Food Journal, 114*(7), 997-1015. http://dx.doi.org/10.1108/00070701211241581

Voona, J. P., Nguib, K. S., & Agrawalc, A. (2011). Determinants of Willingness to Purchase Organic Food: An Exploratory Study Using Structural Equation Modeling. *International Food and Agribusiness Management Review, 14*(2).

Williams, B., Onsman, A., & Brown, T. (2010). Exploratory factor analysis: A five-step guide for novices. *Journal of Emergency Primary Health Care (JEPHC), 8*(3).

Wysong, S. B. (2007). Putting the "brand" back into store brands: an exploratory examination of store brands and brand personality. *Journal of Product & Brand Management, 16*(4), 226-235. http://dx.doi.org/10.1108/10610420710763912

Yangui, A., Font, M. C., & Gil, J. M. (2013). The effect of food related personality traits and lifestyle orientation on consumer's behavior related to extra virgin olive oil: estimation of an extended hybrid choice model. *4th International Conference of the African Association of Agricultural Economists* (pp. 22-25).

Yap, S., & Fen, N. A. (October 2008). An Extended Model of Theory of Planned Behaviour in Predicting Exercise Intention. *International Business Research, 1*(4).

Ye, S. (2012). The impact of destination personality dimensions on destination brand awareness and attractiveness: Australia as a case study. *Original scientific paper, 60*(4), 397-409.

Zakaria, S., & Wen, L. C. (2012). Relationship between Food Choice Motive and Organic Food Buying Decision: A Conceptual Study. *International Journal of Business and Behavioral Sciences, 2*(3).

Zakowska-Biemans, S. (2011). Polish consumer food choices and beliefs about organic food. *British Food Journal, 113*(1), 122-137. http://dx.doi.org/10.1108/00070701111097385

Zhen, J. S. S., & Mansori, S. (2012). Young Female Motivations for Purchase of Organic Food in Malaysia. *International Journal of Contemporary Business Studies, 3*(5).

Appendix

Constructs/ Cronbach's value	Items	Mean	Std. Deviation	Sources
Purchase Intention (0.84)	I intend to purchase organic fast food instead of conventional ones in the forthcoming month. I expect to purchase organic fast food instead of conventional ones in the forthcoming month. I plan to purchase organic fast food instead of conventional ones in the forthcoming month.	3.22	1.01	Adapted from Ajzen I. (2006); Kim, Han et al. (2010)
Subjective Norm (0.68)	Most people who are important to me thinking that I ... purchase organic fast food instead of conventional ones in the near future. I feel under social pressure to purchase organic fast food instead of conventional ones in the near future. My friends think that I… purchase organic fast food instead of conventional ones in the near future. What my friends think I should do are matters to me.	2.73	0.73	
Constructs/ Cronbach's value	**Items**	**Mean**	**Std. Deviation**	**Sources**
Perceived Control (0.70)	How much control do you have whether you do or do not purchase organic fast food? Purchasing of organic fast food or not is completely up to me. Purchasing of organic fast food costs too much money instead of conventional ones. When I have to costs too much money, I am.....to purchase organic fast food instead of conventional ones.	3.19	0.78	Adapted from Ajzen I. (2006); Kim, Han et al. (2010)
Sincerity (0.92)	Wholesome Real Sincere Family-orientation Traditionalism Friendly	3.28	1.00	Adapted from Aaker's (1997); Richard et al. (1998); Lee, (2009)
Excitement (0.89)	Imaginative Excited Cool Unique Trendy Up-to-date	3.03	0.93	
Competence (0.92)	Secure Reliable Intelligent Successful Corporate Leader	3.09	0.98	
Sophistication (0.90)	Upper-class Glamorous Feminine Smooth Charming	2.82	0.99	
Ruggedness (0.87)	Outdoorsy Masculine Tough Strong	2.64	1.03	

Modern Applied Science; Vol. 8, No. 3; 2014
ISSN 1913-1844 E-ISSN 1913-1852
Published by Canadian Center of Science and Education

Transverse Distribution Calculation and Analysis of Strengthened Yingjing Bridge

Liao Xiaofang[1] & Li Dongdong[1]

[1] Department of Civil engineering, Chongqing Jiaotong University, Chongqing, China

Correspondence: Liao Xiaofang, Department of Civil engineering, Chongqing Jiaotong University, Chongqing 400074, China. Tel: 86-136-2844-4207. E-mail: 290943158@qq.com

Received: February 28, 2014 Accepted: March 26, 2014 Online Published: April 23, 2014

doi:10.5539/mas.v8n3p107 URL: http://dx.doi.org/10.5539/mas.v8n3p107

Abstract

Box-girder has been adopted to strengthen bridge as large border girder, in which the original girders can be unloaded with box-girder bearing most loads. However, the load transverse distribution calculation method for it is still imperfect thus a modified calculation method is specially proposed to calculate the load transverse distribution in this case basing on existed methods. An engineering example is introduced to describe the calculation process and corresponding FEM model is established to validate the feasibility and applicability of this calculation method. Besides, comparisons between the load transverse distribution before and after strengthened are conducted which further proves that adding box-girder to the original bridge is an effective strengthening way.

Keywords: bridge strengthening, load transverse distribution, calculation method, box-girder

1. Introduction

Nowadays, strengthening the original bridge by adding large border girder to original girders has been a new tendency in bridge strengthening engineering (Wu & Zheng, 1997). According to the theory that the greater stiffness the girder obtains the more loads it will be subjected to, the risks of original girders can be greatly decreased with large border girder bearing most loads in this condition. So box-girder is naturally preferred as large border girder for strengthening to bear most loads due to its superior bending and torsional stiffness, which has been applied in practical engineering (Nie et al., 2010). Actually, the essential mechanism that this strengthening method works is that the transverse load is redistributed after adding box girder as large border girder. Therefore, exploring the new load transverse distribution becomes particularly necessary for both design and construction. Rigid connected girder method (Fan, 2001; He & Xie, 1996; Li & Shi, 1977) is usually used to calculate the load transverse distribution of assembly T-girder bridge but it can't be used in this condition since the differences of girder size and stiffness can't be taken into consideration.

Nie has proposed a method basing on rigid connected girder method to calculate the load transverse distribution and the cross section diagram of the bridge cited in his paper is shown in Figure 1. In that case, the box-girder is regarded as a large T-girder whose deformation is neglected which makes the results not that correct especially when the box-girder is large to some extent. Therefore, to more accurately calculate the load transverse distribution when strengthening with box-girder, a modified method is proposed in this paper on the basis of existed methods, in which the box-girder is divided into two T-girders with bending stiffness and torsional stiffness equally distributed to them, whose deformation can be taken into consideration.

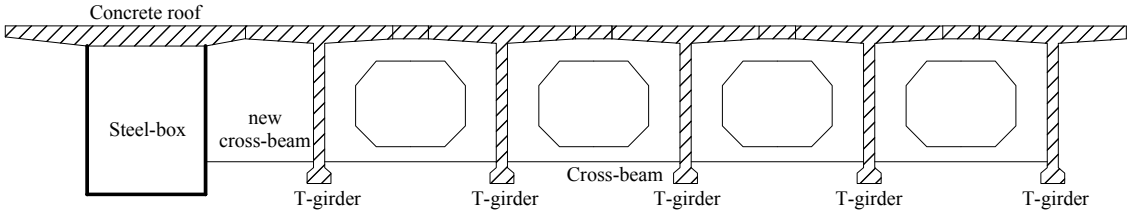

Figure 1. Cross section of bridge in Nie's paper

Calculation mechanism and process of this modified method are described relying on the strengthening project of Yingjing bridge (Zhou & Zhang, 1998; D. Zhang, J. Zhang, & Fan, 2003), whose FEM model is then established (Hambly, 1982) using grillage method to validate the applicability and feasibility of this calculation method. And then, comparisons between the load transverse distribution of Yingjing Bridge before and after strengthened are conducted which further proves that adding box-girder to the original bridge is an effective strengthening way to avoid cracks and improve the bearing capacity.

2. Project Summary

Yingjing Bridge, as a part of National Route 108, is the only bridge crossing Jing River in Sichuan province, China and completed in 1965. This bridge is 111.5 m in length and consists of 6 simply supported beams, with each span of 16.8 m (Figure 2). Cross section diagram of the simply supported beam is shown in Figure 3.

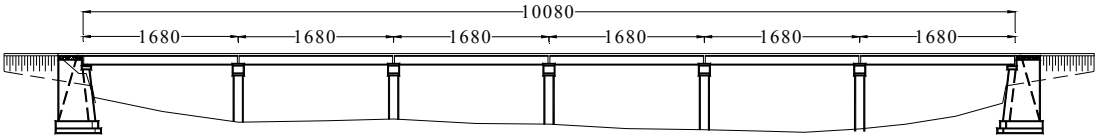

Figure 2. General arrangement diagram of Yingjing Bridge (unit: cm)

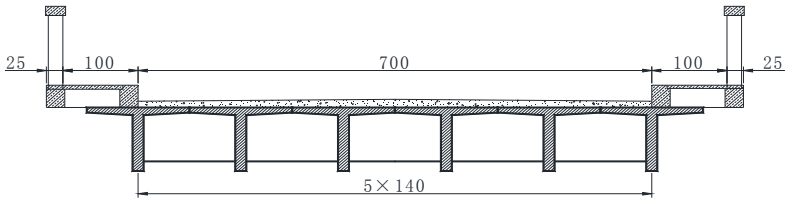

Figure 3. Cross section diagram of Yingjing Bridge (unit: cm)

Due to high traffic, many cracks were found in this bridge and most cracks are wide (the maximum of 2.0 mm) and concentrated especially to those of the T-girders lower edge. Hence, the bridge bearing capacity deduced greatly being only about 90% of the design that it was strengthened and broadened in June, 1997 to meet the increasing traffic requirements by adding two large box girders on both sides. The added box girder is reinforcement concrete, 3.55 m in width and 1.20 m in height (Figure 4(a)) whose detail size are shown in Figure 4(b) and (c).

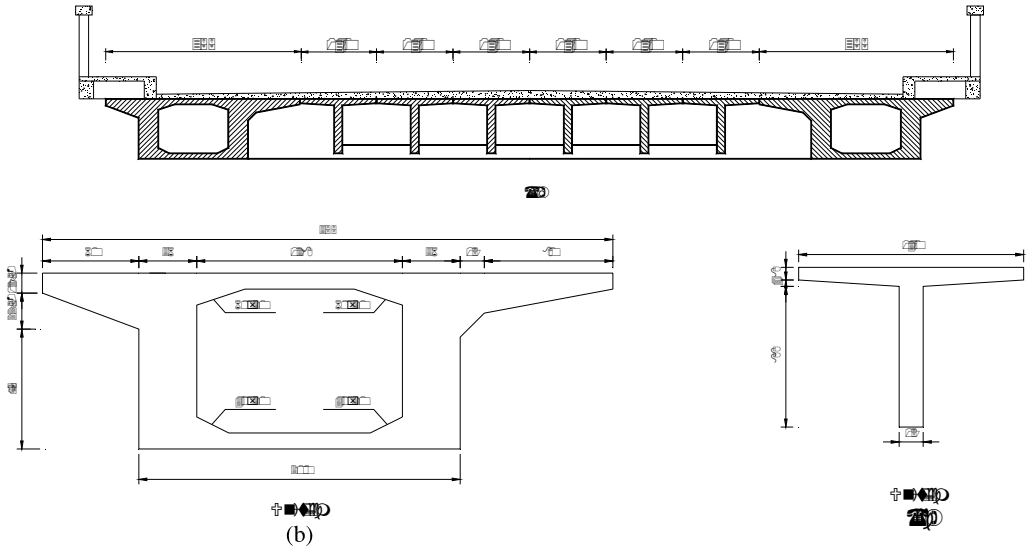

(b)

Figure 4. Cross section diagram of Yingjing Bridge after strengthened (unit: cm)

3. Analysis on Transverse Distribution of Yingjing Bridge

3.1 Calculation Process

To accurately calculate the load transverse distribution of the bridge after strengthened, divide the box girder into two T-girders with bending stiffness and torsional stiffness equally distributed (Figure 5) so that the box-girder deformation can be taken into consideration. It is worth noting that the centroids of the simplified T-girders should be overlapped with the box-girder to better keep the mechanic states and we can take the flange thickness of 1/3 section as the whole flange thickness when the flange thickness changed linearly. Transverse connections between each girder are separated along longitudinal replaced by vertical shear force and pure moment when main girder is subjected to the unit load (Figure 6). Then according to the principle of virtual work, the statically indeterminate canonical equation can be established as follows.

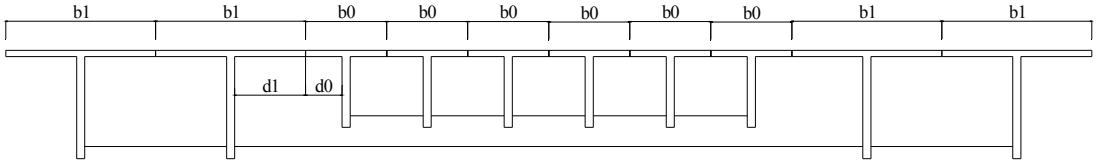

Figure 5. Calculation model of transverse distribution

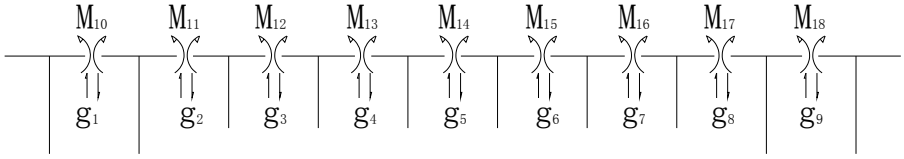

Figure 6. Redundant shear force and moment between girders

$$\sum_{m=1,2...9} \delta_{im} \cdot g_m + \sum_{n=10,11...18} \delta_{in} \cdot M_n + \delta_{ip}{}^{k} = 0 \quad (i = 1,2,....,17,18; m = 1,2...,9; n = 10,11,...,18; k = 1,2..10) \tag{1}$$

Where δ_{ij} means the structural flexibility coefficient, representing the deflection happens in the direction of redundant force i when redundant force j is unit load. And according to elastic reciprocal theory, $\delta_{ij} = \delta_{ji} \cdot \delta_{ip}{}^{k}$ equals to the deflection of beam i when unit load acts at girder k; g_m and M_n mean redundant shear and moment respectively. We can obtain all the δ_{ij} and $\delta_{ip}{}^{k}$ according to static equilibrium. Schematic diagram of calculating flexibility coefficient δ_{11} and $\delta_{10,10}$ is shown in Figure 7.

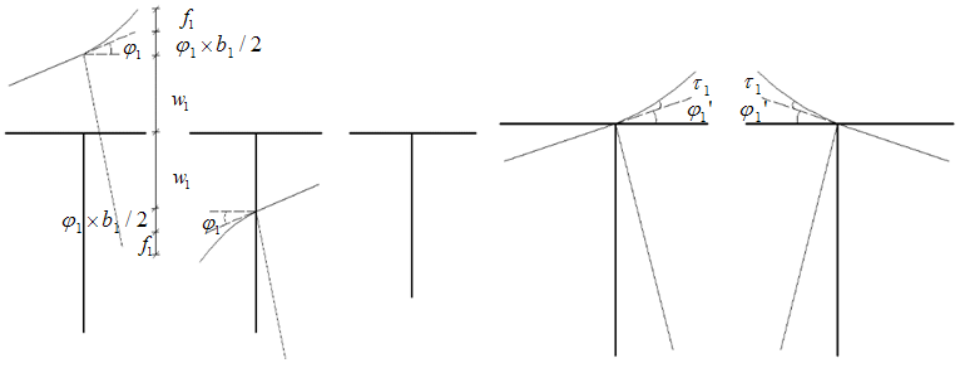

Figure 7. Schematic diagram of flexibility coefficient δ_{11} and $\delta_{10,10}$

$$\delta_{11}=\delta_{99}=2(w_1+\varphi_1\cdot\frac{b_1}{2}+f_1);\quad \delta_{22}=\delta_{88}=w_1+\varphi_1\cdot\frac{b_1}{2}+f_1+w_0+\varphi_0\cdot\frac{b_0}{2}+f_0$$

$$\delta_{33}=\delta_{44}=\delta_{55}=\delta_{66}=\delta_{77}=2(w_0+\varphi_0\cdot\frac{b_0}{2}+f_0);\quad \delta_{12}=\delta_{89}=-(w_1-\varphi_1\cdot\frac{b_1}{2})$$

$$\delta_{23}=\delta_{34}=\delta_{45}=\delta_{56}=\delta_{67}=-(w_0-\varphi_0\cdot\frac{b_0}{2});\quad \delta_{10,10}=\delta_{18,18}=2(2\varphi_1/b_1+\tau_1)$$

$$\delta_{11,11}=\delta_{17,17}=(2\varphi_1/b_1+\tau_1+2\varphi_0/b_0+\tau_0);\quad \delta_{12,12}=\ldots=\delta_{16,16}=2(2\varphi_0/b_0+\tau_0)$$

$$\delta_{1,11}=\delta_{8,18}=\varphi_1=-\delta_{2,10};\quad \delta_{2,11}=\varphi_1-\varphi_0=-\delta_{8,17};\quad \delta_{2,12}=\delta_{3,13}=\delta_{4,14}=\delta_{5,15}=\delta_{6,16}=\delta_{7,17}=\varphi_0$$

The other flexibility coefficients are all zero.

Where b_0,b_1 stands for the width of the inner and border girder while d_0,d_1 stands for the flange length of the inner and border girder; w_0, φ_0, and τ_0 respectively represent the girder deflection under unit load, rotating angle, cantilever deflection under shear force and cantilever deflection under moment of the inner-girder. Accordingly, w_1, φ_1, f_1 and τ_1 respectively represent similar parameter of the border girder. I_{tr1} and I_{tr0} are respectively the bending stiffness of the girder in lateral direction which consist of the bending stiffness of the diaphragms and the one of roof. $k_1=I_1/I_0$, $k_2=I_{t1}/I_{t0}$ respectively mean the bending inertia ratio and torsional inertia ratio between the large border-girder and the inner girder. $k_3=b_1/b_0$, $k_4=d_1/d_0$ respectively mean the flange width ratio and cantilever length of the border-girder to the inner girder.

$\gamma_0=5.8\frac{I_0}{I_{t0}}(\frac{b_0}{l})^2$ stands for the ratio parameter between bending inertia and torsional inertia of the inner girder, $\beta_0=\frac{\pi^4}{3}\frac{I_0}{l^4}\frac{d_0^3}{I_{tr0}}$ stands for the bending inertia ratio parameter between the longitudinal direction and transverse direction of girder. Similarly, $\gamma_1=k_3^2\gamma/k_2$ and $\beta_1=k_4^3\beta_0$ respectively stands for the same parameter of the border girder.

Then, the girder displacement matrix under unit load $[\delta_{ip}^k]$ can be described as follows

$$[\delta_{ip}^k]=\begin{bmatrix}
-1/k_1 & 1/k_1 & 0 & 0 & 0 & 0 & 0 & 0 & 0 & 0\\
0 & -1/k_1 & 1 & 0 & 0 & 0 & 0 & 0 & 0 & 0\\
0 & 0 & -1 & 1 & 0 & 0 & 0 & 0 & 0 & 0\\
0 & 0 & 0 & -1 & 1 & 0 & 0 & 0 & 0 & 0\\
0 & 0 & 0 & 0 & -1 & 1 & 0 & 0 & 0 & 0\\
0 & 0 & 0 & 0 & 0 & -1 & 1 & 0 & 0 & 0\\
0 & 0 & 0 & 0 & 0 & 0 & -1 & 1 & 0 & 0\\
0 & 0 & 0 & 0 & 0 & 0 & 0 & -1 & 1/k_1 & 0\\
0 & 0 & 0 & 0 & 0 & 0 & 0 & 0 & -1/k_1 & 1/k_1\\
0 & 0 & 0 & 0 & 0 & 0 & 0 & 0 & 0 & 0\\
0 & 0 & 0 & 0 & 0 & 0 & 0 & 0 & 0 & 0\\
0 & 0 & 0 & 0 & 0 & 0 & 0 & 0 & 0 & 0\\
0 & 0 & 0 & 0 & 0 & 0 & 0 & 0 & 0 & 0\\
0 & 0 & 0 & 0 & 0 & 0 & 0 & 0 & 0 & 0\\
0 & 0 & 0 & 0 & 0 & 0 & 0 & 0 & 0 & 0\\
0 & 0 & 0 & 0 & 0 & 0 & 0 & 0 & 0 & 0
\end{bmatrix}$$

Divided these flexibility coefficients by w_0 and take the results into Equation (1), the canonical equation can be obtained

$$[\delta_{ij}]\cdot[g_1]+[\delta_{ip}^k]=0 \tag{2}$$

Up to now, the redundant shear force (g_i, M_n) in each section can be obtained through solving the matrix equation. Assuming that unit load acts at 1# girder, then the transverse distribution when loading at 1# girder can be calculated:

$$\eta_{11}=1-g_1,\quad \eta_{21}=g_1-g_2,\quad \eta_{31}=g_2-g_3,\quad \ldots\quad \eta_{91}=g_8-g_9,\quad \eta_{10,1}=g_9$$

Similarly, the load transverse distribution can be also calculated when the unit load acts at 2# girder to 10# girder. In this calculation method, the box-girder is divided into two T-girders with the bending stiffness and torsional stiffness equally distributed thus there are altogether 10 T-girders rather than 6. Therefore, the actual distribution of the box-girder is the sum of two T-girders. And the final results are listed in Table 1 where girders from left to

right in cross section diagram (Figure 4) is numbered 1# to 8# in order and η stands for the transverse distribution coefficient, similarly hereinafter.

Table 1. The calculating result by the method in this paper

η	1#	2#	3#	4#	5#	6#	7#	8#
1#	0.749	0.562	0.450	0.338	0.236	0.148	0.080	0.010
2#	0.075	0.089	0.081	0.069	0.054	0.039	0.026	0.011
3#	0.060	0.081	0.084	0.078	0.067	0.053	0.039	0.020
4#	0.045	0.069	0.078	0.082	0.077	0.067	0.054	0.031
5#	0.031	0.054	0.067	0.077	0.082	0.078	0.069	0.045
6#	0.020	0.039	0.053	0.067	0.078	0.084	0.081	0.060
7#	0.011	0.026	0.039	0.054	0.069	0.081	0.089	0.075
8#	0.010	0.080	0.148	0.236	0.338	0.450	0.562	0.749

3.2 FEM Analysis

A finite element model on the basis of grillage theory is built using MIDAS/CIVIL to validate the accuracy of this calculation method (Figure 8). And the calculating result of load transverse distribution is listed in Table 2.

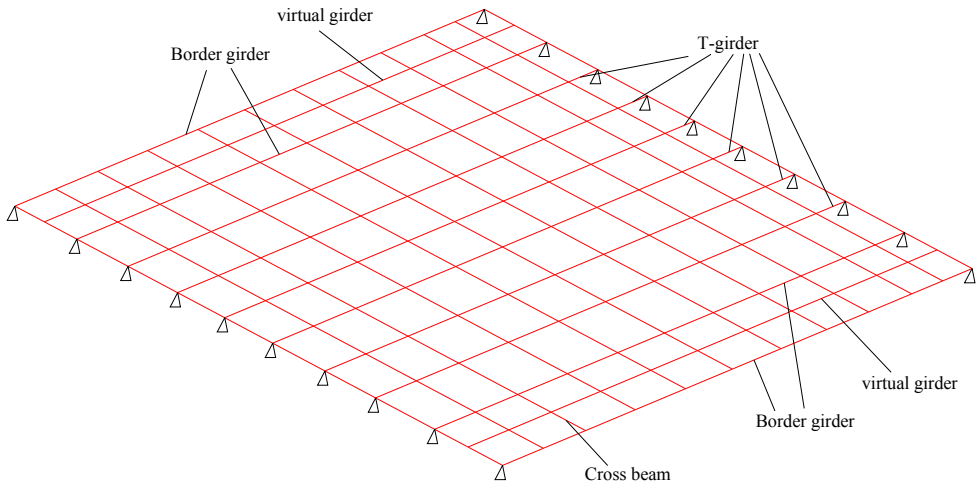

Figure 8. The finite element model on the basis of grillage theory

Table 2. Calculating result of load transverse distribution by FEM

η	1#	#2	3#	4#	5#	6#	7#	8#
1#	0.767	0.608	0.524	0.421	0.305	0.193	0.097	-0.032
2#	0.085	0.046	0.039	0.044	0.049	0.045	0.032	0.005
3#	0.069	0.047	0.039	0.042	0.053	0.060	0.053	0.019
4#	0.052	0.055	0.045	0.041	0.046	0.056	0.060	0.035
5#	0.035	0.060	0.056	0.046	0.041	0.045	0.055	0.052
6#	0.019	0.053	0.060	0.053	0.042	0.039	0.047	0.069
7#	0.005	0.032	0.045	0.049	0.044	0.039	0.046	0.085
8#	-0.032	0.097	0.193	0.305	0.421	0.524	0.608	0.767

It can be concluded that the analytical results in this method conform well to the FEM results as shown in Figure 9(a)-(d), which proves that it is an effective way dividing the box-girder into two T-girders when calculating the load transverse distribution with large box girder whose deformation can't be neglected.

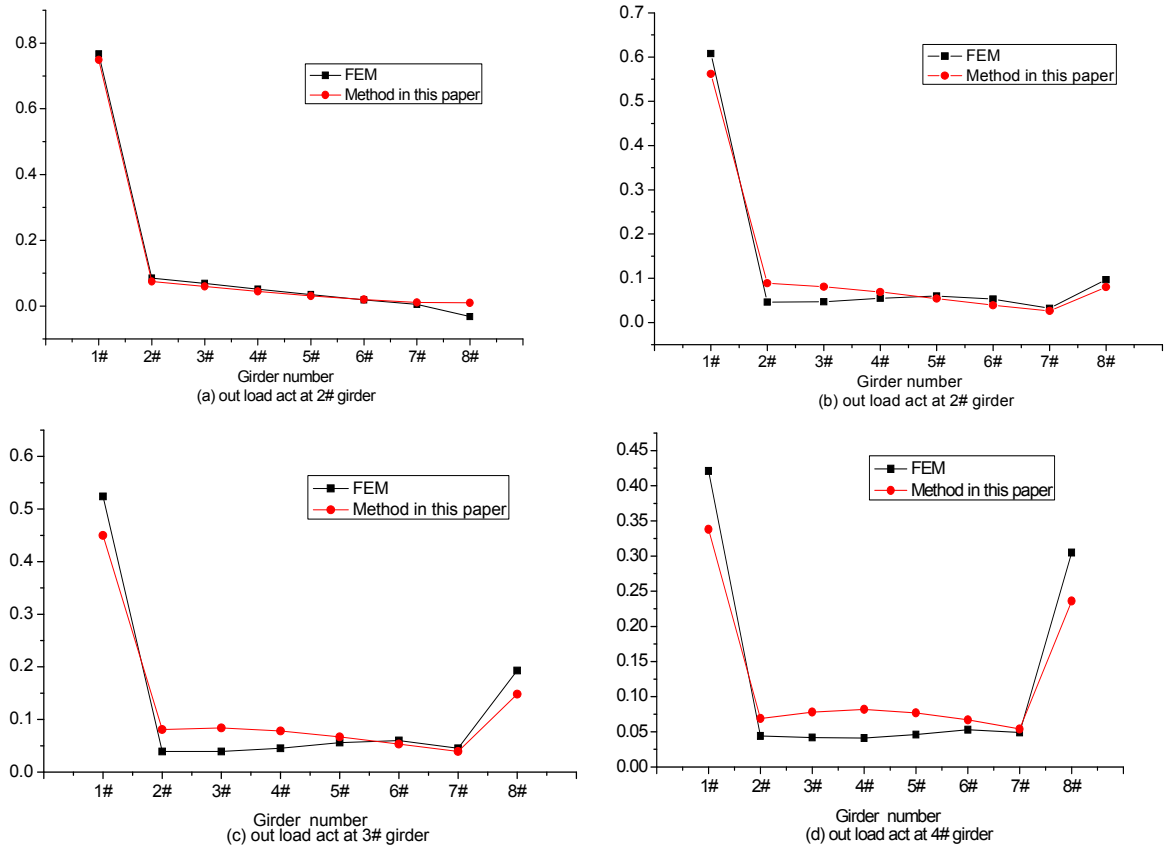

Figure 9. Transverse distribution when load act at different girders

3.3 Comparison to the Transverse Distribution before Strengthened

To explore the strengthening effects, the load transverse distribution of Yingjing Bridge before strengthened (Figure 3) are calculated by conventional rigid connected girder method and the calculation results are listed in Table 3 where girders from left to right in cross section diagram (Figure 3) is numbered 1# to 6# in order.

Table 3. Load transverse distribution of Yingjing Bridge before strengthening

η	1#	2#	3#	4#	5#	6#
1#	0.471	0.347	0.225	0.104	–0.015	–0.133
2#	0.347	0.276	0.203	0.13	0.058	–0.015
3#	0.225	0.203	0.181	0.156	0.13	0.104
4#	0.104	0.13	0.156	0.181	0.203	0.225
5#	–0.015	0.058	0.13	0.203	0.276	0.347
6#	–0.133	–0.015	0.104	0.225	0.347	0.471

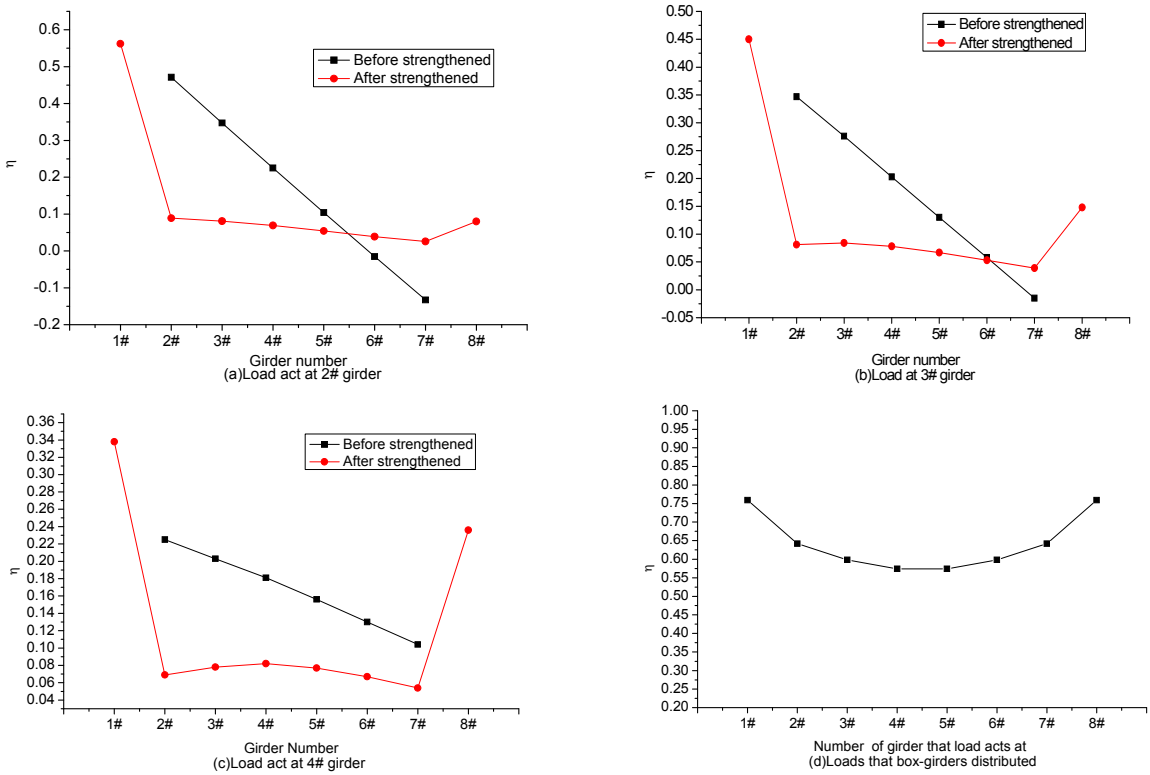

Figure 10. Analysis of strengthening effect

As shown in Table 3 and Figure 10(a)-(c), the loads distributed on T-girders after strengthened decrease greatly than the one before strengthened. Taking 2# girder as an example, the load distributed on 2# girder decreases from 34.7% to 8.9% when the load acts at 2# girder, that is, the girder has been efficiently unloaded due to the large border girder. Besides, the load distributed on added box-girders maintains stable, always being over 55% wherever the load acts (Figure 10(d)), which further proves that adding box-girder to the original bridge is an effective strengthening way to avoiding cracks and improve the bearing capacity.

4. Conclusions and Suggestion

On the basis of analysis above, the following conclusions can be drawn

(a) The load transverse distribution calculation method proposed in this paper takes not only the size differences but also the box girder deformation into consideration, which is especially fit for the load transverse distribution calculation referred to large box-girder whose deformation can't be neglected.

(b) The accuracy of this calculation method is validated through an engineering example whose analytical results conform well to the FEM one.

(c) The comparisons between the loads transverse distributions before and after strengthened further prove that adding box-girder to the original bridge is an effective strengthening way to avoid cracks and improve the bearing capacity.

The load transverse distribution calculation method proposed in this paper can be used to calculate the load transverse distribution of bridge with large box-girder whose deformation can't be neglected. Though the results are correct, there still exists some simplifications and there is still a long way to go to expand its application range.

References

Fan, L. C. (2001). *Bridge Engineering*. Bejing: China Communications Press.

Hambly, E. C. (1982). *Bridge Deck Behaviour* (1st ed.). Beijing: People's Railway Press.

He, S. H., & Xie, R. W. (1996). *Calculation Method of Transverse Distribution in Highway Bridge*. Bejing: China Communications Press.

Li, G. H., & Shi, D. (1977). *Calculation of Load Transverse Distribution in Highway Bridge*. Beijing: China Communications Press.

Nie, J., Zhang, X., Fan, J., Li, Y., & Xu, R. (2010). Transverse Distribution Coefficient of Concrete Bridges Widened with Steel-concrete Composite Beams. Beijing*: Journal of Tsinghua University (Natural Science Edition), 50*(6), 805-809.

Wu, Q. X., & Zheng, Z. F. (1997). The Simplified Calculation of Crosswise Loading Distribution of the Straight Beam Bridge with Large Skirt Beams. *Fuzhou: Journal of Fuzhou University (Natural Science Edition), 25*(2), 86-89.

Zhang, D. Q., Zhang, J. T., & Fan, L. (2003). Investigation on Widening and Reinforcing the Yingjing Bridge by Installing a Box-Girder. *Chongqing: Journal of Chongqing Architecture University, 25*(1), 94-99.

Zhou, Z. X., & Zhang, J. T. (1998). Widening and Strengthening Research on Yingjing Bridge. *Beijing: Engineering Mechanics, A*(02), 425-429.

Modern Applied Science; Vol. 8, No. 3; 2014
ISSN 1913-1844 E-ISSN 1913-1852
Published by Canadian Center of Science and Education

Using Fuzzy Set Approaches in a Raster GIS for Land Suitability Assessment at a Regional Scale: Case Study in Maros Region, Indonesia

Nurmiaty[1] & Sumbangan Baja[2,3]

[1] Department of Estate Crops Cultivation, Pangkep State Polytechnic of Agriculture, South Sulawesi, Indonesia

[2] Department of Soil Science, Hasanuddin University, Makassar, Indonesia

[3] Center for Regional Development and Spatial Information (WITARIS), Hasanuddin University, Jl. Perintis Kemerdekaan Km. 10, Makassar, 95245, Indonesia

Correspondence: Sumbangan Baja, Department of Soil Science, Hasanuddin University, Makassar, Indonesia. Tel (+Fax): 62-0411-587-076, E-mail: sbja02@yahoo.com.au

Received: March 1, 2014 Accepted: March 28, 2014 Online Published: April 23, 2014

doi:10.5539/mas.v8n3p115 URL: http://dx.doi.org/10.5539/mas.v8n3p115

Abstract

Recently, spatial data on land resources have become more available, detailed, and sophisticated. Accordingly, it requires a method that could deal with those complex and detailed data in an effective way. A fuzzy set method with the semantic import model (SIM) was utilized within a raster GIS (geographic information systems) to analyze the area of Maros Regency on a reconnaissance scale basis. In this study, land attribute values were converted into continuous values (ranging from 0 to 1.0), according to the class limit determined based on field experiences, results of experiments, or fixed conventional standards. The evaluation criteria were based on land attributes which are divided into two main components: soil profile and topography. Each of land attributes within each component was valued from 0 (minimum) to 1.0 (maximum) according to the suitability of maize. Those values were represented as membership values, also ranging from 0 to 1.0. The result from land suitability analysis in Maros Regency for maize cultivation indicates that around 25% of land areas have a land suitability index (LSI) value of above 0.70 (suitable and very suitable), about 11% fall between 0.50 and 0.70 (moderately suitable), and 63% under 0.5 (not suitable). The main limiting factor for maize cultivation in this region is topography, especially slope gradient (s).

Keywords: fuzzy set, land suitability index, GIS, Maros Regency

1. Introduction

With the increasing availability of detailed spatial data on land resources, it requires a method that could deal with those data in an effective way, especially in assessing land quality for planning purposes. Basically, two basic types of land suitability evaluation are commonly recognized. The first is a categorical system (CS), and the second is based on continuous functions (CF) (Baja et al., 2001). As its name implies, the CS technique uses categorical classes to examine different levels of land properties and thus to represent the outputs generated. The system is also characterized by an a *priori* determination of 'land mapping units' that apply to all land attributes selected as evaluation criteria: these units will then become the basis for the output delineation of the overall analyses (Albaji et al., 2009; Al-Mashreki et al., 2011; Ashraf et al., 2011; Babalola et al., 2011; Chandio et al., 2011; Chinene et al., 2007; Jafarzadeh et al., 2008). The CF technique, on the other hand, takes into account the spatial continuity of land characteristics, and the outputs of the analysis are then presented as continuous grades (or indices) of land suitability. In the context of land resource assessment, a fuzzy set function (a continuous basis) is commonly used to undertake a CF technique (Baja et al., 2002; Burrough, 1989). Fuzzy set functions are also often used for other than land resources assessment areas, as done by Chen et al. (2010), Chiclana et al. (2007), Nardi and Nazori (2012), Mangaraj and Das (2008), Srivastava et al. (2013), Vucetic and Simonovic (2013), Wang and Chan (2013), and Zhang et al. (2013).

Maros Regency is currently developing a database of the region and runs several projects related to agricultural sector planning and development. The availability of data that has been built is thus important for application of more sophisticated and detailed methods to assist in more accurate land use planning until the stage of

implementation. The main objective of this research is to assess land suitability for maize cultivation using a fuzzy set approach in a GIS. A raster based GIS was used to undertake every stage of spatial analysis in land suitability assessment.

2. Method

2.1 Study Area

The study area (Maros Regency) is located about 30 km north of Makassar City, the capital of South Sulawesi Province (Figure 1). It lies between latitudes 4°711' and 5°2' S, and stretches between longitudes 119°453' to 119°977' W. The area selected for this study includes all parts of Maros District covering a total area of 144,085 ha. Based on the land system map (RePPProT, 1988), the dominant soil type in study area are dystropepts, with an average distribution coverage is 76.236 ha (52.9%), followed by tropaquepts and tropudults, with an average coverage is 38.640 ha (26.8%) and 7.980 ha (5.5%), respectively. Other soil types found in the area are rendolls, eutropepts, haplustults, and paleudults (see Nurmiaty & Baja, 2013).

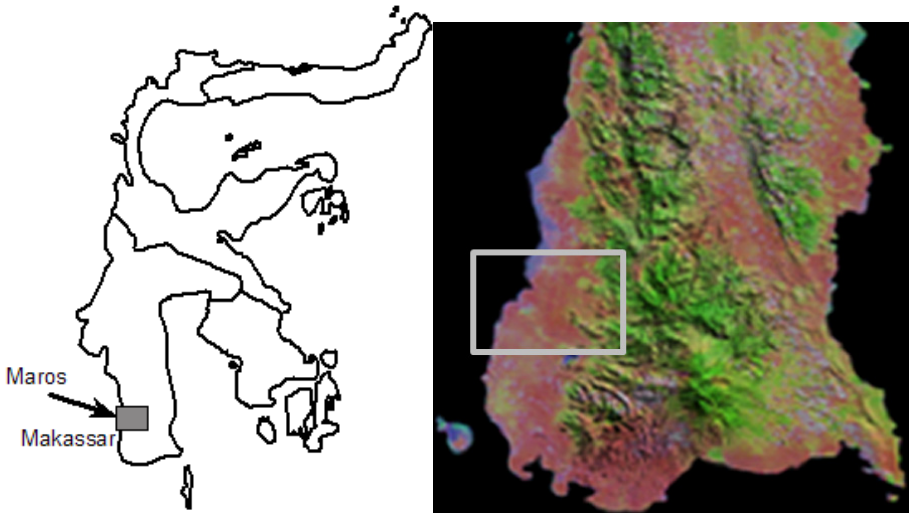

Figure 1. Location of study area (white box, right) in Sulawesi Island (left)

2.2 Database and Preliminary Data Processing

The main sources of database used in this study include: (i) digital topographic map; (ii) soil map and soil characteristics; (iii) climate data; and (iv) digital elevation model (DEM).

The primary reference for soil data layers is the results of soil survey undertaken by the local government of Maros Regency. Land mapping units (based on land system) were derived from a land system map to provide a basis for field survey (Figure 2). As many as 25 homogeneous mapping units were identified in the area of interest, and soil sampling was done in 25 locations. Soil and climate characteristics surveyed and analysed include the followings (see Table 1). The data on climate such as average temperature, rainfall, and number of dry months were obtained from local meteorological station of Maros.

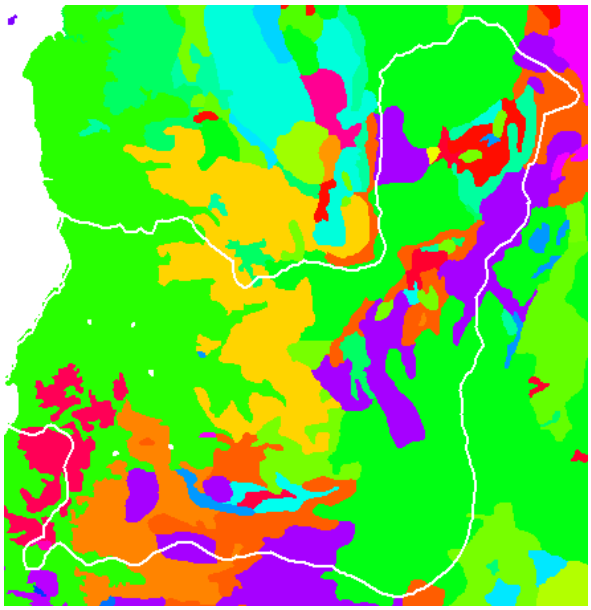

Figure 2. Land mapping unit (LMU) based on land system

Digital topographic maps of study area with a scale of 1:50,000 from the National Agency for Survey and Mapping were used as a reference for generating a DEM (Figure 3). The digital topographic maps were available in a vector GIS format, makes it easier to build database in a standard vector GIS, before converted to a raster format. All the data layers were stored using UTM (Universal Transverse Mercator) coordinate system. As the area of interest covers three sheets of topographic maps, then a process of joining all the elements of map layer was undertaken, before precisely defining the boundary of study area.

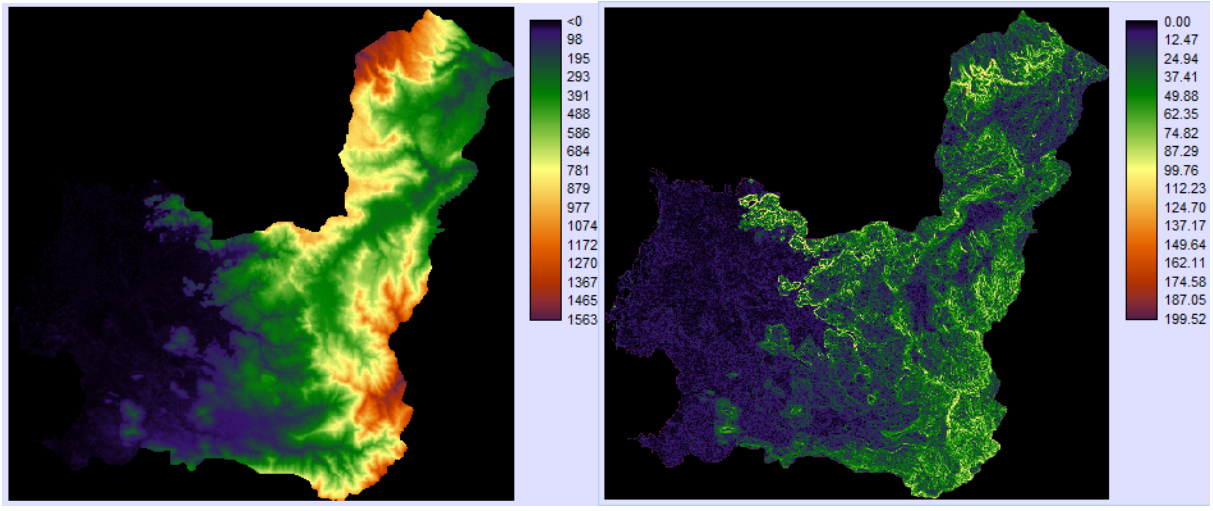

Figure 3. Digital Elevation Model (DEM) and derived slope map of study area

Table 1. Land quality and land characteristics used in the analysis (base on Djaenuddin et al., 2003; FAO, 1976)

Land Qualities	Land Characteristics
Temperature (t)	Average temperature (^oC)
Water availability (w)	Rainfall (mm), number of dry months
Rooting condition (r)	Texture, drainage, soil depth (cm)
Nutrient retention (f)	Clay CEC (cmol/kg), base saturation (%), pH (H2O), organic C (%)
Toxicity (x)	Salinity (dS/m)
Nutrient availability (n)	N, P_2O_5, K_2O
Terrain (s)	Slope (%), surface stoniness (%), surface outcrops (%)

2.3 Fuzzy Set Method

A fuzzy set method with the semantic import model (SIM) was utilized within a GIS to analyze the area of Maros Regency on a reconnaissance scale basis. In this study, land attribute values were converted into continuous values (ranging from 0 to 1.0) (Zadeh, 1965), according to the class limit determined based on field experiences, results of experiments, or fixed conventional standards (Baja, 2012; Galindo et al., 2005; Moreno, 2007; Sediyono et al., 2013; Sui, 1992). The evaluation criteria were based on land attributes which are divided into two main components: soil profile, and topography (Figure 4) (Baja, 2009; Baja et al., 2002). Figure 4 will include climate parameters if they have distinguished sub-region and are limiting for maize cultivation in the study area.

Each of land attributes within each component was valued from 0 (minimum) to 1.0 (maximum) according to the suitability of maize (see Keshavarzi et al., 2010, 2011; Kurtener et al., 2008; Mohammadrezaei et al., 2013; Reshmidevi et al., 2009; Sarmadian et al., 2010). Those values were represented as the membership value ranging from 0 to 1.0. Analytical procedure is conducted through the following steps: (i) selecting and designing evaluation criteria, (ii) standardizing the data set, (iii) determining the field/climate attribute values, (iv) choosing appropriate scoring functions and the parameters (Baja et al., 2001), (v) converting data format between software programs (raster to vector or *vice versa*). The analysis procedure is then continued to three main steps (see Baja et al., 2002, 2007).

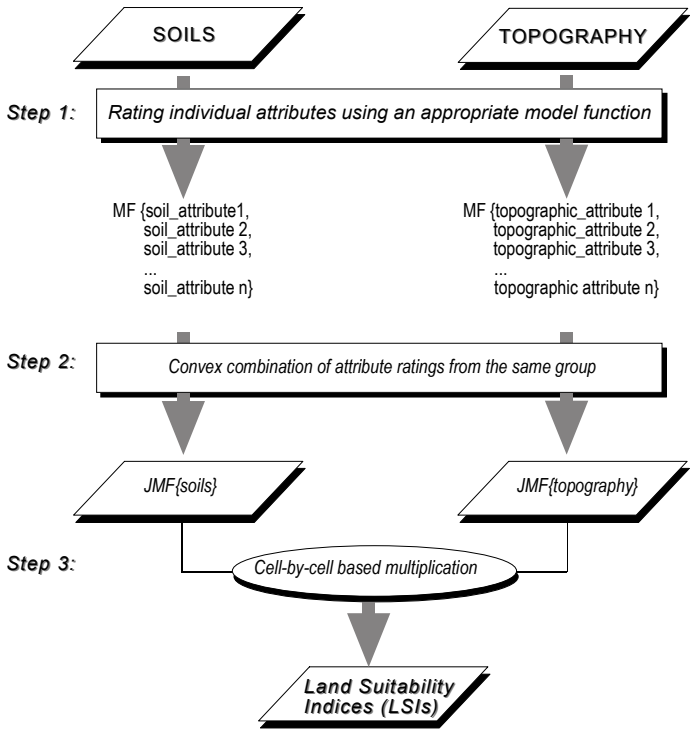

Figure 4. Schematic diagram of the procedure used in this study (source: Baja et al., 2002)

Step 1, determination of the individual rank from the land attributes, using equations (Burrough, 1989):

$$MF(xi) = [1 / (1 + \{(x_i - b) / d\}^2)] \text{ if } 0 < MF(x_i) < 1 \quad (1)$$

For optimum range (Model 2):

$$MF(x_i) = 1 \text{ if } (b_1 + d_1) < x_i < (b_2 - d_2) \quad (2)$$

For asymmetric left (Model 3):

$$MF(x_i) = [1 / (1 + \{(x_i - b_1 - d_1) / d_1\}^2)] \text{ if } x_i < (b_1 + d_1) \quad (3)$$

For asymmetric right (Model 4):

$$MF(x_i) = [1 / (1 + \{(x_i - b_2 + d_2) / d_2\}^2)] \text{ if } x_i > (b_2 - d_2) \quad (4)$$

where $MF(x_i)$ = the individual membership value for the i^{th} soil attribute x, d = the range of transitional zone (that is, x in MF = 0.5 or otherwise mentioned as a crossover point, CP), x_i = the i^{th} soil attribute (x) value, and b = the value of soil attribute x in the ideal point.

Step 2, derivation of the land attribute class rank, through the integration of the land attribute membership values using the following convex combination (Baja et al., 2002):

$$JMF(X) = \sum_{i=1}^{n} \lambda i \, MF(xi) \quad (5)$$

where $0 < JMF(X) < 1$; $0 < MFxi < 1$; $\lambda 1 + \lambda 2 + \lambda 3 + \ldots + \lambda n = 1$, and $0 < \lambda i < 1.0$. The JMF (X) symbol is the plural membership function from the entire variable that considered in the X class, λi is the value factors for land attribute x which in i, MF(xi) is the membership value for the xi land attribute, and n represent the number of land attributes considered.

Step 3, calculating an overall land suitability index (LSI), using the multiplication function which is based on the cell by cell in raster GIS, as follows:

$$LSIp(maize) = JMF(S(p)) \times JMF(T(p) \times JMF(C(p)) \quad (6)$$

where LSIp(*maize*) is LSI for maize at cell p, JMF(S(*p*)), JMF(T(*p*)), and JMF(C(*p*)) are JMF value at cell *p* for soil profile, topography, and climate, respectively. Use of multiplication function indicates that there is no compensation between land attribute. In other words, land area with an extreme limitation could not be compensated, by other excellent land characteristic, or *vice versa* (Baja et al., 2001, 2002). The multiplication function then generates a land suitability index (LSI) which is represented in the form of continuous value, ranging from 0 (not suitable) to 1.0 (very suitable) (Baja et al., 2002; Elaalem, 2010, 2012, 2013).

3. Results and Discussion

3.1 Fuzzy Set Parameters

The rating of soil attributes is established on the basis of the available soil mapping units (SMUs) which have 'crisp' boundaries, while that of topography is based on the DEM which has continuous values. Therefore, at this stage the unit for individual soil attributes is SMUs (see Figure 3), while for topography (slope) it is data cells in the DEM layer. (Nevertheless, it is necessary to point out that it is possible to use different mapping units for different soil attributes by using a *kriging* technique (Chaudhry et al., 2013; Gonzales et al., 2013; Taboada et al., 2013), which is better undertaken in detailed studies involving intensive soil sampling). In the present study, each land attribute is rated with values ranging from 0 (minimum) to 1.0 (maximum) according to its suitability for a nominated land use. Such values are represented as membership grades or membership function (*MF*) values. The analysis indicates that the dominant MF values for internal soil attributes in the study area are between 0.80 and 0.90.

Based on the suitability analysis using fuzzy set method, climate factor in the study area showed that all the data fulfilled the optimum criteria for the evaluation of land suitability of maize in the entire study area. Thus, the fuzzy parameter for climate value of the entire study area is 1.0 (maximum). Furthermore, the study area has a varied topography, ranging from flat to mountainous, with the gentle slope to very steep (Figure 3). The area is relatively flat and gentle slopes generally located in the western part of the study area, while mountainous area and steep terrain are found in the eastern part of the study area. Spatial distribution of land surface parameters using fuzzy method is shown in Figure 5.

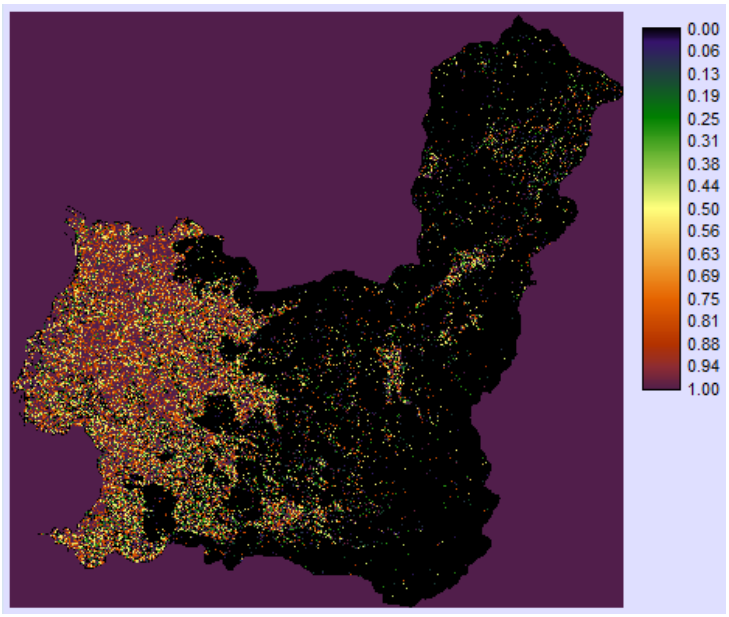

Figure 5. Distribution of MF value for slope gradient

3.2 Land Suitability Index (LSI)

Distribution of LSI derived from applying a fuzzy set method shown in Figure 6. The result from land suitability analysis in Maros Regency for maize cultivation indicates that around 25% of land areas have an LSI value of above 0.70 (suitable and very suitable), ±11% fall between 0.50 and 0.70 (moderately suitable), and ±63% under 0.5 (not suitable) (Figure 6). The main limiting factor for maize cultivation in this region is land surface, especially slope gradient (s).

The figures indicate that three-quarters of the study area is not suitable for the development of maize, and predominantly caused by slope gradient factors, although it was found that soil attributes are in a good condition. Furthermore, about one-third of the study area is available (as appropriate) for the development of maize, by assuming that the decision makers will give the highest priority to areas above LSI values of more than 0,50 (marginally, moderately, and suitable) (see also classification in Table 2).

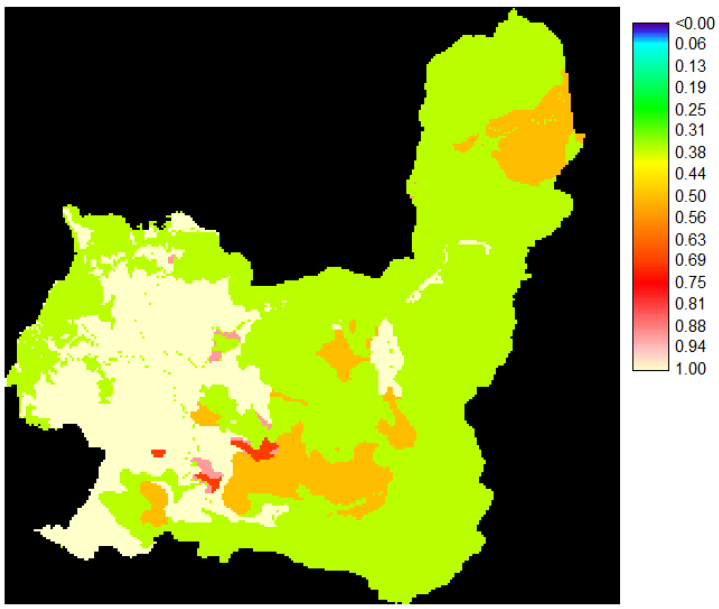

Figure 6. Distribution of LSI derived from applying a fuzzy set method

Figure 7 presents LSI distribution after reclassification into five classes. Percentage of LSI coverage is presented in Table 2. Area with the highest coverage is class 1 (not suitable for corn planting) accounted for 64.21% and followed by class 5 (very suitable for maize) accounted for 24.17%. There is a substantial proportion of area unsuitable for maize due to a sulphuric characteristic and became limiting for the development of maize cultivation.

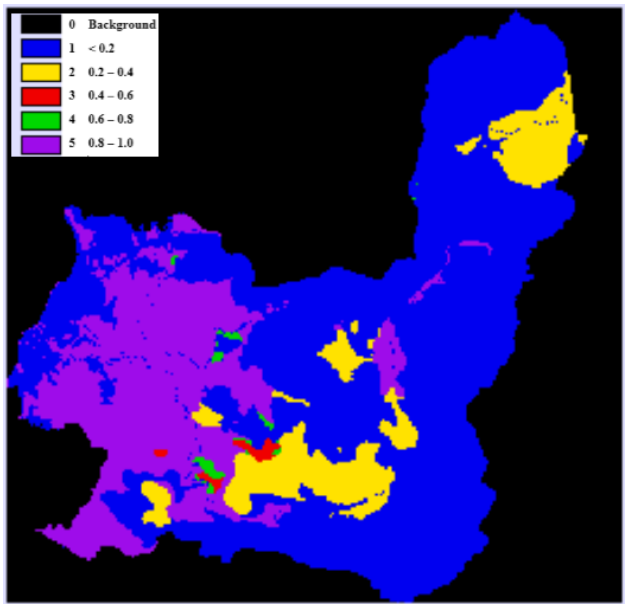

Figure 7. Distribution of LSI after reclassing according to classes

Table 2. Land suitability for maize in the study area

Class	LSI	Land suitability category	Area (ha)	Percent from total area (%)
1	< 0.2	Permanently not suitable	90,568.79	64.21
2	0.2-0.4	Currently not suitable	14,966.75	10.61
3	0.4-06	Marginally suitable	662.63	0.47
4	0.6-0.8	Moderately suitable	749.06	0.53
5	0.8-1.0	Suitable	34,096.54	24.17
Total			141,043.78	100

3.3 Ground Observation

The purpose of ground observation is to see the difference in quality of land in different land index. As shown in Figure 8a with quality land suitable for corn (LSI 0.8-1.0), 8b moderately suitable land quality (LSI 0.6-0.8), 8c marginally suitable (LSI 0.4-06), 8d currently not suitable (LSI 0.2-0.4), and 8e are permanently not suitable (LSI < 0.2). Figure 8d is limited by nutrient deficiency factor and slope, being in the figure 8e constrained by the slope, surface rock and soil depth factors.

Figure 8. Visualisation of land quality in accordance with suitability for corn: a. suitable (LSI 0.8-1.0), b. moderately suitable (LSI 0.6-0.8), c. marginally suitable (LSI 0.4-06), d. currently not suitable (LSI 0.2-0.4), e. permanently not suitable (LSI < 0.2)

The main limiting factor to agricultural development in the study area is slope gradient. In this area, steep slope is quite dominant, especially in the eastern and northeastern parts. Land area with slopes of more than 17% and is not suitable for agricultural development, is found almost half of the total study region (see Figure 9). The rest is areas having a slope of less than 17%, occupying areas currently used for agricultural land, including rice fields, plantations, and dryland agriculture. The area suitable for agriculture development is predominantly found in the western part of the study area (see Figure 3). Other factors that are limiting in the area of interest are soil depth and surface stoniness. Both factors seem to correlate and are generally found in areas that lie within a steep slope (see Figure 8e).

This analysis also confirms that LSI values tend to correspond with the limiting factors mentioned above, where LSI is lower in areas that have heavy limitations (generally in the eastern and northeastern) and higher in areas that have a light limiting condition (in western section). Based on previous study (Nurmiaty & Baja, 2013), most of maize farming areas in Maros regions are found in areas with slope > 17% (Tompobulu, Camba, Moncongloe, Mandai and Mallawa subdistricts) while areas with slope < 17% is generally used for urban areas and paddy fields (Maros Baru, Turikale, Lau, Bantimurung and Simbang subdistricts). Some proportion of land areas for maize is also found in coastal zones (Bontoa Subdistrict). Due to extensive farming of maize in a relatively steep land, farming communities in this area have recently received a negative impact on the environment such as flash floods, droughts, and landslides, and such natural phenomena have never been occurred before in Maros (Nurmiaty et al., 2014).

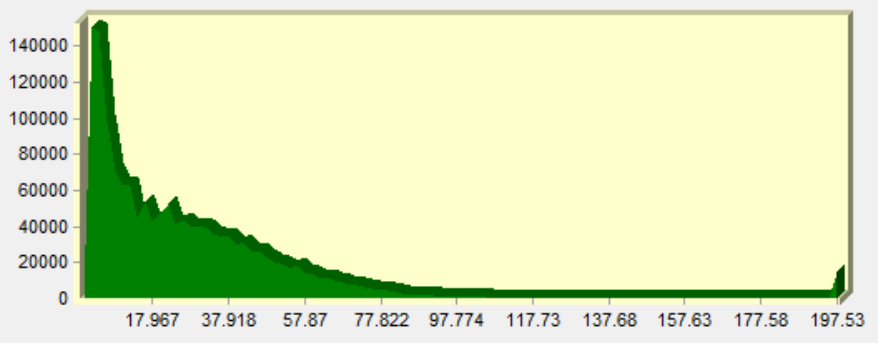

Note: X-axis: slope (degree), Y-ordinat: number of pixels (1 pixel= 30 x 30 meters)

Figure 9. Spatial distribution of slope in the study area

4. Conclusion

This study has performed the use of fuzzy set in the assessing land suitability for maize cultivation in Maros region. The evaluation criteria were based on land attributes which are divided into two main components: soil profile and topography. Each of field attributes within each component was valued from 0 (minimum) to 1.0 (maximum) according to the suitability of maize. Those values were represented as the membership values, also ranging from 0 to 1.0. The results indicate that around 25% of land areas have an LSI value of above 0.70 (suitable and very suitable), ± 11% fall between 0.50 and 0.70 (moderately suitable), and ± 63% under 0.5 (not suitable). Three-quarters of the study area is not suitable for the development of maize, and predominantly caused by slope gradient factors, and the rest one-third of the study area is suitable for the development of maize, with LSI values of more than 0,50 (moderately, suitable, and very suitable).

Acknowledgements

The authors are deeply thankful to the DP2M DIKTI (through the HIBAH KOMPETENSI research grand), Maros Regency government (Bappeda Maros), and The Center for Regional Development and Spatial Information (WITARIS), Hasanuddin University, for providing data, fund, and other supporting facilities in this study.

References

Albaji, M., Naseri, A. A., Papan, P., & Nasab, S. B. (2009). Qualitative evaluation of land suitability for principal crops in The West Shoush Plain, Southwest Iran. *Bulgarian Journal of Agricultural Science, 15*(2), 135-145.

Al-Mashreki, M. H., Akhir, M., Bin, J., Rahim, S. A., Desa, K. M., Lihan, T., & Haider, A. R. (2011). Land suitability evaluation for sorghum crop in the Ibb Governorate, Republic of Yemen using remote sensing and GIS techniques. *Australian Journal of Basic and Applied Sciences, 5*(3), 359-368.

Ashraf, S. H., Manoukyan, R., & Ayoubi, S. H. (2011). Land suitability evaluation in Damghan Plain for Barley, using compare and conformity methods (Northeast-Iran). *Pakistan Journal of Biological Sciences, 14*, 123-127. http://dx.doi.org/10.3923/pjbs.2011.123.127

Babalola, T. S., Oso, T., Fasina, A. S., & Godonu, K. (2011). Land evaluation studies of two wetland soils in Nigeria. *International Research Journal of Agricultural Science and Soil Science, 1*(6), 193-204.

Baja, S. (2009). Land use choice and land resource assessment in agriculture. *CAB Reviews: Perspectives in Agriculture, Veterinary Science, Nutrition and Natural Resources, 4*(15), 1-9. http://dx.doi.org/10.1079/PAVSNNR20094015

Baja, S. (2012). *Perencanaan Tata Guna Lahan dalam Pengembangan Wilayah: Pendekatan Spasial dan Aplikasinya*. Penerbit Andi, Yogyakarta.

Baja, S., Chapman, D. M., & Dragovich, D. (2001). A conceptual model for assessing agricultural land suitability at a catchment level using a continuous approach in GIS. *Proceedings of the Geospatial Information and Agriculture Conference* (pp. 828-841). Sydney NSW Agriculture, Sydney.

Baja, S., Chapman, D. M., & Dragovich, D. (2002). A conceptual model for defining and assessing land management units using a fuzzy modelling approach in GIS environment. *Environmental Management, 29*, 647-661. http://dx.doi.org/10.1007/s00267-001-0053-8

Baja, S., Dragovich, D., & Chapman, D. (2007). Spatial based compromise programming for multiple criteria decision making modeling in land use planning. *Environmental Modelling and Assessment, 12*, 171-184. http://dx.doi.org/10.1007/s10666-006-9059-1

Burrough, P. A. (1989). Fuzzy mathematical methods for soil survey and land evaluation. *Journal of Soil Science, 40*(3), 477-492. http://dx.doi.org/10.1111/j.1365-2389.1989.tb01290.x

Chandio, I. A., Matori, A. N., Lawal, D. U., & Sabri, S. (2011). GIS-based land suitability analysis using AHP for public parks planning in Larkana City. *Modern Applied Science, 5*(4), 177-189. http://dx.doi.org/10.5539/mas.v5n4p177

Chaudhry, A., Khan, A., Kim, J. Y., & Niu, Q. Q. (2013). Intelligent Image Restoration Approach: Using Neural Networks to Eradicate Dilemma in Punctual Kriging. *Life Science Journal, 10*(1), 1631-1641.

Chen, Y., Khan, S., & Paydar, Z. (2010). To retire or expand? A fuzzy GIS-based spatial multi-criteria evaluation framework for irrigated agriculture. *Irrigation and Drainage, 59*, 174-188.

Chiclana, F., Herrera-Viedma, E., Herrera, F., & Alonso, S. (2007). Some induced ordered weighted averaging operators and their use for solving group decision-making problems based on fuzzy preference relations. *European Journal of Operational Research, 182*, 383-399. http://dx.doi.org/10.1016/j.ejor.2006.08.032

Chinene, V. R. N. (2007). Land evaluation using the FAO framework: an example from Zambia. *Soil Use and Management, 8*(3), 130-138. http://dx.doi.org/10.1111/j.1475-2743.1992.tb00908.x

Djaenuddin, D., Marwan, H., Subagjo, H., & dan Hidayat, A. (2003). *Petunjuk Teknis Evaluasi Lahan untuk Komoditas Pertanian*. Versi 3. Balai Penelitian Tanah, Puslitbang Tanah dan Agroklimat, Bogor.

Elaalem, M. (2012). Land suitability evaluation for sorghum based on boolean and fuzzy-Multi-Criteria Decision Analysis Methods. *International Journal of Environmental Science and Development, 3*(4), 357-361. http://dx.doi.org/10.7763/IJESD.2012.V3.247

Elaalem, M. (2013). A comparison of parametric and fuzzy multi-criteria methods for evaluating land suitability for olive in Jeffara Plain of Libya. *APCBEE Procedia, 5*, 405-409. http://dx.doi.org/10.1016/j.apcbee.2013.05.070

Elaalem, M., Comber, A., & Fisher, P. (2010). Land evaluation techniques comparing fuzzy AHP with TOPSIS methods. *Proceeding of the 13th AGILE International Conference on Geographic Information Science* (pp. 1-8). Guimarães, Portugal.

Food and Agriculture Organization (FAO). (1976). *A Framework for Land Evaluation*. FAO Soil Bulletin 32. FAO and Agriculture Organization of the United Nation, Rome.

Galindo, J., Urrutia, A., & Piattini, M. (2005). *Fuzzy Databases: Modelling, Design, Implementation*. Idea Group Publishing, London the United Kingdom and the United States of America. http://dx.doi.org/10.4018/978-1-59140-324-1

Gonzales, A. S., Galan, C. O., Castro, J. T., Perez, E. G., & Fernandez, C. S. (2013). Grade control in a quartz deposit using universal fuzzy kriging. *Dyna, 80*(178), 61-69.

Jafarzadeh, A. A., Alamdari, P., Neyshabouri, M. R., & Saedi, S. (2008). Land suitability evaluation of bilverdy research station for wheat, barley, alfalfa, maize and safflower. *Soil and Water Res., 3*(Special Issue), 581-588.

Keshavarzi, A., Sarmadian, F., Heidari, A., & Omid, M. (2010). Land suitability evaluation using fuzzy continuous calssification (a case study: Ziaran region). *Modern Applied Science, 4*(7), 72-81.

Keshavarzi, A., Sarmadian, F., Labbafi, R., & Vandechali, M. R. (2011). Modeling of soil cation exchange capacity based on fuzzy table look-up scheme and artificial neural network approach. *Modern Applied Science, 5*(1), 153-164.

Kurtener, D., Torbert, H. A., & Krueger, E. (2008). Evaluation of agricultural land suitability: application of fuzzy indicators. In *Computational Science and Its Applications–ICCSA 2008* (pp. 475-490). Springer Berlin Heidelberg. http://dx.doi.org/10.1007/978-3-540-69839-5_35

Mangaraj, B. K., & Das, D. K. (2008). Interactive fuzzy multi-objective programming in land re-organisational planning for sustainable rural development. *World Academy of Science, Engineering and Technology, 23*, 104-113.

Maros, B. P. S. (2012). Kabupaten Maros Dalam Angka. *Kantor Badan Statistik Kabupaten Maros*.

Mohammadrezaei, N., Pazira, E., Sokoti, R., & Ahmadi, A. (2013). Comparing the performance of fuzzy ahp and parametric method toevaluate of land suitability of wheat production in the Southern Plain of Urmia. *International Journal of Agronomy and Plant Production, 4*(12), 3438-3443.

Moreno, J. F. S. (2007). *Applicability of knowledge-based and fuzzy theory-oriented approaches to land suitability for upland rice and rubber, as compared to the farmers' perception, a case study of Lao PDR*. M.S. Thesis, Consortium partners: University of Southampton (UK), Lund University (Sweden), University of Warsaw (Poland), International Institute for Geo-Information Science and Earth Observation (ITC) (The Netherlands).

Nardi, & Nazori A. Z. (2012). Otomasi klasifikasi awan citra satelit MTSAT dengan pendekatan fuzzy logic. *Jurnal Telematika Mkom, 4*(1), 104-117.

Nurmiaty, & Baja, S. (2013). Spatial Based Assessment of Land Suitability and Availability for Maize (Zea mays L.) Development in Maros Region, South Sulawesi, Indonesia. *Open Journal of Soil Science, 3*, 244-251.

http://dx.doi.org/10.4236/ojss.2013.35029

Nurmiaty, Baja, S., & Arif, S. (2014). GIS-Based Modelling of Land Use Dynamics Using Cellular Automata and Markov Chain. *Journal of Environment and Earth Science, 4*(4), 61-66.

RePPProT. (1988). *The Land Resources of Indonesia: A National Overview Main Report*. United Kingdom-ODA NRI, Ditjen Pankim, Department of Transmigration, Jakarta.

Reshmidevi, T. V., Eldho, T. I., & Jana, R. (2009). A GIS-integrated fuzzy rule-based inference system for land suitability evaluation in agricultural watersheds. *J. Agricultural Systems, 101*, 101-109. http://dx.doi.org/10.1016/j.agsy.2009.04.001

Sarmadian, F., Keshavarzi, A., Rajabpour, B., & Askari, S. (2010). Application of MCDM method in fuzzy modeling of land suitability evaluation. *Proceeding of the 19th world congress of soil science, soil solutions fora changing world* (pp. 25-28). Brisbane, Australia, August 1- 6.

Sediyono, E., Setiawan, A., & Kaparang, D. R. (2013). Fuzzy simple additive weighting algorithm to determine land suitability for crop in Minahasa Tenggara. *International Journal of Computer Applications, 84*(7), 26-29. http://dx.doi.org/10.5120/14591-2829

Srivastava, P., Burande, A., & Sharma, N. (2013). Fuzzy environmental model for evaluating water quality of Sangam Zone during Maha Kumbh. *Applied Computational Intelligence and Soft Computing, 2013*, Article ID 265924. http://dx.doi.org/10.1155/2013/265924

Sui, D. Z. (1992). A fuzzy GIS modeling approach for urban land evaluation. *J. Computer, Environment and Urban Systems, 16*, 10l-115. http://dx.doi.org/10.1016/0198-9715(92)90022-J

Taboada, J., Saavedra, Á., Iglesias, C., & Giráldez, E. (2013). Estimating quartz reserves using compositional kriging. *Abstract and Applied Analysis, 2013*, Article ID 716593. http://dx.doi.org/10.1155/2013/716593

Vucetic, V., & Simonovic, S. P. (2013). Evaluation and application of Fuzzy Differential Evolution approach for benchmark optimization and reservoir operation problems. *Journal of Hydroinformatics, 15*(4).

Wang, X., & Chan, H. K. (2013). An integrated fuzzy approach for evaluating remanufacturing alternatives of a product design. *Journal of Remanufacturing, 3*, 10. http://dx.doi.org/10.1186/2210-4690-3-10

Zadeh, L. A. (1965). Fuzzy sets. *J. Information and Control, 8*, 338-353. http://dx.doi.org/10.1016/S0019-9958(65)90241-X

Zhang, Q., Yang, X., Zhang, Y., & Zhong, M. (2013). Risk assessment of groundwater contamination: a multilevel fuzzy comprehensive evaluation approach based on DRASTIC model. *The Scientific World Journal, 2013,* Article ID 610390. http://dx.doi.org/10.1155/2013/610390

Modern Applied Science; Vol. 8, No. 3; 2014
ISSN 1913-1844 E-ISSN 1913-1852
Published by Canadian Center of Science and Education

Study on Shaking Table Model Test Scheme of Tunnel Subjected to Near-Fault Pulse-Like Ground Motions

Xiang Zhao[1], Jiang Shuping[2] & Yi Yi[1]

[1] School of Civil Engineering, Chongqing Jiaotong University, Chongqing 400074, China

[2] Chongqing Communication Research & Design Institute, Chongqing 400067, China

Correspondence: Xiang Zhao, School of Civil Engineering, Chongqing Jiaotong University, Chongqing 400074, China. Tel: 86-188-8384-7221. E-mail: xiangzhaos@126.com

Received: March 9, 2014 Accepted: March 28, 2014 Online Published: April 23, 2014

doi:10.5539/mas.v8n3p126 URL: http://dx.doi.org/10.5539/mas.v8n3p126

The research is financed by the Natural Science Foundation of China (No.51078324).

Abstract

Based on the Natural Science Foundation Project of China "Theoretical study on shock absorption of tunnel subjected to near-fault pulse-like ground motions" (51078324), this research conducts a shaking table model test scheme study to explore the seismic responses of tunnel subjected to near-fault pulse-like ground motions. The test which includes the decision of model similarity ratio, the design of model box and the treatment of boundary, the making of model, the layout of test points and the loading scheme of seismic wave and so on is introduced in detail in this paper. The test focuses on the rule and character of the dynamic response of the tunnel subjected to near-fault pulse-like ground motions. The test results show that the near-fault pulse-like ground motions is destructive. With seismic waves upward propagating, the seismic response of rock and soil is increasing. The tunnel linings were severely damaged.

1. Introduction

A large number of earthquake damage survey showed that the tunnel had a good ability to withstand earthquake damage, but as the result of Wenchuan earthquake in China in 2008, most of the tunnels in Dujiangyan-Wenchuan Highway were subject to varying degrees of damage, in which 73% of the tunnels were damaged severely, especially in the tunnel portal section and the section in fault formation. Near-fault pulse-like ground motions with high peak accelerations and long period velocity pulses are highly destructive. A lot of data statistics show that the tunnels subjected to near-fault ground motions have suffered more serious damages. In addition, it plays a pivotal role to ensure smooth traffic for the tunnel. It is undoubtedly deadly for disaster relief if the tunnels collapse and lose function. Therefore, it is necessary to carry out researches on the tunnel structure subjected to near-fault pulse-type ground motions and to analyze the structural dynamic response of tunnel lining, so as to lay the foundation of shock absorption studies on near-fault tunnel. This paper made a thorough discussion on the specific test scheme and analyzed the test data and failure mode of the tunnel lining.

2. Test Overview

Relying on the Natural Science Foundation Project of China "Theoretical study on shock absorption of tunnel subjected to near-fault pulse-like ground motions", the test was conducted in the State Key Laboratory of Structural Dynamic with earthquake simulation test seismic array system in Chongqing Communications Research and Design Institute. This large high-performance three-axis earthquake simulation seismic array system is the only one that consists of a fixed station and a mobile station all over the world. The level of technology and performance of the system which uses the world's most advanced digital control systems and software are at the international advanced level. The supporting data acquisition, vibration measurement and analysis system are currently the world's most advanced. The three-axial shaking table system is shown in Figure 1. System parameters and technical parameters are shown in Table 1. This model test used the fixed station of the seismic array system. The acceleration, strain and earth pressure dynamic data acquisition is achieved by the 128 channel. Data collecting, storing and processing is running by the vibration measurement and analysis system with hardware of the U.S. HP's VXI system and software of the Belgian company's LMS CADA-X software. It

is one of the world's most powerful and most technologically advanced dynamic data acquisition and analysis of vibration test systems. The main purpose of the test is to analyze and summarize the law of tunnel dynamic response, failure mechanism and failure mode of lining structure when the tunnel is subjected to near-fault pulse-like ground motions, and to lay the foundation of presenting the shock absorption theory of near fault tunnel.

Figure 1. Three-axial shaking table system

Table 1. Main parameters of shaking table system

Technical Parameters		Fixed station	Mobile station
Table size/m×m		3×6	3×6
Maximum specimen weight/ton		35	35
Maximum overturning moment /kN·m		700	700
Maximum turning moment /kN·m		350	350
Operating frequency range /Hz		0.1～50	0.1～50
X-direction movable distance /m		0.0	2.0～20.0
Maximum displacement /mm	*X* direction	±150	±150
	Y direction	±150	±150
	Z direction	±150	±150
Maximum velocity /(mm/s)	*X* direction	±800	±800
	Y direction	±800	±800
	Z direction	±600	±600
Maximum acceleration /g	*X* direction	±1.0	±1.0
	Y direction	±1.0	±1.0
	Z direction	±1.0	±1.0

3. Model Similarity Ratio

Many experimental studies have shown that it is difficult to fully meet the similarity theorem in dynamic model tests due to the complexity of soil traits. We can use approximation similarity method to determine similarity relationships according to the test purposes and the main factors. Moreover, under the current experimental

conditions, the use of artificial methods to simulate the effects of gravity mass of rock and soil is quite difficult, therefore, this test uses gravity distortion model.

Considering the shaking table size, bearing capacity, boundary effect range and other factors, the model similarity ratio refer to Table 2.

Table 2. Similarity relations and rations of physical parameters

Physical parameters	Symbol	Dimension	Similarity ratio	Remark
Length	C_L	L	30	Basic similarity ratio
Modulus of elasticity	C_E	FL^{-2}	30	Basic similarity ratio
Strain	C_ζ	—	1	
Poisson's ratio	C_v	—	1	Basic similarity ratio
Density	C_ρ	FT^2L^{-4}	1	
Stress	C_σ	FL^{-2}	30	
Mass	C_m	$FL^{-1}T^2$	27000	
Time	C_t	T	5.48	
Damping	C_c	$FL^{-1}T$	4929.50	
Frequency	C_f	T^{-1}	0.18	
Cycle	C_T	T	5.48	
Displacement	C_u	L	30	
Velocity	C_v	LT^{-1}	5.48	
Acceleration	C_a	LT^{-2}	1	
Gravitational Acceleration	C_h	LT^{-2}	1	
Area loads	C_q	FL^{-2}	30	

4. Model Box Design and Boundaries

The model box in the test was designed with the following factors:

(1) Solid structure, to avoid losing stability and not to damage the box in the intense vibrating process;

(2) Clear boundary conditions;

(3) The natural frequency of the model box deviating as much as possible from the frequency of soil in order to avoid resonance phenomenon;

(4) Model box size matches the size of the shaking table.

Taking the test and equipment into account, the model box is designed as a cuboid structure with size 3 m × 2.7 m × 2.45 m, in which the length along the tunnel longitudinally is 3 m, the lateral width 2.7 m, and the height 2.45 m.

Model box uses rigidly fixed boundaries with flexible material lined around the box. Its main frame is welded together with 7 equilateral angle steels, surrounded by 5 mm steel plates as enclosure. Considering the convenience of pouring the surrounding rock model, the model box is divided into five layers. The first layer has the thickness of 450 mm, and the other layers have the thickness of 500 mm. 20 M20 bolts are used to rivet every two adjacent layers. Bevel angle steels are added parallel to the sides of the model box to improve the overall vibration frequency to prevent box resonance with the model. Section of the base perimeter uses 100 mm × 50 mm steel frame, as the same, the bottom crossbar of the model box uses l00 mm × 50 mm steel welded trellis. The base reserves bolt holes to connect with the shaking table. Model box front and back (tunnel entrance and exit) reserve 300 × 300 mm square holes for observing. The real model box is shown in Figure 2.

Figure 2. An external view of the model box

After all, the soil of underground structure model test is finite. To make the semi-infinite soil be finite relates to the issue of artificial boundary treatment on which many scholars have done in-depth study.

If the soil contacts the model box sidewalls smoothly, the contacted interfaces have little effect on the soil. On the contrary, the contacted interfaces have a greater impact on the soil if the model box sidewalls are rough. Therefore, when dealing with the boundary of the model box, the sidewalls should be guaranteed smooth so as to reduce experimental error. In the bottom of the box, a layer of crushed stone is paved to increase the soil's friction resistance, and then to prevent relative sliding between the soil and the bottom of the box.

A layer of polystyrene foam board is set around the box sidewalls in order to simulate the semi-infinite soil's deformation and resilient recovery. Under the condition that other parameters are the same, the lighter the foam board is, the better the effects are.

At first, the boundary physical parameters-stiffness and damping should be defined based on three-dimensional viscoelastic artificial boundary equations. Then select the appropriate polystyrene foam board according to the parameters. For the polystyrene foam board, equivalent stiffness and equivalent damping model created by Soong can be recommended to determine the equivalent stiffness k_d and equivalent damping c_d by test methods.

$$c_{\mathrm{d}} = \frac{G''V}{\omega h^2}, \quad k_{\mathrm{d}} = \frac{G'V}{h^2} \tag{1}$$

Where G' is the shear modulus storage of polystyrene foam material; G'' is the shear modulus loss; h is the thickness of the polystyrene foam boards; V is the volume; ω is the natural frequency of model box and soil.

Thereby the determined thickness of the polystyrene foam board is 22.5 cm.

When the ratio of the model box's natural frequency and the soil's natural frequency is between 0.75 and 1.25, resonance phenomenon will be happen. This ratio must be beyond this range in order to prevent this phenomenon. The first-order natural frequency of the model box is 13.72 Hz which is obtained by finite element analysis calculation and that deviate far from the first-order natural frequency of the soil. It is evident that there will be no resonance between the model box and the soil.

5. The Similar Material of Surrounding Rock and the Modeling

After a lot of ratio test, finally we choose gypsum mixes as similar material of surrounding rock, namely: aggregate - quartz; cementing material - gypsum; other materials - water; filling additive - barite powder (barium sulfate).

As the thickness of tunnel lining prototype is 60 cm, based on the similarity theory, model tunnel lining's thickness is 20 mm. The portal section is divided into six sections (each length 400 mm), the deeper buried

section is divided into seven sections (the first six parts each length 400 mm, last one 200 mm). In the reinforced concrete, gypsum is used to simulate the concrete and φ0.7 mm woven barbed wire to steel bars. The simulated linings are prefabricated by a particular mold.

Before making the simulated linings, the mold inner wall is smeared a layer of oil, then pour the prepared gypsum slurry into the mold, standing for half an hour or so to release. And cure 7 days or so to reach a permanent strength at room temperature (25 ~ 35 °C).

We choose gypsum as similar material of surrounding rock and lining, but gypsum can be affected by air humidity and temperature evidently. Especially humidity, we have got great different physical parameters in different weather conditions. To avoid this, we should strictly control the curing of gypsum specimen, and test under the same environmental conditions as possible. A completed specimen can be protected by a thin layer of varnish. Furthermore, different batches and types of similar materials have physical parameters error, effective control is necessary in the test.

Wooden mold has large deformation in contact with water, and not conducive to recycling, so we use steel material. The steel mold is shown in Figure 3.

Figure 3. Steel mold of lining model making

6. Testing Apparatus and Test Points Arrangement

The test data to be collected include acceleration, strain and displacement of lining structure, the contact pressure of surrounding rock and lining structure, the acceleration of side slope in the portal section and acceleration and displacement of the surface above the tunnel.

Optional sensors include: BY-3-type soil micro resistance strain pressure gauge, resistance strain sensor, CA-YD-152-type piezoelectric acceleration sensors and displacement sensors.

In this shaking table test, the arrangement of the sensors must meet the following principles:

(1) Test point arrangement should be based on the purpose of this test;

(2) The limit of the testing ground, equipment and other conditions should be considered for the test point arrangement;

(3) The sensor is preferably arranged based on the existing theory and numerical simulation results so that all measurement results can be compared with the results of numerical simulations;

(4) In the case of meeting the basic information collecting, minimize the number of arranged sensors so as to avoid affecting the integrity of the model because of the arrangement of the sensors and resulting in larger test errors.

The front view of the tunnel and surrounding rock and the arrangement of test points are shown in Figure 4.

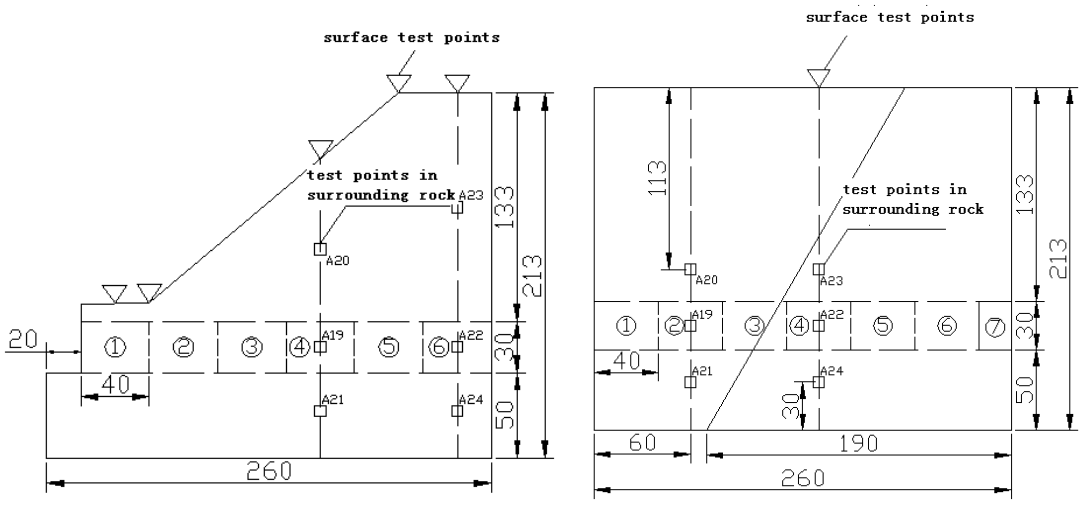

(a) Portal section (b) Tunnel body section

Figure 4. Front view of the arrangement of test points in tunnel and surrounding rock

According to the principles above, the top view of the tunnel and surrounding rock and the arrangement of the test points is as shown below in Figure 5:

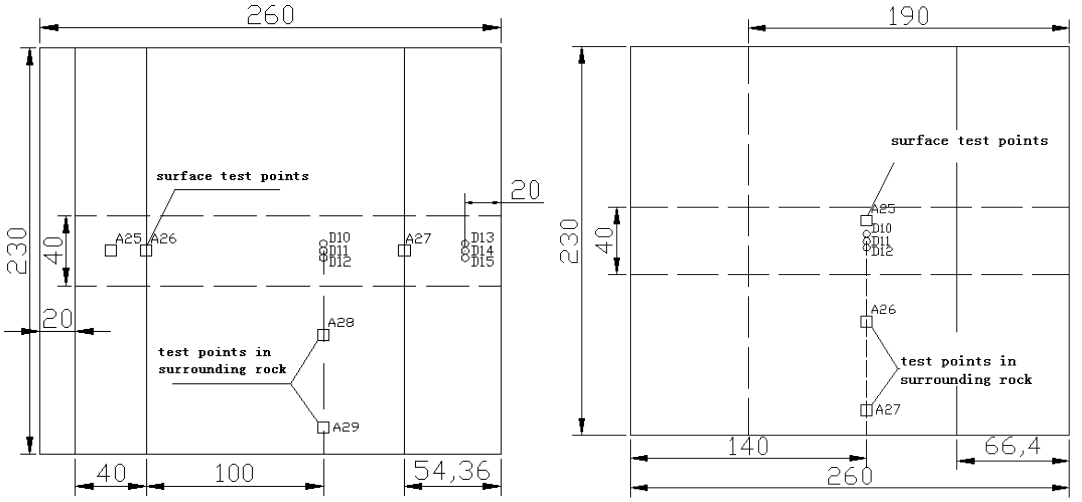

(a) Portal section (b) Tunnel body section

Figure 5. Top view of the arrangement of test points in tunnel and surrounding rock

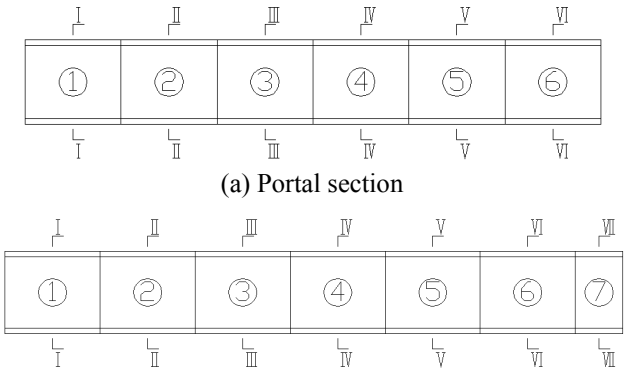

(a) Portal section

(b) Tunnel body section

Figure 6. The layout of the tunnel structure

As can be seen from Figure 4(a) and Figure 5(a), in the portal section, on the surface a total of five test points longitudinally along the tunnel are arranged, the first, second and fourth test point respectively arranged an acceleration sensor, and the third and fifth test point respectively arranged a displacement sensors in three directions. Can also be seen from Figure 4(a), in the middle of 4th and 6th section, three test points are arranged along the vertical direction at the outer surface of lumbar arch in the rock, and each test point is arranged an acceleration sensors. As is shown in Figure 4(b) and Figure 5(b), in the tunnel body section, on the surface only one test point is arranged, and at this point, an acceleration sensor and a displacement sensors in three directions are arranged. Figure 4(b) is showing that in the middle of 2nd and 4th section, three test points are arranged along the vertical direction at the outer surface of lumbar arch in the rock, and each test point is arranged an acceleration sensors. In Figure 5, we can see that in the middle of the 4th section, two test points are arranged along the horizontal direction at the outer surface of lumbar arch in the rock both in the portal section and the tunnel body section, and each test point is arranged an acceleration sensors to verify the treatment effect of model box boundary. Figure 6 shows that both in the portal section and the tunnel body section, longitudinally along the tunnel a total of six typical observation sections are arranged, and the arrangement of each test point of the observation sections is as shown below in Figure 7:

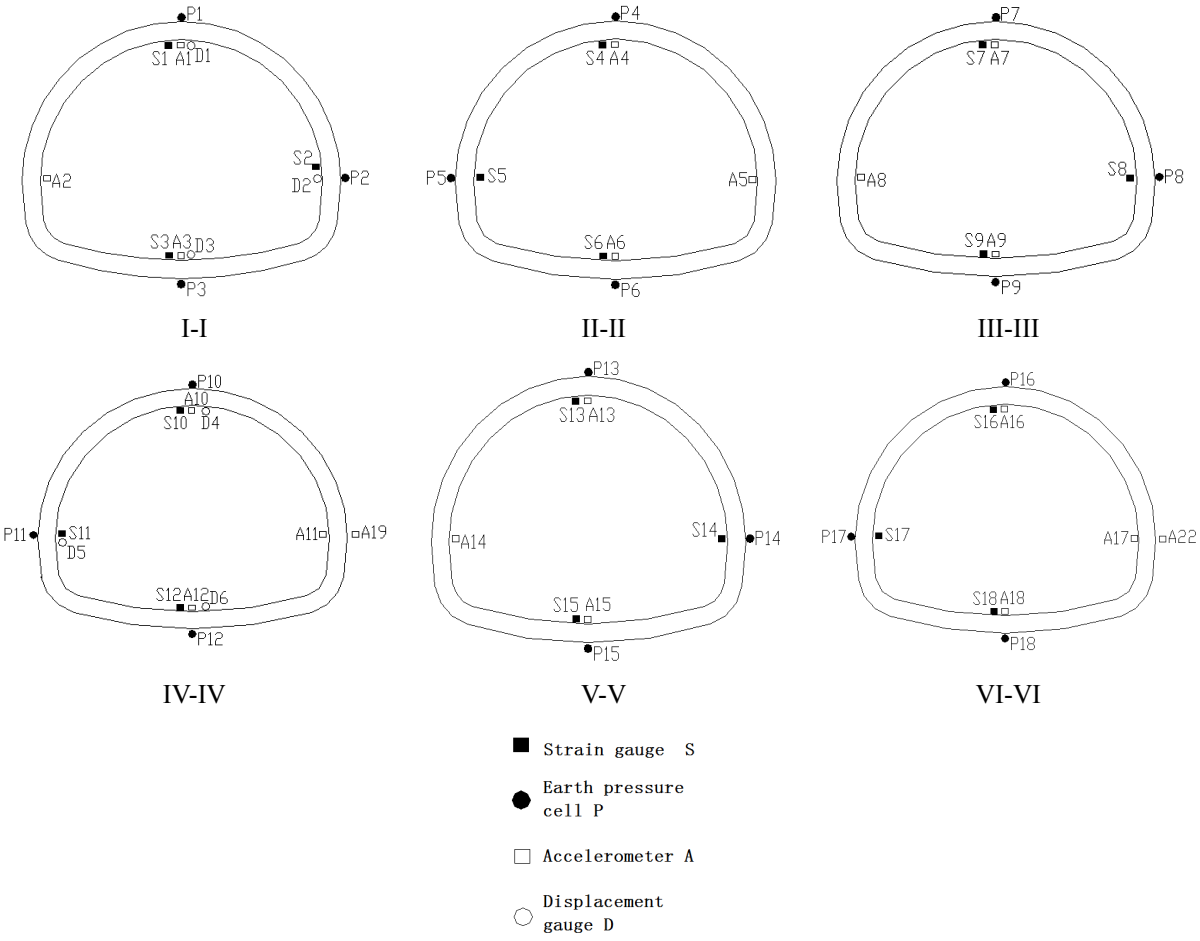

Figure 7. Sectional view of observation sections

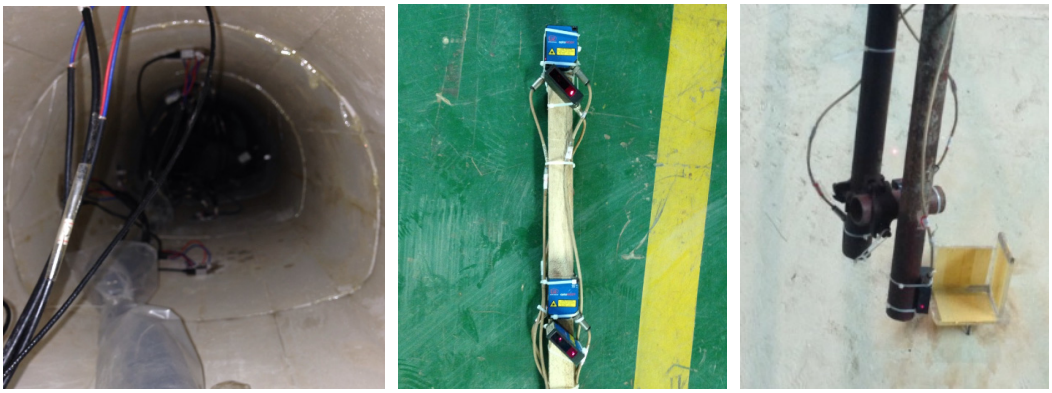

Figure 8. Sensor Installation

The quantities of apparatus in the portal section are shown in Table 3. Table 4 shows the quantities of apparatus in the tunnel body section.

Table 3. Quantities of apparatus in the portal section

Sections	Apparatus			
	Accelerometer	Strain gauge	Earth pressure cell	Displacement gauge
I-I	3	3	3	3
II-II	3	3	3	
III-III	3	3	3	
IV-IV	3	3	3	3
V-V	3	3	3	
VI-VI	3	3	3	
Ground surface	3			6
Surrounding rock	8			
Total	29	18	18	12

Table 4. Quantities of apparatus in the tunnel body section

Sections	Apparatus			
	Accelerometer	Strain gauge	Earth pressure cell	Displacement gauge
I-I	3	3	3	3
II-II	3	3	3	
III-III	3	3	3	
IV-IV	3	3	3	3
V-V	3	3	3	
VI-VI	3	3	3	
Ground surface	1			3
Surrounding rock	8			
Total	27	18	18	9

7. Loading Scheme

Shaking table test should use multiple hierarchical loading ways. The loading principles are as following:

(1) Estimate the successive input table acceleration amplitude based on the model's theoretical elastic and inelastic seismic response;

(2) At elastic stage, input a time history of a certain ground motion acceleration to test the model's seismic response amplification coefficient and elastic properties;

(3) At inelastic stage, increase the amplitude of the input acceleration to make gradual development of the specimen cracking moderately, meanwhile collect the test data and view the cracking or destruction of each part of the specimen;

(4) At failure stage, increase the amplitude of the input acceleration or input a certain peak acceleration repeatedly until the specimen is destroyed to test the seismic capacity of the test specimen.

Based on the test purposes and past experience, we use multiple hierarchical loading ways. The time intervals and peak acceleration was adjusted according to the similarity relationships. The test uses interval 0.00365s. We start with a small amplitude white noise for pre-vibration before intense vibrations, so that the model soil become compact, then the fundamental frequency and damping ratio of the system is obtained. We input white noise to scan at each subsequent change of input peak acceleration to observe the model changes of dynamic characteristics. The specific loading scheme of shaking table test is in Table 5.

8. Analysis of Test Results

Large amounts of data is obtained in the model test, but this paper only lists some representative record results of the load order 30 inputting seismic waves of Landers earthquake in Table 5 in the portal section because of the limited space. The results of the 4th section in the portal section model are listed in the following figures. The other detailed analysis of the results data can be referred to other papers. In this chosen condition, the seismic waves are input from X, Y, Z three directions simultaneously. Figure 9 to Figure 11 are the acceleration time histories of test points of the 4th lining and shaking table. In the condition, the peak accelerations of the 4th lining arch crown are 0.503g in X-direction, 0.83g in Y-direction and 0.473 g in Z-direction. The peak accelerations of the 4th lining arch shoulder are 0.397 g in X-direction, 0.689 g in Y-direction and 0.492 g in Z-direction. The peak accelerations of the 4th lining invert arch are 0.403 g in X-direction, 0.669 g in Y-direction and 0.462 g in Z-direction.

Table 5. Loading scheme of shaking table test

Load order	Waveforms	Recording stations	Amplitude adjustment coefficients	Peak acceleration (m/s^2)			Duration (s)	
				X-direction	Y-direction	Z-direction	Origin	Model
1	White noise	/	/	/	/	/	/	/
2	Kocaeli, Turkey	Duzce	1/5	—	0.716	—	27.18	4.96
3				0.624	—	—		
4				—	—	0.458		
5				0.624	0.716	0.458		
6	White noise	/	/	/	/	/	/	/
7	Landers, USA	Cool water	1/5	—	0.834	—	27.96	5.10
8				0.566	—	—		
9				—	—	0.347		
10				0.566	0.834	0.347		
11	White noise	/	/	/	/	/	/	/
12	Chichi	Tcu52	1/5	—	0.838	—	90.00	16.42
13				0.696	—	—		
14				—	—	0.482		
15				0.696	0.838	0.482		
16		Tcu68	1/5	—	1.132	—	90.00	16.42
17				0.924	—	—		
18				—	—	0.972		
19				0.924	1.132	0.972		
20	White noise	/	/	/	/	/	/	/
21	Kobe, Japan	Takarazuka	1/5	—	1.388	—	40.95	7.47
22				1.386	—	—		
23				—	—	0.866		
24				1.386	1.388	0.866		
25	White noise	/	/	/	/	/	/	/
26	Kocaeli, Turkey	Duzce	1	—	3.580	—	27.18	4.96
27				3.120	3.580	2.290		
28	White noise	/	/	/	/	/	/	/
29	Landers, USA	Cool water	1	—	4.169	—	27.96	5.10
30				2.828	4.169	1.736		
31	White noise	/	/	/	/	/	/	/
32	Chichi	Tcu52	1	—	4.190	—	90.00	16.42
33				3.480	4.190	2.410		
34		Tcu68	1	—	5.660	—	90.00	16.42
35				4.620	5.660	4.860		
36	White noise	/	/	/	/	/	/	/
37	Kobe, Japan	Takarazuka	1	—	6.940	—	40.95	7.47
38				6.930	6.940	4.330		
39	White noise	/	/	/	/	/	/	/

Note: X-direction is the direction of the tunnel cross section; Y-direction is the tunnel axis direction; Z-direction is vertical direction.

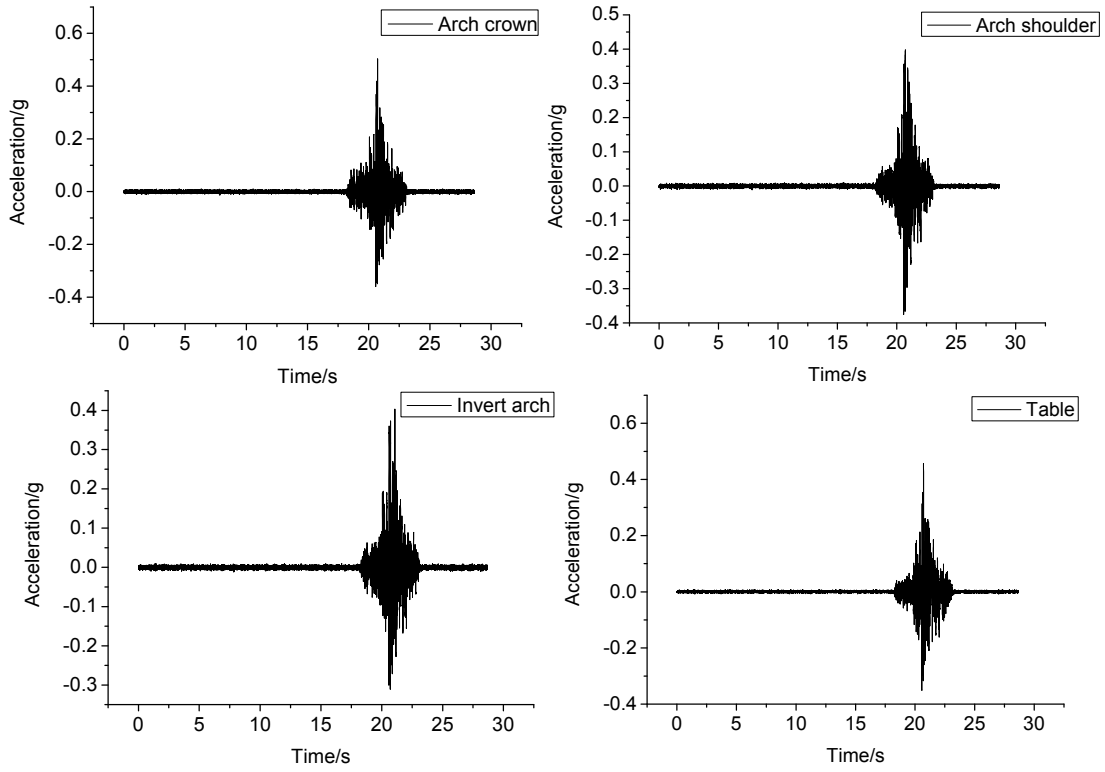

Figure 9. Acceleration time histories of model and shaking table in X-direction

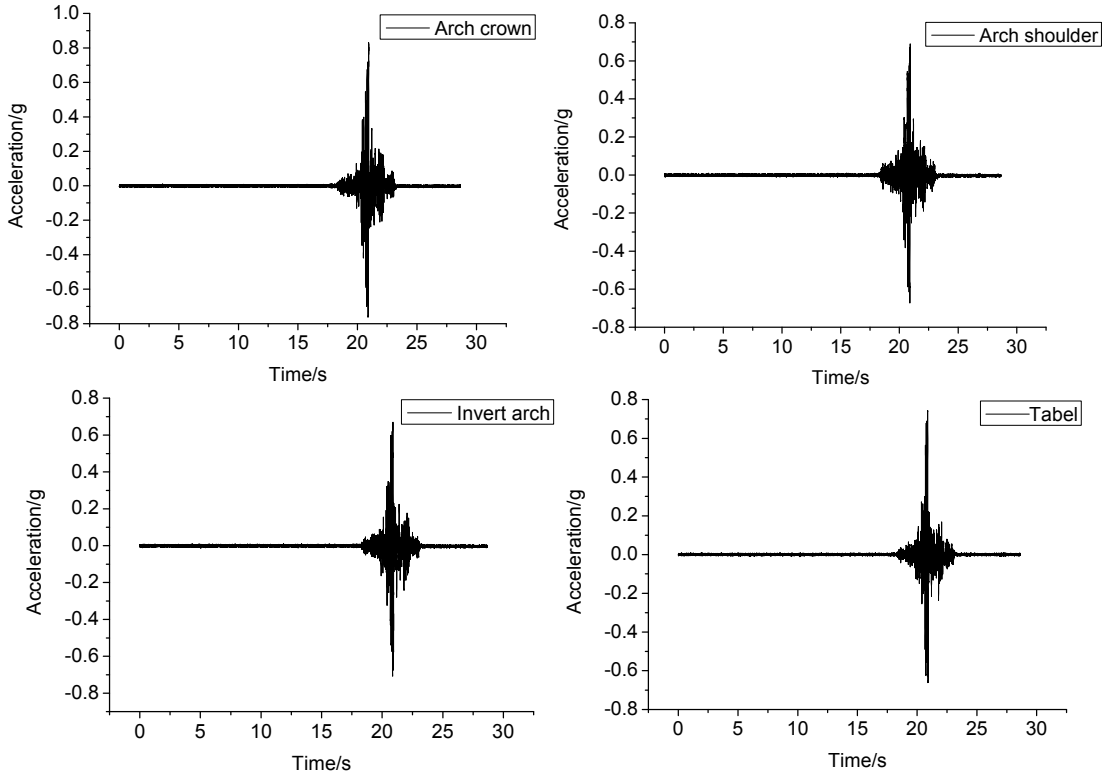

Figure 10. Acceleration time histories of model and shaking table in Y-direction

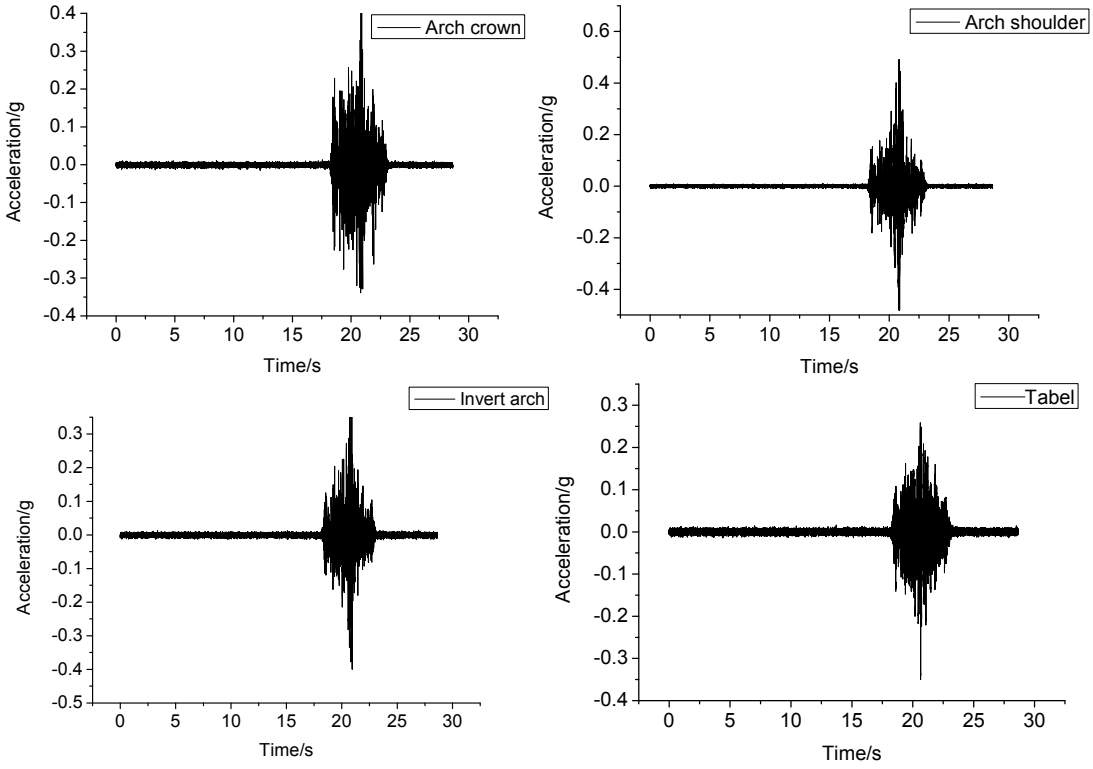

Figure 11. Acceleration time histories of model and shaking table in Z-direction

Figure 12 shows the earth pressures of the 4th lining model in different positions. The earth pressure of arch crown has a significant fluctuation in which the peak pressure is 4.26×10^{-3} MPa at the moment 22 s, while the earth pressures of arch shoulder and invert have small fluctuations in which the peak pressure also occurred at the moment 22 s.

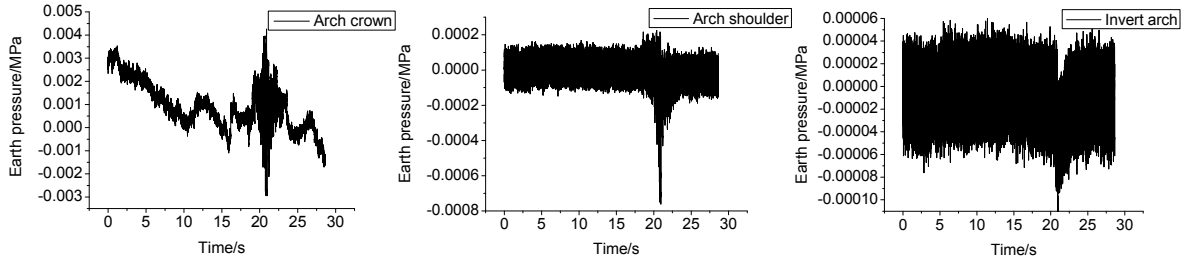

Figure 12. Earth pressure time histories of the surrounding rock in different places

Pictures in Figure 13 are the displacement time histories of different test points of the 4th lining model. The arch shoulder has the maximum displacement of 4 mm at the moment 20 s. In the third picture, the displacement of invert arch changes from 0mm to -1.5 mm finally. And in the first picture, the displacement of arch crown changes from 0mm to 0.3 mm. It is evident that the 4th lining model has a permanent deformation after the strong vibration.

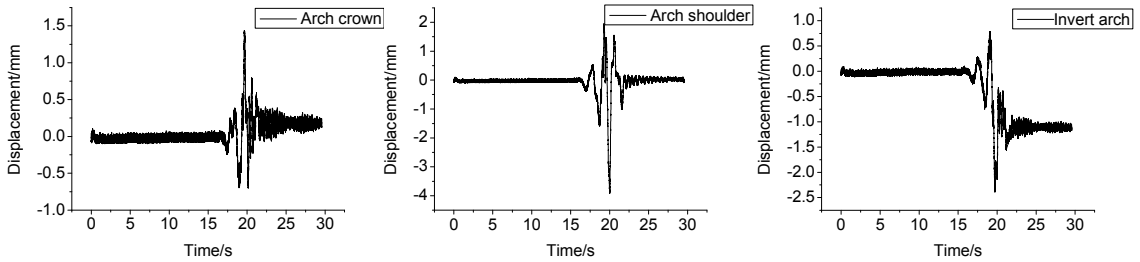

Figure 13. Displacement time histories of different test points of the 4th lining model

The peak acceleration variation of the 4th lining model with the increase of seismic waves is shown in Figure 14 in which the contrast of peak accelerations of arch crown, arch shoulder and invert arch when inputting different seismic waves is demonstrated.

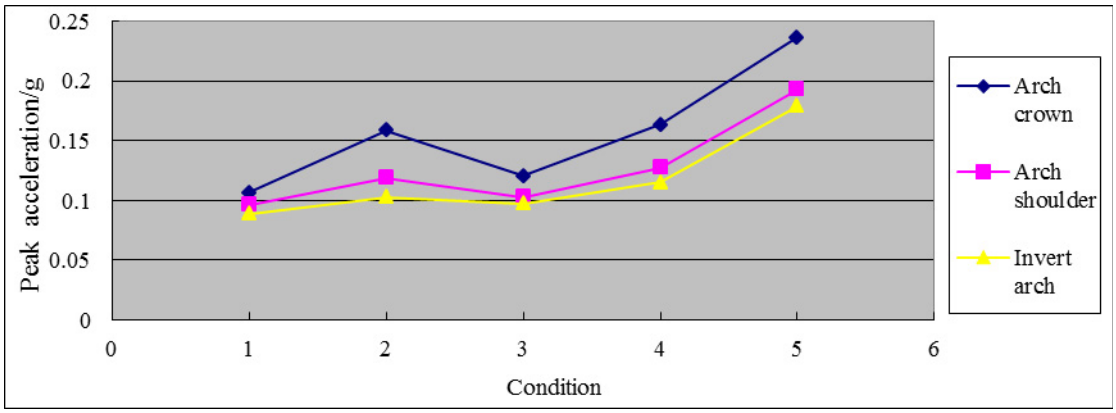

Figure 14. The acceleration variations of the 4th lining model with the increase of seismic waves

9. Summary and Conclusions

In this paper, research on a shaking table model test scheme of tunnel subjected to near-fault pulse-like ground motions is carried out based on the Natural Science Foundation Project of China "Theoretical study on shock absorption of tunnel subjected to near-fault pulse-like ground motions". The paper lays emphasis on the details of the design of the test scheme which contain the model similarity ratio, model box, model boundaries, the similar material of surrounding rock and lining, testing apparatus and test point arrangement and loading scheme. The following conclusions can be drawn from this research:

(1) Near-fault pulse-like ground motions is destructive to tunnel structures.

(2) Seismic responses of surrounding rock and lining soil increase with the upward propagation of seismic waves. Arch crown has larger accelerations and displacements than arch shoulder and invert arch. This should be taken into consideration in the tunnel's anti-seismic structure design.

(3) Cracks occur on the side slope above the tunnel and near the tunnel portal. Therefore, taking some anti-seismic measures of side slope is necessary for those tunnels in near-fault high-intensity earthquake area.

(4) In the same condition, the acceleration of arch crown varies with a trend of increasing along the tunnel in the portal section while the accelerations of arch shoulder and invert arch variation trends are not obvious.

References

Alavi, B., & Krawinkler, H. (2000, March). Design considerations for near-fault ground motions. In *Proceedings of the US–Japan Workshop on the Effects of Near-Fault Earthquake Shaking* (pp. 20-21).

Bray, J. D., & Rodriguez-Marek, A. (2013). Characterization of forward-directivity ground motions in the near-fault region. *Soil Dynamics and Earthquake Engineering, 24*(11), 815-828. http://dx.doi.org/10.1016/j.soildyn.2004.05.001

Chen, G., Zhuang, H., Du, X., Li, L., & Cheng, S. (2007). Analysis of large-scale shaking table test of dynamic soil-subway station interaction. *Earthquake Engineering and Engineering Vibration, 27*(2), 171-176.

Fang, L., Jiang, S., Lin, Z., & Wang, F. (2011). Shaking table model test scheme study on the tunnel through fault. *Rock and Soil Mechanics, 32*(9), 2709-2713.

Khoshnoudian, F., Ahmadi, E., & Sohrabi, S. (2014). Response of nonlinear soil-MDOF structure systems subjected to distinct frequency-content components of near-fault ground motions. *Earthquake Engineering & Structural Dynamics, 43*(5), 701-716. http://dx.doi.org/10.1002/eqe.2367

Lou, M., Wang, W., Ma, H., & Zhu, T. (2001). Study on soil-pile-structure interaction system by shaking table model test. *Journal of Tongji University, 29*(7), 763-768.

Martinelli, P., & Filippou, F. (2009). Simulation of the shaking table test of a seven-story shear wall building. *Earthquake Engineering & Structural Dynamics, 38*(5), 587-607. http://dx.doi.org/10.1002/eqe.897

Moustafa, A., & Takewaki, I. (2010). Characterization and modeling of near-fault pulse-like strong ground motion via damage-based critical excitation method. *Structural Engineering and Mechanics, 34*(6), 755-778. http://dx.doi.org/10.12989/sem.2010.34.6.755

Phillips, B. M., Wierschem, N. E., & Spencer, B. F. (2014). Model-based multi-metric control of uniaxial shake tables. *Earthquake Engineering & Structural Dynamics, 43*(5), 681-699. http://dx.doi.org/10.1002/eqe.2366

Shang, S, Liu, F., Lu, H., & Du, Y. (2006). Design and experimental study of a model soil used for shaking table test. *Earthquake Engineering and Engineering Vibration, 26*(4), 199-204.

Xie, L., Xu, L., & Rodriguez-Marek, A. (2005). Representation of near-fault pulse-type ground motions. *Earthquake Engineering and Engineering Vibration, 4*(2), 191-199. http://dx.doi.org/10.1007/s11803-005-0002-2

Modern Applied Science; Vol. 8, No. 3; 2014
ISSN 1913-1844 E-ISSN 1913-1852
Published by Canadian Center of Science and Education

Boltzmann Machine and Hyperbolic Activation Function in Higher Order Network

Saratha Sathasivam[1] & Muraly Velavan[2]

[1] School of Mathematical Sciences, Universiti Sains Malaysia Penang, 11800 USM, Malaysia

[2] School of General and Foundation Studies, AIMST University, 08100 Bedong, Kedah, Malaysia

Correspondence: Saratha Sathasivam, School of Mathematical Sciences, Universiti Sains Malaysia Penang, 11800 USM, Malaysia. E-mail: saratha@usm.my

Received: February 9, 2014 Accepted: April 7, 2014 Online Published: April 23, 2014

doi:10.5539/mas.v8n3p140 URL: http://dx.doi.org/10.5539/mas.v8n3p140

Abstract

For higher-order programming, higher-order network architecture is necessary to provide faster convergence rate, greater storage capacity, stronger approximation property, and higher fault tolerance than lower-order neural networks. Thus, the higher-order clauses for logic programming in Hopfield Networks have been considered in this paper. The goal is to perform logic programming based on the energy minimization scheme is to achieve the best global minimum. However, there is no guarantee to find the best minimum in the network. However, by using Boltzmann Machines and hyperbolic tangent activation function this problem can be overcome.

Keywords: Higher Order Hopfield Network (HONN), Boltzmann machine and hyperbolic tangent activation function

1. Introduction

Neural Networks is a mathematical model or computational model that is inspired by the structure of biological neurons such as the brain process information. It can solve sophisticated recognition and analysis problems. It is because it composed of huge amount of interconnected neurons to solve specific problems. However in this paper, we are concentrated on Hopfield network. Hopfield network is a recurrent neural network (Hopfield, 1982) invented by John Hopfield, consists of a set of N interconnected neurons which all neurons are connected to all others in both directions. It has synaptic connection pattern which involving Lyapunov function E (energy function) for dynamic activities. It serves as content addressable memory systems with binary threshold units.

Logic is deals with true and false while in the logic programming, a set of Horn clauses that formed by atoms are represented to find the truth values of the atoms in the clauses. It is using neurons to store the truth value of atoms to write a cost function for minimization when all the clauses are satisfied. In addition, a bi-directional mapping between propositional logic formulas and energy functions of symmetric neural networks had defined by Gadi Pinkas (Pinkas, 1991, 1992) and Wan Abdullah (Wan Abdullah, 1991, 1992). Further detail can refer to the references. The advantages by using Wan Abdullah's method are it can revolves around propositional Horn clauses and learning ability of the Hopfield network and hunts for the best solutions, given the clauses in the logic program, and the corresponding solutions may change as new clauses added.

This paper is organized as follows. In section 2, an outline of Hopfield network is given and in section 3, method of doing logic programming in neural network is described. Meanwhile in section 4 contain discussions regarding the Boltzmann machine and Hyperbolic Tangent activation function. Finally, section 5 and 6 occupy the simulation results and concluding remarks regarding this work.

2. Higher Order Hopfield Networks

Discrete Hopfield network is shown in Figure 1, as an expanded form of a common representation of the Hopfield network. Hopfield had stated that this network is useful for solving combinatorial optimization problems as a content addressable memory or an analog computer. Combinatorial optimization includes looking for the combination of choices from a discrete set which produces an optimum value for some related cost function.

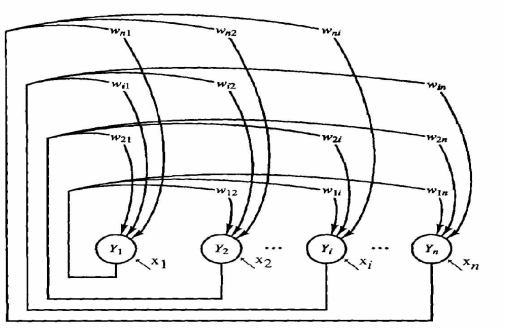

Figure 1. Discrete hopfield network

In neural network, higher order logic programming is highly regarded as the essential method in Hopfield Networks. When the Hopfield neural network is used to solve NP-complete optimization problem (Brenton, 2002; Ding et al., 2010; Cheung & Lee, 1993) such as travelling salesman problem, positive solutions would be produced. From literature review, few papers had carried out that applying higher order Hopfield networks such as using HOHN (Ding et al., 2010) to solve N-queens problem and construction method of energy function and neural computing method also shown. Besides, comparison with the first order Hopfield network and the method how to speed the convergence and escape from the local minima also had discussed in those papers. While according to Cheung and Lee (1993), the convergence property had restudied before put in application in real life. Besides, Ising spin problem also had carried out in it. The most important paper that affects the main backbone of this paper is explained by Joya et al. (2002). It is a study of the different dynamics in HOHN and problem affecting practical application of these networks are brought to light such as incoherence between the network dynamics and the associated energy function, error due to discrete simulation on a digital computer, existence of local minima and convergence depends on coefficients weighting the cost function terms. However, in this paper only local minima and convergence are concentrated. Further explanation can refer to reference. From those stated above, Hopfield network has overcome the difficulty to find suitable parameters to guarantee convergence and explore a new path for artificial intelligence and intellectual computer.

Other than that, higher-order Hopfield network can solve non-linear and discontinuous data in larger field and connections. For example, it is well performed in nonlinear statistical modelling and it can provide a new alternative to logistic regression in bigger state and numbers. Furthermore, it is able to detect all possible interactions between predictor variables such as detect complex nonlinear relationships between dependent and independent variables. Lastly, it can be used as research tool like neurobiologists use it for interpretation of neurobiological phenomena. From here, researchers know that Hopfield network can use to minimize a configurationally energy function and thus can solve the combinatorial optimisation problem. It is a reason why there are good solutions can be found.

The higher-order Hopfield Networks with the order = n-1 is stated as below. The energy function is

$$E = -\frac{1}{n}\sum_{i_1}\sum_{i_2}\sum_{i_3}\dots\sum_{i_n} w_{i_1 i_2 i_3 \cdots i_n} x_{i_1} x_{i_2} x_{i_3} \dots x_{i_n} - \frac{1}{n-1}\sum_{i_1}\sum_{i_2}\sum_{i_3}\dots\sum_{i_{n-1}} w_{i_1 i_2 i_3 \cdots i_{n-1}} x_{i_1} x_{i_2} x_{i_3} \dots x_{i_{n-1}} -$$

$$\cdots - \frac{1}{2}\sum_{i_1}\sum_{i_2} w_{i_1 i_2} x_{i_1} x_{i_2} - \sum_i w_i x_i \quad (1)$$

where x_i is the state value of i^{th} neuron , $w_i$defines the connection weights of the nth order connection from neurons $i_1 i_2 i_3 \dots i_n$ to neuron I, h_i is the input potential to neuron i and x_i is the state of neuron i. In the high-order model each node is assigned a sigma-pi unit that updates its activation value by first computing the partial derivative of the energy function. The dynamic equation or the updating rule of the network is

$$x_i(t) = sgn(h_i(t)),$$

$$h_i = \sum_{i_1}\sum_{i_2}\sum_{i_3}\dots\sum_{i_n} w_{i_1 i_2 i_3 \cdots i_n} x_{i_1} x_{i_2} x_{i_3} \dots x_{i_n} + \sum_{i_1}\sum_{i_2}\sum_{i_3}\dots\sum_{i_{n-1}} w_{i_1 i_2 i_3 \cdots i_{n-1}} x_{i_1} x_{i_2} x_{i_3} \dots x_{i_{n-1}} + \cdots +$$

$$\sum_{i_1}\sum_{i_2} w_{i_1 i_2} x_{i_1} x_{i_2} + \sum_i w_i x_i \quad (2)$$

where sgn is signum function. The connection weight of higher-order Hopfield networks is symmetrical. This condition is analogical to the symmetric requirement of the Hopfield Netowrks connection weight matrix.

As the dynamic equation is derived by partial derivative, it only guarantees convergence towards local minimum. It is affected by the value of the coefficients that weight the different terms of the cost function (Joya et al., 2010). Thus, the Boltzmann machine and Hyperbolic Tangent activation function will carry out in this paper.

3. Logic Programming

Logic programming is the use of mathematical logic for computer programming. Thus, higher order Hopfield network (HONN) had carried out in logic programming model. A HOHN is used to minimise logical inconsistency in interpretations of logic programs and clauses. To apply it, first of all need to understand what logic program play in the system. Following is the logic program that built by using Wan Abdullah's method in HN.

Following is the algorithms.

i) Given a logic program, translate all the clauses in the logic program into basic Boolean algebraic form. It like A← B, C as A ∨ ⌐(B ∧ C) = A ∨ ⌐B ∨ ⌐C

ii) Identify a neuron to each ground neuron.

iii) Initialize all connections strengths to zero. It assumed the connection with A, B and C is zero value.

iv) Derive a cost function that is associated with the negation of all the clauses, such that $\frac{1}{2}(1 + S_A)$ represents the logical value of a neuron *A,* where S_A is the neuron corresponding to *A*. The value of $S_A$is define in such a way that it carries the values of 1 if *A* is true and -1 if *A* is false. Negation (neuron *A* does not occur) is represented by, $\frac{1}{2}(1 - S_A)$; $E_p = \frac{1}{2}(1 - S_A)\frac{1}{2}(1 + S_B)\frac{1}{2}(1 + S_C) + \ldots\ldots$ a conjunction logical connective 'and' is represented by multiplication whereas a disjunction connective 'or' is represented by addition.

v) Obtain the values of connection strengths by comparing the cost function with the energy, *H* which in the section 2 that had recognized in Hopfield network.

vi) Let the neural networks evolve until minimum energy is reached. The neural states then provide a solution interpretation for the logic program, and the truth of ground atom may be checked then consider the solution obtained is a global solution or not.

A logic program contains of program clauses and it is activated by an initial goal. It is easy to understand, modify and verify. For example in a simple propositional case, logic clauses had formed as $A <- B_1, B_2, B_3, \ldots\ldots, B_n$ where the arrow can be read as 'if' while the comma can be read as 'and' for the purpose of interpretation the clauses by using truth value. Thus, a model or pattern can be found to the given logic program and it can be a way to solve the combinational optimization problem. Consequently, to carry out a logic program, we need to build up a simulator to run it. However, to solve the global minima problem, in next section, an introduction about Boltzmann machine and Hyperbolic Tangent activation function will carry out.

4. Boltzmann Machine

Hopfield networks have recognized that some relaxation schemes have a joined cost function and the states of the network converge to local minima of this function. It had performed optimization of a well-defined function. However, there is no guarantee to find the best minimum in the network. Thus, Boltzmann Machines had introduced to overcome this problem. A Boltzmann machine is a network of units which are fully interconnected by bidirectional connections with symmetric weights. There are no self-connections are allowed. These units have binary values 0 and 1 that referring to states ON and OFF for each unit. The major difference from Hopfield networks is the way of updating the states which determined by stochastic decisions. Boltzmann machines have a simple learning algorithm that allows them to discover interesting features that represent complex regularities in the training data. Furthermore, it extends the concept of Hopfield networks by a stochastic update method.

A Boltzmann machine, like a Hopfield network, is a network of units with an "energy" defined for the network. Unlike Hopfield networks, binary units of Boltzmann Machine are stochastic. By referring to the energy function, $E(u)$ for Hopfield networks, due to the probabilistic update rule, a Boltzmann machine is able to transit the states on higher energy level in contrast to Hopfield network. This feature can avoid the network getting stuck in local minima of the energy function in minimization problems (Sathasivam & Wan Abdullah, 2010). The difference in the global energy that results from a single unit *i* being 0 versus 1, written ΔE_i, is given by:

$$\Delta E_i = \sum_{j=1}^{n} u_j w_{ij} - \theta_i \tag{3}$$

Thus, $\Delta E_i > 0$ means that the energy of the whole system is higher if $u_i = 0$ and higher energy for $\Delta E_i < 0$ with $u_i = 1$. A Boltzmann machine is made up of stochastic units. The probability, p_i of the i–th unit being on is given by:

$$p_i = \frac{1}{1+e^{\left(-\frac{\Delta E_i}{T}\right)}} \tag{4}$$

where the scalar T is referred to as the temperature of the system. The network is run by repetitively choosing a unit and setting its state. After running for long period at a certain temperature, the probability of a global state of the network will depend only upon that global state's energy based on Boltzmann distribution. It is true when the probability distribution of global states has converged. A temperature value is needed to influence the output from the network. As this temperature decreases from a high temperature to reach a thermal equilibrium at a low temperature, we are guaranteed to converge to a distribution where the energy level fluctuated around the global minimum. This process is called simulated annealing. This material is subjected to high temperature and then gradually cooled. The gradual cooling allows the material to cool to a state in which there are few weak point, the molecule system becomes more and more stable. The heat causes the atoms to become unstuck from their initial position (local minimum) and move randomly to the states of higher energy. It achieves global optimum whereas the entire object achieves a minimum energy crystalline structure.

4.1 Hyperbolic Tangent Activation Function in Hopfield Network

Hyperbolic tangent activation function is one of well know activation function. However, logistic function which was frequently in use in neural network, introduced by McCulloch-Pitts where it is already established in original method of doing logic programming in Hopfield network proposed by Wan Abdullah. Since McCulloch-Pitts function is unbounded, smoother function such as hyperbolic tangent which have output range between -1 and +1 are preferred. In this section, we will discuss the application and implementation of Hyperbolic Tangent activation function.

Most neurons in neural networks using a scalar-to-scalar function which was called activation function to transform their net input while the activation value is fed via synaptic connections to one or more other neurons. The activation function is sometimes called a transfer function. The transfer function with a bounded range are frequently called squashing functions. Hyperbolic tangent activation function is one of an example of squashing function.

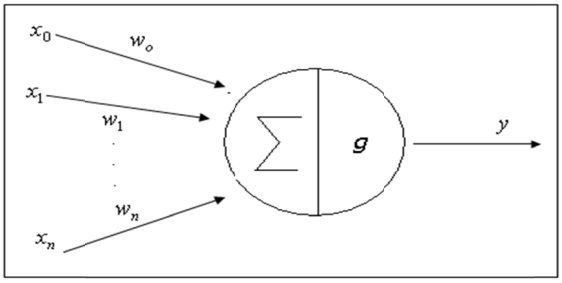

Figure 2. An artificial neuron with activation function

Figure 2 shows the artificial neuron x which is a neuron with n input dendrites ($x_0 \ldots x_n$) and where ($w_0 \ldots w_n$) are weights of inputs and one output axon $y(x)$. g is an activation function that weights how dominant the output should be from the neuron based on the sum of the input. Equation 3.6 shows the equation of activation function.

$$y(x) = g\left(\sum_{i=0}^{n} w_i x_i\right) \tag{5}$$

where $g(x)$ used the hyperbolic tangent function as below,

$$g(x) = \frac{1-e^{-2x}}{1+e^{-2x}} \tag{6}$$

At first, we substitute the total of weights and inputs into Hyperbolic Tangent function to achieve the value. If it surpasses the threshold (θ = 0), the actual output will be 1 else the value of the actual output is -1. After obtained an output pattern during the network computation, if error exists, or a difference between actual and desired output patterns, the weights will be adjusted to reduce the error.

5. Experimental results and discussion

We used *C++* as a platform to simulate the programs.

5.1 Maximum Complexity

Maximum complexity means the maximum or the limitation of the system can be afford to run before oscillation occurred. In this paper, we want to figure out the maximum complexity that can be reached when higher order clause was applied in logic programming. We did trial and error technique to determine the maximum capacity for the system. From the technique we selected number of neurons (NN) = 30. The system started having overload error for running more than 30 neurons for higher orders. We used fifth dimension arrays to represent the higher order logic programming.

5.2 Hamming Distances

Hamming distance was originally conceived for detection and correction of errors. It is simply defined as the number of bits that are different between two bit vectors. It is easier to discuss closeness of a bit pattern to another bit pattern by determining the number of bit positions in which the two patterns being compared differs. Thus, at here hamming distance is measured between the final state and global state of the neurons upon relaxation.

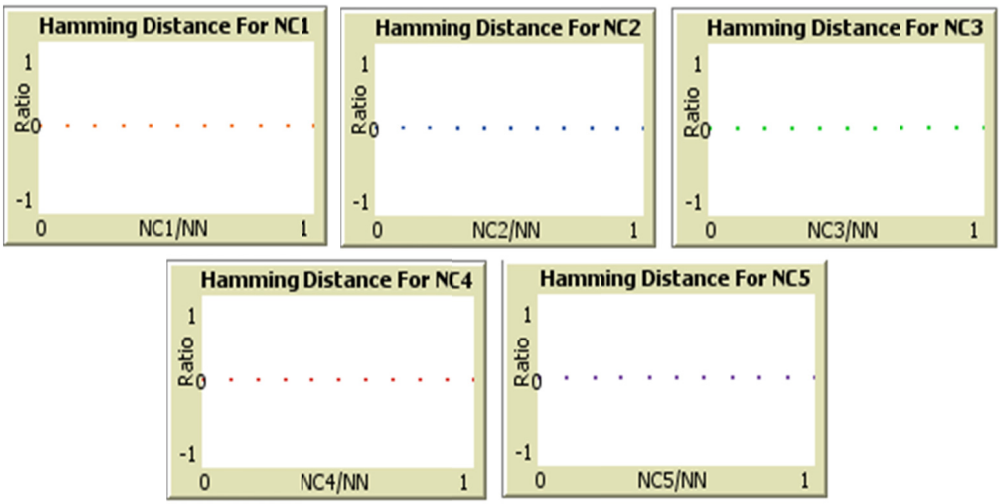

Figure 3. Hamming distance for NC1~NC5

In Figure 3, it shows that the hamming distance graphs of every level of clauses such as NC1, NC2, NC3, NC4 and NC5. It shows that the hamming distance is approximately to zero for all the cases, (NC1 (one literal), NC2 (two literals), NC3 (three literals), NC4 (four literals), NC5 (five literals)). The value of hamming distance was approximately to zero due to all the neurons reached a stable state. So, the distance between the stable states and global states are almost zero. Due to this, similar statistical error was obtained for all the cases.

5.3 Global Minima

From the global minima graphs, when the neurons relaxed to global solutions the ratio will approached 1.

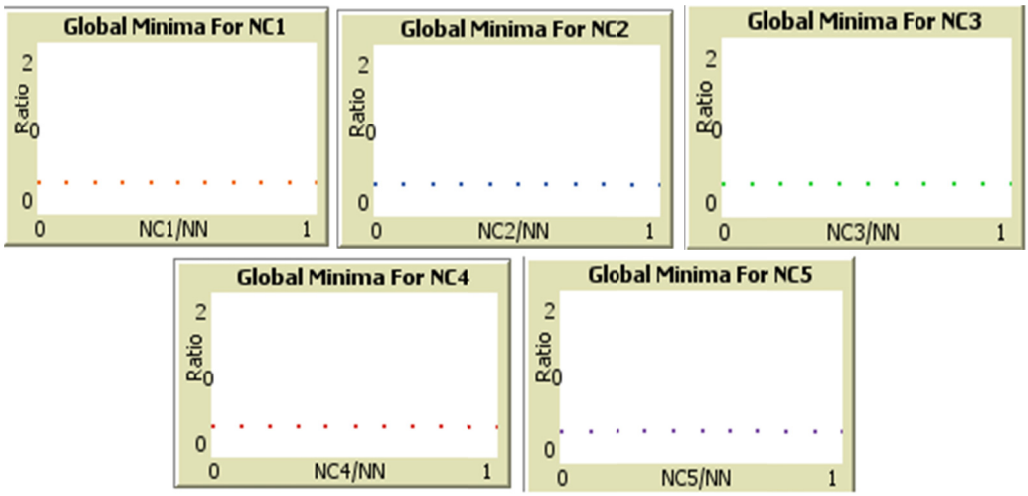

Figure 4. Graphs of global minima for NC1~ NC5

From the Figure 4 obtained, the ratio of global solutions is approximately to 0.375 for all cases when the number of neurons and number of literals per clause (NC1, NC2, NC3, NC4, and NC5) increased. It is because by using Higher Order Hopfield Network (HOHN), it was guaranteed to yield convergence towards toward local minima. When the network gets more complex due to increasing complexity, the neurons start to oscillate and stuck in local minima values.

Furthermore, the abrupt energy surface does not allow for the existence of local minima escape trajectories. This problem is increasing proportionally to the size of the error surface, and there is no universal solution (Joya et al., 2002). However, it stills have some ways to escape the local minima. One way to escape the local minima in order to find the global minimum is to resort to simulated annealing. Thus, Boltzmann machine and hyperbolic tangent activation function in higher order to show which method will enhance a better global minima.

5.4 Comparing Global Minima in Higher Order Logic Programming

We simulated the network by using two methods, Boltzmann machine and hyperbolic tangent activation function to accelerate the performance of doing logic programming. Thus a comparison of the Wan Abdullah method, Boltzmann machine and hyperbolic tangent activation function in logic programming in Hopfield networks is carried out.

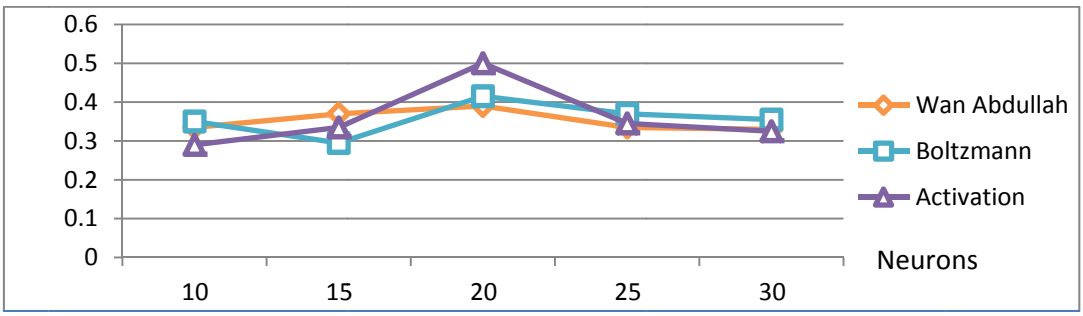

Figure 5. Global minima ratio show according to number of neurons in higher order logic programming

From the Figure 5, it shows that the global minimum ratios at first are different for each method. The ratio for Wan Abdullah method is 0.335, the Boltzmann method is 0.35 and hyperbolic method is 0.29. All the global minima values obtained are not more than 0.4. This problem occurs for higher order Hopfield network. To address this problem, the application of arbitrary order Hopfield neural networks to optimization problems is studied (Joya et al., 2002). This paper studied about the main problems affecting practical applications of higher order Hopfield networks such as existence of local minima and others. From the paper, it had made justification that a high probability of evolution to local minima occurs when involving higher order Hopfield networks. One of the simulation results for the evolution of a higher order Hopfield networks oriented for solving a Diophantine equation had shown that the percentage of correct solution (to achieve global minima) is only 38% (almost the

same ratio value when run for fifth order clause). To help to get through the problem of local minima, Boltzmann machine and hyperbolic tangent activation functions are implemented to enhance the global minima. Among the methods, Boltzmann method achieves the best value among. When the networks get larger or more complex, more neurons are applied in the program, Boltzmann method also have better performance than hyperbolic method and the Wan Abdullah method. It is because when using Boltzmann machine, after running for a long enough time at a certain temperature, the probability of a global state of the network will depend only upon that global state's energy, according to a Boltzmann distribution. When temperature decreases from a high temperature to reach a thermal equilibrium at a low temperature, we are guaranteed to converge to a distribution where the energy level fluctuated around the global minimum. The heat cause the neurons unstuck from local minima. As a result, Boltzmann machine is having the best result among the others methods.

From the overall comparison in logic programming that perform higher order Horn clause, each method had achieved low and non-ideal global minima. However for Boltzmann machine, it produces better global minima among them.

6. Conclusion

From the theory and experimental result, the ability of Boltzmann machine in doing logic programming on Hopfield network is better than Wan Abdullah method, which is based on Mc Culloch Pitts updating rule, and hyperbolic tangent activation function. It provides a better result in term of global minima ratio and hamming distance for higher order clauses. However, for higher order, the result of global minima that obtained was very low due to the complexity of network.

Acknowledgement

This research is partly financed by Fundamental Research Grant Scheme (203/ PMATHS/6711368) by Ministry of Higher Education and Universiti Sains Malaysia.

References

Brenton, C. (2002). Stability analysis of higher-order neural networks for combinatorial optimization. *International Journal of Neural Systems, 12*, 177-186. http://dx.doi.org/10.1142/S0129065702001151

Cheung, K. W., & Lee, T. (1993). Boundary Detection by Artificial Neural Network. *IEEE Proceeding of 1993 International Joint Conference on Neural Networks, Nagoya, 2*, 1189-1194.

Ding, Y., Dong, L., Wang, L., & Wu, G. (2010). A high order neural network to solve crossbar switch problem. In *Neural Information Processing, Models and Applications* (pp. 692-699). Springer Berlin Heidelberg.

Hopfield, J. J. (1982). Neural networks and physical systems with emergent collective computational abilities. *Proceedings National Academy of Science USA, 79*, 2554-2558. http://dx.doi.org/10.1073/pnas.79.8.2554

Joya, G., Atencia, M. A., & Sandoval, F. (2002). Hopfield neural networks for optimization: study of the different dynamics. *Neurocomputing, 43*, 219-237. http://dx.doi.org/10.1016/S0925-2312(01)00337-X

Pinkas, G. (1991a). Energy minimization and the satisfiability of propositional calculus. *Neural Computation, 3*, 282-291. http://dx.doi.org/10.1162/neco.1991.3.2.282

Pinkas, G. (1991b). Propositional no monotonic reasoning and inconsistency in symmetric neural networks. *Proceedings of the 12th International Joint Conference on Artificial Intelligence* (pp. 525-530).

Roweis, S. (n.d.). *Boltzmann Machines*. Retrieved May 15, 2013, from www.cs.nyu.edu/~roweis/notes/botlz.pdf

Sathasivam, S., & Wan Abdullah, W. A. T. (2010). The Satisfiabilty Aspect of Logic on Little Hopfield Network. *American Journal of Scientific Research, 7*, 90-105.

Wan Abdullah, W. A. T. (1991). Neural Network Logic. In O. Benhar, C. Bosio, P. del Giudice & E. Tabet (Eds.), *Neural Networks: From Biology to High Energy Physics* (pp. 135-142). Pisa: ETS Editrice.

Wan Abdullah, W. A. T. (1992). Logic Programming on a Neural Network. *Int. J. Intelligent Sys, 7*, 513-519. http://dx.doi.org/10.1002/int.4550070604

Modern Applied Science; Vol. 8, No. 3; 2014
ISSN 1913-1844 E-ISSN 1913-1852
Published by Canadian Center of Science and Education

Analysis and Research on Deformation Monitoring of Large Span Cable-stayed Bridge during Operating Period

Jun Cheng[1], Cheng Zhang[1], Zengshun Chen[1] & Jun Yang[1]

[1] School of Civil Engineering & Architecture, Chongqing Jiaotong University, Chongqing, China

Correspondence: Zengshun Chen, School of Civil Engineering & Architecture, Chongqing Jiaotong University, Chongqing 400074, China. E-mail: chenzs2007@163.com

Received: March 19, 2014 Accepted: April 15, 2014 Online Published: April 23, 2014

doi:10.5539/mas.v8n3p147 URL: http://dx.doi.org/10.5539/mas.v8n3p147

Abstract

This paper studies the alignment of bridge, the vertical displacement of the pier, the offset of the tower, the deformation of the expansion joints and cable force based on an extra large span cable-stayed bridge in Chongqing. Secondly, the contents and methods of large span cable-stayed bridge monitoring were introduced. Then, the theoretical value related to deformation of the bridge is calculated by using finite element software. After that, the bridge deformation data on the site was measured. Finally, the bridge alignment, tower vertical displacement, tower deformation, expansion joints, tower of the measured values and the theoretical calculation values were analyzed on the basis of comparison. It is concluded that the bridge is in normal working condition. The analysis and research of large span bridge in this paper provides the basis for similar Bridges, which has good practical value.

Keywords: bridge alignment, tower vertical displacement, tower deformation, expansion joints deformation, cable force, comparison analysis

1. Introduction

With the rapid development of China's economic, the bridge spans increase day by day. The cable-stayed bridge is one of popular styles of the long-span bridges. Compared with the suspension bridge, cable-stayed bridge is preferable in rigidity, economy, wind resistant stability, erection and so on (Zhou, 2004). However, factors, such as the heavy car traffic volume, destructive effects of overload and overweight vehicles, natural ageing of structures and materials cause large deformation of bridge structures. Thus, the deformation monitoring of bridge structure is more and more important.

The distress and accidents of cable-stayed bridge mainly occur on corrosions and wire broken, crack and deformation of girder and main tower. There are many related researches about deformation monitoring of long-span cable-stayed in China and abroad (Chen, Zhang, Zhou, Song, & Huang, 2013; Cho et al., 2010; Lekidis, Papadopoulos, Karakostas, & Sextos, 2013; Li, & Ou, 2006a, 2006b; Macdonald, 2003; Si, Au, & Li, 2013; Zengshun, Jun, Cheng, Guanrong, & Haoyang, 2013). Li Shunlong and other researchers assessed the conditions of stayed cable and damage monitoring of girder through the structural health monitoring system (Li et al., 2014). Cho, Soojin used wireless smart sensor technology to monitor the health of cable-stayed bridge under vibration load monitoring (Cho et al., 2010). However, the contents of the monitoring for large span cable-stayed bridge system are not comprehensive enough, especially in short-term deformation monitoring. Based on a long-span cable-stayed bridge, this paper analyzed the monitoring deformation value by finite element analysis software. And then, the calculated values and measured values were analyzed on the basis of comparison. The analysis of the long-span cable-stayed bridge deformation monitoring can provide a certain basis for similar bridge deformation monitoring and has good popularization value.

2. Engineering Situation

The large span cable-stayed bridge is located in the territory of the Shanghai-Chengdu Expressway in Chongqing. The total length of the Bridge is 992 m, of which the main bridge is 632 m. The main bridge is a pre-stressed concrete cable-stayed bridge with double pylons and double cable planes, total bridge span combination: 2 × (4 × 40 m (pre-stressed T beam) + (50 +108 +316 +108 +50) m (cable-stayed) +1 × 40 m (pre-stressed T beams) deck. Horizontal layout: 0.50 m (crash barrier) +10.75 (lane) +2.00 m (median strip) +10.75 (lane) +0.50 m (crash

barrier).

The main Bridge girder used pre-stressed concrete structures separate trapezoidal cross-section with girder center height 3.00 m, roof thickness 0.25 m, width of the bottom of the triangular box 2.50 m, flanks thickness 0.25 m, vertical web thickness 0.35 m, box beam full width 27.40 m. The bridge was set two-way cross slope of 2%, formed by the box girder roof. The start block from the tower, No. 0 block length is 13.00 m and the standard block length is 6.00 m. The tower is of "H" shaped tower with hollow thin-walled box section. The tower along the bridge is 6.20 m and along width transverse direction is 4.00 m. the width of medial pylons is 4.00 m and the width of the under pylons grades by 5.85 m to 8.50 m and the width of the central pylons along the bridge to the top of the pylons to the bottom grades by 6.20 m to 10.00 m. The height of upper tower is 45.671 m and the medial tower is 43.379 m and the lowers tower is 25.15 m.

The top of auxiliary pier which under main girder and at the junction of the pier top was set with tension compression bearing. The top of the abutment and the 4th pier was set with a SSFB-80 expansion joint respectively; Each ends of the main bridge was set with a SSFB-320 expansion joint respectively.

Superstructure of the main bridge box girder used C60 concrete, tower and approach bridge with T beam by using C50 concrete. The main bridge pier, the junction pier, the auxiliary pier, the approach bridge pier and cap beam all with C40 concrete. All caps, juncture pier pile foundation, auxiliary pier pile foundation and abutment cap by using C30 concrete, the main bridge pier pile foundation by using C30 underwater concrete. Bridge elevation layout is shown in Figure 1.

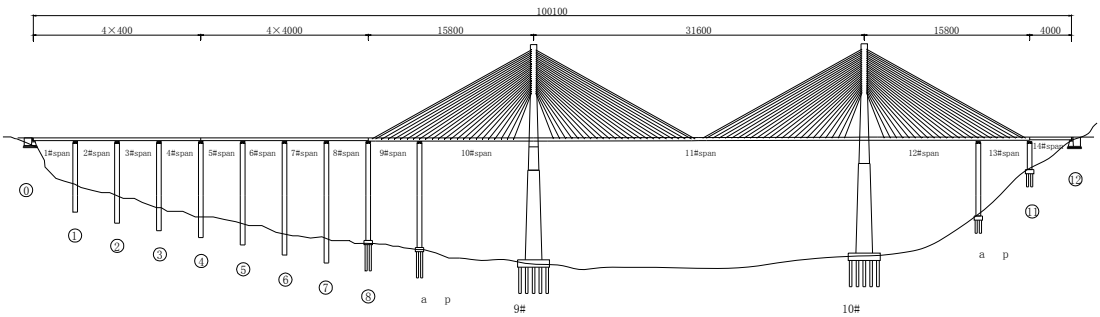

Figure 1. Bridge elevation layout (units: cm)

3. Deformation Monitoring Methods and Arrangement of Measuring Points

According to the usage of the bridge, the plane control network elevation control points, bridge alignment, tower deformation and expansion joints deformation of the bridge were monitored.

3.1 Deformation Monitoring Methods

3.1.1 Plane Control Network

Triangulation method is adopted to establish the plane control network, using LeicaTCR1201 total station (1 "level) with optical prism and the base, in accordance with the requirements for second grade leveling plane control network technology USES the traverse survey measured in the form of plane control network monitoring data.

3.1.2 Elevation Control Points

Elevation data were measured by NA2 Leica Precision Level (0.1 mm) with indium ruler. All level line observations in accordance with the requirements of national second-class leveling method form close level line. Station observation sequence, observation method, the results of overrun return measurements, weight measurements and so on are in accordance with the provisions.

3.1.3 The Bridge Alignment

Bridge deck alignment observation uses NA2 Leica Precision Level (0.1 mm) with indium ruler, according to the second-class leveling, the length of sighting line, sighting distance from start to finish and repeat counts of precision level measurements are conformed to the specification requirements of "Secondary Precision Level". Inspect on I Angle of the Level before measurements, constitute the benchmark and bridge deck alignment observation points to a closed loop, measurements are in accordance with the observation sequence (1) odd

station “back-front-front- back”, (2) even station “front- back- back - after”, the observation results are adjusted in addition.

3.1.4 Tower Deformation

Tower deformation monitoring usies Leica TCR1201 Total Station (1 "level) with optical prism. According to the requirements of secondary surface accuracy, the polar coordinate method is adopted to.

3.1.5 Expansion Joints Deformation

Expansion joints deformation monitoring includes both sides of the expansion joints (large pile side, small pile side) the deck transverse stagger displacement monitoring and transverse stagger displacement changes of itself (steel clearance) monitoring. Expansion joints on both sides of the bridge deck transverse stagger displacement monitoring uses total station with optical prism for measurement. And steel tape measurement is adopted to steel clearance changes of expansion joint itself directly.

3.1.6 Cable Force

(1) Test Methods

This test uses the frequency method to measure the cable force. When expressways completely closed, use precision vibration pick-up to pick up vibration signals under environment excitation or the attenuation of vibration signal after hitting. When testing, fixing the vibration pick-up on the cable so that the transverse vibration of the cable can be measured. Vibration pick-up transform random vibration signal into electrical signal, the electric signal was send to the dynamic signal acquisition system after enlargement and then was taken samples and stored. Through filtering, amplifying and spectrum analysis and the spectrum diagram again to determine the natural frequencies of the cable. Then calculate the cable force according to the measured natural vibration frequencies.

(2) The Cable Force Calculation Method

Regardless of the cable sag and the stiffness of the cable, and suppose the cable hinged at both ends, the cable force calculation formula as follow:

$$F = 4ml^2 \frac{f_n^2}{n^2} = K \frac{f_n^2}{n^2} \tag{1}$$

Where;

n is cable natural frequency modal order of natural vibration frequency of a cable (is: half wave numbers in the cable length)

f_n is the natural vibration frequency of the related order of a cable

l is the free length or bending length of a cable

K is the proportional coefficient ($KN \cdot s^2$)

3.2 Monitoring Points Arrangement

3.2.1 Layout Principles

The deformation monitoring networks are divided into base point, work datum point and deformation observation point. The layout should follow the principles below:

(1) Base point: shall be in stable and reliable positions outside the deformation influential area, and each bridge should have at least three base points;

(2) Work datum point: Shall be in a rather stable and user-friendly position;

(3) Deformation observation point: Shall be set up in the position where can reflect the detection deformation characteristics or a test section.

3.2.2 Measuring Points Layout

(1) The Plane Control Network

Select positions which can reflect the detection plane characteristics or three points on the test section as measuring points;

(2) Elevation Control Points

Select positions which can reflect the control elevation characteristics or two points on the test section as

measuring points.

(3) The Bridge Deck Line

The bridge deck line monitoring points makes full use of historical monitoring points and sets up additional liner measuring points for those unsatisfied ones, specific arrangements of measuring points are as follows: the bridge deck line monitoring is only in view of the main line. Linear observation points in longitudinal direction of each corresponding cross-section and main span, L / 4, supporting point and other control sections were set up. And according to the requirements of the stationing spacing is not more than 20 m, additional linear observation points were added.

Linear observation points are set on the bridge to the right or left medial part of bridge deck against a wall at the bottom of the picture, the right side of the median fence outside concrete base side decorate. According to the bridge longitudinal, it was divided into three measuring lines (L, Z, R line).They are left, middle and right lines. The whole bridge has 312 deck linear observation points. The observation points uses stainless steel round head nail, implant inserted bar glue after drilling hole with churn drill and identified with red paint. Arrangements of measuring points are shown in Figure 2 and Figure 3:

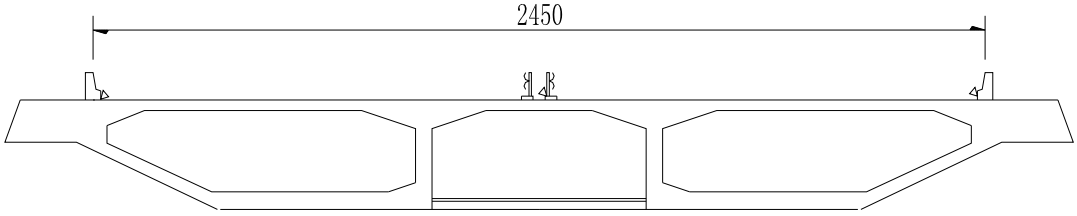

Figure 2. The deck arrangement of measuring points in alignment profile (unit: cm)

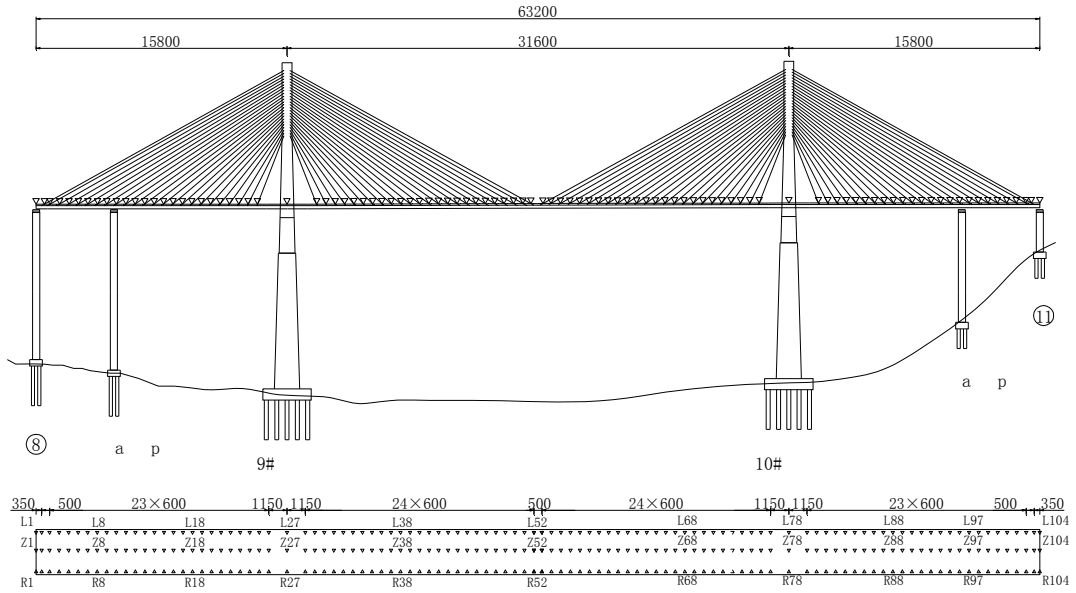

Figure 3. The deck arrangement of measuring points in alignment profile (unit: cm)

(4) The Deformation of Cable Tower

In this deformation monitoring, there are 8 deformation observation points on the cable tower and 4 points on each pylon which arrange at the top and the middle of the pylon. Arrangements of observation points are shown in Figure 4.

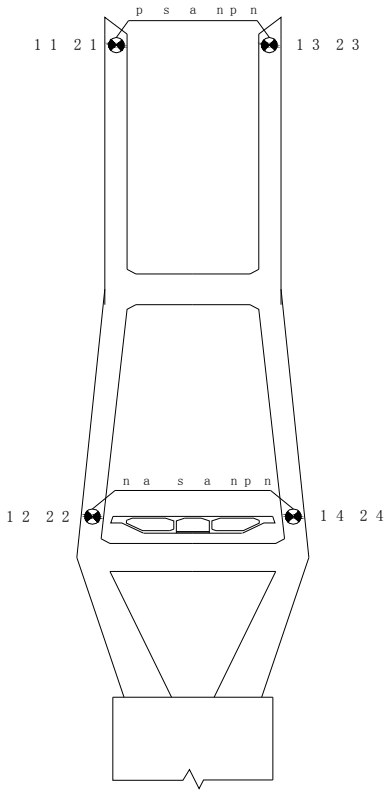

Figure 4. The arrangement of measuring points in cable tower deformation

(5) The Deformation of Expansion Joint

In this expansion joint monitoring, every 1 observation section was set at each expansion joint of the main bridge. And observation sections were set outside of the deck when laterally and each observation section has 2 observation points, a total of 4 observation sections, 8 observation points. Arrangements of measuring points are shown in Figure 5.

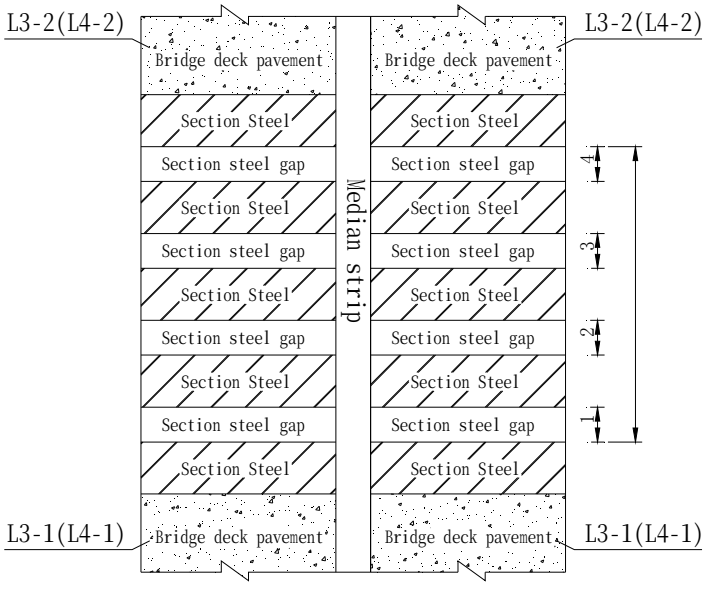

Figure 5. Monitoring point arrangement on expansion joint deformation

(6) Cable Force

In order to pick up vibration signal of stayed cable under environment excitation accurately, cable force test points should be chosen in the part of a larger vibration amplitude of the cable stayed and the maximum to avoid the influence of damper and steel thimble. According to the test conditions, the cable force measuring points is close to the PE thimble of the bridge deck, specific arrangement of measuring points are shown in Figure 6.

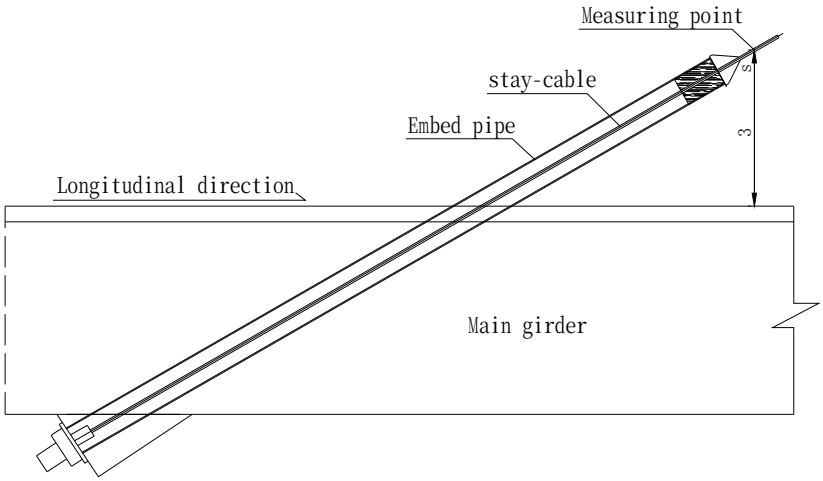

Figure 6. The arrangement of testing points in cable force

4. Monitoring Results and Analysis

4.1 Theoretical Calculation of Deformation Monitoring

According to the material parameters and usage of the bridge, using the FEA software calculates the theoretical value of the bridge deformation. Stayed cable adopts truss element to simulate, and the main girder adopts beam element to simulate. Stay-cables, the girder and cable pylons adopt rigid connection. The master nodes are respectively set in the main pylons and the girder, the main tower beam is simulated according to actual condition, the main girder diaphragms adopt the equivalent load to simulate, a total of 865 nodes, 648 units. The main types of bridge load in the model include dead load, temperature load, cable force, wind loads, etc. Discrete graph structure model is as shown in Figure 7.

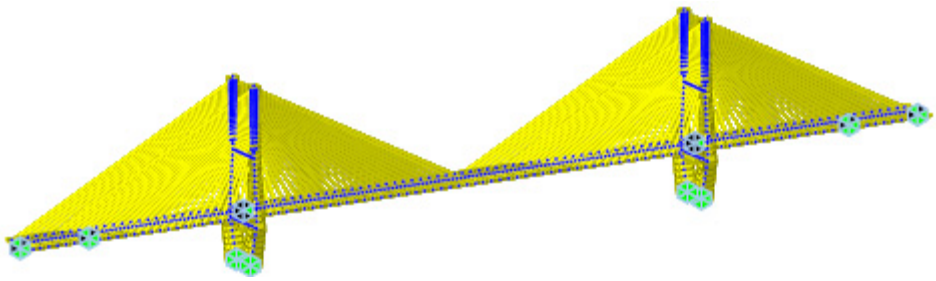

Figure 7. discrete graph structure model

Through the model analysis, theory values of the geometry of bridge deck, tower deformation, expansion joint deformation and cable force can be obtained.

4.2 Contrastive Analysis of Theoretical and Measured Values

After the theoretical results obtained by using finite element analysis software, the measured values of the bridge deformation can be obtained according to the contents and methods of monitoring the bridge. After obtaining theoretical and measured deformation values, then the measured values with calculated values can be compared. Deflection of the bridge, tower vertical displacement, tower deviation, expansion joints deformation, cable force comparative analysis results are as follows.

4.2.1 Contrastive Analysis of the Bridge Deck Linear Deflection

Contrastive analysis of two measurement results, “the measured deflection” is the “second phase (December 2012) the relative elevation data” subtract “the first phase (September 2012) the relative elevation data”. A positive value indicates up-flexion, a negative value indicates down deflection. Theoretical value extracted from the finite element program structural model. Comparison of measured deflection and theoretical deflection is as shown in Figures 8-10.

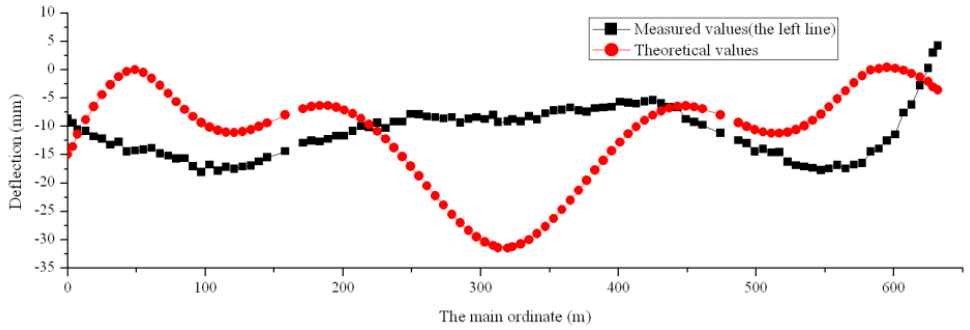

Figure 8. The measured deflection and the theory of the left line of bridge deck alignment deflection comparison chart

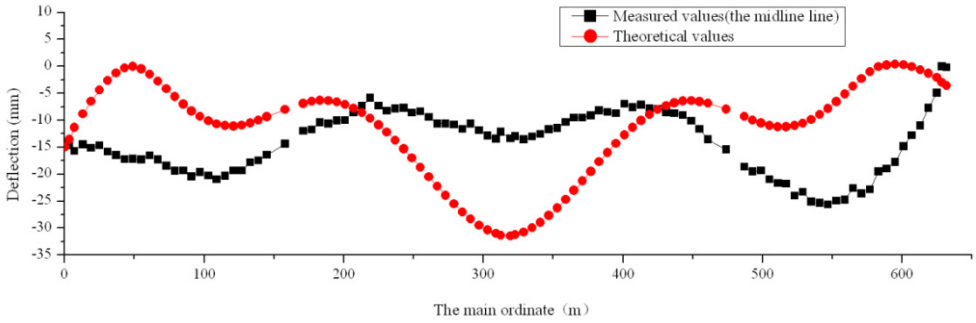

Figure 9. The measured deflection and the theory of the center line of bridge deck alignment deflection comparison chart

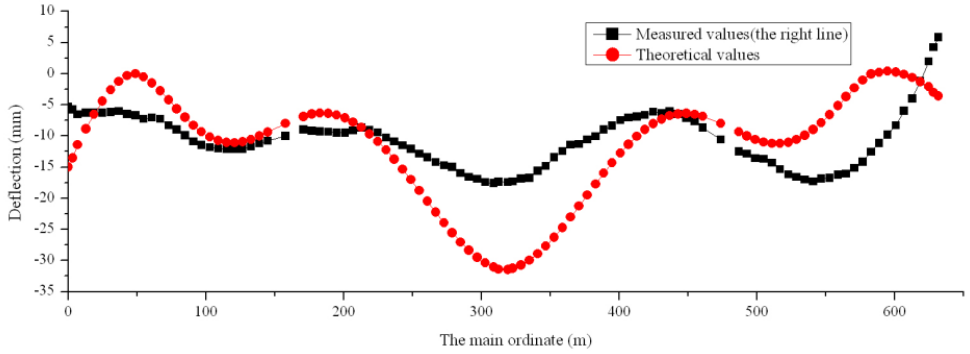

Figure 10. The measured deflection and the theory of the right line of bridge deck alignment deflection comparison chart

Thus it can be seen that the deflection of the bridge deck, the left side of the maximum deflection occurs in the cross-section 0.445L of the 10# span, deflection value is 18.06 mm, 8.72 mm larger than the theoretical value. The middle of the maximum deflection occurs in the cross-section 0.664L of the 12# span, deflection value is 25.61 m, 17.75 m larger than the theoretical value. The right side of the maximum deflection occurs in the

cross-section 0.609L of the 12# span, deflection value is 17.59 mm, 8.36 mm larger than the theoretical value.

4.2.2 Contrastive Analysis of the Results of the Tower Vertical Displacement

In order to understand the situation of tower settlement in monitoring period and its influence on the deck line, the vertical displacement of the bridge were measured. “Measured Vertical Displacement of the Tower” stands for “Relative Elevation of 1st Phase subtract Relative Elevation of 2nd Phase”. Calculated Vertical Displacement is the theoretical value in consideration of the overall temperature drop and shrinkage and creep. “The vertical displacement of the Tower” as a negative value indicates downward deformation. Contrastive results are shown in Table 1.

Table 1. Test result of Cable tower vertical deformation (unit: m)

No.	Measuring Point	Location	Relative Elevation of 1st Phase	Relative Elevation of 2nd Phase	Measured Vertical Displacement of the Tower (10^{-3})	Calculated Vertical Displacement (10^{-3})
1	T1-2	Middle of 9# tower of left bridge	111.586	111.5741	-11.89	-14.27
2	T1-4	Middle of 9# tower of right bridge	111.6264	111.6149	-11.47	-14.27
3	T2-2	Middle of 10# tower of left bridge	118.2727	118.2585	-14.19	-15.34
4	T2-4	Middle of 10# tower of right bridge	118.2874	118.274	-13.46	-15.34

As can be seen from test results of the main bridge tower observation point, under the conditions of cooling 16.7 °C, the central position of the pylon of 9# tower’s vertical deformation is 11.89 mm, 14.27 mm less than the theoretical value, the central position of the pylon of 10# tower’s vertical deformation is 14.19 mm, 15.34 mm less than the theoretical value. The above analysis shows that the measured vertical displacement of each main bridge tower is less than the calculated value, so that we can make a preliminary determine that there was no obvious settlement deformation of each main tower during the initial monitoring period.

4.2.3 The Tower Deviation Comparison Analysis

In order to get the status of bridge tower deformation during monitoring period, measurements of the bridge axial displacement were taken “Measured Axial Displacement” is the value that the measuring point displacement converts to the axis of the bridge based on the first and the second phase measured data; “Theoretical Axial Displacement” is the theoretical calculation value which in according with the test conditions including the overall cooling, cable force change, wind load effects, and the shrinkage and creep value; Positive values in “Axial Displacement” means deviating to the north, while negative value to the south. The theory and the measured results are shown in Table 2:

Table 2. Comparison on theoretical and practical results of Cable tower deviation (unit: mm)

No.	Measuring Point	Location	Measured Axial Displacement(10^{-3})	Theoretical Axial Displacement(10^{-3})
1	T1-1	Top of 1# tower of left bridge	29	33.68
2	T1-3	Top of 1# tower of right bridge	27	33.78
3	T2-1	Top of 2# tower of left bridge	-28	-33.69
4	T2-3	Top of 2# tower of right bridge	-27	-33.8

According to the test results of main tower observation points and under the condition of temperature cooling is 14.3 °C, 9 # tower location along the bridge to the river's side tilts 29 mm, 33.68 mm less than the theoretical value; 10 # tower location along the bridge to the river's side tilts 28 mm, 33.69 mm less than the theoretical value. Tower deviation measured value is less than the theoretical calculation shows that the deformation is in normal range.

4.2.4 The Expansion Joint Deformation Comparison Analysis

By comparing and analysis the measured value and theoretical value of 4 expansion joints clearance on both the left and right sides of the bridge with total station and steel tape, the results are shown in Table 3.

Table 3. Comparison on theoretical and practical expansion joint clearance of deck (unit: mm)

Side	Expansion Joint No.	Total Station Measured Deformation	Steel Tape Measured Deformation	Theoretical Deformation
The left bridge	L3#	41	41	50.91
	R3#	42	42	50.91
The right bridge	L4#	33	34	48.05
	R4#	35	35	48.05

According to the measuring results of expansion joints that under the condition of temperature cooling 14.3 °C, the width of each expansion joints is in expanding condition, the expansion joints of the main tower 3# expanded 42 mm, 50.91 mm less than the theoretical value while the expansion joints of 4 # 35mm, 48.05 mm less than the theoretical value. The measured expansion deformation value is less than the theoretical value. Comparatively speaking, the expansion joints of 3# are larger than 4#, which means that every expansion joint is in good working condition during the monitoring period.

(5) Cable Force Test Results and Contrastive Analysis

In order to know the change of cable force, make a test for each cable, the measured cable force and the designed cable force comparison results are shown in Figures 11 ~ 13.

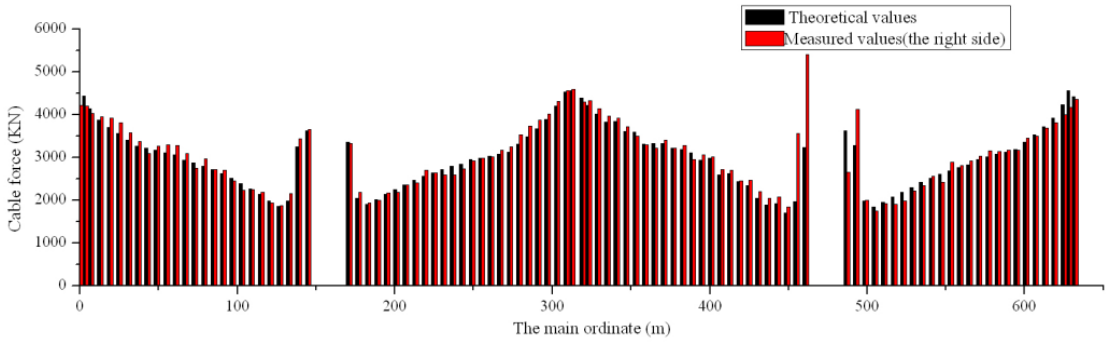

Figure 11. The right side measured cable force and the design force comparison chart

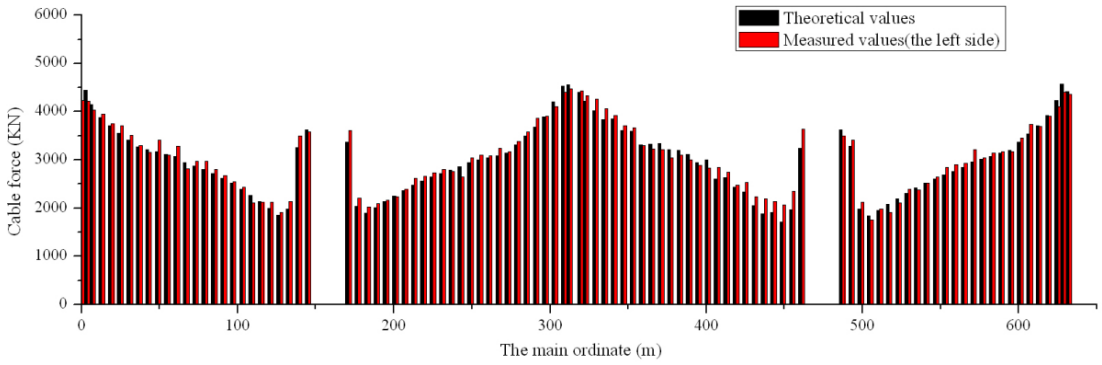

Figure 12. The left side measured cable force and the design force comparison chart

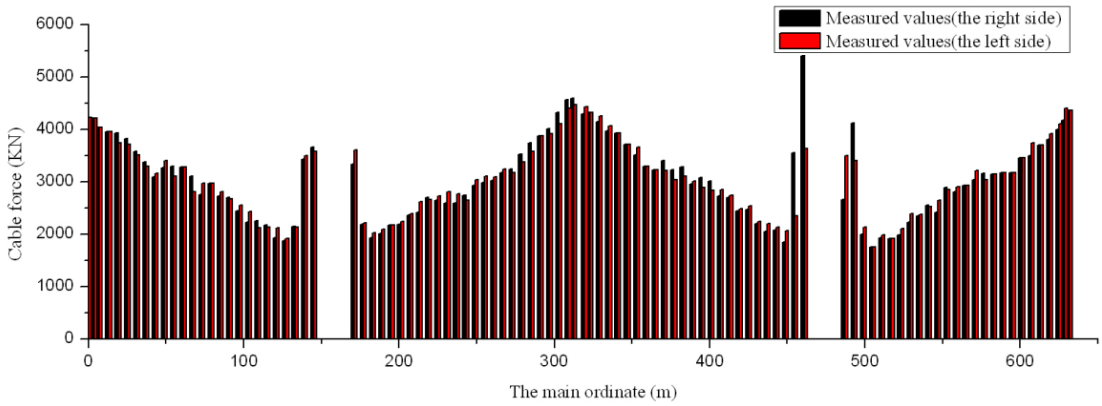

Figure 13. The left and right side measured cable force comparison chart

Figures 11 -13 show that the regularity of stayed-cable force on the left and the right side of the large bridges basically the same. The measured values and designed values of the two phases completed accord well with each other.

5. Conclusion

Through the results of contrastive analysis by field measured data and the theory data calculated by finite element software, conclusions can be got as follows:

(1) We can know from the bridge deck deflection testing results and deflection analysis diagram: change rules of three measured deflection curves which correspondently in the left, middle and right sides is the same with theoretical curve. Measured deflection values and the calculated values of each measuring point are in or near the theoretical value scope, deformation belongs to the normal range;

(2)The vertical deformation values of the middle part in pylons are less than the calculated values. Thus a preliminary determination that no obvious settling deformation of each main tower occurred during the monitoring period can be made;

(3) The top of the two pylons along the bridge to the river's side direction deviations are less than the calculated values, which shows that the deformation is in normal range;

(4) Under the condition of the site environment, the measured values of bridge expansion joint deformation are less than the calculated values, and the expansion joint is in good working condition.

(5) The regularities of dead load cable force on both left and right sides are basically the same. The measured values and designed values completed accord well with each other.

Currently, the bridge is only under the condition of no moving load monitoring. We measure structure performance by static deformation of the structure. We suggest to establish health and safety monitoring system at an appropriate time, using modern sensor technology to real-time monitor the structural response parameters of bridge operation stages under various environment (dynamic characteristics and vibration, dynamic strain and

dynamic deflection), acquire all kinds of information which can reflect the status of structure and environmental factors and make a comprehensive evaluation of bridge structure conditions.

References

Chen, Z., Zhang, C., Zhou, J., Song, J., & Huang, C. (2013). Study of Cable Force of Construction Control and Alignment Control of Main Girders for Long-Span Railway Cable-Stayed Bridges. *Modern Applied Science, 7*(9).

Cho, S., Jo, H., Jang, S., Park, J., Jung, H. J., Yun, C. B., ... Seo, J. W. (2010). Structural health monitoring of a cable-stayed bridge using wireless smart sensor technology: data analyses. *Smart Structures and Systems, 6*(5), 461-480. http://dx.doi.org/10.12989/sss.2010.6.5_6.461

Lekidis, V., Papadopoulos, S., Karakostas, C., & Sextos, A. (2013). Monitored Incoherency Patterns of Seismic Ground Motion and Dynamic Response of a Long Cable-Stayed Bridge. *Computational Methods in Earthquake Engineering, 30*, 33-48. http://dx.doi.org/10.1007/978-94-007-6573-3_2

Li, H., & Ou, J. (2006a). The Design and Implementation of Cable-stayed Bridge Structural Health Monitoring System (I): Design System. *Journal of Civil Engineering, 39*(4), 39-44.

Li, H., & Ou, J. (2006b). The Design and Implementation of Cable-stayed Bridge Structural Health Monitoring System (I): Implementation System. *Journal of Civil Engineering, 39*(4), 45-53.

Li, S., Li, H., Liu, Y., Lan, C., Zhou, W., & Ou, J. (2014). SMC structural health monitoring benchmark problem using monitored data from an actual cable-stayed bridge. *Structural Control and Health Monitoring, 21*(2), 156-172. http://dx.doi.org/10.1002/stc.1559

Macdonald, J. H. G. (2003). Evaluation of buffeting predictions of a cable-stayed bridge from full-scale measurements. *Journal of wind engineering and industrial aerodynamics, 91*(12), 1465-1483. http://dx.doi.org/10.1016/j.jweia.2003.09.009

Si, X. T., Au, F. T., & Li, Z. H. (2013). Capturing the long-term dynamic properties of concrete cable-stayed bridges. *Engineering Structures, 57*, 502-511. http://dx.doi.org/10.1016/j.engstruct.2013.10.007

Zengshun, C., Jun, S., Cheng, Z., Guanrong, H., & Haoyang, W. (2013). Study of Different Construction Processes Affecting the Installation of Appropriate Cambers for Long-Span Railway Cable-Stayed Bridges. *Modern Applied Science, 7*(8), 89. http://dx.doi.org/10.5539/mas.v7n8p89

Zhou, M. (2004). *Cable-stayed Bridge Handbook*. Beijing: China Communications Press.

Copyrights

Modern Applied Science; Vol. 8, No. 3; 2014
ISSN 1913-1844 E-ISSN 1913-1852
Published by Canadian Center of Science and Education

Software Sensor to Enhance Production of Fructose

Norliza Abd. Rahman[1], Mohd. Azlan Hussain[2], Jamaliah Md. Jahim[1] & Siti Rozaimah Sheikh Abdullah[2]

[1] Department of Chemical Engineering & Process, Faculty of Engineering and Built Environment, Universiti Kebangsaan Malaysia, Malaysia

[2] Department of Chemical Engineering, Faculty of Engineering, University Malaya, Malaysia

Correspondence: Norliza Abd. Rahman, Department of Chemical Engineering & Process, Faculty of Engineering and Built Environment, Universiti Kebangsaan Malaysia, 43600 Bangi, Malaysia. Tel: 60-389-216-115. E-mail: liza@eng.ukm.my

Received: September 2, 2013 Accepted: February 12, 2014 Online Published: April 30, 2014

doi:10.5539/mas.v8n3p158 URL: http://dx.doi.org/10.5539/mas.v8n3p158

Abstract

Present studies describe the on-line prediction of fructose concentration by using Artificial Neural Network (ANN) that employed as software sensor in the batch reactor for the biosynthesis of fructose by Immobilised Glucose Isomerase (IGI) of *S.murinus*. The process of fermentation was carried out in a 2-L batch bioreactor (New Brunswick Scientific, USA) with a working volume of 1.5 L reactor. All of the parameters were automatically controlled with the help of attached software. The optimum pH and temperature, for the production of fructose by Immmobilised Glucose Isomerase (IGI) of *S.murinus* were found to be 8 and 60 ^{o}C, respectively. Accuracy of the proposed soft sensor was calculated by the correlation coefficient (R^2) and mean square error (MSE). In this study, value R^2 were greater than 0.95 and the values of MSE were less than 0.2, indicating a good fit of the ANN-soft sensor to the experimental data, accurate up to 95.7% for training and 100% for testing. Thus, the proposed ANN-soft sensor was the most precise in predicting fructose concentration.

Keywords: fructose, on-line prediction, batch bioreactor, mean square error

1. Introduction

Artificial Neural Networks (ANN) is defined as structures comprised of densely interconnected adaptive simple processing elements similar to the biological neurons that are capable of performing massively parallel computations for data processing and knowledge representation (Serra et al., 2003; Molga & Cherbanski, 2003; Chen et al., 2004; Basheer & Hajmeer, 2000). Researcher successfully applied using artificial neural network in modeling of biological system (Boyaci, 2005; Geeraerd et al., 1998; Hajmeer et al., 1997; Lou, 2001; Sun, 2003; Torrecilla et al., 2004). According to Jain et al. (1996), the attractiveness of ANNs comes from the remarkable information processing characteristics of the biological system such as non-linearity, high parallelism, robustness, fault and failure tolerance, learning, ability to handle imprecise and fuzzy information and their capability to generalize.

The analogy between biology neuron and artificial neuron is; the connections between nodes represent the axons and dendrites, the connections weights represent the synapses and the threshold approximates the activity in soma. Figure 1 illustrates *n* biological neurons with various signals of intensity *x* and synaptic strength *w* feeding into the neuron with the threshold of *b* and the equivalent artificial neurons system.

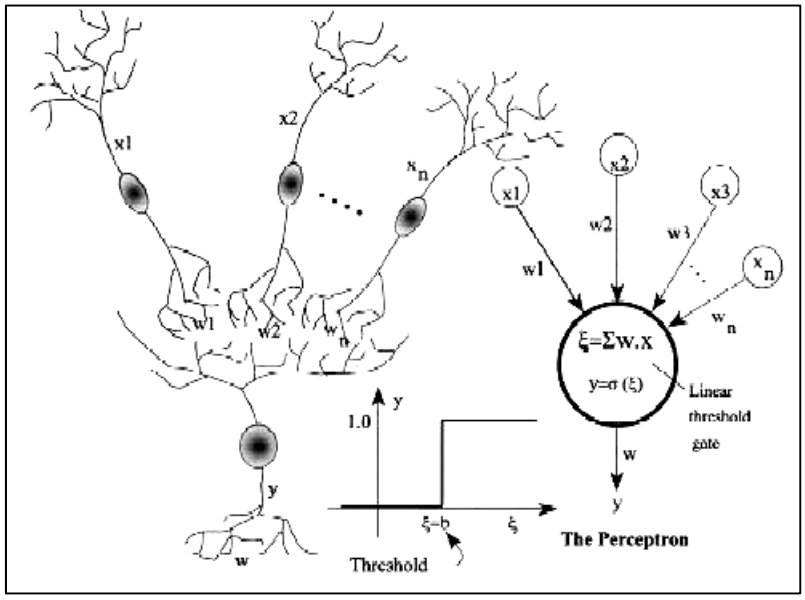

Figure 1. Signal interaction from n neurons and analogy to signal summing in an artificial neuron comprising the single layer perceptron (Basheer & Hajmeer, 2000)

Generally the applications of ANNs fall into seven categories known as pattern classification, clustering, function approximation, forecasting, optimization, association and control. In this study the application of ANNs is under the function approximation. Function approximation (modeling) involves training ANN on input–output data so as to approximate the underlying rules relating the inputs to the outputs. Function approximation is applied to problems (i) where no theoretical model is available, i.e., data obtained from experiments or observations are utilized, or (ii) to substitute theoretical models that are hard to compute analytically by utilizing data obtained from such models.

Bioprocess and chemical process systems are instrumented with a large number of sensors and require precious instrumental analysis or statistical analysis with a large amount of experimental data (Chung et al., 2010). According to previous researcher (Mithra, 2011; Norliza et al., 2011; Yu et al., 2011; Ferreira et al., 2003; Crabb & Shetty, 1999; Luong et al., 1997; Lammers & Scheper, 1997; Crabb & Mitchinson, 1997) application of soft sensors is still relatively inadequate for enzymatic reaction due to numerous factors such as need for regular calibration and maintenance, high cost, short operational life, unreliable supervisory systems for on-line fault detection and correction.

According to (Kadlec et al., 2009), soft sensors are predictive model and the term soft refers to "software" whereas sensors are delivering similar information as their hardware counterparts. In general, there are two different types of soft sensors, namely model-driven and data-driven.

First Principle Models (FPM) is commonly used in model-driven soft sensors but their drawback is an assumption of steady-states of the processes. As a result, data-driven soft sensors gained increasing popularity in the process industry as shown by previous researcher (Yuan et al., 2000; Yang et al., 1998; Chen & He, 1997; Latrille, 1997; Rouzic & Le, 1997; Acuna et al., 1995; Thibault et al., 1990; Pfaff, 1995; Oh, 1995). Therefore in this work, data-driven soft sensors are used since they are based on the data measured within the processing plants, and thus describe the real process conditions. The applications of soft sensors are mostly for on-line prediction, process fault detection, process monitoring and sensor fault detection.

In this proposed study, we apply neural network data-driven soft sensor is applied in a batch process to estimate fructose concentration for on-line prediction. This is due to the dynamic behaviour during the process where there is no steady state operating point and wide operating ranges may be encountered due to frequent start-up and shutdown (Seborg et al., 2004).

The research conducted will then be described, starting with the research procedures (Section 2), some results and discussion (Section 3) and the conclusion.

2. Materials and Methods

This section describes close-loop studies, batch systems and computer accessories firstly for conventional control followed by development of a software sensor which acts as an estimator or prediction.

2.1 Close-loop Studies and Batch Systems

Preliminary experiment for glucose isomerisation was conducted in a 2 liter stirred double-jacketed bioreactor made of Borosilicate glass 3. 3 DN 120 043943 with 3 blades of propeller agitator. Figure 2 and Table 1 give the dimension of the batch bioreactor used in this study. The speed of the agitator in the experiment was set in the range of 100 to 200 rpm. The heater was installed to control the temperature and a dosing pump was added of pH by addition of NaOH. For temperature control, the usage of heater of 21 cm in length (only 8 cm for heating zone) with diameter of 1.3 cm was implemented inside the reactor. The function of the waterbath was to maintain the reactor temperature.

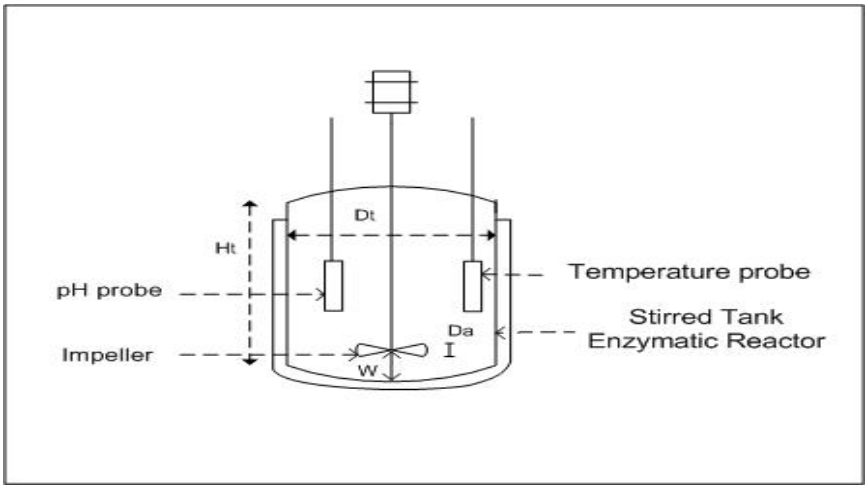

Figure 2. Dimension of a batch reactor

Table 1. The dimension of the batch reactor

Parameters	Dimensions
Diameter of impeller, D_a	5 cm
Diameter of reactor, D_t	11.5 cm
Height of impeller blade, W	0.5 cm
Height of reactor, H_t	20.9 cm
Height of liquid in the reactor, H_L	8.5 cm

The objective of this experiment was to determine the optimum values for the reaction conditions such as temperature, pH, enzyme activity, and kinetic parameters for the reaction. 0.1 M of glucose solution and 12 g of rehydrated IGI were added to give one liter of solution A in the reactor and heated up to the reaction temperature of 55 °C, 60 °C, 65 °C and 70 °C and pH of 3, 4, 5, 6, 7, 8, 9 and 10. The glucose-IGI mixture was agitated for 2 hours at 150 rpm. Once the experiment was completed, the samples were deactivated and analysed for the fructose content.

2.2 Computer and Accessories

The main purpose in the closed-loop system was to control the temperature and pH of the reaction at the desired set point. Figure 3 shows the schematic diagram for wiring of both the temperature and pH control, where the interface card of RS232 type was used to connect the reactor with the computer. The PC used in this work operated with Intel Celeron 667/800 MHz, with more than 1 GB. For proper installation and execution, the following software specifications were installed as shown in Table 2.

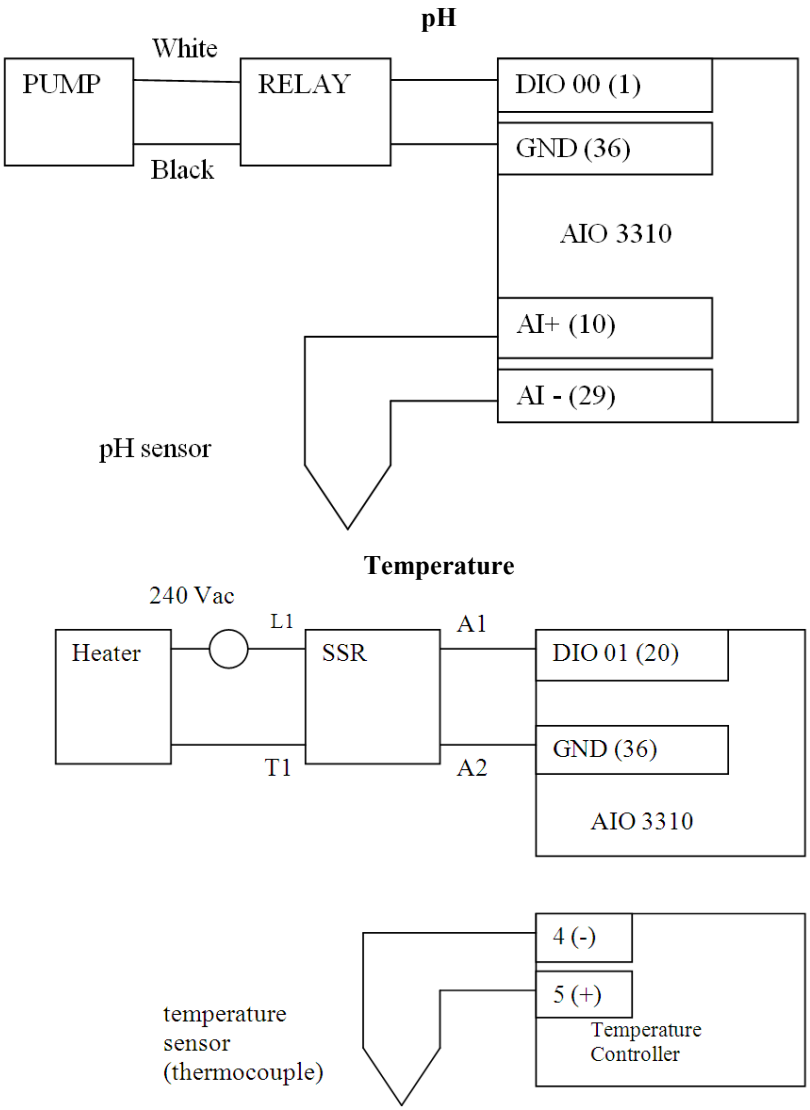

Figure 3. The schematic diagram of wiring for both temperature and pH control

Table 2. Software specifications

Software	Description
Operating system	Window XP
C Compiler	Microsoft Visual Basic
FULDEK	Version 1.0
MATLAB/Simulink	Version 12a

The control hardware consists of the following items below;

- **Sensors:** Mattec-T PT100, thermocouple, temperature sensor (from 0 ^{o}C to 100 ^{o}C) with 4mm diameter and 150 mm in length and pH probe (Amphel) (pH from 3 to 10).
- **Transmitter:** Temperature transmitter; (FlexTop 2202, Baumer, 4 to 20 mA signal, 3 wire sensors, accurancy better than 0.25 ^{o}C). pH transmitter; (FlexTop 2202, Baumer, 4 to 20 mA signal, 3 wire sensors, accurancy better than 0.1).
- **Converter:** SSR and RS232 for Heater converter.
- **Analog-digital interface card:** AIO-3310/1/2 (JS Automation Corp., Taipei, Taiwan); PCI plug and

play function with 16 identical cards. Analog function: for software selectable input range; -10 V~+10 V. For Digital I/O function; 232 bit multifunction up to 33 MHz.

2.3 Software Sensor for Estimation of Fructose Concentration

The experimental work so far in this study used analytical method for determination of fructose concentration. Time consuming and high maintenance cost for the analysis of fructose concentration using analytical method trigger the development of a software sensor which acts as an estimator or prediction. The application of ANN has been widely used as a prediction for the fructose formation in the glucose isomerisation. The proposed sensor was introduced into the batch reactor due to the dynamic and variation of the process. Figure 4 shows the schematic diagram of batch reactor with the software sensor.

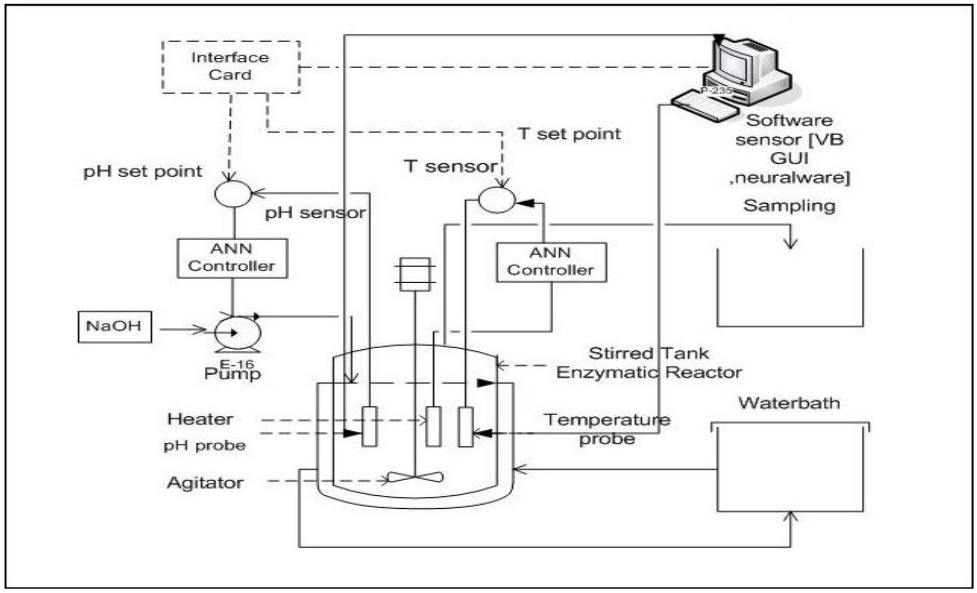

Figure 4. Schematic diagram of batch reactor for glucose isomerisation process with software sensor

Based on the initial data of closed-loop experiment for temperature and pH effect (inputs for the software sensor) the software sensor was introduced to estimate the fructose concentration (output). The procedure and control hardware to perform this experiment is similar with the closed loop experiment.

3. Results and Discussion

Analytical methods for the determination of simple sugar are generally based on the HPLC column using RI detector such as by (Gram & Bang, 1990) followed by several researchers (Bhosale et al., 1996; Crabb & Shetty, 1999; Salehi et al., 2004; Lee & Hong, 2000). Rački et al. (1991) reported a Dische-Borenfreund method for the determination of fructose concentration. This method is time consuming and costly for material in handling the HPLC as well as maintenance of it. For this purpose, Artificial Neural Networks was used in this study for the estimation of fructose concentration instead of chemical analysis.

According to (Anantachar et al., 2010), there are two main advantages for the application of Artificial Neural Networks. The primary advantage is that, it does not require a user-specified problem solving algorithm, instead it 'learns" from examples, much like human being. Moreover, it has inherent generalization ability. The alternative method has the following properties: (i) it is applicable for all type of reactors without any limitations (ii) it does not require any assumptions about kinetic study.

The Artificial Neural Networks was carried out using the Neuralware Product and Predict Software (Neuralware Carnegie, USA, product release 3.2, February, 2007). By using data of experiment for batch reactor, Stirred Tank Reactor (STR), the ANN was developed. For the STR, the ANN was built up which consists of five inputs, one output with linear transfer function, and ten hidden layers, using sigmoid as a transfer function in the hidden layers. The inputs of the neural network were temperature, (T_k), previous temperature, (T_{k-1}), glucose concentration, [G], pH_k and previous pH, (pH_{k-1}). The output of the system was the fructose concentration, $[Fr]_k$.

3.1 On-Line Prediction

The application of soft sensor in this study is for on-line prediction of fructose concentration which is the most common application (Kadlec et al., 2009). These ANN- based software sensors are used coupled with the primary on-line sensors, which capture large volumes of real-time isomerisation data (Rivera et al., 2010). Accuracy of the proposed soft sensor was calculated by the correlation coefficient (R^2) and mean square error (MSE) (Rivera et al., 2010).

The performances of the ANN- soft sensor for the effect of temperature and pH in the batch reactor are shown in Figure 5 and Figure 6. Table 3 and 4 summarized the values of R^2 and MSE.

Figure 5 shows the proposed soft sensors predicting (named PT55, PT60, PT65 and PT70) accuracy of fructose concentration from easily measurable input variables at each temperature. The experimental results refer to the off-line analysis of fructose concentration using HPLC (named ExT55, ExT60, ExT65 and ExT70). The results were further emphasized in terms of R^2 and MSE.

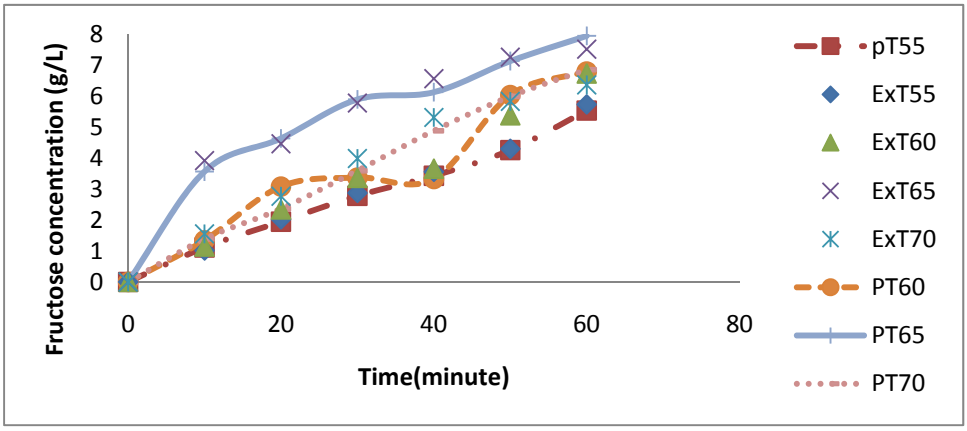

Figure 5. Experimental (filled shapes) and performance of the ANN- soft sensor for the fructose concentration (lines) in the Batch Reactor (change of temperature)

The accuracy of ANN-soft sensor with the effect of pH is shown in Figure 6. From Figure 6, throughout the reaction time for each pH under study, the ANN-soft sensor prediction of fructose concentration function almost as accurately as the experimental works (refer to off-line analysis by HPLC method). The performance of the soft sensor was indicated by the values of R^2 and MSE.

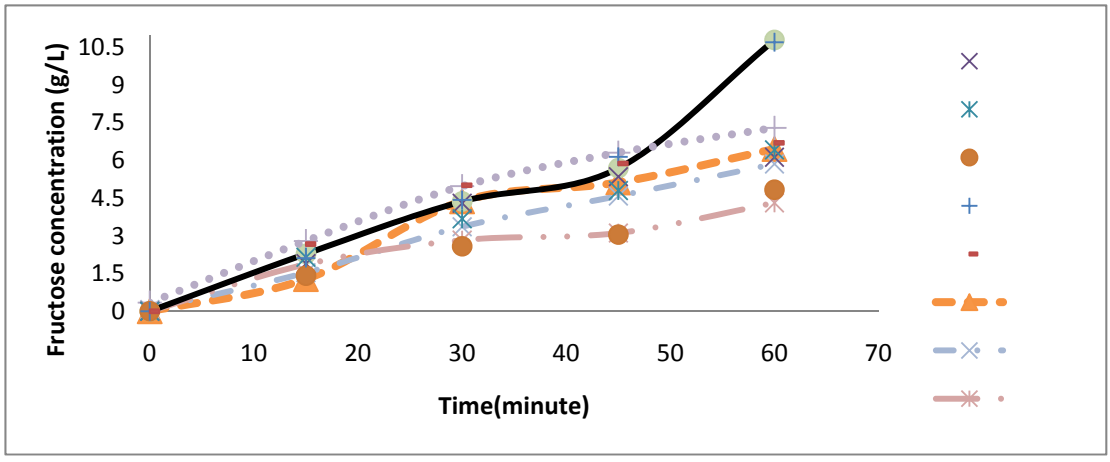

Figure 6. Experimental (filled circles) and performance of the ANN- soft sensor for the fructose concentration (lines) in the Batch Reactor (change of pH)

Table 3. Performance of Soft sensor in the Batch reactor with temperature effect

Temperature (^{0}C)	R^2	MSE
55	0.993	0.056
60	0.987	0.165
65	0.993	0.107
70	0.991	0.116

Table 4 Performance of Soft sensor in the Batch reactor with pH effect

pH	R^2	MSE
5	0.993	0.122
6	0.996	0.069
7	0.984	0.137
8	0.998	0.077
9	0.998	0.043
10	0.996	0.110

From Table 3 and 4, R^2 were greater than 0.95 and the values of MSE were less than 0.2, indicating a good fit of the ANN-soft sensor to the experimental data, accurate up to 95.7% for training and 100% for testing. From these criteria, it was concluded that the proposed ANN-soft sensor was the most precise in predicting fructose concentration.

4. Conclusion

ANN soft sensor was the most precise in predicting fructose concentration with R^2 were greater than 0.95 and the values of MSE were less than 0.2, indicating a good fit of the ANN-soft sensor to the experimental data. From these criteria, it concludes that the proposed ANN-soft sensor for on-line prediction is capable of achieving a satisfactory prediction performance. Based on the results of this study, artificial intelligence techniques of other different process are proposed using other types of reactor such as fluidized reactor for higher values of product and lower cost of operating should be studied. Beside that implementation of other control strategies such as model predictive control to the batch and continuous system should be introduced.

Acknowledgment

The research is funded by Universiti Kebangsaan Malaysia (UKM) (GGPM- 2012- 072) which are duly acknowledge by authors.

References

Acuna, G., Latrille, E., & Corrieu, G. (1995). Biomass estimation using neural networks and the extended kalman filter. *Preprints of the 6th Intern. Conf. Comp. Appl. Biotech. Germany* (p. 209).

Anantachar, M., Kumar, P. G. V., & Guruswamy, T. (2010). Neural network prediction of performance parameters of an inclined plate seed metering device and its reverse mapping for the determination of optimum design and operational parameters. *Comput. Electron. Agric., 72*(2), 87-98. http://dx.doi.org/10.1016/j.compag.2010.03.001

Basheer, I. A., & Hajmeer, M. (2000). Artificial neural networks: fundamentals, computing, design, and application. *Journal of Microbiological Methods, 43*, 3-31. http://dx.doi.org/10.1016/S0167-7012(00)00201-3

Bhosale, H. S., Rao, B. M., & Deshpande, V. V. (1996). Molecular and Industrial Aspects of Glucose Isomerase. *Microbiological Review, 60*(2), 280-300.

Boyaci, İ. H. (2005). A new approach for determination of enzyme kinetic constants using response surface methodology. *Biochemical Eng. J., 25*, 55-62. http://dx.doi.org/10.1016/j.bej.2005.04.001

Chen L. Z., Nguang, S. K., Chen, X. D., & Li, X. M. (2004). Soft sensors for on-line biomass measurements. *Bioprocess and Biosystems Engineering, 26*(3), 191-195. http://dx.doi.org/10.1007/s00449-004-0350-8

Chen, B. Z., & He, X. R. (1997). Neural networks intelligent system for the on-line optimization in chemical plants. *Chinese J. Chem. Eng., 5*(1), 57-62.

Chung, C. C., Chen, H., & Ting, C. H. (2010). Grey prediction fuzzy control for ph processes in the food industry. *J. Of Food Eng., 96*, 575-582. http://dx.doi.org/10.1016/j.jfoodeng.2009.09.004

Crabb, W. D., & Mitchinson, C. (1997). Enzymes involved in the processing of starch to sugars. *Tibtech., 15*, 349-352. http://dx.doi.org/10.1016/S0167-7799(97)01082-2

Crabb, W. D., & Shetty, J. K. (1999). Commodity Scale Production of sugars from starches. *Microbiology., 2*, 252-256.

Ferreira, L. S., Souza Jr., M. B., Trierweiler, J. O., Hitzmann, B., & Folly, R. O. M. (2003). Analysis of experimental biosensor/FIA biomeasurements. *Brazilian Journal of Chemical Engineering, 20*(1), 7-13. http://dx.doi.org/10.1590/S0104-66322003000100003

Geeraerd, A. H., Herremans, C. H., Cenens, C., & Van Impe, J. F. (1998). Application of artificial nueral networks as a non-linear modular modeling technique to describe bacteria growth in chilled food products. *International Journal of Food Microbiology, 44*, 49-68. http://dx.doi.org/10.1016/S0168-1605(98)00127-5

Gram, J., & Bang, De. M. (1990). An automated glucose isomerase reactor system with online flow injection analysers for monitoring of pH, glucose and fructose concentrations. *Chem.Eng. Sci., 45*, 1031-1042. http://dx.doi.org/10.1016/0009-2509(90)85023-7

Hajmeer, M. N., Basheer, I. A., & Najjar, Y. M. (1997). Computional neural networks for predictive microbiology II.Application to microbial growth. *International Journal of Food Microbiology, 34*, 51-66. http://dx.doi.org/10.1016/S0168-1605(96)01169-5

Jain, A. K., Mao, J., & Mohiuddin, K. M. (1996). Artificial neural networks: A tutorial. *Comput. IEEE* (pp. 31-44). March. http://dx.doi.org/10.1109/2.485891

Kadlec, P., Gabrys, B., & Strandt, S. (2009). Data- driven Soft sensors in the Process Industry. *Comput. and Chemical Eng., 33*, 795-814. http://dx.doi.org/10.1016/j.compchemeng.2008.12.012

Lammers, F., & Scheper, T. (1997). On-line monitoring of enzyme-catalyzed biotransformations with biosensors. *Enzyme and Microbial Technology., 20*, 432-436. http://dx.doi.org/10.1016/S0141-0229(96)00171-8

Latrille, E. (1997). Neural networks modelling and predictive control of yeast starter production in champagne. *In CD –ProcECC'97, European Control Conference '97.*

Lee, H. S., & Hong, J. (2000). Kinetic of glucose isomerization to fructose by immobilized glucose isomerase: Anomeric reactivity of D-glucose in kinetic model. *J. of Biotechnology., 84*, 145-153. http://dx.doi.org/10.1016/S0168-1656(00)00354-0

Lou, W., & Nakai, S. (2001). Application of artifical neural networks for predicting the thermal inactivation of bacteria: A combined effect of temperature, pH and water activity. *Food Research International, 34*(7), 573-579. http://dx.doi.org/10.1016/S0963-9969(01)00074-6

Luong, J. H. T., Bouvrette, P., & Male, K. B. (1997). Development and applications of biosensors for food analysis. *Trends Biotechnol., 15*, 369-377. http://dx.doi.org/10.1016/S0167-7799(97)01071-8

Mithra, S. (2011). *What is Glucose, 2003-2011 Conjecture Corporation*. Retrieved October 29, 2011, from http://www.wisegeek.com/what-is-glucose.htm

Molga, E., & Cherbanski, R. (2003). Catalytic reaction performed in the liquid-liquid system: Comparison of conventional and neural networks modelling methods. *Catalysis Today., 79-80*, 241-247. http://dx.doi.org/10.1016/S0920-5861(03)00011-7

Norliza, A. R., Hussain, M. A., Hasan, M., &Jahim, M. (2011). Mathematical modeling of fructose production by immobilised glucose isomerase as a function of temperature and pH variations. *African Journal of Biotechnology, 10*(14), 2766-2799.

Oh, G. S. (1995). Neural netwoks in estimation and control of antibody production using hybridoma cells in fed-batch cultures. *Preprints of the 6th Intern. Conf. Comp. Appl. Biotech. Germany* (p. 183).

Pfaff, M. (1995). Model-aided on-line glucose monitoring for computer-controlled high cell density fermentation. *Preprints of the 6th Intern. Conf. Comp. Appl. Biotech. Germany* (p. 6).

Rački, D. V., Pavlović, N., Čižmek, S., Dražić, M., & Husadžić, B. (1991). Development of reactor model for glucose isomerization catalyzed by whole-cell immobilized glucose isomerase. *Bioprocess Eng., 7*, 183-187. http://dx.doi.org/10.1007/BF00387415

Rivera, E. C., Atala, D. I. P., Filho, F. M., Costa, A. C., & Filho, R. M. (2010). Development of real-time state estimators for reaction-separation processes: A continuous flash fermentation a study case. *Chemical Eng. And Processing: Process Intensification, 49*, 402-409.

Rouzic, Y., & Le. (1997). Soft sensor for adaptive pH control, an industrial application. *Proc. European Control Conf. ECC'97* (p. 297).

Salehi, Z., Sohrabi, M., Kaghazchi, T., & Bonakdarpour, B. (2004). Application of down flow jet loop bioreactors in implementation and kinetic determination of solid-liquid enzyme rections. *Process Biochemistry., 40*(7), 2455-2460. http://dx.doi.org/10.1016/j.procbio.2004.09.027

Seborg, D. E., Edgar, T. F., & Mellichamp, D. A. (2004). *Process Dynamic and Control* (2nd ed.). USA: John Wiley & Son Inc.

Serra, J. M., Corma, A., Chica, A., Argente, E., & Botti, V. (2003). Can artifical neural networks help the experimentation in catalysis? *Catalysis Today, 81*, 393-403. http://dx.doi.org/10.1016/S0920-5861(03)00137-8

Sun, Y., Peng, Y., Chen, Y., & Shukla, A. J. (2003). Application of artificial neural networks in the design of controlled release drug delivery systems. *Advanced Drug Delivery Reviews, 55*, 1201-1215. http://dx.doi.org/10.1016/S0169-409X(03)00119-4

Thibault, J., Breusegemvan, V., & Cheruy, A. (1990). On-line prediction of fermentation variables using nerural networks. *Biotech. And Bioeng., 36*, 1041. http://dx.doi.org/10.1002/bit.260361009

Torrecilla, J. S., Otero, L., & Sanz, P. D. (2004). A neural network approach for thermal/pressure food processing. *Journal of Food Eng., 62*, 89-95. http://dx.doi.org/10.1016/S0260-8774(03)00174-2

Yang, S. H., Wang, X. Z., McGreavy, C., & Chen, Q. H. (1998). Soft sensor based predictive control of industrial fluid catalytic cracking processes. *Chem. Eng. Res. Des.-Trans. IChemE., 76*(4), 499-508. http://dx.doi.org/10.1205/026387698525126

Yuan, B., Wang, X. Z., & Morris, T. (2000). Software analyser design using data mining technology for toxicity prediction of aqueous effluents. *Waste Managment, 20*, 677-686. http://dx.doi.org/10.1016/S0956-053X(00)00045-3

Yu, H., Guo, Y., Wu, D., Zhan, W., & Lu, G. (2011). Immobilization of glucose isomerase onto GAMM support for isomerization ofglucose to fructose. *Journal of Molecular Catalysis B: Enzymatic, 72*(2011), 73-76. http://dx.doi.org/10.1016/j.molcatb.2011.05.006

Modern Applied Science; Vol. 8, No. 3; 2014
ISSN 1913-1844 E-ISSN 1913-1852
Published by Canadian Center of Science and Education

Bridge Assessment, Management and Life Cycle Analysis

Antonio Saviotti[1]

[1] U+P Consulting Engineers, Brescia, Italy

Correspondence: U+P Consulting Engineers, Via Ferrini 30, Brescia, Italy. E-mail: lar_consulting@libero.it

Received: February 14, 2014 Accepted: March 17, 2014 Online Published: April 30, 2014

doi:10.5539/mas.v8n3p167 URL: http://dx.doi.org/10.5539/mas.v8n3p167

Abstract

Existing bridges represents strategic components of infrastructural nets, actually matching with an increasing traffic flow. Despite their increasing age, and even if subjected to an increasing heavy traffic, these nets stands generally in a good structural health. At the same time, prolonged out of service due to structural problems are rare. Nevertheless, it is important to highlight the major causes of degradation reported in bridges, to achieve an adequate maintenance and design. In particular, the design stage should be aware that new structures should ensure growing capacity and structural performance along its lifetime. Bridge assessment help in this way: it is a relatively recent bridge engineering science growing faster, as the amount of resources needed for the complete repair of existing bridges is absolutely impossibile to be retrieved for the managing authorities. It is a scientific based and technical procedure, mainly not coded, aiming at producing evidences on the bridge health, of the structural reliability, and of the suggested procedure to prolong its life. The purpose of this study, is to provide a review of recent studies and research accomplishments in the field of bridge assessment, management and life cycle analysis.

Keywords: bridge, structural analysis, seismic assessment, fatigue and fracture, retrofit and rehabilitation

1. Introduction

The American Society of Civil Engineers (ASCE 2009) has recently highlited that more than 26% of the existing bridges in US are structurally deficient or is characterized by obsolescence in functionality. A total investment of one thousand billion dollars (ASCE 2009) has been estimated to be necessary only in the next five years to cover these deficiencies only in US. These costs, will certainly increase in the near future, and are mainly covered by public income, so there is a need to manage as well this problem, as at the same time the socio-economical growth of nations is strictly related with the functionality of its infrastructural system. Among infrastructural systems, transport infrastructures cover a large part of the lifeline system, able to connect cities, regions and nations. It is a preliminary need of every state to provide adequate infrastructures, reliable, functional, updated, safe. The approach to manage such an amount of bridges should be as much scientific as it is possible.

2. Assessment Procedures of Existing Bridges

The assessment of an existing bridge aims at producing evidence to demonstrate it will function safely over a specified residual service life, taking into account a specific code reference. It is mainly based on the results of assessing hazards and load effects to be anticipated in the future, and of assessing material properties, the geometry and the structural state of the bridge. Guidelines for assessment of existing structures have been developed in many countries; however, the occurrence of bridge assessment guidelines coming from codes or standards is rare. More frequently, such guidelines are prepared at a detailed level by scientific groups or research organisations. Whatever the source, the first issue deals with fixing risk acceptance criteria, which is quite difficult since it must be compatible to the code for new structures (limit state analysis, safety factor format, etc.). The second issue deals with the process of the assessment procedure, which is commonly separated in phases, starting from preliminary evaluation, through to detailed investigation, expert and finally advanced assessment, depending on the structural condition of the investigated structure (Pipinato, 2010a). A four phases assessment procedure is presented in the following (Pipinato, 2014).

2.1 First Level: Preliminary Evaluation

The preliminary evaluation is the first level of investigation aiming at removing existing doubts about the safety of existing structures, adopting fairly simple methods and identifying critical parts or members in the structure. In order to identify critical members, it is necessary to carry out an intensive study of the available original

design documents, along with a visual inspection of the structure and a photographic survey. The inspection procedure is often coded by infrastructural agencies manuals and procedures; however, at least the following points must be checked:

- The bridge construction is conforming to the original drawings and/or differences between as-built and drawings.
- Bridge modification during service (rehabilitation, strengthening, changes in the static system, etc.).
- Presence of any visual evidence of degradation (damaged expansion joints, supports, corrosion, cracks, vibration or loose rivets, collision, lack of structural members etc.).

Moreover, if available, inspection and maintenance reports can be used, and reference should be made to the evaluation report. The preliminary evaluation should include codes and recommendations analysis procedure where available, and conservative assumptions where information is lacking or doubtful. In this way, critical construction details can be identified.

2.2 Second Level: Detailed Investigation

The aim of the detailed investigation is to update the information obtained in other analysis by carrying out a refined assessment, especially for those members for which adequate safety was not confirmed by preliminary evaluation. At this stage a specialised consultant should assist. In this phase a FEM numeric model of the entire structure is developed. Based on the current code provisions, the structure should be recalculated and verification tables should report whether the structural members are safe or not. Concerning specific issues, such as the fatigue and seismic behaviour of the bridge, detailed code provisions should be referred to. From this step-level investigation, non-destructive testing (NDT) could be used in order to characterise the basic material properties of the structure. The final report of the investigation should establish whether the structure is verified against specific issues and has sufficient static strength against actual loadings.

2.3 Third Level: Expert Investigation

In case of key structures that have major consequences in terms of risks or costs related to a decision, a team of experts is needed in order to carefully check the conclusions and proposals reached in the last phase. Discussions and further assessments using specific tools can also be carried out to help reach decisions. At this level, on-site testing could be adopted in order to provide the dynamic identification of the structure, as reported in the following example.

2.4 Fourth Level: Advanced Testing

This advanced level of investigation should be reserved for recurrent bridges along infrastructural nets, in which a rational procedure of analysis and intervention could help in determining if retrofitting interventions could be adopted, or if rational dismantling large scale operations are required. The procedure is based on a detailed survey of the existing bridge, a FEM analysis, a code verification procedure, NDT diffused sampling, and, based on these data on real scale testing of one case study structure, aims to determine the global static and cyclic behaviour of the bridge. In specific cases, on-site dynamic identification could be performed. Concerning the fatigue assessment, in this case a LEFM (linear elastic fracture mechanics) investigation is required. Concerning seismic analysis, non-linear analysis is required. Specific material testing analysis should be performed dealing with the case analysed. The advanced testing result should report on the various analysis performed, and should clearly state verification results indicating the specific retrofit needed for recurrent interventions. An advanced testing operation is reported in the following section, dealing with a recurrent existing bridge type in service along the railway lines.

2.5 Literature Review on Bridge Assessment

A wide amount on studies on the specific issue of bridge assessment could be found in literature, however, only some of these studies are strictly related to useful procedures aiming at producing evidences that a bridge should be retrofitted, as a result of a scientific and practical at the same time procedures. The general procedure is reported in a study dealing with the assessment of existing bridges, considering safety and security issues (Pipinato, 2011). Among specific studies, the applications of B-WIM (bridge-weight in motion) technology to bridge assessment (Znidaric, 2010) relates to a useful procedure of investigation using WIM approach; the use of B-WIM data for bridge assessment is described in Petschacher (2011); the bridge assessment and health monitoring with distributed long-gauge FBG sensors (fiber Bragg grating) and detailed investigations using HM (health managment) procedures could be found in Chunfeng et al. (2013); recommendations for dynamic allowance in bridge assessment are well described in O'Brien et al. (2010); concerning the FEM approach on the

assessment of existing bridges, the role of finite element analysis in bridge assessment and design could be found in Cakebread (2010), and similarly, the benefits and use of FE modelling in bridge assessment and design could be found in Icke (2012); going on with the multiple reference impact testing for bridge assessment with drop hammer (Liao et al., 2013), which contains a more practical approcach to the assessment of existing bridges; the reliability-based bridge assessment using enhanced Monte Carlo to simulate extreme traffic loading by Enright et al. (2013) is more focused on theoretical applications, that are useful in case that the loads distribution in the past is not available or with difficult could be assessed; at the same level, concering SHM (structural health monitoring tecnicques), the deployment of a dense hybrid wireless sensing system for bridge assessment is accurately described in Gangone et al. (2011), and similarly the assessment of structural health condition through static and dynamic monitoring is reported in Sigurdardottir et al. (2011). Concerning the specific matter of metal bridges, the structural analysis and assessment tecniques of historical metal bridges has been described in Pipinato et al. (2010a); moreover, the residual service life of existing railway bridges and structural analysis and the fatigue reliability assessment of the Paderno bridge is highlighted respectively in Pipinato et al. (2010b) and Pipinato and Modena (2010); and an advanced application Is reported in Pipinato et al. (2012a). If a specific step level procedure for remaining fatigue life evaluation of one railway bridge is of interest, an introductive study is in Pipinato (2010a), while an application is reported in Pipinato (2010b). Finally it is of interest to cite methods for determining differences of attribute weight between evidences in bridge assessment, accounted for in Li et al. (2013), and similarly, an improved one-dimensional optimization algorithm in non-probabilistic reliability investigation and its application in bridge assessment is reported in Chen and Fan (2011).

3. Bridge Managment

Probably one of the most significant applications of contemporary BMSs (bridge management systems) could be found in the US. In 1991, the Intermodal Surface Transportation Efficiency Act (ISTEA) required all states to develop, establish and implement a BMS by October 1998. The ISTEA requirements, first distributed in 1991, stated that the BMS must be implemented on all state and local bridges. New Federal legislation, however, required implementation of BMS only for bridges on the National Highway System (NHS); therefore, use of BMS inspection for non-NHS bridges was optional (Sunley, 1995). The principle BMS used in the US is PONTIS (the acronym), developed in the early 1990s for the Federal Highway Administration (FHWA) and became an American Association of State Highway and Transportation Officials (AASHTO) product in 1994. It performs functions such as recording bridge inventory and inspection data, simulating condition and suggesting actions, developing preservation policy and developing an overall bridge program. The system allows representation of a bridge as a set of structural elements, with each element reported based on its condition. In 2002, 46 agencies throughout the nation had PONTIS licensing, and each State Highway Administration (SHA) could customize the system according to its needs (Robert et al., 2003). BRIDGIT was developed in 1985 by the National Cooperative Highway Research Program (NCHRP) and the National Engineering Technology Cooperation in an attempt to improve bridge management networks. This system has capabilities similar to the PONTIS system. There have been many research projects throughout the nation on which local agencies have worked with universities to develop their own BMS. Other BMSs developed by individual state agencies do have good specific functions and qualities, but they lack features that can satisfy all the demands of effective bridge management and maintenance procedures on a national scale. Other notable research and development efforts on BMSs took place in Iowa, Washington, Connecticut, Texas and South Carolina (Czepiel, 1995). Among recent European experience that we should remember is the TISBO (the acronym) Infrastructure Maintenance Management System, currently being developed by The Netherlands Ministry of Transportation, Public Works and Water Management. It is a system that integrates inspection registration and maintenance management. Concerning the Italian current situation regarding BMSs, owner agencies usually manage their network with self-developed codes/procedures. The policy of the main Italian agencies is briefly presented in the following: Rete Ferroviaria Italiana (RFI), is the National agency for the whole Italian railway network, consisting of about 16,000 km. The BMS is based on periodical visual inspections supported by special testing trains. All data are elaborated with specific software developed by the agency with the aim of defining economical and technical convenience of possible maintenance/rehabilitation/ strengthening interventions. Autostrade per l'Italia is the most relevant highway agency in Italy and manages a network of about 3400 km. The BMS is based on the SAMOA programme for surveillance, auscultation and maintenance of structures. ANAS (1997) is the Italian agency for roads having national interest and manages a network of about 26,700 km. The BMS is based on the 'National Road Inventory' and in-situ survey and is a web-based management application that is developed by the agency and updated regularly. Also in Japan a wide amount of experience could be cited in the framework of bridge management system, as in Yokohama et al. (2006), where the development of bridge management system for expressway bridges in Japan is described; or in Soma (2006) where the development and implementation of

bridge management system in aomori prefectural government is delineated.

3.1 Literature Review on Bridge Managment

The specific matter of bridge management is not already deepen with a practical and useful way in the current literature. For this reason, in the following are reported some relevant studies related to the argument, that could help in understanding the basic and more scientifical advanced research on the matter. An introductive study on the bridge information modeling in sustainable bridge management could be found in Marzouk (2011); concerning the specific argument of railway, the network rail's bridge asset management could be found in Griffin and Patro (2013); while a more complicated approach is deepen in the description of deformation predication and management of large bridge based on radial basis function neural network by Linya et al. (2010). An accurate description of the the life-cycle information management practice of Shanghai Yangtze River Tunnel and Bridge Project is in Tian et al. (2012); while delaing with an approach considering bridge management and GIS instruments, the study dealing with management information system of road and bridge infrastructure based on ArcGIS engine (Xiaofang et al., 2012) is very interesting. A relative contemporary problem is faced in the study of the analysis and design of urban bridge safety early-warning management system by Rong et al. (2010) generally approaching the problematic of early warning systems, while a more focused article consider an integrated system for bridge management using probabilistic and mechanistic deterioration models, with specific application to bridge decks by Morcous et al. (2010); the scheduled maintenance and management actions, considering the residual life evaluation of railway infrastructures is described in Pipinato et al. (2008), while in Pellegrino et al. (2011b) a simplified management procedure for bridge network maintenance is deepen and applied; if a more deep approach on the risk modelling is requested, the advanced deterioration in bridge management systems by Thompson et al. (2013) should be of interest; while a very useful and interesting application of the integration of SHM into bridge management systems, with a case study, is presented in Figueiredo et al. (2011). As a fact, the economical aspects involving bridge management are increasingly important, so a stakeholder probability-based optimization approach for cost-effective bridge management under financial constraints by Orcesi and Frangopol (2011) should be a necessary lecture for these types of problems; and if a more complicated tools is desired, the multiobjective optimization for project selection in network-level bridge management incorporating decision-maker's preference using the concept of holism (Qiang et al., 2013) is very useful.

Figure 1. I35 bridge, Minneapolis bridge collapse (2007)

4. Bridge Detrimental Factors

4.1 Fatigue and Fracture

Monotonically application of static loads in structural component may produce fracture and fail if the same load or even smaller is applied cyclically at a large number of times. For example a thin plate bent back and forth beyond yielding fails after a few cycles of such repeated bending: this is termed as the 'fatigue failure'. Examples of structures prone to fatigue failure, are bridges, cranes, offshore structures and slender towers, etc., which are subjected to cyclic loading. The fatigue failure is due to progressive propagation of flaws in steel under cyclic loading. This is partially enhanced by the stress concentration at the tip of such flaw or crack, as also recent collapse have evidenced (Figure 1). The presence of a hole in a plate or simply the presence of a notch in the plate creates stress concentrations. The stress at these points could be three or more times the average applied stress. These stress concentrations may occur in the material due to some discontinuities in the material itself and are not serious when a ductile material like steel is subjected to a static load, as the stresses redistribute themselves to other adjacent elements within the structure. At the time of static failure, the average stress across the entire cross section would be the yield stress; however when the load is repeatedly applied or the load fluctuates between tension and compression, the hot spot points experience a higher range of stress reversal than the applied average stress. These fluctuations involving higher stress ranges, cause minute cracks at these points, which open up progressively and spread with each application of the cyclic load and ultimately lead to rupture. The fatigue failure occurs after four different stages, namely: crack initiation at points of stress concentration; crack growth; crack propagation; final rupture. Fatigue failure can be defined as the number of cycles and hence time taken to reach a pre-defined or a threshold failure criterion. Fatigue failures are classified into two categories namely the high cycle and low cycle fatigue failures, depending upon the number of cycles necessary to create rupture. Low cycle fatigue could be classified as the failures occurring in few cycles to a few tens of thousands of cycles, normally under high stress/ strain ranges. High cycle fatigue requires about several millions of cycles to initiate a failure. However this distinction is not strictly defined. The common form of presentation of fatigue data is by using the S-N curve, where the total cyclic stress (S) is plotted against the number of cycles to failure (N) in logarithmic scale. Typical S-N curve are shown in codes and standards. It could be seen that the fatigue life reduces with respect to increase in stress range and at a limiting value of stress, the curve flattens off. The point at which the S-N curve flattens off is commonly called the 'endurance limit'. To carry out fatigue life predictions, a linear fatigue damage model is used in conjunction with the relevant S-N curve. One such fatigue damage model is that postulated by Wohler. It becomes very important to avoid any local structural discontinuities and notches by good design and this is the most effective means of increasing fatigue life.

4.1.1 Literature Review

The fatigue argument is more related to bridge specialists, increasingly in the last years, as weight control in new bridges is becoming of importance to reduce the use of material, and to accelerate bridge construction. The Modelling and fatigue life assessment of orthotropic bridge deck details using FEM is deepen in Mustafa et al. (2012); while, the integrating reliability and structural health monitoring in the fatigue assessment of concrete bridge decks is studied in Newhook and Edalatmanesh (2013); the Fatigue assessment of a composite railway bridge for high speed trains is reported in Liu (2013) for the analysis of conditions for which a dynamic analysis is needed, while in Zhou et al. (2013) it could be found the modeling and fatigue critical details; if considering at the same time the monitoring option, the fatigue reliability assessment for bridge welded details using long-term monitoring data (by Deng Yang et al., 2011) is very useful; while the fatigue assessment of orthotropic steel bridge deck based on hot spot stress method by Qianhui et al. (2013) is of interest; a general approach to consider the Fatigue assessment and strengthening measures to upgrade a steel railway bridge is in Stamatopoulos (2013); while, the evaluation of fatigue strength of one riveted historical railway bridge (Pipinato et al., 2008b) is of interest for historical construction, as the high-cycle fatigue behavior of riveted connections for railway metal bridges (Pipinato et al., 2009, 2011c, 2014) where also full scale investigations are reported; the bridge fatigue reliability assessment using probability density functions of equivalent stress range based on field monitoring data (Kwon & Frangopol, 2010) is a very useful study for expert of the matter; while for a more mechanical engineering based study, the crack water interaction and fatigue life assessment of reinforced concrete bridge decks is of interest (Maekawa & Fujiyama, 2013), as the fracture mechanics approach as an improvement of fatigue life assessment in orthotropic bridge decks, by Nagy et al. (2013), or the fatigue damage assessment of steel bridge members using paint cracking (Okumura et al., 2010); a specific view on the fatigue damage estimation in existing railway steel bridges by detailed loading history analysis could be of interest for railway engineers (Pipinato et al., 2012e), and alsoconsidering fatigue/corrosion issues (Pipinato, 2012a, b), or

FRP strengthening (Pipinato et al., 2012d); the Fatigue reliability assessment of steel bridge details integrating weigh-in-motion data and probabilistic finite element analysis is described in Guo (2012), while the fatigue crack assessment of asphalt concrete pavement on a single span highway bridge subjected to a moving truck is introduced in Youngguk et al. (2012), and the Bridge fatigue reliability assessment using probability density functions of equivalent stress range based on field monitoring data in Kwon and Frangopol (2010). Concerning new constructions, the influence of fatigue on cable arrangement in cable-stayed bridges could be finally found in Pipinato et al. (2012b), or as the structural analysis of the cantilever construction process in cable-stayed bridges found in Pipinato et al. (2012c); and if the moving load and fatigue analysis of a long span high speed railway bridge or the moving loads bridge response, considering the structural analysis and eurocode provisions are investigated, a good reference should be found in Pipinato (2013b, c).

4.2 Seismic Issues

As observed by Albon (1988) "bridges should be designed to absorb seismic forces without collapse to ensure that main arterial routes remain open after major seismic events. This helps the movement of aid and rescue services in the first instance and underpins the ability of the local community to recover in the long term". The following are the primary causes of the bridge seismic damage:

a) effects of site conditions: the significant impact that local site conditions have on amplifying strong ground motion, and the subsequent increased vulnerability of bridges on soft soil sites; furthermore, in some specific sites sites liquefaction and lateral spreading could enable permanent substructure deformations and loss of superstructure support;

b) correlation of damage with construction era: an excellent example of the effect of construction era is provided by observing the relative performances of bridges on Routes 3 (built in 1965) and 5 (built in 1990) of the Hanshin Expressway in Kobe, as in the first damages were catastrofics, while in the latter only concentrated damage were found; this is principally related to the new design method and awareness of the potential damage of eartquakes on infrastructures in critical zones; moreover, the use of benchmark years as a crude but effective method for rapidly assessing the likely performance of bridge construction;

c) design or construction changes: both changes are potentially very dangerous, as they could greatly affect its seismic performance; the first being a cause coming for the deterioration of the structure during the service life, while the latter due to construction modifications, not checked for the earthquake design requirements;

d) irregularities of the bridge: excessive deformation demands occuring in a few brittle elements, or the complex structural configuration, or a bridge lacks of redundancy could negatively influence the structural performance of a bridge during the seismic event;

e) unseating: expansion joints introduce a structural irregularity that can have catastrophic consequences;

f) special situations: these occurs for specific structures, as for skewed bridges (in which a rotation of the deck about a vertical axis could led to the collapse of the superstructure), curved bridges (for the asymmetrical response similar to that of skewed bridges);

g) superstructure: the most common form of damage to superstructures is due to pounding of adjacent segments at the expansion hinges; in particular, for steel girder, buckling of cross braces beneath the roadway could be found;

h) damage to bearings: in steel superstructures, the bearings commonly consist of steel components designed to provide restraint in one or more directions and, in some cases, to permit movement in one or more directions; failure of these bearings in an earthquake can cause redistribution of internal forces, which may overload specific structural members;

i) damage to substructures: also in older bridges, columns tend to be weaker than the beam–diaphragm–slab assembly to which they connect. Consequently, columns can be subjected to large inelastic demands during strong earthquakes; this is often the primary cause of the whole structure collapse.

The risk associated to the seismic vulnerability of bridges and infrastructure in general is a relevant issue to guarantee standard safety and security of citizens in everyday life and moreover in the case of disaster. The example of this risk has been evidenced in Italy, where tragic events have kicked the nation also recently (Aquila, 2009; Emilia, 2012), and in the past -in the second half of the 20th century (Friuli, 1976; Irpinia, 1980)- even if the transportation infrastructure has not suffered significantly. In the Apennine mountains crossing of the A16

highway the bridges did undergo some damage, mainly due to the inadequacy of the bearing devices, but this was promptly remedied by the owner through the systematic adoption of the seismic isolation. The delay in the appreciation of the risk is not exclusive to Italy, but also in US, the Federal Highway Administration (FHWA) published a first document titled "Retrofitting guidelines for Highway Bridges" some years after (FHWA-ATC, 1983) the San Fernando (1971) earthquake. Still, in 1989, despite of the large retrofit program developed, the Loma Prieta earthquake exposed substantial deficiencies in bridges in California (Pinto et al., 2011). Although, a relevant amount of bridges and viaduct, of medium and large span are present in the national infrastructural system (Figure, 1-2). The situation as briefly outlined above is sufficient to understand that the state of the art on seismic assessment and retrofit of bridges still needs to be advanced in several areas. The areas considered to be of priority interest were assessment methods, retrofit criteria and intervention techniques. Although, a relevant amount of work on existing bridge network has been performed in the past, a comprehensive overview of recent studies should help in the identification of the state of knowledge of the matter.

Figure 2. I5 bridge, Gavin Canion (1994)

Figure 3. Hanshin Expressway elevated road, Japan (1995)

4.2.1 Literature Review

The seismic hazard, and the inherent difficulties of upgrading existing bridges to current structural standards, is not a very interesting matter for the whole engineering world, as this specific problem is not relevant for all nations. However, the tragedy of the past, highlighted that research and studies are needed expecially in those countries where this is really a structural and safety problem (Figures 3 and 4). The literature is very rich of studies and research on the matter, as hidden nations have invested a wide amount of money to bridge the gap on not known seismic resistant solutions. The recent main relevant studies are enclosed in Aman et al. (2010) dealing with the seismic assessment of an existing non-seismically designed major bridge-abutment-foundation system, in (Nguyen et al., 2008) where a system modeling for seismic performance assessment and evaluation of reinforced concrete bridge columns is described, or in Taner and Caner (2012) where the target damage level assessment for seismic performance evaluation of two-column reinforced concrete bridge bents, or in Lau et al. (2012), where the fragility relationships for probabilistic performance-based seismic risk assessment of bridge inventories is explained, and finally in Ghosh and Padgett (2010) where the probabilistic seismic loss assessment of aging bridges using a component-level cost estimation approach is presented; specific applications for the seismic risk assessment for highway bridge system (by Chen et al., 2013), or concerning geotechnical probabilistic aspects (Bradley et al., 2010) and geotechnical applications (Thavaraj et al., 2012; Bayram et al., 2013) are useful for the completeness of the approach; if particular bridge geometrical shape are present, specific studies should be addressed: for e.g. curved bridges (Junwon & Linzell, 2012), long span structures (Wen et al., 2013), hollow columns (Kim et al., 2012), cable stayed (Pipinato, 2012c), viaducts (Pipinato, 2011a, 2012b), existing bridges (Pipinato, 2012d), or bridge networks (Pipinato, 2013a). However, one of the most interesting chapter of this argument, deals with bridge isolation, as well illustrated in the Seismic assessment of bridge structures isolated by a shape memory alloy/rubber-based isolation system by Ozbulut and Hurlebaus (2011). According to the financial needs cited before, the study of the Performance-based Seismic Financial Risk Assessment for Bridge Structure by Zhang et al. (2011) is a reasonable approach to the matter. Other specific and relevant studies, involves for instance the Regional seismic risk assessment of bridge network (by Padgett et al., 2010), the nonlinear seismic assessment for the post-repair response of RC bridge piers by Do Hyung Lee et al. (2011), the analysis of seismic risk probability assessment of lower-tower cable-stayed bridge based on LHS-MC method (Yin et al., 2013), the performance Assessment of a Highway Bridge Structure Employing Adaptive Negative Stiffness for Seismic Protection (Attary et al., 2013), and inally as a comprehensive case study, the Probabilistic perforcemance-based seismic risk assessment of a bridge network should be cited (Waller & Lau, 2010). The severe seismic hazard risk and recent events in Japan are related to a high level research and studies production: for e.g. in Zhang et al. (2013) the seismic damage of retrofitted highway bridges in the 2011 great east japan earthquake is described; Hisaya et al. (2012) describe the maintenance planning of deteriorating highway bridges with seismic risk; Iida et al. (2012) discussed the seismic performance evaluations of bridge-pier systems with uncertainty; Ge et al. (2012) presented a relevant study on the demand on stiffened steel shear panel dampers in a rigid-framed bridge pier under repeated seismic ground motions; Nogami et al. (2013) discussed on the seismic design of RC bridge piers to ensure the post-disaster functionality of road network.

5. Conclusion

In this study, a wide amount of very recent research have been reported on the general matter of bridge assessment, management and life cycle analysis. As existing bridges represents a strategic components of infrastructural nets, an accurate study of their remaining life basing on evidences is more often required. Matching with an increasing traffic flow, despite their increasing age, and even if subjected to an increasing heavy traffic, these nets stands generally in a good structural health, as prolonged out of service due to structural problems are rare. Nevertheless, it is important to highlight the major causes of degradation reported in bridges, so that to achieve an adequate maintenance and a design stage aware that new structures should ensure - during the lifetime - growing capacity and structural performance. At the same time it is crucial to understand how much work is undergoing in the specific matter of bridge assessment, a relatively recent bridge engineering science that is growing faster, because the whole amount of resources needed for the complete repair of existing bridges is absolutely impossibile to be retrieved for the owner or managing public authorities. Bridge assessment is in this case a scientific based and technical procedure, mainly not coded, aiming at producing evidences on the bridge health, of the structural reliability, and of the suggested procedure to prolong its life. According to this framework, this study, has provided a review of recent studies and research accomplishments in the field of bridge assessment, management and life cycle analysis, highlighting that there is a need to focus these studies on relevant problems.

References

ANAS. (1997). Material and techniques of intervention for the restoration of the concretes of the bridges and viaducts (in Italian). Rome, Italy: Gangemi Ed.

ASCE. (2009). Report Card 2009 Grades. *Asce web-site*.

Attary, N., Symans, M., Nagarajaiah, S., Reinhorn, A. M., Constantinou, M. C., Taylor, D., & Pasala, D. T. R. (2013). Performance Assessment of a Highway Bridge Structure Employing Adaptive Negative Stiffness for Seismic Protection. *Proceedings of the Structures Congress 2013* (pp. 1736-46). http://dx.doi.org/10.1061/9780784412848.152

Aygül, M., Almrani, M., & Urushadze, S. (2012). Modelling and fatigue life assessment of orthotropic bridge deck details using FEM. *International Journal of Fatigue, 40*, 129-142. http://dx.doi.org/10.1016/j.ijfatigue.2011.12.015

Aygün, B., Dueas-Osorio, L., & Padgett, J. E. (2011). Efficient longitudinal seismic fragility assessment of a multispan continuous steel bridge on liquefiable soils. *Desroches, Reginald Source: Journal of Bridge Engineering, 16*(1), 93-107. http://dx.doi.org/10.1061/(ASCE)BE.1943-5592.0000131

Bradley, B. A., Cubrinovski, M., Dhakal, R. P., & MacRae, G. A. (2010). *Probabilistic seismic performance and loss assessment of a bridge-foundation-soil system.* Soil-Foundation-Structure Interaction - Selected Papers from the International Workshop on Soil-Foundation-Structure Interaction, SFSI 09 (pp. 221-228).

Bradley, B. A., Cubrinovski, M., Dhakal, R. P., & MacRae, G. A. (2010). Probabilistic seismic performance and loss assessment of a bridge-foundation-soil system. *Soil Dynamics and Earthquake Engineering, 30*(5), 395-411. http://dx.doi.org/10.1016/j.soildyn.2009.12.012

Cakebread, T. (2010). *The role of finite element analysis in bridge assessment and design.* Bridge Maintenance, Safety, Management and Life-Cycle Optimization - *Proceedings of the 5th International Conference on Bridge Maintenance, Safety and Management* (pp. 2433-2439), 2010.

Chen, L., Zhang, J., & Zhuo, W. (2013). Seismic risk assessment for highway bridge system in the Wenchuan region. *Tumu Gongcheng Xuebao/China Civil Engineering Journal, 46*(SUPPL. 2), 242-248.

Chen, X. Y., & Fan, J. P. (2011). An improved one-dimensional optimization algorithm in non-probabilistic reliability investigation and its application in bridge assessment. *Gongcheng Lixue/Engineering Mechanics, 28*(5), 21-25, 30.

Chunfeng W., Wan H., Jianxun L., Zhishen W., Zhaodong X., & Shu L. (2013). Bridge Assessment and Health Monitoring with Distributed Long-Gauge FBG Sensors. *International Journal of Distributed Sensor Networks,* 494260, 2013.

Czepiel, E. (1995). *Bridge management systems literature review and search*. Technical report no. 11, Northwestern University BIRL Industrial Research Laboratory, Evanston, IN, USA.

Deng Y., Ding Y., Li A., & Zhou G. D. (2011). Fatigue reliability assessment for bridge welded details using long-term monitoring data. *Science in China Series E: Technological Sciences, 54*(12), 3371-3381. http://dx.doi.org/10.1007/s11431-011-4526-6

Do, H. L., Joonam P., Kihak, L., & Byeong, H. K. (2011). Nonlinear seismic assessment for the post-repair response of RC bridge piers. *Composites Part B: Engineering, 42*(5), 1318-1329. http://dx.doi.org/10.1016/j.compositesb.2010.12.023

Enright, B., Hajializadeh, D., & Obrien, E. J. (2013). Reliability-based bridge assessment using enhanced Monte Carlo to simulate extreme traffic loading. Safety, Reliability, Risk and Life-Cycle Performance of Structures and Infrastructures - *Proceedings of the 11th International Conference on Structural Safety and Reliability, ICOSSAR* 2013 (pp. 3703-3708).

Figueiredo, E., Radu, L., Park, G., & Farrar, C. (2011). Integration of SHM into bridge management systems: Case study-Z24 bridge. Structural Health Monitoring 2011: Condition-Based Maintenance and Intelligent Structures - *Proceedings of the 8th International Workshop on Structural Health Monitoring, vol. 1*, (pp. 725-732).

Gangone, M. V., Whelan, M. J., & Janoyan, K. D. (2011). Deployment of a dense hybrid wireless sensing system for bridge assessment. *Structure and Infrastructure Engineering, 7*(5), 369-378. http://dx.doi.org/10.1080/15732470802670842

Ghosh, J., & Padgett, J. E. (2011). Probabilistic seismic loss assessment of aging bridges using a component-level cost estimation approach. *Earthquake Engineering and Structural Dynamics, 40*(15), 1743-1761. http://dx.doi.org/10.1002/eqe.1114

Griffin, M., & Patro, S. (2013). Shaping Network Rail's bridge asset management. *IET & IAM Asset Management Conference 2013* (p. 104). http://dx.doi.org/10.1049/cp.2013.1924

Gu, Y., Zheng, W. T., & Zhuo, W. D. (2013). Analysis of seismic risk probability assessment of lower-tower cable-stayed bridge based on LHS-MC method. *Gongcheng Lixue/Engineering Mechanics, 30*(8), 96-102.

Hisaya, F., Tanaka, S., Furuta, H., & Dogaki, M. (2012). Maintenance planning of deteriorating highway bridges with seismic risk. *Zairyo/Journal of the Society of Materials Science, Japan, 61*(2), 133-140.

Iida T., Lim D., & Kawano K. (2012). Seismic performance evaluations of bridge-pier systems with uncertainty. Bridge Maintenance, Safety, Management, Resilience and Sustainability - *Proceedings of the Sixth International Conference on Bridge Maintenance, Safety and Management* (pp. 2517-2524), Bridge Maintenance, Safety, Management, Resilience and Sustainability - *Proceedings of the Sixth International Conference on Bridge Maintenance, Safety and Management*.

Icke, P., & Margheriti, C. (2012). *The benefits and use of FE modelling in bridge assessment and design*. Bridge Maintenance, Safety, Management, Resilience and Sustainability - *Proceedings of the Sixth International Conference on Bridge Maintenance, Safety and Management* (pp. 3191-3197).

Jin, Q. W., Wang, T. N., Sun, Y. L., & Hu, Z. T. (2013). Seismic performance assessment of long span continuous rigid bridge. *Applied Mechanics and Materials, 353*, 2033-2038. http://dx.doi.org/10.4028/www.scientific.net/AMM.353-356.2033

Kihyon, K., & Frangopol, D. M. (2010). Bridge fatigue reliability assessment using probability density functions of equivalent stress range based on field monitoring data. *International Journal of Fatigue, 32*(8), 1221-32. http://dx.doi.org/10.1016/j.ijfatigue.2010.01.002

Kim, T. H., Seong, D. J., & Shin, H. M. (2012). Seismic Performance Assessment of Hollow Reinforced Concrete and Prestressed Concrete Bridge Columns. *International Journal of Concrete Structures and Materials, 6*(3), 165-176. http://dx.doi.org/10.1007/s40069-012-0015-y

Kwon, K., & Frangopol, Dan M. (2010). Bridge fatigue reliability assessment using probability density functions of equivalent stress range based on field monitoring data. *International Journal of Fatigue, 32*(8), 1221-1232. http://dx.doi.org/10.1016/j.ijfatigue.2010.01.002

Lau, D. T., Waller, C. L., Vishnukanthan, K., & Sivathayalan, S. (2012). Fragility relationships for probabilistic performance-based seismic risk assessment of bridge inventories. *Proceedings, Annual Conference - Canadian Society for Civil Engineering* (vol. 4, pp. 2765-2774) 2012, Annual Conference of the Canadian Society for Civil Engineering 2012: Leadership in Sustainable Infrastructure, CSCE 2012.

Li, X. F., Ding, S. C., & Wang, X. M. (2013). Methods for determining differences of attribute weight between evidences in bridge assessment. *Advanced Materials Research, 760*, 2172-2176. http://dx.doi.org/10.4028/www.scientific.net/AMR.760-762.2172

Liao, Y., Zhou, Y., & Qin, P. (2013). Multiple reference impact testing for bridge assessment with drop hammer. *Source: Advanced Materials Research, 605*, 718-772.

Linya T., Xiaotao Y., & Hui Z. (2010). Deformation predication and management of large bridge based on radial basis function neural network. *2010 International Conference on Management and Service Science (MASS 2010)* (p. 4).

Liu, K., Zhou, H., Shi, G., Wang, Y. Q., Shi, Y. J., & De Roeck, G. (2013). Fatigue assessment of a composite railway bridge for high speed trains. Part II: conditions for which a dynamic analysis is needed. *Journal of Constructional Steel Research, 82*, 246-254. http://dx.doi.org/10.1016/j.jcsr.2012.11.014

Maekawa, K., & Fujiyama, C. (2013). Crack Water Interaction and Fatigue Life Assessment of RC Bridge Decks. *Poromechanics V. Proceedings of the Fifth Biot Conference on Poromechanics* (pp. 2280-9). http://dx.doi.org/10.1061/9780784412992.267

Marzouk, M. M., & Hisham, M. (2011). Bridge information modeling in sustainable bridge management. ICSDC 2011: Integrating Sustainability Practices in the Construction Industry - *Proceedings of the International Conference on Sustainable Design and Construction 2011* (pp. 457-466).

Morcous, G., Lounis, Z., & Cho, Y. (2010). An integrated system for bridge management using probabilistic and

mechanistic deterioration models: Application to bridge decks. *KSCE Journal of Civil Engineering, 14*(4), 527-537. http://dx.doi.org/10.1007/s12205-010-0527-4

Mwafy, A., Kwon, O., & Elnashai, A. (2009). Seismic assessment of an existing non-seismically designed major bridge-abutment-foundation system. *Engineering Structures, 32*(8), 2192-2209. http://dx.doi.org/10.1016/j.engstruct.2010.03.022

Nagy, W., De Backer, H., & Van Bogaert, Ph. (2013). Fracture mechanics as an improvement of fatigue life assessment in orthotropic bridge decks. Research and Applications in Structural Engineering, Mechanics and Computation - *Proceedings of the 5th International Conference on Structural Engineering, Mechanics and Computation, SEMC 2013* (pp. 579-584).

Newhook, J. P., & Edalatmanesh, R. (2013). Integrating reliability and structural health monitoring in the fatigue assessment of concrete bridge decks. *Structure and Infrastructure Engineering, 9*(7), 619-633. http://dx.doi.org/10.1080/15732479.2011.601745

Nguyen, T. L. T., Silva, P. F., Manzari, M. T., & Belarbi, A. (2010). *System modeling for seismic performance assessment and evaluation of reinforced concrete bridge columns.* American Concrete Institute, ACI Special Publication, n 271 SP, p 125-146, 2010, Structural Concrete in Performance-Based Seismic Design of Bridges - Technical Session at the ACI Fall 2008 Convention.

Nogami, Y., Akiyama, M., & Frangopol, D. M. (2013). Seismic design of RC bridge piers to ensure the post-disaster functionality of road network. Safety, Reliability, Risk and Life-Cycle Performance of Structures and Infrastructures - *Proceedings of the 11th International Conference on Structural Safety and Reliability, ICOSSAR 2013* (pp. 3581-3586).

O'Brien, E. J., González, A., & Znidaric, A. (2010). *Recommendations for dynamic allowance in bridge assessment.* Bridge Maintenance, Safety, Management and Life-Cycle Optimization - *Proceedings of the 5th International Conference on Bridge Maintenance, Safety and Management* (pp. 3434-3441).

Okumura, Y., Sakano, M., Horie, Y., & Kobayasi, H. (2010). *Fatigue damage assessment of steel bridge members using paint cracking.* Bridge Maintenance, Safety, Management and Life-Cycle Optimization - *Proceedings of the 5th International Conference on Bridge Maintenance, Safety and Management* (pp. 2103-2105).

Okumura, Y., Sakano, M., Horie, Y., & Kobayasi, H. (2010). *Fatigue damage assessment of steel bridge members using paint cracking.* Bridge Maintenance, Safety, Management and Life-Cycle Optimization - *Proceedings of the 5th International Conference on Bridge Maintenance, Safety and Management* (pp. 2111-2113).

Orcesi, A. D., & Frangopol, D. M. (2011). A stakeholder probability-based optimization approach for cost-effective bridge management under financial constraints. *Engineering Structures, 33*(5), 1439-1449.

Ozbulut, O. E., & Hurlebaus, S. (2011). Seismic assessment of bridge structures isolated by a shape memory alloy/rubber-based isolation system. *Smart Materials and Structures, 20*(1).

Padgett, J. E., Desroches, R., & Nilsson, E. (2010). Regional seismic risk assessment of bridge network in Charleston, South Carolina. *Journal of Earthquake Engineering, 14*(6), 918-933.

Pellegrino, C., Pipinato, A., & Modena, C. (2011b). A simplified management procedure for bridge network maintenance. *Structure and Infrastructure Engineering, 7*(5), 341-351. http://dx.doi.org/10.1080/15732470802659084

Petschacher, M. (2011). Use of b-wim data for bridge assessment. Applications of Statistics and Probability in Civil Engineering-*Proceedings of the 11th International Conference on Applications of Statistics and Probability in Civil Engineering* (pp. 2642-2648).

Pipinato, A. (2010a). *Structural analysis and fatigue life assessment of the Paderno Arch Bridge.* IABMAS 2010 - Bridge Maintenance, Safety, Management, Resilience and Sustainability - *Proceedings of the Sixth International Conference on Bridge Maintenance, Safety and Management* (pp. 1003-1007). Philadelphia, USA, 11-15 July 2010.

Pipinato, A. (2012b). Life cycle assessment of existing steel bridges considering corrosion and fatigue coupled problems. IABMAS 2012 - Bridge Maintenance, Safety, Management, Resilience and Sustainability - *Proceedings of the Sixth International Conference on Bridge Maintenance, Safety and Management* (pp. 1003-1007). Stresa, Lake Maggiore, Italy, 8-12 July 2012. ISBN: 9780415621243.

Pipinato, A. (2012c). Coupled damage in assessing the lifetime of bridge and viaducts. Life-Cycle and Sustainability of Civil Infrastructure Systems - *Proceedings of the 3rd International Symposium on Life-Cycle Civil Engineering, IALCCE 2012* (pp. 2292-2297). Vienna, Austria, October 3-6, 2012. ISBN 9780415621267.

Pipinato, A. (2012d). Assessment procedures and strengthening of an existing metal bridge. IABMAS 2012 - Bridge Maintenance, Safety, Management, Resilience and Sustainability - *Proceedings of the Sixth International Conference on Bridge Maintenance, Safety and Management* (pp. 3651-3655). Stresa, Lake Maggiore, Italy, 8-12 July 2012. ISBN: 9780415621243.

Pipinato, A. (2014a). Orthotropic steel deck design to extend the lifetime of plate and box girder bridge and viaducts. IABMAS 2014 - Bridge Maintenance, Safety, Management, Resilience and Sustainability - *Proceedings of the Seventh International Conference on Bridge Maintenance, Safety and Management*. Shangai, China, 7-11 July 2014 (in print).

Pipinato, A. (2014b). Longitudinal web stiffening in steel girders: fracture propagation and life cycle design. IABMAS 2014 - Bridge Maintenance, Safety, Management, Resilience and Sustainability - *Proceedings of the Seventh International Conference on Bridge Maintenance, Safety and Management*. Shangai, China, 7-11 July 2014 (in print).

Pipinato, A. (2014c). Steel bridges: codes, design specifications and construction issues. IABMAS 2014 - Bridge Maintenance, Safety, Management, Resilience and Sustainability - *Proceedings of the Seventh International Conference on Bridge Maintenance, Safety and Management.* Shangai, China, 7-11 July 2014 (in print).

Pipinato A. (2014d). Steel bridge coatings and corrosion protection. IABMAS 2014 - Bridge Maintenance, Safety, Management, Resilience and Sustainability - *Proceedings of the Seventh International Conference on Bridge Maintenance, Safety and Management*. Shangai, China, 7-11 July 2014 (in print).

Pipinato, A., Pellegrino, C., & Modena, C. (2010b). Residual service life of existing railway bridges. IABMAS 2010 - Bridge Maintenance, Safety, Management, Resilience and Sustainability - *Proceedings of the Sixth International Conference on Bridge Maintenance, Safety and Management* (pp. 1003-1007). Philadelphia, USA, 11-15 July 2010. ISBN: 9780415877862.

Pipinato, A. (2010a). Step level procedure for remaining fatigue life evaluation of one railway bridge. *Baltic Journal of Road and Bridge Engineering, 5*(1), 28-37. http://dx.doi.org/10.3846/bjrbe.2010.04

Pipinato, A. (2011). Assessment of existing bridges: Safety and security issues [Problemi di sicurezza nelle valutazioni strutturali di ponti esistenti]. *Ingegneria Ferroviaria, 66*(4), 355-371.

Pipinato, A. (2012c). Coupled safety assessment of cable stay bridges. *Modern Applied Science, 6*(7), 64-78. http://dx.doi.org/10.5539/mas.v6n7p64

Pipinato, A. (2013a). Retrofit procedures of bridge networks against seismic actions in Italy. *Durability of Bridge Structures Proceedings of the 7th New York City Bridge Conference* (pp. 215-228), 26-27 August 2013. Edited by Khaled M. Mahmoud, CRC Press 2013 Print ISBN: 978-1-138-00112-1 eBook ISBN: 978-1-315-85684-1.

Pipinato, A. (2013b). Moving load and fatigue analysis of a long span high speed railway bridge. *Advanced Materials Research, 629*, 403-408.

Pipinato, A. (2013c). Moving loads bridge response: Structural analysis and eurocode provisions. *Advanced Materials Research, 629*, 409-417.

Pipinato, A., & Modena, C. (2010). Structural analysis and fatigue reliability assessment of the Paderno bridge. *Practice Periodical on Structural Design and Construction, 15*(2), 109-124. http://dx.doi.org/10.1061/(ASCE)SC.1943-5576.0000037

Pipinato, A., Molinari, M., Pellegrino, C., Bursi, O. S., & Modena, C. (2011c). Fatigue tests on riveted steel elements taken from a railway bridge. *Structure and Infrastructure Engineering, 7*(12), 907-920. http://dx.doi.org/10.1080/15732470903099776

Pipinato, A., Pellegrino, C., & Modena, C. (2008). Scheduled maintenance actions and residual life evaluation of railway infrastructures for metallic structure bridges [Interventi di manutenzione programmata e valutazione della vita residua delle infrastrutture ferroviarie da ponte a struttura metallica]. *Ingegneria Ferroviaria, 63*(2), 125-134.

Pipinato, A., Pellegrino, C., & Modena, C. (2008b). Evaluation of fatigue strength of one riveted historical

railway bridge. Bridge Maintenance, Safety Management, Health Monitoring and Informatics IABMAS '08 *Proceedings of the Fourth International IABMAS Conference*, Seoul, Korea, July 13-17 2008. Edited by Hyun-Moo Koh and Dan M . Frangopol, Taylor & Francis 2008, Print ISBN: 978-0-415-46844-2, eBook ISBN: 978-1-4398-2843-4.

Pipinato, A., Pellegrino, C., & Modena, C. (2010a). Structural analysis of historical metal bridges in Italy. *Advanced Materials Research, 133*, 525-530. http://dx.doi.org/10.4028/www.scientific.net/AMR.133-134.525

Pipinato, A., Pellegrino, C., & Modena, C. (2011a). Fatigue assessment of highway steel bridges in presence of seismic loading. *Engineering Structures, 33*(1), 202-209. http://dx.doi.org/10.1016/j.engstruct.2010.10.008

Pipinato, A., Pellegrino, C., & Modena, C. (2012a). Assessment procedure and rehabilitation criteria for the riveted railway Adige Bridge. *Structure and Infrastructure Engineering, 8*(8), 747-764. http://dx.doi.org/10.1080/15732479.2010.481674

Pipinato, A., Pellegrino, C., & Modena, C. (2012c). Structural Analysis of the Cantilever Construction Process in Cable-Stayed Bridges. *Periodica Polytechnica: Civil Engineering, 56*(2), 141-166.

Pipinato, A., Pellegrino, C., & Modena, C. (2012d). Fatigue behaviour of steel bridge joints strenghtened with FRP laminates. *Modern Applied Science, 6*(10), 1-15.

Pipinato, A., Pellegrino, C., & Modena, C. (2014). *Residual life of historic riveted steel bridges: an analytical approach*. ICE-Bridge Engineering, UK Institution of Bridge Engineers. http://dx.doi.org/10.1680/bren.11.00014.

Pipinato, A., Pellegrino, C., & Modena, C. (2012e). Fatigue Damage Estimation in Existing Railway Steel Bridges by Detailed Loading History Analysis. *ISRN Civil Engineering, 2012*, Article ID 231674. http://dx.doi.org/10.5402/2012/231674.

Pipinato, A., Pellegrino, C., Bursi, O. S., & Modena, C. (2009). High-cycle fatigue behavior of riveted connections for railway metal bridges. *Journal of Constructional Steel Research, 65*(12), 2167-2175. http://dx.doi.org/10.1061/(ASCE)SC.1943-5576.0000037

Pipinato, A., Pellegrino, C., Fregno, G., & Modena, C. (2012b). Influence of fatigue on cable arrangement in cable-stayed bridges. *International Journal of Steel Structures, 12*(1), 107-123. http://dx.doi.org/10.1007/s13296-012-1010-5.

Pipinato, A. (2014). *Assessment and rehabilitation of steel railway bridges using fi bre-reinforced polymer (FRP) composites*. Rehabilitation of Metallic Civil Infrastructure using Fiber-reinforced Polymer (FRP) Composites, Edited by Vistasp M. Karbhari. Woodhead Publishing Series in Civil and Structural Engineering: Number 51.

Pu, Q., Gao, L., Liu, Z., & Shi, Z. (2013). Fatigue assessment of orthotropic steel bridge deck based on hot spot stress method. *Source: Xinan Jiaotong Daxue Xuebao/Journal of Southwest Jiaotong University, 48*(3), 395-401.

Qiang B., Labi, S., Sinha, K. C., & Thompson, P. D. (2013). Multiobjective Optimization for Project Selection in Network-Level Bridge Management Incorporating Decision-Maker's Preference Using the Concept of Holism. *Journal of Bridge Engineering, 18*(9), 879-89.

Robert, W., Marshall, A., Shepard, R., & Aldayuz, J. (2003). The Pontis bridge management system: state-of-thepractice in implementation and development. *Proceedings of 9th international bridge management conference* (pp. 49-60). Transportation Research Board, Washington, DC, USA.

Rong, L. (2010). The analysis and design of urban bridge safety early-warning management system. *2010 IEEE International Conference on Industrial Engineering & Engineering Management (IE&EM 2010)* (pp. 1786-90).

Seo, J., & Linzell, D. G. (2012). Horizontally curved steel bridge seismic vulnerability assessment. *Engineering Structures, 34*, 21-32.

Sigurdardottir, D., Hubbell, D., Sousa Afonso, J. P., & Glisic, B. (2011). Streicker bridge: Assessment of structural health condition through static and dynamic monitoring. *SHMII-5 2011 - 5th International Conference on Structural Health Monitoring of Intelligent Infrastructure*.

Soma M. (2006). *Development and implementation of bridge management system in aomori prefectural government*. Advances in Bridge Maintenance, Safety Management, and Life-Cycle Performance,

Proceedings of the Third International Conference on Bridge Maintenance, Safety and Management (pp. 16-19). July 2006, Porto, Portugal - IABMAS '06.

Stamatopoulos, G.N. (2013). Fatigue assessment and strengthening measures to upgrade a steel railway bridge. *Journal of Constructional Steel Research, 80*, 346-54.

Sunley, W. (1995). Pontis: a bridge inspection. *Illinois Department of Transportation, Illinois Municipal Review* (pp. 13-15).

Teresa, R. A., Premavathi, N., & Gunasekaran, U. (2012). Seismic performance assessment of an existing road bridge using standard pushover analysis. *Applied Mechanics and Materials, 147*, 278-282.

Thavaraj, T., Sy, A., Hamersley, B., Woolford, D. (2012). Geotechnical aspects of the seismic safety assessment and retrofit of the Knight Street Bridge. *Proceedings, Annual Conference - Canadian Society for Civil Engineering* (vol. 1, pp. 607-616), 2012, Annual Conference of the Canadian Society for Civil Engineering 2012: Leadership in Sustainable Infrastructure, CSCE 2012.

Thompson, P., Sobanjo, J., & Kerr, R. (2013). Modeling the risk of advanced deterioration in bridge management systems. *Transportation Research Record, 2360*, 52-59.

Tian, H. Y., & Liu, Q. W. (2012). The life-cycle information management practice of Shanghai Yangtze River Tunnel and Bridge Project. Harmonising Rock Engineering and the Environment - *Proceedings of the 12th ISRM International Congress on Rock Mechanics* (pp. 2157-2162).

Tong G., Frangopol, D. M., & Yuwen, C. (2012). Fatigue reliability assessment of steel bridge details integrating weigh-in-motion data and probabilistic finite element analysis. *Computers & Structures, 112*, 245-57.

Walbridge, S., Fernando, D., & Adey, B. T. (2012). Modelling inspection and fatigue retrofitting by post-weld treatment in bridge management systems. Bridge Maintenance, Safety, Management, Resilience and Sustainability - *Proceedings of the Sixth International Conference on Bridge Maintenance, Safety and Management* (pp. 3960-3967).

Waller, C. L., & Lau, D. T. (2010). *Probabilistic perforcemance-based seismic risk assessment of Canadian bridges - A pilot study*. 9th US National and 10th Canadian Conference on Earthquake Engineering 2010, Including Papers from the 4th International Tsunami Symposium, v 6, p 5003-5012, 2010, 9th US National and 10th Canadian Conference on Earthquake Engineering 2010, Including Papers from the 4th International Tsunami Symposium.

Wang, J., & Melbourne, C. (2010). Mechanics of MEXE method for masonry arch bridge assessment. *Proceedings of the Institution of Civil Engineers: Engineering and Computational Mechanics, 163*(3), 187-202.

Xiaofang, W., Hongchun, Y., Dongqing, X., & Ziyong, X. (2012). Developing of management information system of road and bridge infrastructure based on ArcGIS engine. *2012 Proceedings of 2nd International Conference on Remote Sensing, Environment and Transportation Engineering (RSETE 2012)* (pp. 3-10).

Yilmaz, T., & Caner, A. (2012). Target damage level assessment for seismic performance evaluation of two-column reinforced concrete bridge bents. *Bridge Structures, 8*(3-4), 135-146.

Yokoyama, K., Inaba, N., Honma, A., & Ogata, N. (2006). Development of Bridge Management System for Expressway Bridges in Japan. Advances in Bridge Maintenance, Safety Management, and Life-Cycle Performance, *Proceedings of the Third International Conference on Bridge Maintenance, Safety and Management*, 16-19 July 2006, Porto, Portugal - IABMAS '06.

Youngguk, S., Cheolmin, B., & Kim, Y. R. (2012). Fatigue crack assessment of asphalt concrete pavement on a single span highway bridge subjected to a moving truck. *Journal of Testing and Evaluation, 40*(6), JTE104200.

Zhang, K., Zhu, X., Ni, Y., & Jiang, H. (2011). Performance-based Seismic Financial Risk Assessment for Bridge Structure. *China Railway Science, 32*(1), 68-74.

Zhou, H., Liu, K., Shi, G., Wang, Y. Q., Shi, Y. J., & De Roeck, G. (2013). Fatigue assessment of a composite railway bridge for high speed trains. Part I: Modeling and fatigue critical details. *Journal of Constructional Steel Research, 82*, 234-45.

Znidaric, A., & Lavric, I. (2010). Applications of B-WIM technology to bridge assessment. Bridge Maintenance, Safety, Management and Life-Cycle Optimization - *Proceedings of the 5th International Conference on Bridge Maintenance, Safety and Management* (pp. 1001-1008).

Modern Applied Science; Vol. 8, No. 3; 2014
ISSN 1913-1844 E-ISSN 1913-1852
Published by Canadian Center of Science and Education

Investigation of Passive Design Techniques for Pitched Roof Systems in the Tropical Region

Karam M. Al-Obaidi[1], Mazran Ismail[1] & Abdul Malek Abdul Rahman[1]

[1] School of Housing, Building and Planning, Universiti Sains Malaysia, 11800, Penang, Malaysia

Correspondence: Karam M. Al-Obaidi, School of Housing, Building and Planning, Universiti Sains Malaysia, 11800, Penang, Malaysia. Tel: 60-174-039-378. E-mail: karam_arc@yahoo.com

Received: March 13, 2014 Accepted: April 1, 2014 Online Published: May 5, 2014

doi:10.5539/mas.v8n3p182 URL: http://dx.doi.org/10.5539/mas.v8n3p182

Abstract

Pitched roof design represents the common system for the most tropical houses in Malaysia. Different angles and colours of this roof deliver various impacts on the indoor environment. This study focuses on estimating the amount of heat gain and roof surface temperature obtained from different roofing aspects. The paper hypothesizes that colour technique could change pitched roof design more than roof angles and materials. The research was based on simulation analysis applied on an actual room size with different roof angles (0°, 30°, 45° and 60°) in the Malaysian environment. As a result, the findings of different roofing systems affirm the hypothesis and show the significant of roof colour compare to area, angles and materials. This study contributes efficiently to the knowledge of the roofing design in the tropics. In addition, it will shed light on the economic sector and sustainability for optimum roofing concept particularly for low cost housing components in Malaysia.

Keywords: pitched roofs, roof angles, roof colours, roof materials, tropical houses

1. Introduction

Research studies have estimated that urban areas could be covered by 60% of roofs and pavements (Akbari, Arthur, & Rosenfeld, 2008). In addition, this estimation is increasing as there are around 50% of the world population currently in urban regions, with expected increases to 70% at the end of 2040. Furthermore, roofing systems represent the main body of urban area that interact directly with solar rays. Therefore, roof angles and claddings are one of the most elements that may lead to effect considerably the indoor environment. Generally, pitched roof system represents the most common construction design for traditional and modern buildings in hot humid regions. This type of roof has been extensively used in order to protect against rain water and strong sunshine as well as its consequent of lower heat transfer into the building. The rapid development of building design were the reason for the selection of concrete tiles, cement tiles, clay tiles and aluminium sheets for this type of system in the specific environment. However, concrete and cement tiles have the priority in the Malaysian urban area not due to thermal properties but because of low cost and good resistance to the weather conditions.

The climatic condition, sun position, orientation, tilt of building external elements, surface reflectance, thermal capacity, area of the surface must be considered in evaluating heat gain (Mahdavinejad, Ghasempourabadi, Nikhoosh, & Ghaedi, 2012). According to Vijaykumar, Srinivasan and Dhandapani (2007) indicate that roofing system represents 70% of the total heat gain in a building. The colour of the external surfaces especially the roof has a remarkable effect on the level of heat gain in buildings and on the indoor temperature, particularly in unair-conditioned spaces. This technique is widely recognized and clearly observed in the hot regions, but its application is poor in the tropics. Based on a study in Malaysia conducted by Yacouby, Khamidi, Nuruddin, Farhan and Razali (2011), the results indicated that the majority roof tiles colours are dark as Red 38%, Brown 25.9%, White 9.5%, Beige and Blue 7.8% Black 4.9% and Grey 2.9%. In Malaysia, Allen et al. (2008) showed that concrete roof tiles are the most commonly used roofing materials, as it represents 85% followed by clay tiles and metal deck with 10% and 5% respectively. Yacouby, Khamidi, Nuruddin, Farhan, & Razali (2011) tested two roof slopes 30° and 45° consist of concrete and clay tiles which are commonly used in Malaysia.

Experimental and Numerical researches in buildings in the United States as well as in Europe (Bozonnet, Doya, & Allard, 2011; Pisello & Cotana, 2013) indicated the reduction of the cooling peak load by up to 70% and of the indoor free-floating temperature up to 3°C in the thermal zones adjacent to the roof features implementation.

Pearlmutter (1993) made the first attempt to quantitatively compare thermal behaviour of several roof designs in terms of indoor temperatures. Runsheng, Meir and Etzion (2003) compared the amount of solar heat to domed roofs and flat roofs. The authors stated that the ratio of radiation absorbed by a curved roof to that absorbed by a flat one rises with increase of rim angle however it is insignificantly affected by climate characteristics and site latitude. Hadavand, Yaghoubi and Emdad (2007) in another study compared flow field around different building geometries of several roofs and also determined corresponding heat flow and Nusselt number for these roofs. According to Hadavand and Yaghoubi (2008) temperature difference of two sides of vaulted roofs increases with rim angle. Fitzgerald et al. (2011) have studied on the assessment of roof space solar gains in a temperate maritime climate. Al-Obaidi, Ismail and Abdul Rahman (2014) reviewed the performance of pitched roof angles and pitched roof with an attic in the tropics.

In addition, Jayasinghe, Attalage and Jayawardena (2003) investigated roof orientation, roofing materials and roof surface colour: their influence on indoor thermal comfort in warm humid climates. The recommendations stated in this study have lead to; (i) The effect of the roof orientation on indoor thermal conditions is insignificant. (ii) Prefer clay tiles to cement fibre sheets as a roof covering material. (iii) An improvement can be obtained by using an aluminium foil with or without polystyrene over the ceiling. (iv) Paint the exterior surface of the roof with a light colour such as off-white, especially if the roof covering is cement fibre sheets. In Malaysia, Al-Obaidi, Ismail and Abdul Rahman (2013) tested the effect of pitched roof integrated with aluminium sheet and reflective roof however this study was based on determine the level of daylight and heat gain from skylight system. Moreover, Rahman, Rahim, Al-Obaidi, Ismail and Mui (2013) investigated the performance of affordable housing design in the tropics which targeted with the cement roof tiles for a single story low cost terrace house. However both studies have not compared different types of roofs.

As a result, most of researchers have not shed light on the investigation of heat gain with roof angles associated with different colours and materials. Therefore, this paper hypothesizes that colour technique could change pitched roof design more than roof angles and materials. Therefore, this paper targets the roof construction system (structure angles, colours and materials) as keys to identify the design controllers. The paper aims to investigate these properties in same room size to shift the paradigm in the understanding of passive roofing design in the tropical architecture.

2. Methodology

The study was conducted on several roof types applied on a single room in the area of Penang (latitude 5.3° and longitude 100.3°), Malaysia. The testing room was constructed from brickwork for the walls and exposed to full sunlight from all directions. The long side of the room was oriented to east and west side to experience worst case condition. The investigational work consists of one unit experimental model of 5.0 m (L) x 4.0 m (W) and 3.0 m (H) contains of a door without any windows as shown in Figure 1 the door was shut during the measurement for eliminating any additional heat gain. The floor was covered with cement sand screed. External walls were constructed with thick brick. External and internal walls were white paint finish.

The experimental work was conducted on the same room size with different roof designs and mainly focusing on two different roofing materials i.e. clay tiles and aluminum sheets which are commonly used in Malaysia. The above parameters were tested for flat and sloped roofs 0° (20 m^2), 30° (47 m^2), 45° (56 m^2), 60° (73 m^2). In addition, three types of roof colours selected as Black, Red and White to represents different solar reflectance from 0.9 to 0.2. The thicknesses of roof materials were clay tiles 15 mm with cement board 3 mm while aluminum sheets used 0.8 mm. The measurement targeted outdoor and indoor environments i.e. outdoor air temperature, solar radiation, surface temperature, indoor air temperature were measured to evaluate the thermal performance of the room under the roofs.

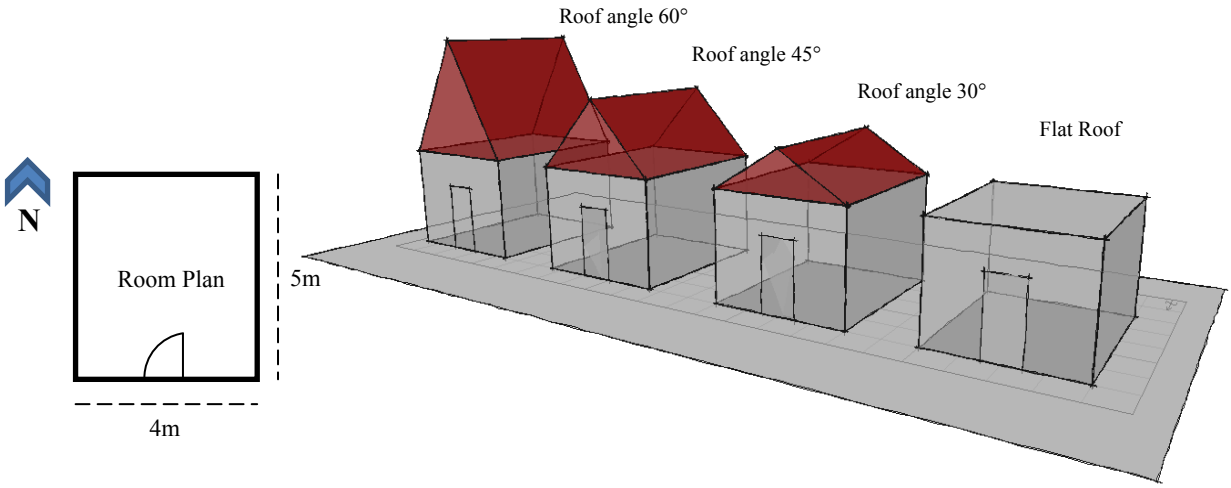

Figure 1. Graphical models

The findings were obtained using the building energy simulation tool "Integrated Environmental Solutions" <Virtual Environment> version 6.4 (IES, 2013) used for the investigations. The simulation program is recommended for the Malaysian conditions by Green Building Index (2011) and Building Sector Energy Efficiency Project (2013). The weather data used for the simulation study is the Test Reference Year (TRY) weather data from an analysis of 21 years of weather data from the weather station of Penang Airport in Bayan Lepas, Malaysia. The selected days for the measurement were based on targeting the hottest days of the year (mid of March) to compare the different types of roofs for constant evaluation. Due to the large amount of information generated, this paper only reports the reading of 14th March as the hottest day to perform the testing for several types of investigations. The data presents the maximum outdoor air temperature which was around 34.6 °C while maximum outdoor solar radiation was around 1060 W/m^2. These readings demonstrate the most common levels of the current condition.

3. Results and Discussion

3.1 The Performance of Roof with Clay Tiles

Figure 2 shows the indoor temperature for roof with clay tiles in different roof colours and angles. The results indicate that in various roof colours the behaviour of roof angle was varied significantly. It was noticed that the indoor temperature with Black colour 0° angle represents the highest level whereas with White colour shows the lowest. These performances give an interesting understanding to the design of roofing systems. The readings show that maximum indoor air temperature with Black roof was 40.06 °C for roof (60°), 39.9 °C for roof (45°), 40.17 °C for roof (30°) and 40.61 °C for roof (0°). For Red colour was 36.13 °C for roof (60°), 35.69 °C for roof (45°), 35.64 °C for roof (30°) and 35.81 °C for roof (0°). For the White colour was 33.32 °C for roof (60°), 32.76 °C for roof (45°), 32.49 °C for roof (30°) and 32.46 °C for roof (0°). The readings show that colours play a significant role in every roof angle more than material properties and roof shapes. The findings show that the difference of maximum - minimum indoor temperature with same colour but with different angles was for Black colour with angle 0° - 45° was 0.71 °C (40.61 - 39.9). For Red colour with angle 60°- 30° was 0.49 °C (36.13 - 35.64) and for White colour with angle 60° - 0° was 0.85 °C (33.32 - 32.46). The readings show that in every colour the maximum and minimum readings were for different roof angles. This findings approved that roof colour is important compare to roof angles. The reading show that the maximum value recorded for Black - Red roof colour was 4.48 °C (40.61 - 36.13) and for Black - White roof colour was 7.29 °C (40.61 - 33.32). Table 1 tabulated the main indoor temperature for worst and best conditions with different roof angles.

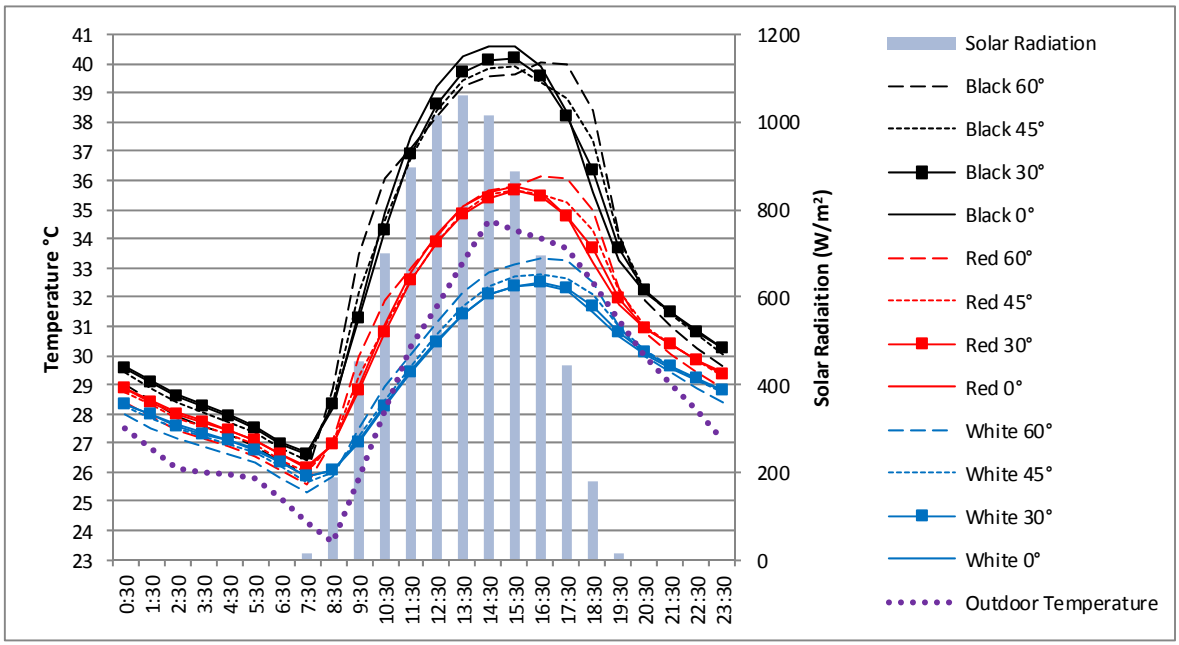

Figure 2. Indoor temperature for roof with clay tiles associated with different roof angles and colours

Table 1. Indoor temperature for roof (clay tiles) in Black and White colours with different roof angles

	Black 60°	Black 45°	Black 30°	Black 0°	White 60°	White 45°	White 30°	White 0°
Max	40.06	39.9	40.17	40.61	33.32	32.76	32.49	32.46
Mean	32.78	32.77	32.76	32.89	29.24	29.22	29.14	29.13
Min	25.94	26.37	26.58	26.65	25.29	25.68	25.84	25.86

Figure 3, Figure 4 and Figure 5 present the behaviour of clay tiles surface temperature with various roof angles and colours. The readings indicate varied patterns. Figure 3 shows that roof with Black colour, the maximum surface temperature was for flat roof 0° which it reached 57.45 °C around 01:30 pm. However, for other roof angles the two sides was not stable as the highest temperature recorded for the east side more than west side. The findings for Black colour show that roof angle (60°) east side was 55.52 °C and west side was lower with 55.27 °C, roof angle (45°) east side was 55.64°C and west side was lower with 55.13°C, for roof angle (30°) east side was 55.74°C and west side was also lower with 55.26°C and finally roof angle (0°) was the highest with 57.45 °C.

The results from Figure 4 show the performance of clay tiles surface temperature for Red colour which presents varied patterns for east and west side. The maximum surface temperature was for roof angle 60° which it extended to 45 °C around 04:30 pm. However, the comparison of two sides shows that west side was always higher than east side. The findings point out that maximum reading for roof angle (60°) east side was 43.19°C while west side was 45.01°C, roof angle (45°) east side was 43.65°C while west side was 44.84°C, for roof angle (30°) east side was 43.58°C while west side was 44.68°C and finally roof angle (0°) was 44.54°C. The readings show that even roof angle (60°) was recorded highest temperature however the east side of this roof was lower than roof angle of 45° and 30°.

Figure 5 also shows different patterns for east and west side for White colour. The maximum surface temperature was for roof angle 60° which hit 37.69 °C between 03:30 pm and 04:30 pm. However, the figure shows that west side was significantly higher than east side. The outcomes indicate that maximum reading for roof angle (60°) east side was 35.96 °C while west side was higher with 37.69 °C, roof angle (45°) east side was 36.14 °C while west side was higher with 37.49 °C, for roof angle (30°) east side was 36.16 °C whereas west side was 37.13 °C and finally roof angle (0°) was 35.35 °C. The recording results in Table 2 affirm that even roof angle (60°) was recorded highest temperature however the east of this roof was lower than roof angle of 45° and 30°.

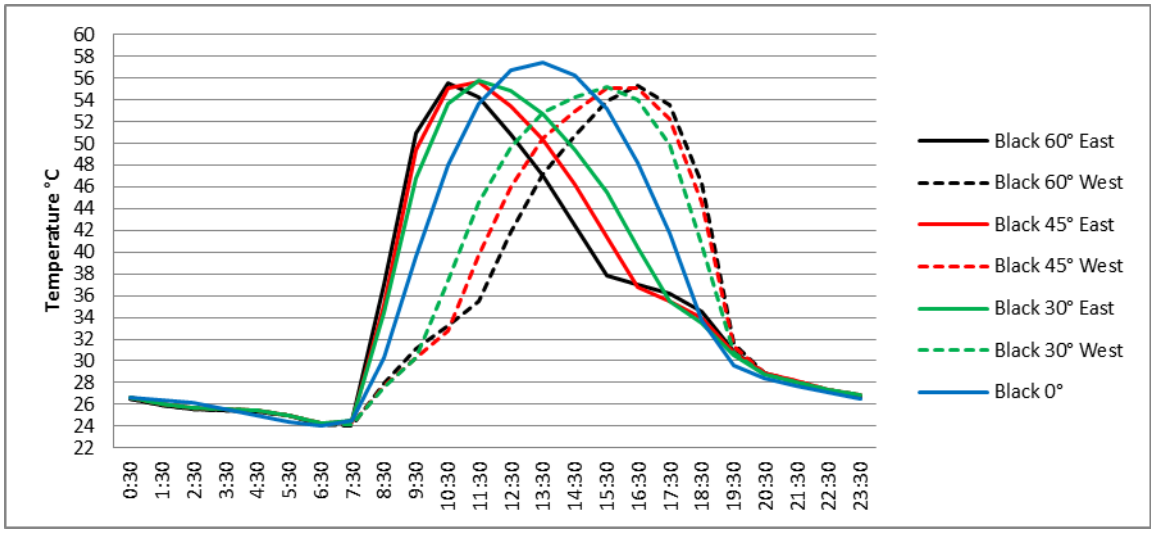

Figure 3. Surface temperature of clay tiles with Black colour in two sides (East and West)

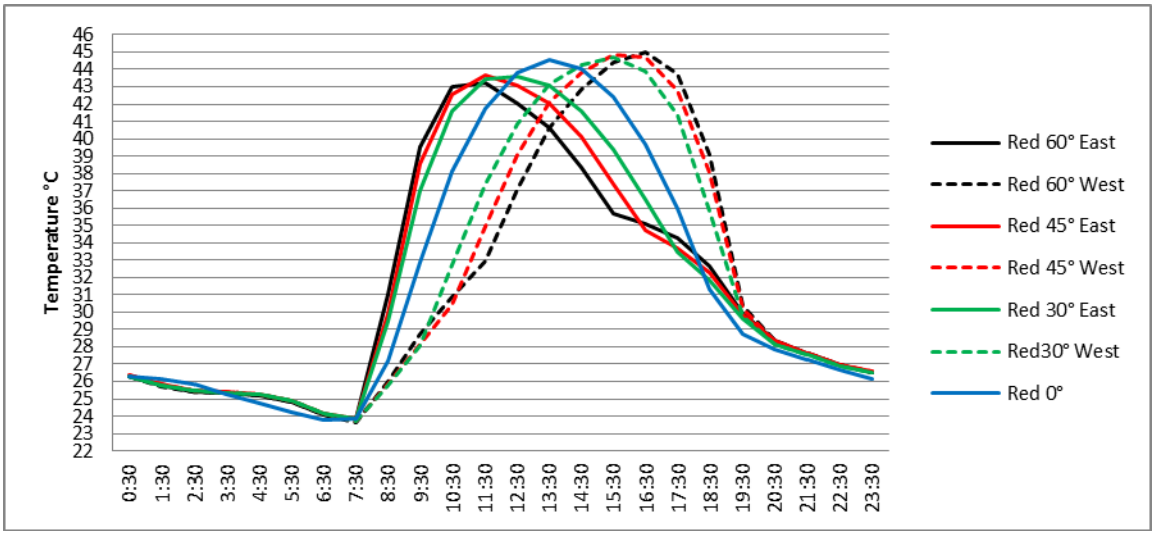

Figure 4. Surface temperature of clay tiles with Red colour in two sides (East and West)

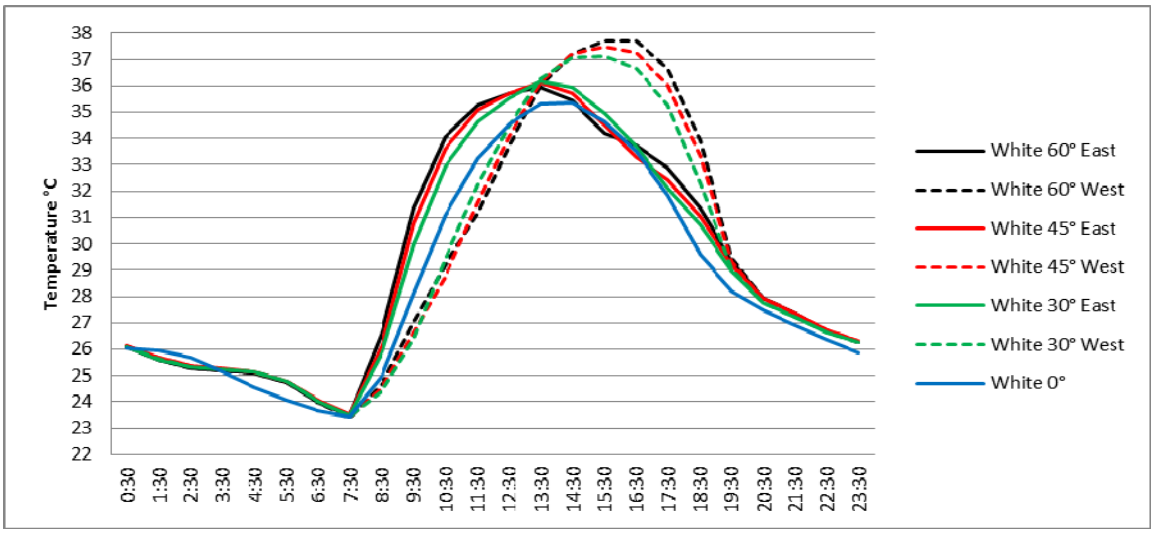

Figure 5. Surface temperature of clay tiles with White colour in two sides (East and West)

Table 2. The performance of surface temperature (°C) for clay tiles in worst and best conditions

	Black 60° East	Black 60° West	Black 45° East	Black 45° West	Black 30° East	Black 30° West	Black 0°	White 60° East	White 60° West	White 45° East	White 45° West	White 30° East	White 30° West	White 0°
Max	55.52	55.27	55.64	55.13	55.74	55.26	57.45	35.96	37.69	36.14	37.49	36.16	37.13	35.35
Mean	34.51	34.22	34.92	34.68	35.3	35.05	35.86	29.32	29.25	29.25	29.19	29.12	29.09	28.57
Min	24.17	24.02	24.27	24.13	24.26	24.15	24.01	23.47	23.37	23.5	23.43	23.46	23.41	23.44

3.2 The Performance of Roof with Aluminium Sheets

Figure 6 shows the indoor temperature for roof with aluminium sheets for different roof colours and angles. The results indicate that in various roof colours the behaviour of roof angle was varied considerably. It was observed that maximum indoor temperature with Black colour 0° angle represent the highest reading whereas with White colour shows the lowest. The behaviour of different roofs gives an interesting indication. The findings show that maximum indoor air temperature with Black was 40.76 °C for roof (60°), 40.81 °C for roof (45°), 41.13 °C for roof (30°) and 41.66 °C for roof (0°). For Red colour was 36.58 °C for roof (60°), 36.23 °C for roof (45°), 36.22 °C for roof (30°) and 36.4°C for roof (0°). For the White colour was 33.6 °C for roof (60°), 33.02 °C for roof (45°), 32.75 °C for roof (30°) and 32.71 °C for roof (0°). Support the outcomes that mentioned earlier, the findings show that colours play a considerable role in every roof angle compare to property, area and shape. The findings indicate that the difference of maximum - minimum indoor temperature with same colour but with different angles was for Black colour with angle 0° - 60° was 0.9 °C (41.66 - 40.76). For Red colour with angle 60°- 30° was 0.36 °C (36.58 - 36.22) and for White colour with angle 60° - 0° was 0.89 °C (33.6 - 32.71). In fact, the results show that minimum readings for aluminium sheets with Black colour was for roof angle (60°) while for the clay tiles was for roof angle (45°). The readings present that in every colour the maximum and minimum readings were for different roof angles. These outcomes approved that roof colour is more important than roof angles. The analysis show that the maximum value for Black - Red roof colour was 5.08 °C (41.66 - 36.58) and for Black - White roof colour was 8.06 °C (41.66 - 33.6). Table 3 tabulated the main indoor temperature for worst and best conditions with different roof angles.

Table 3. Indoor temperature for roof (aluminium sheets) in Black and White colours with different roof angles

	Black 60°	Black 45°	Black 30°	Black 0°	White 60°	White 45°	White 30°	White 0°
Max	40.76	40.81	41.13	41.66	33.6	33.02	32.75	32.71
Mean	32.99	33.01	33.03	33.18	29.26	29.23	29.15	29.13
Min	25.74	26.18	26.4	26.47	25.1	25.49	25.64	25.67

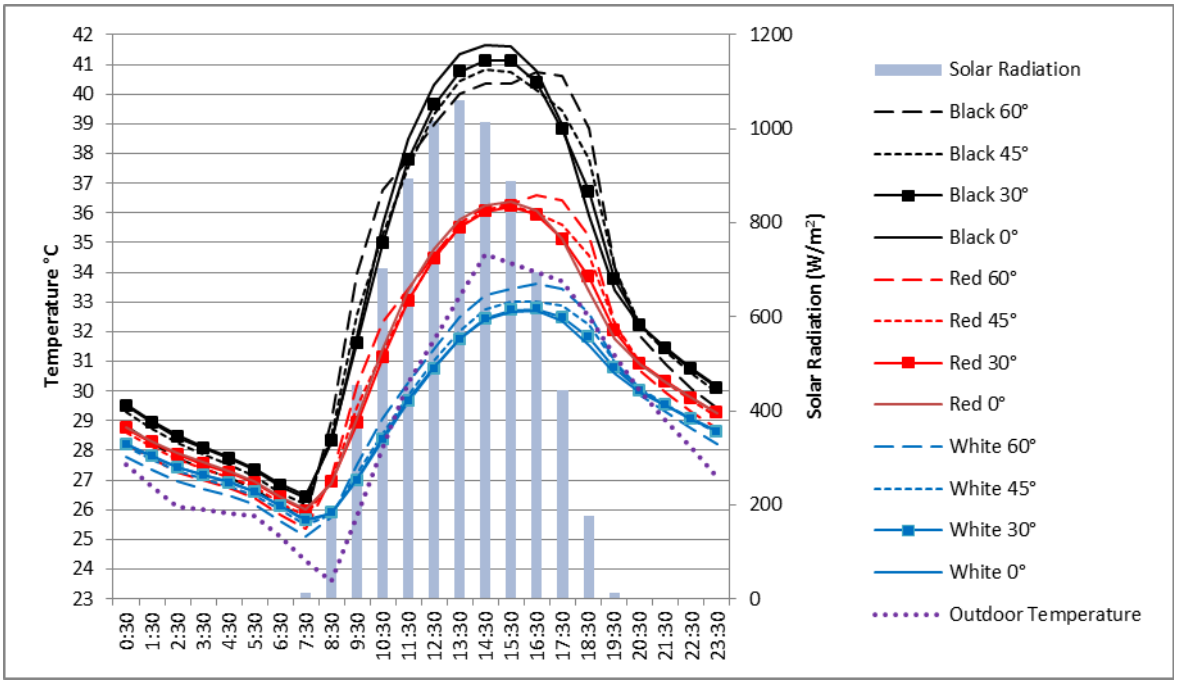

Figure 6. Indoor temperature for roof with aluminium sheets associated with different roof angles and colours

Figure 7, Figure 8 and Figure 9 present the behaviour of aluminium sheets surface temperature with various roof angles and colours. The readings draw varied patterns. Figure 7 indicates that roof with Black colour the maximum surface temperature was for flat roof 0° which reached 60.15 °C around 01:30 pm. However, the outcomes show that roof sides were also different as east side was higher than west side. The findings for Black colour show that roof angle (60°) east side was 58.49 °C and west side was 57.75 °C, roof angle (45°) east side was 58.63 °C and west side was 57.68°C, for roof angle (30°) east side was 58.73 °C and west side was 57.8 °C and finally roof angle (0°) was 60.15 °C.

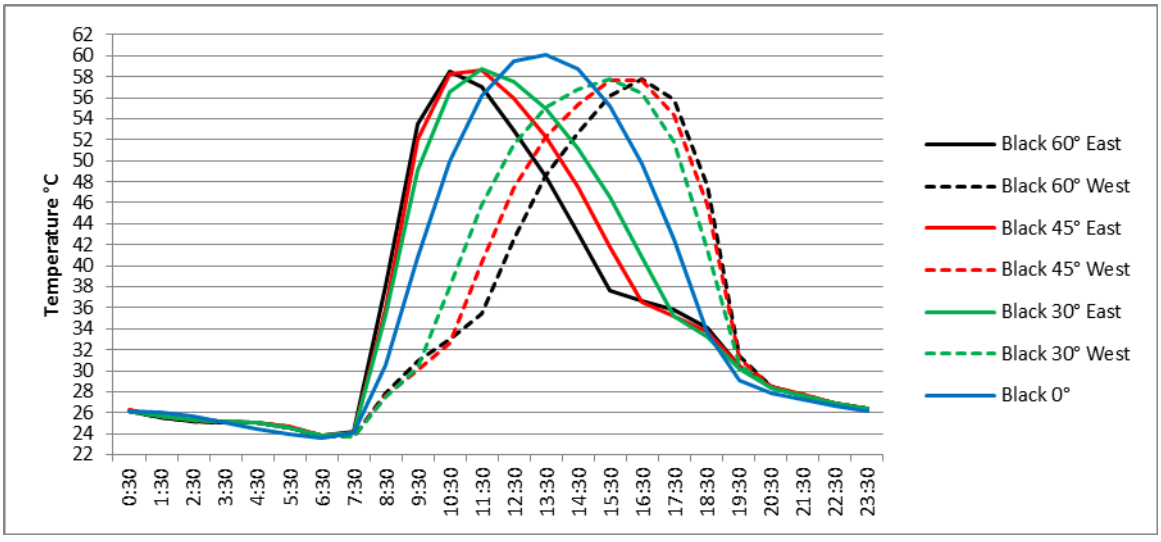

Figure 7. Surface temperature of aluminium sheets with Black colour in two sides (East and West)

Figure 8 shows the readings of surface temperature that painted with Red colour which indicate of varied patterns for east and west side. The maximum surface temperature was with roof angle 60° which reached 46.47 °C around 04:30 pm. In addition, the findings assert that two sides of roof were higher for west on contrary of the Black colour. The maximum reading for roof angle (60°) east side was 44.81 °C while it was

higher for west side with 46.47 °C, roof angle (45°) east side was 45.39 °C while it was higher for west side with 46.38 °C, for roof angle (30°) east side was 45.19 °C while it was higher for west side with 46.21 °C and finally roof angle (0°) was 46.07 °C. The readings show that even roof angle (60°) recorded highest temperature however the east of this roof angle was lower than roof angle of 45° and 30°.

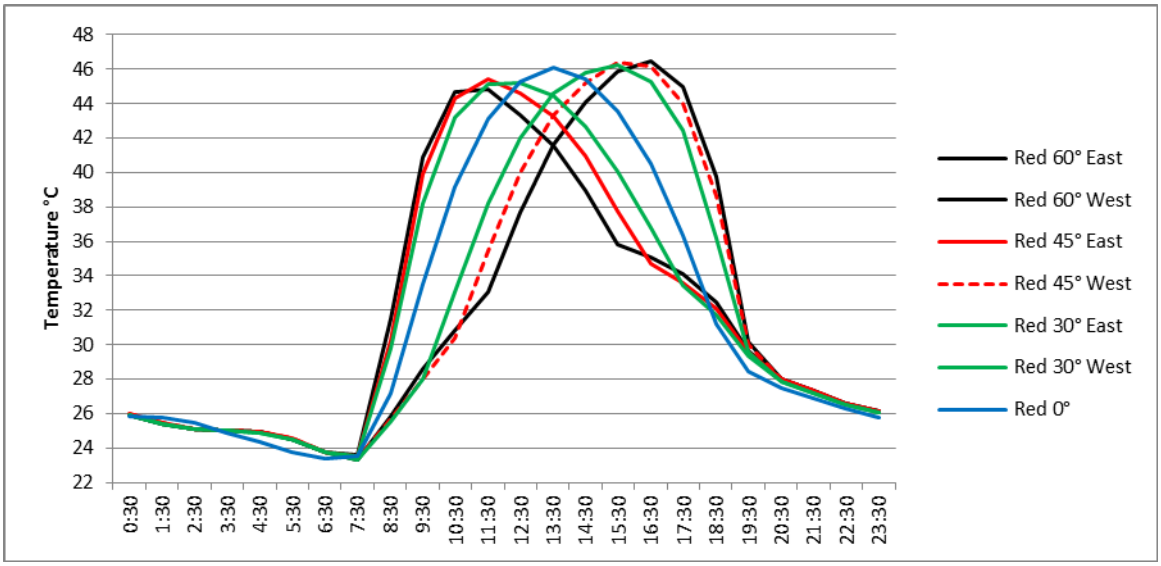

Figure 8. Surface temperature of aluminium sheets with Red colour in two sides (East and West)

Figure 9 for White colour also presents varied patterns for east and west side. The maximum surface temperature was with roof angle 60° which hit 38.46°C around 03:30 pm. The findings indicate that west side was always higher than east side. The results show that maximum reading for roof angle (60°) east side 36.62 °C and west side 38.46 °C, roof angle (45°) east side 36.9°C and west side 38.3°C, for roof angle (30°) east side 36.97 °C and west side 37.93 °C and finally roof angle (0°) was 36.02 °C. The findings in Table 4 affirm that that even roof angle (60°) was recorded highest temperature however the east of this roof was lower than roof angle of 45° and 30°.

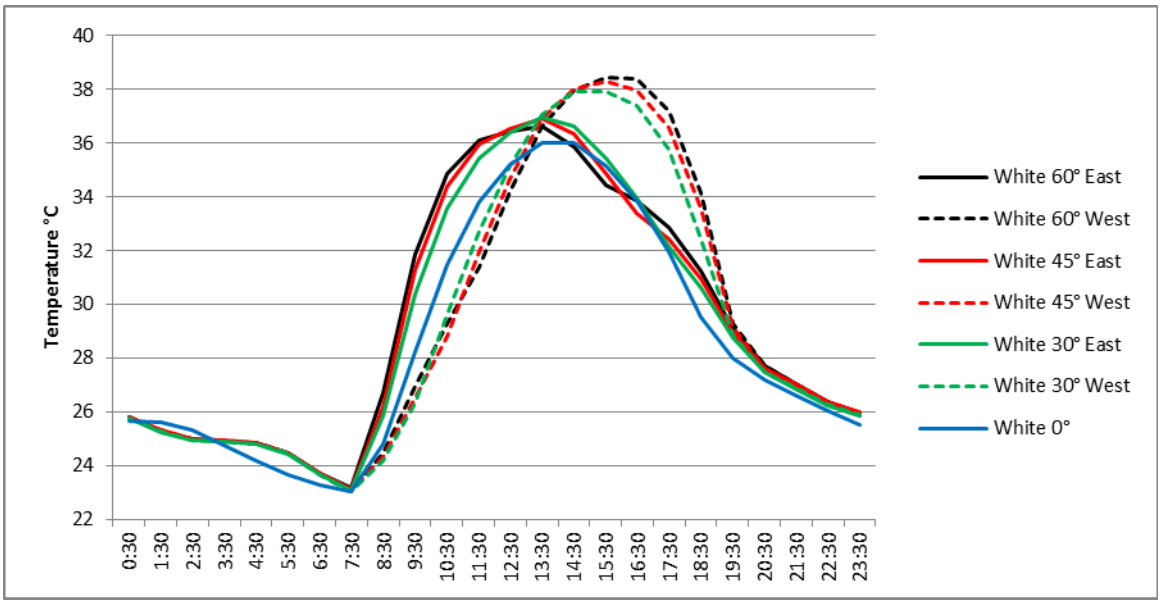

Figure 9. Surface temperature of aluminium sheets with White colour in two sides (East and West)

Table 4. Surface temperature (°C) for aluminium

	Black 60° East	Black 60° West	Black 45° East	Black 45° West	Black 30° East	Black 30° West	Black 0°	White 60° East	White 60° West	White 45° East	White 45° West	White 30° East	White 30° West	White 0°
Max	58.49	57.75	58.63	57.68	58.73	57.8	60.15	36.62	38.46	36.9	38.3	36.97	37.93	36.02
Mean	34.82	34.51	35.32	35.06	35.76	35.49	36.38	29.34	29.27	29.27	29.2	29.14	29.11	28.54
Min	23.81	23.7	23.86	23.77	23.83	23.77	23.56	23.16	23.05	23.14	23.07	23.09	23.02	23.05

4. Conclusion

The paper focuses on different techniques to develop the understanding of pitched roof systems in the tropics. The research hypothesizes that colour approach could change pitched roof angle more than material properties. The results of different roofing systems affirm this theory and show the significance of roof colour more than the roof area, angle and material. Furthermore, it was noticed that pitched roof sides have played a significant role to determine the heat gain. In addition, it was realized that highest temperature for lighter colour was for roof angle 60° more than lower angles and especially flat roof while for darker colours the highest temperature for roof angle was 0° or flat roof. Moreover, the results from surface temperature display that even 60° was recorded the highest indoor temperature for lighter colour such as Red and White however the east side of this roof angle was lower than roof with angle 45° and 30°. Additionally, the study shows the differences of roof angles with same roof materials found with clay tiles, the difference between roof angles was around 0.71 °C (Black colour), 0.49 °C (Red colour) and 0.85 °C (White colour). However for aluminium sheets was 0.9 °C (Black colour), 0.36 °C (Red colour) and 0.89 °C (White colour). Also with clay tiles the difference of roof colour shows the maximum value for Black - Red roof colour which was 4.48 °C and for Black - White roof colour was 7.29 °C. However for the aluminium sheets, the reading indicates that maximum record for Black - Red roof colours was 5.08 °C and for Black - White roof colours was 8.06 °C.

The findings also indicate that the thickness of roof tiles for clay and aluminium sheets have not affected significantly on the behaviour of the temperature patterns. Even though, the pattern of two roof systems (clay tiles 15 mm + 3 mm cement board) and aluminium sheet just (0.8 mm) was similar, the indoor temperature was lower for clay with maximum temperature for Black around 1 °C and for White colour was 0.28 °C. As a result, the study identifies the passive factors that could help any designer in order to shift the paradigm in the understanding of passive roofing design in the tropical architecture. These results will shed light on more economic decision for optimum roofing design especially for affordable quality housing components in Malaysia.

Acknowledgements

The authors would like to thank Universiti Sains Malaysia (USM) for the financial support provided for this research project.

References

Akbari, H., Arthur, H., & Rosenfeld. (2008). *White roofs cool the world, directly offset CO_2 and delay global warming*. Retrieved from http://www.whiteroofsalliance.org/wp-content/uploads/2010/12/White-Roofs-Cool-World-2ppNewCntct.pdf

Allen, L. K. K., Elias, S., & Lim, C. H. (2008). The thermal performance of evaluation of roofing systems and materials in Malaysian Residential Development. *Proceedings of SENVAR, ISESEE, Humanity and Technology* (pp. 387-395).

Al-Obaidi, K. M., Ismail, M., & Abdul Rahman, A. M. (2013). An innovative roofing system for tropical building interiors: Separating heat from useful visible light. *International Journal of Energy & Environment, 4*(1).

Al-Obaidi, K. M., Ismail, M., & Abdul Rahman, A. M. (2014). A review of the potential of attic ventilation by passive and active turbine ventilators in tropical Malaysia. *Sustainable Cities and Society, 10*, 232-240. http://dx.doi.org/10.1016/j.scs.2013.10.001

Bozonnet, E., Doya, M., & Allard, F. (2011). Cool roofs impact on building thermal response: A French case study. *Energy Build, 43*, 3006-3012. http://dx.doi.org/10.1016/j.enbuild.2011.07.017

Building Sector Energy Efficiency Project (BSEEP). (2013). *Building Energy Efficiency Technical Guideline for Passive Design*. Malaysia.

Fitzgerald, W. B., Fahmy, M., Smith, I. J., Carruthers, M. A., Carson, B. R., Sun, Z., & Bassett, M. R. (2011). An assessment of roof space solar gains in a temperate maritime climate. *Energy and Buildings, 43*(7), 1580-1588. http://dx.doi.org/10.1016/j.enbuild.2011.03.001

Green Building Index. (n.d.). *RESIDENTIAL NEW CONSTRUCTION (RNC)*. Retrieved from http://www.greenbuildingindex.org/Resources/GBI%20Tools/GBI%20Design%20Reference%20Guide%20-%20Residential%20New%20Construction%20(RNC)%20V1.02.pdf

Hadavand, M., & Yaghoubi, M. (2008). Thermal behavior of curved roof buildings exposed to solar radiation and wind flow for various orientations. *Applied Energy, 85*(8), 663-679. http://dx.doi.org/10.1016/j.apenergy.2008.01.002

Hadavand, M., Yaghoubi, M., & Emdad, H. (2007). Thermal exchange of flat and vaulted roofs exposed to solar radiation for various building geometries. *Proceedings of the 15th ISME conference*, Tehran, Iran.

Integrated Environmental Solutions (IESVE). (n.d.). *Home page*. Retrieved from http://www.iesve.com/

Jayasinghe, M. T. R., Attalage, R. A., & Jayawardena, A. I. (2003). Roof orientation, roofing materials and roof surface colour: their influence on indoor thermal comfort in warm humid climates. *Energy for Sustainable Development, 7*(1), 16-27. http://dx.doi.org/10.1016/S0973-0826(08)60345-2

Mahdavinejad, M., Ghasempourabadi, M., Nikhoosh, N., & Ghaedi, H. (2012). The Role of Roof Shapes in Design of Green Building Systems (Case Study: Iran, Tehran). *International Conference on Future Environment and Energy IPCBEE, 28* (2012). Singapoore: IACSIT Press.

Pearlmutter, D. (1993). Roof geometry as a determinant of thermal behavior: A comparative study of vaulted and flat surface in a hot-arid zone. *Architect Sci Rev, 36*(2), 75-86. http://dx.doi.org/10.1080/00038628.1993.9696740

Pisello, A. L., & Cotana, F. (2014). The thermal effect of an innovative cool roof on residential buildings in Italy: Results from two years of continuous monitoring. *Energy and Buildings, 69*, 154-164. http://dx.doi.org/10.1016/j.enbuild.2013.10.031

Rahman, A. M. A., Rahim, A., Al-Obaidi, K., Ismail, M., & Mui, L. Y. (2013). Rethinking the Malaysian Affordable Housing Design Typology in View of Global Warming Considerations. *Journal of Sustainable Development, 6*(7).

Runsheng, T., Meir, I. A., & Etzion, Y. (2003). An analysis of absorbed radiation by domed and vaulted roofs as compared with flat roofs. *Energy and buildings, 35*(6), 539-548. http://dx.doi.org/10.1016/S0378-7788(02)00165-2

Vijaykumar, K. C. K., Srinivasan P. S. S., & Dhandapani S. (2007). A performance of hollow tiles clay (HTC) laid reinforced cement concrete (RCC) roof for tropical summer climates. *Energy and Buildings, 39*, 886-892. http://dx.doi.org/10.1016/j.enbuild.2006.05.009

Yacouby, A. M. A., Khamidi, M. F., Nuruddin, M. F., Farhan, S. A., & Razali, A. E. (2011). Study on roof tile's colors in Malaysia for development of new anti-warming roof tiles with higher Solar Reflectance Index (SRI). In *National Postgraduate Conference (NPC), 2011* (pp. 1-6). IEEE. http://dx.doi.org/10.1109/NatPC.2011.6136358

Modern Applied Science; Vol. 8, No. 3; 2014
ISSN 1913-1844 E-ISSN 1913-1852
Published by Canadian Center of Science and Education

Factors Analysis for E-Services Adoption in Jordan: A Technology Acceptance Study

Ja'afer AL-Saraireh[1] & Mohammad Alnabhan[2]

[1] Applied Science University, Amman, Jordan

[2] Jerash University, Jerash, Jordan

Correspondence: Ja'afer AL-Saraireh, Applied Science University, Amman, 11931, Jordan. E-mail: sarjaafer@yahoo.com

Received: March 18, 2014 Accepted: April 2, 2014 Online Published: May 5, 2014

doi:10.5539/mas.v8n3p192 URL: http://dx.doi.org/10.5539/mas.v8n3p192

Abstract

This work investigates the factors affecting the adoption and acceptance of e-services in Jordan. In which, requirements for successful e-services implementation is addressed, and significant barriers being faced by e-services users and developers are described. Results have indicated that ease of use, usefulness, credibility, self-efficacy and trust had positive effects on the e-services adoption in Jordan. However, risk and cost at the other spectrum had a significant negative effect. Outcomes of this research have drawn a number of practical implications achieving positive attitude towards e-services adoption and developing the employment of e-services applications. Such implications include; promoting its trust, decreasing the perceived risk and cost, overcoming services development obstacles, considering user's capability concerns and increasing the awareness of e-services usefulness and ease of use.

Keywords: TAM, perceived usefulness, e-service, ease of use, trust, risk

1. Introduction

E-services experience is considered as a continuous emerging interest among information system researchers. Hence, there have been many surveys conducted regarding the factors affecting successful acceptance of e-services, especially in developing countries (Pi et al., 2012). There have been a few localized and comparative studies regarding e-services adoption in Jordan. These studies indicated that less than 5 percent of clients in Jordan are using e-services. Although, Jordan has set up many initiatives focusing on access and usage of e-services, and a set of legal service utilization frameworks has been developed, still E-services adoption and usage is considered very slow (Al-gaith et al., 2010) and (Al-Shboul & Alsmadi, 2010). Hence, understanding e-services adoption drivers and barriers among clients in Jordan becomes increasingly important for researchers, as well as for decision and policy makers (Alateyah et al., 2013). Accordingly, this research work was motivated by two key questions: (1) what are the factors affecting the e-services adoption among Jordanian residents? (2) what are the barriers and inhibitors causing slow adoption and usage of e-services?

The following section presents literature review, in which the conceptual model was developed and research hypotheses are then presented in section 3, in section 4, research method is presented, data analysis and results are presented in section 5. The paper concludes in section 6.

2. Literature Review

Technology acceptance model (TAM) is used to study the adoption of technology (Lule et al., 2012). In addition, TAM is used to analyze how external factors affect internal beliefs, attitudes, and aims (Davis, 1989). The perceived Usefulness (U) and perceived Ease of Use (EoU) are two factors effecting users attitude toward using technology (A). There are external variables effecting the usefulness and ease of use (Davis et al., 1992). TAM is presented in Figure 1.

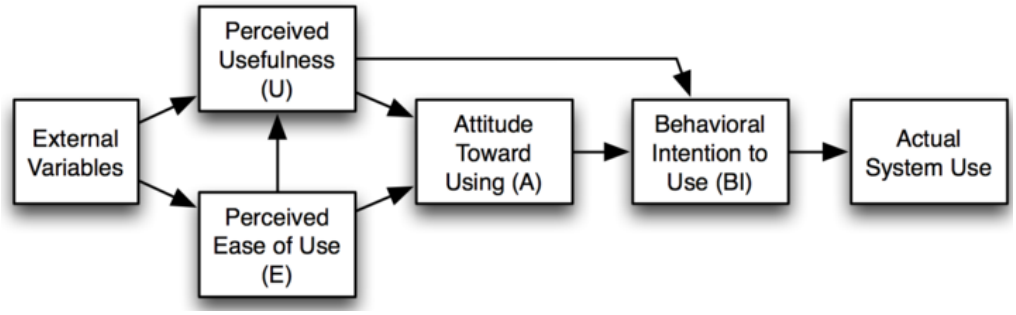

Figure 1. TAM (Davis, 1989)

Information Technology (IT) usage and adoption encompasses not only the simple use of hardware and software, but also the services that surround the IT, and the clients and procedures required for sustainability. E-service presents a singular chance to examine a user's interaction with a complex IT system (Alomari et al., 2012). The development of e-services and its adoption in Jordan has been recognized, and considered within the country's IT development vision. Jordan has embarked on two ambitious strategies that revolve around the development, deployment, and use of IT systems in Jordan.

The first strategy is a comprehensive plan to develop globally competitive software and IT service industry (Al-Shboul & ALsmadi, 2010). The second plan requires endeavors to stimulate the development of the IT service industry through public- and private-sector collaboration (Alomari et al., 2012). Most significantly, both initiatives are planned to complement public-sector reform projects that can be traced to Jordan's attempt during the 1990s to implement (a) the National Information System (NIS) to support public decision makers, planners, and policy makers in decision-making activities (Abdel-Rahim, 1998) and (b) to allow public administration modernization (Jreisat, 1997). Despite the substantial increase in the number of Internet users in Jordan and the high demand in the IT products, there is no reading for potential growth of e-services. Drawing upon these literatures, this paper theoretically builds a model based on a modified of TAM by adding new variables as the independent variables. The modification of the model and the selection of variables are based on a scenario of Jordan and considering the fact that e-services is still at its early stage in Jordan. The main research issues are:

- Deciding on the drivers of Jordanian users to accept e-services and engage in the online transaction behavior.
- Deciding whether and how to integrating TAM under the nomological structure of Theory of Reasoned Action (TRA) to jointly predict clients' online behavior.

3. Research Model and Hypothesis

This work has addressed a set of variables affecting e-service adoption which are not described in the TAM. Hence, TAM should be modified relating to the specific nature and uniqueness of e-services adoption, in which new variables have been included in the model as indicated in Table 1. This study integrates TAM with five additional variables to examine the implementation of e-services as shown in Figure 2 and Table 1. The perceived Usefulness, perceived Ease of Use, attitude to use and adoption were retained according to TAM. In addition, variables such as Credibility, Self-Efficacy, Trust, and Transaction Cost were included in this study.

Table 1. Descriptions of the constructs added to the original TAM

Construct	Definition
Behavioural Intention	Refers to a person's intention to perform a behaviour and is a function of Attitude and Perceived Usefulness (Lule et al., 2012) and (Davis, 1989).
Attitudes	Refers to individual's positive or negative evaluation of the behavior and is a function of Perceived Usefulness and Perceived Ease of Use (Lule et al., 2012) and (Davis, 1989).
Perceived Ease of Use (X_1)	Refers to person's beliefs that using a specific system would be free of effort (Lule et al., 2012) and (Davis, 1989).
Perceived Usefulness (X_2)	Discusses to a person's belief that using a system would increase his work performance (Lule et al., 2012) and (Davis, 1989).
Perceived Risk (X_3)	Touches to the possible to lose in the pursuance of a desired outcome of utilizing e-services (Al-Shafi & Weerakkody).
Perceived Trust (X_4)	Refers to the degree to which an individual has sufficient trust on the particular to place an order online and still take his financial info and other personal data in undertaking other financial transactions.
Perceived Credibility (X_5)	Refers to individual's behavioral intention to use the system. It contains security and privacy (Lule et al., 2012) and (Luarn & Lin, 2005).
Perceived Transaction Cost (X_6)	The transaction cost of using e-services (Luleet al., 2012) and (Luarn & Lin, 2005).
Perceived Self-Efficacy (X_7)	Means to the degree to which a person's trust in his capability to usage e-services (Lule et al., 2012) and (Bandura, 1982).

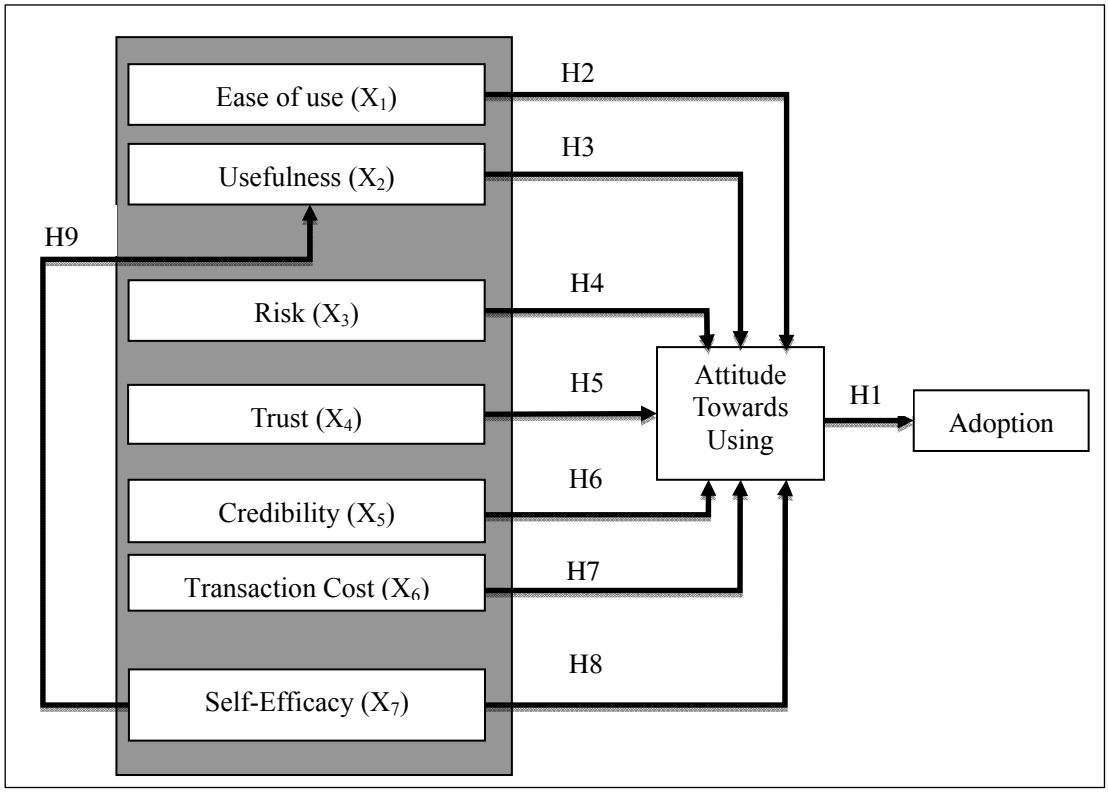

Figure 2. Proposed e-services adoption model

3.1 Attitude towards Using E-services (ATU)

TAM assumes that individuals' use of e-services is influenced by individual's intention to use such services, $X_1$and X_2 can predict the usage intention, and X_1 is hypothesized as a predictor of X_2. Transacting with e-services system requires the user to apply to this proposed scheme. Granting to the original TAM, it is anticipated that X_1 and X_2 of the scheme would be positively linked to the intention to transact with the system. Accordingly, the following hypotheses are presented:

H1: Individuals' attitude to employ e-services has no effect on behavioral intention to apply.

H2: Usefulness has no effect on attitude to employ e-services.

H3: Ease of use has no effect on attitude to employ e-services.

3.2 Perceived Risk (X_3)

The potential of being unsure about the certainty and accuracy of e-services transaction results, described as the perceived risk, will affect the clients' intention to transact with e-services system (Stone & Gronhaug, 1993). The original TAM tends to concentrate on the positive prospects of technology (X_1 and X_2). This weakens the explanatory power of TAM in circumstances where users' perceived risk degrades the system use. Accordingly, the following hypothesis is presented:

H4: The perceived risk has a significant negative effect on behavioral intention to use e-services.

3.3 Perceived Trust (X_4)

Various researchers have presented trust as an important component of e-services. It is believed that Trust creates positive attitudes and perceived behavioral control toward e-services, reducing uncertainty and providing expectations for a satisfactory transaction, thus positively influencing client behavioral intentions to transact. Hence, the following hypothesis is considered:

H5: The perceived trust will have a positive effect on attitude to employ e-services.

3.4 Perceived Credibility (X_5)

Credibility consists of privacy and security. Security is the protection of information from unauthorized users (Nysveen et al, 2005) and (Lule et al., 2012). Lack of security is one of the elements holding back the growth and development of e-services adoption. Hence, the following hypothesis is considered:

H6: Perceived credibility will have a negative effect on behavioral intention to utilize e-services.

3.5 Perceived Transaction Cost (X_6)

Transaction Cost is an essential factor that effect using e-services. If this factor is considered satisfactory for e-services users', then they are more likely to take and practice it (Lule et al., 2012). The transaction cost may prevent many users from choosing e-services. The following hypothesis is being considered:

H7: Transaction cost will have a positive effect on behavioral intention to utilize e-services.

3.6 Perceived Self Efficacy (X_7)

The Self Efficacy is an important factor in the adoption of e-services. Many research studies (Nysveen et al., 2005), (Wang et al., 2003) and (Mathioeson et al., 2004) have confirmed the significance of X_7 in technology acceptance. In these studies, X_7 affect the X_1 and assume that individuals' with higher degrees of X_7, will be more positive towards using e-services than others. Accordingly, the following hypotheses are considered:

H8: Self Efficacy has negative effect on attitude to the use e-services.

H9: Self Efficacy has negative effect on perceived ease of use of e-services

4. Research Methodology

The purpose of this work is to contribute to the extension of TAM within e-services context. Hence, attempts were made to prevent the research method from being similar to that employed by earlier studies on TAM (Gefen & Straub, 2004; Pavlou, 2003; Men et al., 2011). However, as noted above, the modification of the model and the selection of variables are based on Jordanian users' requirements and considering the fact that e-service in Jordan is yet in its early phase.

4.1 The Research Instrument

This research was conducted using a set of qualified and comprehensive questionnaire consisting of three main sections. The first section contained basic demographic characteristics including gender, age, measures for

assessing the degree of Internet usage, e-service's experience. In the second section, respondents were required to indicate the level of their risk, perception relative to the use of e-services. In the third part, the study participants were required to reply to inquiries on the other constructs of the model. For each section, Likert scale of five-point was employed.

4.2 Sample

The questionnaire was sent to 300 survey participants. In which, 265 replies were received with a response rate more than 80%, of which 261 completed and 4 uncompleted questionnaires were received.

4.3 Data Collection

The research work concentrated on how to measure factors contributing to e-services adoption from the users' perspective; based on their experience, requirements and intellect. The data needed for fulfilling this purpose was obtained using a quantitative approach. A survey questionnaire was chosen as the most appropriate research strategy in this work. In which, the collection of information from a large population was considered.

5. Results and Discussion

5.1 Descriptive Statistics

As noted above, 265 questionnaires were returned from study participants. Using relatively large sample size and hatching a can measure the external validity of the survey. Table 2 lists the sample demographics.

The data indicated that 77.8% of respondents are from the age group of (19-23) years. This was because young people are more likely to use the internet than older people in Jordan, according to the statistics of Jordan National Information Center in 2005. In addition, it is shown that female respondents have a higher percentage (58.3%) compared to male respondents. There are more respondents (95%) who have e-mail address and most of the respondents have Internet Access (88%). In addition, (75.1%) of the respondents have their internet connection from home. Lastly, and in terms of using e-services transaction, only (14.9%) of the respondents had online service experience. This conforms with previous research studies (Ment et al., 2011; Alghamdi et al., 2011; Yonazi et al., 2010; Colesca, 2009; Alawadhi & Morris, 2009; Zarmpou et al., 2011) which indicated that users are more comfortable in accepting and using new technology innovations, when they have prior related experience, which might be the case with Jordanian users. However, it is the purpose of this research to recover out the factors and barriers affecting such a low adoption rate of e-services transaction.

Table 2. Demographic attributes of the responders

Description	Variable	Result	Percentage
Gender	Male	109	41.7%
	Female	152	58.3%
Age	19-23 years	203	77.8%
	24-28	34	13%
	29-33	8	3.1%
	Up to 30	16	6.1%
Have an email address	Yes	248	95%
	No	13	5%
Internet Access	Yes	230	88 %
	No	31	12 %
Connect to the Internet	Home	196	75.1%
	Office	46	17.6%
	Internet Café	19	7.3%
Used the internet for e-services	Yes	39	14.9
	No	222	85.1

5.2 Reliability and Validity

To ascertain the reliability and strength of the survey, some measures are used when a questionnaire is designed. The reliability of the items is evaluated by Cronbach's alpha (Cronbach, 1951). Table 3 shows the results of the validity and reliability, representing suitable reliability.

Table 3. Reliability and validity analysis

Construct	# of Items (Questions in Questioners)	Reliability
Adoption (Y_1)	3	0.765
Attitudes Toward Using (Y_2)	5	0.724
Ease of Use (X_1)	4	0.797
Usefulness (X_2)	5	0.783
Risk (X_3)	4	0.782
Trust (X_4)	4	0.747
Credibility (X_5)	4	0.737
Transaction Cost (X_6)	4	0.756
Self-Efficacy (X_7)	4	0.771

Table 4. Correlation between Latent variables ($*10^{-2}$)

Variable		X_1	X_2	X_3	X_4	X_5	X_6	X_7	Y_2	Y_1
X_1	Q1	63	17	15	08	20	07	22	34	22
	Q2	75	14	22	06	13	13	18	22	24
	Q3	72	16	11	10	17	17	15	26	25
	Q4	68	18	12	09	18	10	12	18	23
X_2	Q1	24	72	21	12	21	17	11	17	24
	Q2	26	65	14	17	14	14	11	12	21
	Q3	22	75	09	21	09	12	17	09	14
	Q4	18	62	18	08	18	21	19	10	09
	Q5	19	68	19	09	19	15	21	12	18
X_3	Q1	23	19	56	11	15	23	14	21	19
	Q2	37	23	67	18	09	19	09	18	27
	Q3	19	21	58	09	18	21	18	21	17
	Q4	24	16	69	12	21	17	19	23	08
X_4	Q1	08	14	32	72	23	08	17	16	19
	Q2	09	21	27	64	16	09	16	29	09
	Q3	15	08	16	53	28	17	09	21	09
	Q4	09	11	18	58	17	12	18	08	18
X_5	Q1	07	15	21	11	56	09	14	19	18
	Q2	16	09	15	08	62	10	09	17	21
	Q3	21	12	09	19	57	12	18	21	23
	Q4	15	18	18	13	64	21	19	08	16
X_6	Q1	18	15	21	27	18	69	19	29	21
	Q2	05	19	23	24	15	72	23	21	21
	Q3	12	21	16	31	09	70	33	18	14
	Q4	14	07	21	13	18	69	21	19	09
X_7	Q1	09	17	23	18	21	19	62	21	18
	Q2	13	12	21	22	23	14	54	18	19
	Q3	14	09	15	19	16	18	56	25	15
	Q4	09	10	19	17	21	21	54	21	17
Y_2	Q1	17	12	18	16	23	21	17	54	12
	Q2	19	21	23	21	21	14	12	56	09
	Q3	21	24	26	25	17	09	09	61	10
	Q4	18	26	21	21	16	18	10	58	12
	Q5	23	19	16	24	18	19	12	60	21
Y_1	Q1	17	15	19	19	21	21	21	19	80
	Q2	18	17	23	16	09	08	14	18	78
	Q3	13	16	26	21	17	15	09	15	79

Convergent validity is considered to confirm that each item correlates to hypothetical assumption, validity needs to fit within Average Variance Extracted (AVE) (Lule et al., 2012). This validity is extended out to determine that square base of AVE should be higher than any correlation between any couple of latent variables. The correlation between latent variable and AVE are represented in Tables 4 and 5.

Table 5. AVE ad Square Root AVE

Variables	AVE*10^{-3}	Square Root AVE *10^{-3}
X_1	655	764
X_2	694	798
X_3	543	675
X_4	672	714
X_5	581	636
X_6	723	758
X_7	623	670
Y_2	427	625
Y_1	783	875

5.3 Model Validity and Hypotheses Testing

A various modifications for proposed model are carried out by analysis test. Table 6, presents the fit measures for the proposed model. The overall fit for Chi-Square/Degree Freedom for Model (CSM/DFM) is 2.615 (less than 3) significant and P value 0.

Table 6. Fit measures of the proposed model

Fit Measures	Standards Fit	Model Fit
Chi-Square for Model (CSM)		81.350
Degree Freedom for Model (DFM)		29.734
Chi-Square/Degree Freedom for Model (CSM/DFM)	Fit when value approximately = 1 and ≤ 3 fit.	2.736
Incremental Fit Index (IFI)	Fit when value approximately = 1	0.871
Tucker-Lewis Index (TLI)	Fit when value approximately = 1	0.867
Normed Fit Index (NFI)	Fit when value approximately = 1	0.852
Comparative Fit Index (CFI)	Fit when value approximately = 1	0.893
Relative Fit Index (RFI)	Fit when value approximately = 1	0.826
Root Mean-Square Error of Approximation (RMSEA)	Fit when value ≤ 0.1	0.078

5.4 Hypotheses Analyses

Analysis of variance (ANOVA) is applied to examine the proposed theories. The results in Table 7 represent the test hypothesis by using ANOVA, based on the significant level of (0.05). The hypothesis is accepted if the significance level was more than (0.05).

To determine the relationships among the variables, β is very important as it compares the contribution of each independent variable for explaining the dependent variable. A large value indicates that a unit change in this predictor or independent variable has a large effect on the dependent variable. The t and Sig (p) values give a rough indication for the impact of each predictor variable, a big absolute t value > 3 and small p value ≤ 0.05, suggests that a predictor variable is having a large impact on the criterion variable (Hair et al., 2005).

As a result, in Table 7, the variance in e-services adoption accounted by user's attitude is 8.2%, the t value is 14.2, and the H1 is rejected because t value is greater than 0.05. This pointed out that user's attitude to use e-services affects the behavioral intention to use. In addition, Table 7 shows that 9.5% of the variance in user perspective of e-services adoption accounted by easy to use, the t value is 15.3, hence H2 is rejected because t value is greater than 0.05. This indicates that usefulness has a direct effect on using e-services. In addition, results has described 8.4 % disagreement in user viewpoint towards e-services usefulness, the t value is 14.4, hence H3 is rejected because t value is greater than 0.05. This point indicated that the ease of use has a substantial influence on attitude to use e-services.

The correlation between perceived risk and intention to use e-services (H4), is also supported (β: 2.1%, t: 12.2, sig: 0:000). This implies that if the users consider using e-services is risky, the intention to e-services adoption will be low. H5, measures the correlation between the trust and the intention of using e-services, is supported (β: 8.3%, t: 14.5 sig: 0:000). This indicates that if the users consider using e-services is trustworthy, the intention of e-services adoption will be high. H6, which indicates perceived credibility will have a negative effect on behavioral intention to utilize e-services, (β: 8.1%, t: 14.1 sig: 0:000). H6 is rejected because t value is greater than 0.05. Moreover, 2.3% of the variance in user perspective of e-services adoption is accounted by cost, the t value is 11.2, and the H7 is rejected because t value is greater than 0.05. This confirms that there is an effect of cost on e-services adoption, this result is supported by previous studies. At last, perceived credibility and Self Efficacy has an important influence on attitude to the use e-services. Therefore, H8 and H9 are rejected because t value is greater than 0.05.

Table 7. Summary of the regression results and test of hypotheses

Hypotheses	Independent Variables	Dependent variables	B	T	Sig p	Support
H1	User's attitude to use e-services	Intention to Usage	0.082	14.2	0.00	Yes
H2	Ease of use	Attitude to Use E-Services	0.095	15.3	0.00	Yes
H3	Perceived Usefulness	Attitude to Use E-Services	0.084	14.4	0.00	Yes
H4	Perceived Risk	Attitude to use E-Services	0.021	12.2	0.00	Yes
H5	Perceived Trust	Attitude to Use E-Services	0.083	14.5	0.00	Yes
H6	Perceived Credibility	Attitude to Use E-Services	0.081	14.1	0.00	Yes
H7	Perceived Cost	Attitude to Use E-Services	0.023	11.2	0.00	Yes
H8	Perceived Self-Efficacy	Attitude to Use E-Services	0.078	13.8	0.00	Yes
H9	Perceived Self-Efficacy	Ease of Use E-Services	0.076	13.6	0.00	Yes

6. Conclusion

This research work has described a theoretical model for investigating factors influencing Jordanian clients' adoption of e-services. These factors correspond to a set of hypotheses used to determine the pertinence of the theoretical model. E-services successful implementation was determined by users' behavior while dealing with electronic arrangements being experienced during the evaluation study. An intensive questionnaire was used within the evaluation study and ANOVA statistical analysis was used to confirm or reject the proposed model hypothesis. Results have described major e-services adoption and acceptance determinants. In addition, empirical results explain interesting insights into factors affecting users' intention toward e-services adoption, taking into consideration Jordanian users' requirements. It was measured that that ease of use, usefulness, credibility, self-efficacy and trust had positive effects on the e-services adoption in Jordan. However, e-services

deployment risk and utilization cost have a negative influence towards using and adopting e-services. In addition, users' capability including self efficiency is significantly related to perceived usefulness and ease of use.

Based on these conclusions, the successful adoption of e-services in Jordan implies considering more attention on cost, security and information privacy. In addition, user's capability concerns and preferences, are required to be addressed while designing and developing e-services. The awareness and understanding of e-services needs to be increased and new policies needs to be adopted allowing for an simple transition from tradition to digital systems.

References

Abdel-Rahim, S. (1998). The impact of the information revolution on society and state in Jordan. *The information revolution and the Arab World* (pp. 160-175).

Alateyah, S., Crowder, R., & Wills, G., (2013). An Exploratory study of proposed factors to Adopt e-government Services Saudi Arabia as a case study. *International Journal of Advanced Computer Science and Applications, 4*(11), 57-66.

AlAwadhi, S., & Morris, A. (2009). Factors influencing the adoption of e-government services. *Journal of Software, 4*, 584-590.

Al-Ghaith, W., Sanzogni, L., & Sandhu, K. (2010). Factors Influencing The Adoption And Usage Of Online Services In Saudi Arabia. *The Electronic Journal on Information Systems in Developing Countries EJISDC, 40*(1), 1-32.

Alghamdi, I., Goodwin, R., & Rampersad, F. (2011). E-government readiness assessment for government organizations in developing countries. *Computer and Information Science, 4*, 3-17. http://dx.doi.org/10.5539/cis.v4n3p3

Alomari, M. K., Woods, P., & Sandhu, K. (2012). Predictors for e-government adoption in jordan: Deployment of an empirical evaluation based on a citizen-centric approach. *Information Technology & People, 25*(2), 207-234. http://dx.doi.org/10.1108/09593841211232712

Al-Shafi, S., & Weerakkody, V. (2010). Factors affecting e-government adoption in the state of Qatar. *European and Mediterranean Conference on Information Systems (Emcis)* (pp. 1-23). Abu Dhabi, UAE, April 12-13 (2010).

Al-Shboul, M., & Alsmadi, I. (2010). Jordan E-Government Challenges and Progresses. *International Journal of Advanced Cooperating Learning, 3*(1), 37-41.

Bandura, A. (1982). Self-Efficacy mechanism in Human Agency. *American Psychologist, 37*(2), 122-147. http://dx.doi.org/10.1037/0003-066X.37.2.122

Colesca, S. E. (2009). Increasing e-trust: A solution to minimize risk in e-government adoption. *Journal of Applied Quantitative Methods, 4*, 31-44.

Cronbach, L. J. (1951). Coefficient alpha and the internal structure of tests. *Psychometrika, 16*, 297-333. http://dx.doi.org/10.1007/BF02310555

Davis, F. D. (1989). Perceived Usefulness, Perceived Ease of Use, and User Acceptance of Information Technology. *MIS Quarterly, 13*(3), 319-339. http://dx.doi.org/10.2307/249008

Davis, F. D., Bagozzi, R. P., & Warshaw, P. R. (1992). Extrinsic and Intrinsic Motivation to Use Computers in the Workplace. *Journal of Applied Social Psychology, 22*(14), 1111-1132. http://dx.doi.org/10.1111/j.1559-1816.1992.tb00945.x

Gefen, D., & Straub, D. W. (2004). Consumer Trust in B2C e-Commerce and the Importance of Social Presence: Experiments in e-2 Products and e-Services. *Omega: The International Journal of Management Science, 32*(6), 407-424.

Hair, J. F. (2005). *Multivariate data analysis*. Upper Saddle River: Pearson, Prentice Hall.

Jreisat, J. E. (1997). *Politics without process: Administering Development in the Arab World*. Lynne Rienner Publishers.

Luarn, P., & Lin, H. H. (2005). Toward an understanding of the behavioral intention to use mobile banking. *Computers in Human Behavior, 21*, 873-891. http://dx.doi.org/10.1016/j.chb.2004.03.003

Lule, I., Omwansa, T., & Waema, M. (2012). Application of Technology Acceptance Model (TAM) in M-Banking Adoption in Kenya. *International Journal of Computing and ICT Research, 6*(1), 31-43.

Mathieson, K., Peacock, E., & Chin., W. W. (2001). Extending the technology acceptance model: The influence of perceived user resources. *Data Base for Advances in Information Systems, 32*(3), 86-112. http://dx.doi.org/10.1145/506724.506730

Nysveen, H., Pedersen, P. E., & Thorbjornsen, H. (2005). Intentions to Use Mobile Services: Antecedents and Cross-Service Comparisons. *Journal of the Academy of Marketing Science, 33*(3), 330-346. http://dx.doi.org/10.1177/0092070305276149

Pavlou, P. A. (2003). Consumer Acceptance of Electronic Commerce: Integrating Trust and Risk with the Technology Acceptance. *International Journal of Electronic Commerce, 7*(3), 101-134.

Pi, S. M., Liao, H. L., & Chen, H. M. (2012). Factors that affect consumers' trust and continuous adoption of online financial services. *International Journal of Business and Management, 7*, 108-119. http://dx.doi.org/10.5539/ijbm.v7n9p108

Seng Wong, M., Hideki, N., & George, P. (2011). The use of importance-performance analysis (ipa) in evaluating japan's e-government services. *Journal of Theoretical and Applied Electronic Commerce Research, 6*, 17-30.

Stone, R. N., & Gronhaug, K. (1993). Perceived Risk: Further Considerations for the Marketing Discipline. *European Journal of Marketing, 27*(3), 39-50. http://dx.doi.org/10.1108/03090569310026637

Taylor, S., & Todd, P. (1995). Assessing IT Usage: The Role of Prior Experience. *MIS Quarterly, 19*(4), 561-570. http://dx.doi.org/10.2307/249633

Wang, Y. S., Wang, Y. M., Lin, H. H., & Tang, T. I. (2003).Determinants of user acceptance of internet banking: An empirical study. *International Journal of Service Industry Management, 14*(5), 501-519. http://dx.doi.org/10.1108/09564230310500192

Yonazi, J., Sol, H., & Boonstra, A. (2010). Exploring issues underlying citizen adoption of e-government initiatives in developing countries: The case of Tanzania. *Electronic Journal of e-Government, 8*, 176-188.

Zarmpou, T., Saprikis, V., & Vlachopoulou, M. (2011). Examining Behavioral Intention toward Mobile Services: An Empirical Investigation in Greece. *International Journal of E-Services and Mobile Applications, 3*(2), 1-19. http://dx.doi.org/10.4018/jesma.2011040101

Modern Applied Science; Vol. 8, No. 3; 2014
ISSN 1913-1844 E-ISSN 1913-1852
Published by Canadian Center of Science and Education

On the Use of Multidimensional Data Analysis Techniques for Corporate Valuation

Georgeta Vintilă[1] & Ştefan Cristian Gherghina[1]

[1] Department of Finance, Bucharest University of Economic Studies, Bucharest, Romania

Correspondence: Ştefan Cristian Gherghina, Bucharest University of Economic Studies, 6 Romana Square, district 1, 010374, Bucharest, Romania. Tel: 40-21-319-1900. E-mail: stefan.gherghina@fin.ase.ro

Received: March 12, 2014 Accepted: April 4, 2014 Online Published: May 5, 2014

doi:10.5539/mas.v8n3p202 URL: http://dx.doi.org/10.5539/mas.v8n3p202

Abstract

The aim of this research consists in the investigation of a random sample of companies which belong to five European emerging countries, respectively Hungary, Poland, Russia, Slovakia, and Ukraine, from the valuation perspective, by using multidimensional data analysis techniques. Thus, by employing the principal component analysis, after transforming the initial characteristics there resulted two principal components, also considering the restriction of minimizing the loss of information. Subsequently, by the instrumentality of factor analysis, there resulted two factors required to explain the correlations existing between variables. The usefulness of both multidimensional data analysis techniques emerges from the reduction of the significant number of variables in a lesser number of principal components, respectively factors.

Keywords: principal component analysis, factor analysis, eigenvalues, eigenvectors, firm value

1. Introduction

Often, in order to establish the value of a given company we could own an exhaustive set of indicators from financial statements or which could be computed based on financial reports. However, the significant dimensionality of the employed measures with the purpose previously mentioned, frequently conduct to the impairment of the valuation process. On the other hand, the availability of more indicators in order to reflect firm value could support contradictory results. Besides, the task of the valuator could be more facile if the indicators used would be reduced to some components as linear combinations of the original variables. Thus, applying the principal component analysis could represent a proper technique in order to facilitate the evaluation process. Likewise, by employing the factor analysis we will identify the essential factors through which we could explain the interdependencies existing between the indicator variables represented by the valuation ratios. This paper aims at exploring a random sample of companies which belong to five European emerging countries, respectively Hungary, Poland, Russia, Slovakia, and Ukraine, in order to determine their value, by using the aforementioned multidimensional data analysis techniques. The novelty of current research consists in using SAS 9.2 by the valuators in order to establish the value of the companies. SAS (Statistical Analysis System)is a software suite which began at North Carolina State University as a project to analyze agricultural research. Since demand for such software grew, SAS was founded in 1976 to help all sorts of customers, from pharmaceutical companies and banks to academic and governmental entities. The utility of current paper consists inthe reduction of the significant number of variables in a lesser number of principal components, respectively factors.

The rest of this paper proceeds as follows. In Section 2 we emphasize the numerous important applications of multidimensional data analysis techniques, while Section 3 describes the data and the research methodology, as well as the fundamentals of principal component analysis and factor analysis. The results of the empirical research are presented in Section 4, while Section 5 concludes the paper.

2. The Applications of Multidimensional Data Analysis Techniques

Principal component analysis (hereafter PCA) technique was developed by Pearson (1901), having a great usefulness in the exploratory data analysis and in the achievement of the prediction models. Depending on the field of application, this multidimensional data analysis technique is also named the discrete Karhunen-Loève transform (KLT), the Hotelling transform, or the proper orthogonal decomposition (POD). In fact, there are many fields such as ecology, chemometrics, or economy, where multivariate analyses are employed in order to

describe and summarize large data sets by removing any redundancy existing in the data (Dray, 2008; Zou, Hastie & Tibshirani, 2006). Likewise, PCA is the most popular multivariate statistical technique used by almost all scientific disciplines (Abdi & Williams, 2010) and the simplest multivariate method (Jackson, 1993). Thereby, we acknowledge numerous important applications such as human face recognition (Hancock, Burton & Bruce, 1996) or handwritten zip code classification (Hastie, Tibshirani & Friedman, 2009). We emphasize that PCA was employed on facial images and bounded these to human performance on recognition of own and other-race facial images (O'Toole, Deffenbacher, Valentin & Abdi, 1994). Withal, PCA was used in gene expression data analysis (Alter, Brown & Botstein, 2000). Subsequently, the gene shaving method was employed to analyze gene expression measurements based on samples from patients with diffuse large B-cell lymphoma (Hastie et al., 2000). Thus, the gene shaving technique using PCA identified a small cluster of genes whose expression was highly predictive of survival. In the financial field, PCA is widely used thanks to its multiple applications. Thus, this technique was employed in order to estimate the bankruptcy risk (Altman, 1968; Conan & Holder, 1979). Further, bankruptcy prediction models recorded a broader usage. Also, Meric, Leal, Ratner, & Meric (2001) examined the possibilities of international portfolio diversification through investment in the principal capital markets from Latin America. Leger and Leone (2008) analysed the economic variables which could help to explain the principal components in UK stock returns.

Factor analysis (hereafter FA) was introduced by the American psychologist Thurstone (1931). Accordingly, exploratory factor analysis (EFA) is an important tool for organizational researchers (Conway & Huffcutt, 2003). Thus, Ford, MacCallum and Tait (1986) investigated the application of EFA as regards 152 studies published in the Journal of Applied Psychology, Personnel Psychology, and Organizational Behavior and Human Performance, over the period 1975-1984. The results showed the fact that the components model was the most popular factor model employed (N=64; 42.1 percent), in contrast to common factor model (N=52; 34.2 percent), whereas in 36 papers (23.7 percent) was impossible to determine which factor model was used. As well, Fabrigar, Wegener, MacCallum and Strahan (1999) reported for Journal of Applied Psychology, over the period 1991-1995, that PCA was used in 48.3 percent of the cases in contrast to common factors (22.4 percent), whilst in 25.9 percent of the cases the factor extraction model was unknown. Park, Dailey, & Lemus (2002) reviewed the articles published in three major communication journals: Human Communication Research, Communication Monographs, and Communications Research, from 1990 to 2000, and found an usage of principal component analysis in 52.94 percent of cases, common factors in 11.76 percent of papers, while 31.93 percent did not specify the type of analysis. As regards financial investigations, since the research of FA pioneers (Pinches, Mingo,& Caruthers, 1972) which tried to realize a classification of financial ratios related to US industrial firms, FA is used as a way in order to remove the redundancy and to reduce the number of financial ratios required for empirical researches. Therefore, Ali and Charbaji (1994) used this technique within the international commercial airlines sector to reduce 42 financial ratios to five underlying factors. Tan, Koh and Low (1997) applied FA for the companies listed on the Stock Exchange of Singapore, thus reducing 29 financial ratios to eight underlying factors. De, Bandyopadhyay and Chakraborty (2011) employed FA for a set of 44 financial ratios corresponding to a sample of companies from the Indian iron and steel industry and derived eight underlying factors.

Thus, compared with previous studies, our paper employs multidimensional data analysis techniques in order to determine the value of a random sample of companies out of European emerging countries. Firm value is very important for individual investors since it reflects the underlying value of their stake in an enterprise. As the estimated value is more accurate, the investors could take the proper investment decisions, respectively to sell, to buy, or to maintain their holdings.

3. Data and Research Methodology

The aim of this research consists in the valuation of a random sample of companies which belong to five European emerging countries. Thus, the randomly selected sample comprises 310 companies as follows: 11 companies from Hungary, 125 companies from Poland, 89 companies from Russia, 5 companies from Slovakia, and 80 companies from Ukraine. Thereby, in order to evaluate the selected companies we will use ten financial ratios which were computed based on the data from financial statements of the companies, the values corresponding to 2009. The indicators employed and their computation method will be described below. The financial statement data was provided by ISI Emerging Markets. We will use the software instrument SAS 9.2 in order to apply the multidimensional data analysis techniques. We will employ the **PRINCOMP** procedure in order to perform principal component analysis, as well **PROC FACTOR** statement towards factor analysis (Delwiche & Slaughter, 2008; Fernandez, 2010).

I1: DE = the debt to equity ratio, calculated through dividing total liabilities by stockholders' equity. Also known as global financial autonomy, this indicator assesses the size of external funds compared with the funds from shareholders;

I2: DTA = the debt to total assets ratio. Also known as the general indebtednessratio, this indicator reflects the means in which the company's assets are financed by debt;

I3: LEV = the financial debt to equity ratio signifies financial leverage ratio, through which is reflected the financial managers' ability to collect outside resources in order to stimulate the equity' efficiency;

I4: EPS = earnings per share or the internal return of a certain share in terms of the income which is generated by that share in a financial year, is computed through dividing net income by total number of capital stock shares. This ratio allows the investors to compare the results recorded by the company in order to decide if the owned capital stock shares will be kept, cleared, or raised;

I5: PER = price/earnings ratio, computed by dividing the company's current share price by its per-share earnings, is showing the market return of a certain share in terms of the amount which the investors are willing to pay per dollar of company's earnings. Also, this ratio shows the period required to a shareholder in order to recover the invested capital;

I6: ROS = return on sales is the ratio of net income before interest and tax divided by net sales, usually reported in percentage. On the one hand, ROS highlights the part of each dollar of sales that the company is able to turn into income. On the other hand, ROS shows the contribution of company's income in order to strengthen the self-financing ability;

I7: CR = current ratio is the ratio of current assets recorded in the balance sheet of a particular company for a given period of time divided by its current liabilities (short-term liabilities). This indicator reflects the possibility of current patrimonial elements to transform into liquidity in a short time in order to pay the current liabilities;

I8: QR = quick ratio, also known the Acid-test ratio is calculated as the difference between current assets and inventory, divided by current liabilities. This indicator reflects the possibility of current assets represented by accounts receivable and short-term investments to cover the current liabilities;

I9: ROA = return on assets is computed by dividing the company's income after interest and tax by its total assets. This indicator shows the efficiency recorded in company's assets utilization;

I10: ROE = return on equity is equal to net income divided by shareholders' equity. The contribution of shareholders in order to finance the company is measured through shareholders' equity, thus return on equity reflecting the efficiency of the company at generating profits from every unit of shareholders' equity.

3.1 Principal Component Analysis Description

By employing the multidimensional data analysis technique entitled principal component analysis, there will result the decomposition of total variability from the initial causal space through a reduced number of components. However, this decomposition will not contain informational redundancy. Thus, it is followed a collapse of the variables to a reduced number of composite variables. By the instrumentality of PCA our purpose is to synthesize the distinctions amongst the 310 selected companies, existing at the ten researched factors, through a reduced number of components which are uncorrelated.

The principal components are abstract vector variables defined as linear combinations of the original variables, characterized by the following two fundamental properties: the principal components are uncorrelated two by two, and the sum of squares of the coefficients which define the linear combination corresponding to a principal component is equal to one. Peres-Neto, Jackson and Somers (2005) noticed that detecting certain relationships by generating linear combinations of variables showing common trends of variation exhibit a significant scientific contribution as regards the recognition of patterns in the data. Thus, the first principal component is a linear normalized combination whose variance is maximum. The second principal component is an uncorrelated linear combination with the first principal component, whose variance is as high as possible, but lesser than the variance of the first principal component. The initial causal space subject to our research is figured by ten explanatory variables x_1, x_2, …, x_9, x_{10}, thus signifying the fact that each of the 310 companies is evaluated by ten financial indicators, as defined previously.

The principal components corresponding to the researched causal space are described through a vector with ten dimensions, labeled with w:

$$w = \begin{pmatrix} w_1 \\ w_2 \\ \cdots \\ w_9 \\ w_{10} \end{pmatrix} \quad (1)$$

Each coordinate w_i of this vector represents a principal component defined compared with the original variables through the following linear combination:

$$w_i = \alpha_1^{(i)} * x_1 + \alpha_2^{(i)} * x_2 + \ldots + \alpha_9^{(i)} * x_9 + \alpha_{10}^{(i)} * x_{10} \quad i = 1, 2, \ldots, 9, 10 \quad (2)$$

The coefficients $\alpha_j^{(i)}$ are the coordinates of the eigenvectors corresponding to the covariance matrix of the original variables $x_1, x_2, \ldots, x_9, x_{10}$, while the principal components' variances are the eigenvalues of this matrix.

Thereby, it is followed to solve the following extreme problem. Depending on the type of the function ϕ, the optimum criterion could be maximum or minimum.

$$\begin{cases} \text{Opt } \phi(x, w) \\ w = A^T * x \end{cases} \quad (3)$$

We will consider the fact that the vectors $\alpha^{(i)}$ are the columns of matrix A of dimensions 10×10, having the following form:

$$A = \begin{pmatrix} \alpha_1^{(1)} \alpha_1^{(2)} \cdots \alpha_1^{(9)} \alpha_1^{(10)} \\ \ldots \quad \ldots \quad \cdots \quad \ldots \quad \ldots \\ \alpha_{10}^{(1)} \alpha_{10}^{(2)} \cdots \alpha_{10}^{(9)} \alpha_{10}^{(10)} \end{pmatrix} \quad (4)$$

Besides, we will suppose the fact that x is the vector whose coordinates are the original variables $x_1, x_2, \ldots, x_9, x_{10}$, whereas w is the vector whose coordinates are the principal components $w_1, w_2, \ldots, w_9, w_{10}$.

Thus, the linear combinations which define the principal components could be represented as below:

$$\begin{cases} w_1 = \alpha_1^{(1)} * x_1 + \alpha_2^{(1)} * x_2 + \cdots + \alpha_9^{(1)} * x_9 + \alpha_{10}^{(1)} * x_{10} \\ w_2 = \alpha_1^{(2)} * x_1 + \alpha_2^{(2)} * x_2 + \cdots + \alpha_9^{(2)} * x_9 + \alpha_{10}^{(2)} * x_{10} \\ \ldots\ldots\ldots\ldots\ldots\ldots\ldots\ldots\ldots\ldots\ldots\ldots\ldots\ldots\ldots\ldots\ldots\ldots\ldots\ldots\ldots\ldots\ldots\ldots\ldots\ldots\ldots\ldots \\ w_9 = \alpha_1^{(9)} * x_1 + \alpha_2^{(9)} * x_2 + \cdots + \alpha_9^{(9)} * x_9 + \alpha_{10}^{(9)} * x_{10} \\ w_{10} = \alpha_1^{(10)} * x_1 + \alpha_2^{(10)} * x_2 + \cdots + \alpha_9^{(10)} * x_9 + \alpha_{10}^{(10)} * x_{10} \end{cases} \quad (5)$$

Under matrix form, the linear combinations related to the principal components could be represented as follows:

$$\begin{pmatrix} w_1 \\ w_2 \\ \cdots \\ w_9 \\ w_{10} \end{pmatrix} = \begin{pmatrix} \alpha_1^{(1)} & \alpha_2^{(1)} & \ldots & \alpha_9^{(1)} & \alpha_{10}^{(1)} \\ \alpha_1^{(2)} & \alpha_2^{(2)} & \cdots & \alpha_9^{(2)} & \alpha_{10}^{(2)} \\ \ldots & \ldots & \cdots & \ldots & \ldots \\ \alpha_1^{(2)} & \alpha_2^{(2)} & \cdots & \alpha_9^{(2)} & \alpha_{10}^{(2)} \\ \alpha_1^{(10)} & \alpha_2^{(10)} & \cdots & \alpha_9^{(10)} & \alpha_{10}^{(10)} \end{pmatrix} * \begin{pmatrix} x_1 \\ x_2 \\ \cdots \\ x_9 \\ x_{10} \end{pmatrix} \quad (6)$$

The mathematical model of principal component analysis is defined as follows:

$$\begin{cases} \max \text{Var}(w) \\ w = A^T * x \end{cases} \quad (7)$$

3.2 Factor Analysis Description

The multidimensional data analysis technique entitled factor analysis is employed in order to explain the correlations between several variables named indicators, by the instrumentality of a lower number of sorted and uncorellated factors, named common factors. However, the common factor represents a fundamental concept within factor analysis which could be considered as a random variable with a certain probability distribution. Likewise, with the aim of numerical valuations' achievement we distinguish the variable entitled indicator, whose observations are known as scores. Additionally, the indicators have associated unique factors. The unique factor is exerting the influence in a one-sided manner on a single indicator (measured) variable. Besides, the unique factor could not be subject to a direct observation and measurement process. Outside the influence exerted by the common factor and by the unique factor, we distinguish in addition the influence of the measurement errors, considered negligible.

The factor model has the following mathematical form, considering the fact that the measured variables are marked with x_j, the common factors are marked with f_j, the unique factors are marked with u_j, while a_{ij} represents the intensity of the common factor f_j compared with the measured variable x_j:

$$\begin{cases} x_1 = a_{1.1} * f_1 + a_{1.2} * f_2 + \cdots + a_{1.9} * f_9 + a_{1.10} * f_{10} + a_1 * u_1 \\ x_2 = a_{2.1} * f_1 + a_{2.2} * f_2 + \cdots + a_{2.9} * f_9 + a_{2.10} * f_{10} + a_2 * u_2 \\ \cdots\cdots\cdots\cdots\cdots\cdots\cdots\cdots\cdots\cdots\cdots\cdots\cdots\cdots\cdots\cdots\cdots\cdots\cdots\cdots\cdots \\ x_9 = a_{9.1} * f_1 + a_{9.2} * f_2 + \cdots + a_{9.9} * f_9 + a_{9.10} * f_{10} + a_9 * u_9 \\ x_{10} = a_{10.1} * f_1 + a_{10.2} * f_2 + \cdots + a_{10.9} * f_9 + a_{10.10} * f_{10} + a_{10} * u_{10} \end{cases} \quad (8)$$

Under matrix form, the factor model has the following representation:

$$x = F*f + D*u \quad (9)$$

$$\begin{pmatrix} x_1 \\ x_2 \\ \cdots \\ x_9 \\ x_{10} \end{pmatrix} = \begin{pmatrix} a_{1.1} \cdots a_{1.10} \\ a_{2.1} \cdots a_{2.10} \\ \cdots \quad \cdots \quad \cdots \\ a_{9.1} \cdots a_{9.10} \\ a_{10.1} \cdots a_{10.10} \end{pmatrix} * \begin{pmatrix} f_1 \\ f_2 \\ \cdots \\ f_9 \\ f_{10} \end{pmatrix} + \begin{pmatrix} a_1 \cdots 0 \\ 0 \cdots 0 \\ \cdots \cdots \cdots \\ 0 \cdots 0 \\ 0 \cdots a_{10} \end{pmatrix} * \begin{pmatrix} u_1 \\ u_2 \\ \cdots \\ u_9 \\ u_{10} \end{pmatrix} \quad (10)$$

However, unlike principal component analysis in the context of which the variability that characterizes the initial causal space is undifferentiated considered, in factor analysis, the variability of the initial causal space is considered as a composition of variances which are constituted under the influence of the factors previously mentioned. The variance σ_j^2 related to the variable x_j could be shared in three important components: the communality h_j^2 (that part of the total variance σ_j^2 that explains the information which is common to all the variables which define the causal space and which are forming under the influence of common factors), the uniqueness a_j^2 (that part of the total variance σ_j^2 that expresses significant information of specific type which characterizes the particular variable x_j and which is constituted under the influence of the unique factor), and the residuality e_j^2 (that part of the total variance σ_j^2 which is formed under the influence of the residual factor that is associated with the considered variable and which shows insignificant information with specific feature related to the variable x_j).

4. Empirical Research Results

4.1 The Results of the Principal Component Analysis

The script related to the principal component analysis employed in SAS 9.2 is showed in Apendix . The covariance matrix of the original variables is presented in Table 1. However, the covariance matrix is very important within current empirical research due to the principal components' properties. The total variance recorded is **26.4257**.

Table 1. Covariance matrix

Variable	DE	DTA	LEV	EPS	PER	ROS	CR	QR	ROA	ROE
DE	14.7157	0.3548	2.2354	-0.0288	-0.3265	-0.0118	-0.4418	-0.2174	-0.0529	-0.8544
DTA	0.3548	0.0628	0.1268	-0.0019	-0.0305	0.0028	-0.1907	-0.1579	-0.0085	-0.0190
LEV	2.2354	0.1268	3.6779	-0.0025	-0.0270	0.0712	-0.3715	-0.3432	-0.0018	-0.0614
EPS	-0.0288	-0.0019	-0.0025	0.0041	0.0016	0.0055	-0.0051	-0.0037	0.0024	0.0051
PER	-0.3265	-0.0305	-0.0270	0.0016	0.7399	0.1380	0.0065	-0.0051	0.0041	0.0189
ROS	-0.0118	0.0028	0.0712	0.0055	0.1380	0.9886	0.0057	-0.0112	0.0262	0.0515
CR	-0.4418	-0.1907	-0.3715	-0.0051	0.0065	0.0057	3.4419	2.8056	0.0327	0.0745
QR	-0.2175	-0.1579	-0.3432	-0.0037	-0.0051	-0.0112	2.8056	2.5909	0.0249	0.0501
ROA	-0.0529	-0.0085	-0.0018	0.0024	0.0041	0.0262	0.0327	0.0249	0.0102	0.0227
ROE	-0.8544	-0.0190	-0.0614	0.0051	0.0189	0.0515	0.0745	0.0501	0.0227	0.1938

The principal components are sorted in Table 2 in a descending order of the retained information as percentage from the total variance. The column entitled **Proportion** highlights the percentage out of the initial information of each variable from the ten selected variables, which is synthesized in the extracted principal components.

Thereby, the first principal component explains about 57.72 percent out of the total variance, the second principal component explains about 22.29 percent out of the total variance, the third principal component explains about 12.06 percent out of the total variance, while the fourth principal component explains about 3.97 percent out of the total variance. As well, the first four principal components record eigenvalues greater than one, values which could be noticed in the **Eigenvalue** column. However, the first four principal components cumulate 96.05 percent out of total information, fact presented in the **Cumulative** column. Thus, if it is added a new principal component there would result 98.60 percent out of total information.

Table 2. Eigenvalues of the covariance matrix

	Eigenvalue	Difference	Proportion	Cumulative
1	15.2523	9.3610	0.5772	0.5772
2	5.8914	2.7033	0.2229	0.8001
3	3.1881	2.1393	0.1206	0.9208
4	1.0488	0.3748	0.0397	0.9605
5	0.6740	0.4968	0.0255	0.9860
6	0.1772	0.0366	0.0067	0.9927
7	0.1406	0.0968	0.0053	0.9980
8	0.0438	0.0373	0.0017	0.9996
9	0.0065	0.0036	0.0002	0.9999
10	0.0030		0.0001	1.0000

The both of graphs showed in Figure 1, proposed by Cattell (1966), are used in order to establish the number of principal components. Thus, in the first graph is remarked that after the second point which symbolizes the second principal component, the slope decreases. However, we could retain two principal components.

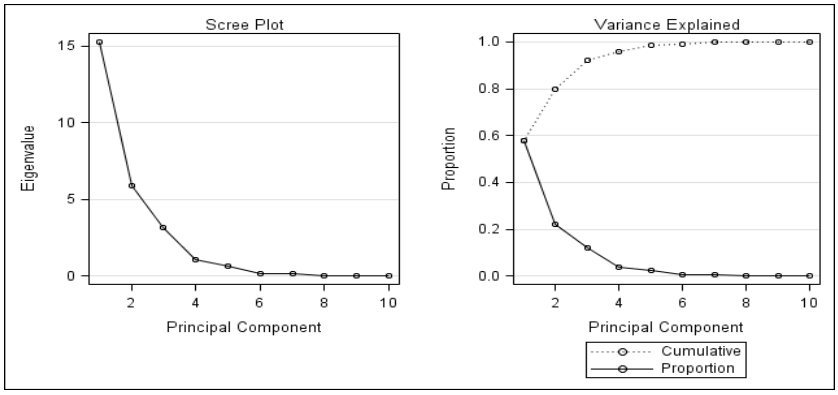

Figure 1. Eigenvalue plot

The number of principal components which are retained in the analysis is determined based on a cut in the graph parallel with the ordinate. Thereby, the number of principal components is the first number from the left of the cut so the part of the graph from the right of the cut have a slope equal to zero. In the graph from the left side each point represents an eigenvalue, while in the graph from the right side each point represents the proportion (cumulative) out of the variance explained by each component. However, in order to express the ten variables there could be satisfactory only a single principal component, but this could not adequately cover the variability from the space of the ten variables because the proportion is only 57.72 percent. Thus, based on the slope criterion, there will be retained two principal components. Likewise, by considering the covering criterion, the first two principal components ensure a cover of 80.01 percent out of the variability from the space of the ten variables. On the other hand, according to the Kaiser criterion there should be retained only the eigenvalues greater than one. However, within current empirical research we could not employ the Kaiser criterion because

data standardization was not employed. We notice the fact that the data was not standardized because there were not recorded high standard deviation of the variables. The standard deviation of the ten variables employed in this analysis in order to evaluate the companies is presented in Table 3.

Table 3. Standard deviation of the variables

	DE	DTA	LEV	EPS	PER	ROS	CR	QR	ROA	ROE
StD	3.8361	0.2506	1.9178	0.0639	0.8602	0.9943	1.8552	1.6096	0.1009	0.4402

The eigenvectors of the covariance matrix are presented in Table 4. The importance of the eingenvectors is emphasized by the fact that they provide the coefficients of the original variables out of the linear equations related to the principal components. We underline that the technique of PCA represents a multidimensional method of analysis which has the aim of determining new variables entitled principal components expressed as linear combinations of the original variables. Thereby, these new resulted variables are characterized by a maximum variability.

Table 4. Eigenvectors of the covariance matrix

Variable	Prin1	Prin2	Prin3	Prin4	Prin5	Prin6	Prin7	Prin8	Prin9	Prin10
DE	0.9772	0.0897	-0.1788	0.0195	0.0188	-0.0138	0.0606	-0.0194	-0.0069	0.0035
DTA	0.0255	-0.0394	0.0067	-0.0077	-0.0347	0.0165	0.0191	0.9834	0.1644	-0.0419
LEV	0.1920	-0.1369	0.9706	-0.0365	0.0044	0.0124	-0.0219	-0.0166	-0.0021	0.0005
EPS	-0.0019	-0.0014	0.0007	0.0053	-0.0021	0.0037	0.0251	-0.0457	0.4915	0.8693
PER	-0.0225	-0.0045	0.0154	0.3960	0.9170	0.0057	0.0164	0.0345	0.0049	-0.0017
ROS	-0.0003	-0.0029	0.0341	0.9156	-0.3948	0.0167	-0.0633	-0.0026	-0.0197	0.0061
CR	-0.0514	0.7459	0.1236	0.0067	0.0007	-0.6493	-0.0470	0.0423	0.0011	0.0067
QR	-0.0339	0.6444	0.0885	-0.0123	0.0004	0.7578	0.0357	0.0119	0.0030	-0.0043
ROA	-0.0037	0.0062	0.0049	0.0248	-0.0123	-0.0152	0.1292	-0.1644	0.8454	-0.4904
ROE	-0.0567	0.0036	0.0364	0.0478	-0.0393	-0.0548	0.9851	0.0054	-0.1276	0.0437

Thus, the first and the second principal components could be represented as linear combinations out of the original variables, as follows:

- **Prin1** = 0.9772*DE + 0.0255*DTA + 0.1920*LEV + (-0.0019)*EPS + (-0.0225)*PER + (-0.0003)*ROS + + (-0.0514)*CR + (-0.0339)*QR + (-0.0037)*ROA + (-0.0567)*ROE
- **Prin2** = 0.0897*DE + (-0.0394)*DTA + (-0.1369)*LEV + (-0.0014)*EPS + (-0.0045)*PER + + (-0.0029)*ROS + 0.7459*CR + 0.6444*QR + 0.0062*ROA + 0.0036*ROE

The financial ratios corresponding to the first ten companies from the sample are showed in Table 5. Therefore, the objects' coordinates in the new space which is constituted, respectively the principal components' scores for the first ten companies are presented in Table 6 being entitled **'Prin1'** and **'Prin2'**.

Table 5. Financial ratios for the first ten companies

Company	DE	DTA	LEV	EPS	PER	ROS	CR	QR	ROA	ROE
1	1.5508	0.6079	2.5512	0.0041	0.0779	0.0095	1.2606	0.7506	0.0400	0.1020
2	0.9232	0.4800	1.9232	0.0797	0.0242	0.8600	1.3944	1.1457	0.2474	0.4758
3	0.5437	0.3522	1.5437	0.0003	0.3649	0.0100	2.0413	1.8580	0.0321	0.0496
4	0.2581	0.2052	1.2581	0.0016	0.3393	0.0400	2.3969	2.3341	0.0266	0.0335
5	0.4952	0.3309	1.4967	0.0002	0.6569	0.0300	2.2580	1.6246	0.0282	0.0422
6	1.5727	0.6113	2.5727	-0.0224	-0.0284	-0.0700	0.4301	0.1483	-0.0912	-0.2345
7	1.2981	0.5273	2.4616	0.0005	0.3167	0.0100	1.7384	0.9651	0.0117	0.0289
8	1.8130	0.6010	3.0166	0.0025	0.1742	0.0081	1.2499	0.9884	0.0097	0.0291
9	-3.5705	1.3890	-2.5705	0.0617	0.0046	0.2900	0.2165	0.1638	0.0807	-0.2074
10	2.0612	0.6674	3.0886	0.0066	0.3043	0.0100	0.3821	0.3484	0.0332	0.1026

Table 6. Principal components' scores matrix

Company	Prin1	Prin2
1	0.0150	-1.1199
2	-0.7636	-0.7305
3	-1.2503	0.2321
4	-1.6210	0.8234
5	-1.3167	0.2449
6	0.1258	-2.1299
7	-0.2842	-0.6341
8	0.3550	-1.0155
9	-5.8606	-2.0672
10	0.6722	-2.0656

We take into consideration the property that the sum of squares of the coefficients which define the linear combination corresponding to a principal component is equal to one. Thus, the examination of this property by the linear combinations' coefficients which define the principal components, determine the fact that these coefficients under vectorial form compose an orthonormal system.

Thereby, for the first principal component:

$$(0.9772|0.0255|0\ .1920|-0.0019|-0.0225|-0.0003|-0.0514|-0.0339|-0.0037|-0.0567)$$
$$* (0.9772|0.0255|0.1920|-0.0019|-0.0225|-0.0003|-0.0514|-0.0339|-0.0037|-0.0567)^t$$
$$= 0.9549 + 0.0007 + 0.0369 + 0.0000 + 0.0005 + 0.0000 + 0.0026 + 0.0011 + 0.0000 + 0.0032 = 1$$

Additionally, for the second principal component:

$$(0.0897|-0.0394|-0.1369|-0.0014|-0.0045|-0.0029|0.7459|0.6444|0.0062|0.0036) *$$
$$* (0.0897|-0.0394|-0.1369|-0.0014|-0.0045|-0.0029|0.7459|0.6444|0.0062|0.0036)^t$$
$$= 0.0080 + 0.0016 + 0.0187 + 0.0000 + 0.0000 + 0.0000 + 0.5564 + 0.4153 + 0.0000 + 0.0000 = 1$$

Figure 2 shows the 310 companies' scores in the first two principal axes plan. We notice a fairly compact group of companies which are inclined to be similarly valued, but also several companies which are detached from the rest of the companies.

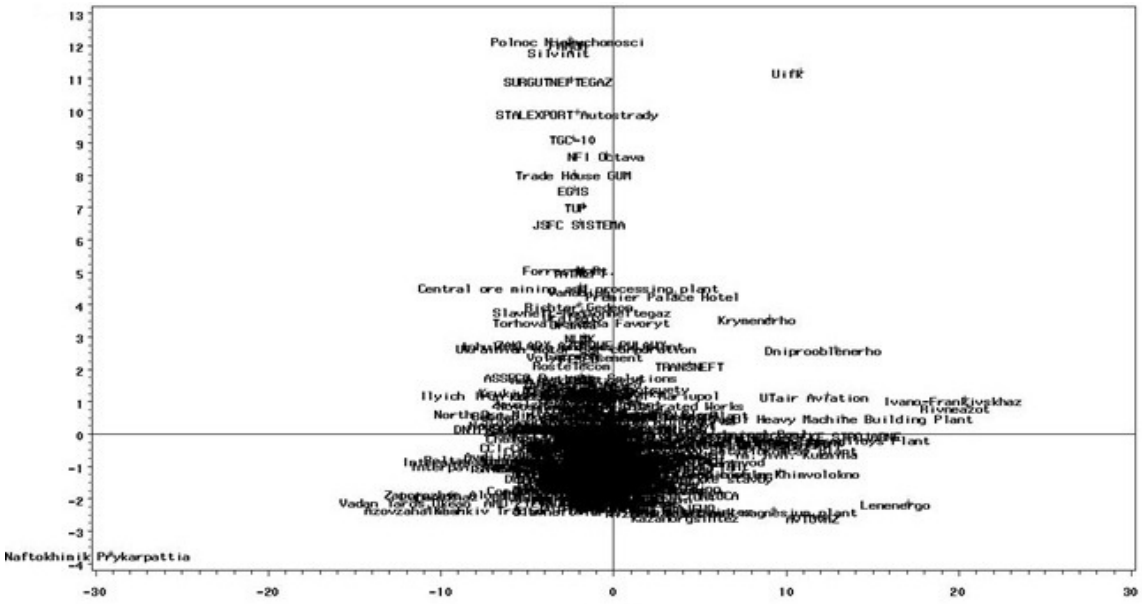

Figure 2. Companies' scores in the first two principal axes plan

The principal components are orthogonal vectors which take as much from the original vector variables' variance as follows: the first principal component take maximum possible out of the original variables' variance, while the second principal component take maximum out of the remained variance after is removed the variance taken by the first principal component.

$$<\text{Eigenvector1; Eigenvector2}> =$$
$$(0.9772|0.0255|0.1920|-0.0019|-0.0225|-0.0003|-0.0514|-0.0339|-0.0037|-0.0567)$$
$$* (0.0897|-0.0394|-0.1369|-0.0014|-0.0045|-0.0029|0.7459|0.6444|0.0062|0.0036)^t = 0.0001 \approx 0$$

From a geometrical point of view, the variables named principal components are defining a new objects' space in the context of which the axes corresponding to the new created space are orthogonal two by two and ascertain the new variables. Moreover, the principal components own a feature which determines their adequacy from the informational point of view in order to substitute the original variables. Thus, this feature refers to the fact that through the principal components is ensured the variability' preservation from the initial causal space. Besides, the diagonal elements of the covariance matrix (Table 1) corresponding to the observations performed to the ten variables are the variances related to the ten original variables, as follows:

$\sigma_1^2 = 14.7157$, $\sigma_2^2 = 0.0628$, $\sigma_3^2 = 3.6779$, $\sigma_4^2 = 0.0041$, $\sigma_5^2 = 0.7399$, $\sigma_6^2 = 0.9886$, $\sigma_7^2 = 3.4419$, $\sigma_8^2 = 2.5909$, $\sigma_9^2 = 0.0102$, $\sigma_{10}^2 = 0.1938$

The eigenvalues of the covariance matrix (Table 2) are presented below:

$\lambda_1 = 15.2523$, $\lambda_2 = 5.8914$, $\lambda_3 = 3.1881$, $\lambda_4 = 1.0488$, $\lambda_5 = 0.6740$, $\lambda_6 = 0.1772$, $\lambda_7 = 0.1406$, $\lambda_8 = 0.0438$, $\lambda_9 = 0.0065$, $\lambda_{10} = 0.0030$

Thus, the feature previously mentioned is demonstrated as follows:

$\text{tr}(\hat{\Sigma}) = \sigma_1^2 + \sigma_2^2 + \sigma_3^2 + \sigma_4^2 + \sigma_5^2 + \sigma_6^2 + \sigma_7^2 + \sigma_8^2 + \sigma_9^2 + \sigma_{10}^2 =$ **26.4257**

$= \lambda_1 + \lambda_2 + \lambda_3 + \lambda_4 + \lambda_5 + \lambda_6 + \lambda_7 + \lambda_8 + \lambda_9 + \lambda_{10} = \text{tr}(\hat{\Lambda})$

Another noteworthy property of the principal components consists in the fact that these are ensuring the whole conservation of the generalized variance corresponding to the original variables. Thus, the determinant of the covariance matrix is equal with the multiplication of the ten eigenvalues, respectively it is equal with the covariance matrix' determinant corresponding to the ten principal components:

$|\Sigma| = 0.0000043 = 15.2523 * 5.8914 * 3.1881 * 1.0488 * 0.6740 * 0.1772 * 0.1406 * 0.0438 * 0.0065 * 0.0030$
$= 0.0000043 = |\Lambda|$

4.2 The Results of the Factor Analysis

The script related to the factor analysis employed in SAS 9.2 is showed in Apendix . The Pearson correlation coefficient matrix related to the original variables is showed in Table 7.

Table 7. Pearson correlation coefficients

Variable	DE	DTA	LEV	EPS	PER	ROS	CR	QR	ROA	ROE
DE	1.0000	0.3691	0.3039	-0.1174	-0.0990	-0.0031	-0.0621	-0.0352	-0.1366	-0.5060
DTA	0.3691	1.0000	0.2639	-0.1158	-0.1416	0.0114	-0.4102	-0.3915	-0.3358	-0.1725
LEV	0.3039	0.2639	1.0000	-0.0207	-0.0163	0.0373	-0.1044	-0.1112	-0.0094	-0.0727
EPS	-0.1174	-0.1158	-0.0207	1.0000	0.0294	0.0870	-0.0434	-0.0362	0.3783	0.1820
PER	-0.0990	-0.1416	-0.0163	0.0294	1.0000	0.1614	0.0041	-0.0037	0.0471	0.0499
ROS	-0.0031	0.0114	0.0373	0.0870	0.1614	1.0000	0.0031	-0.0070	0.2610	0.1178
CR	-0.0621	-0.4102	-0.1044	-0.0434	0.0041	0.0031	1.0000	0.9395	0.1745	0.0913
QR	-0.0352	-0.3915	-0.1112	-0.0362	-0.0037	-0.0070	0.9395	1.0000	0.1534	0.0706
ROA	-0.1366	-0.3358	-0.0094	0.3783	0.0471	0.2610	0.1745	0.1534	1.0000	0.5106
ROE	-0.5060	-0.1725	-0.0727	0.1820	0.0499	0.1178	0.0913	0.0706	0.5106	1.0000

The correlation coefficient matrix have a particular importance in order to employ factor analysis because based on the correlations between variables will result a lower number of variables entitled factors. Besides, the factors will explain the variance related to observations.

Table 8 reveals the eigenvalues of the correlation matrix.

Table 8. Eigenvalues of the correlation matrix

	Eigenvalue	Difference	Proportion	Cumulative
1	2.6342	0.8243	0.2634	0.2634
2	1.8099	0.5036	0.1810	0.4444
3	1.3063	0.2289	0.1306	0.5750
4	1.0774	0.1913	0.1077	0.6828
5	0.8861	0.0605	0.0886	0.7714
6	0.8256	0.2250	0.0826	0.8540
7	0.6006	0.0434	0.0601	0.9140
8	0.5572	0.3142	0.0557	0.9697
9	0.2431	0.1835	0.0243	0.9940
10	0.0595		0.0060	1.0000

Table 9 shows the factor pattern matrix before rotation, thus being retained two factors.

Table 9. Factor pattern

Variable	Factor1	Factor2
DE	-0.5154	-0.3850
DTA	-0.7219	0.0762
LEV	-0.3332	-0.0017
EPS	0.2684	0.4714
PER	0.1510	0.1703
ROS	0.1507	0.3085
CR	0.7029	-0.6376
QR	0.6836	-0.6549
ROA	0.5952	0.4369
ROE	0.5507	0.5322
Variance Explained by Each Factor	2.6342	1.8098

However, the orthogonal rotation of factors using the **Varimax** rotation method determined the factor structure showed in Table 10. Besides, the Varimax rotation represents an orthogonal rotation method through which is minimized the number of variables with high loadings on each factor.

Table 10. Rotated factor pattern

Variable	Factor1	Factor2
DE	-0.1913	-0.6142
DTA	-0.6292	-0.3621
LEV	-0.2688	-0.1969
EPS	-0.0594	0.5392
PER	0.0223	0.2265
ROS	-0.0591	0.3382
CR	**0.9434**	-0.1036
QR	**0.9378**	-0.1289
ROA	0.2254	**0.7031**
ROE	0.1335	**0.7541**
Variance Explained by Each Factor	2.3501	2.0939

Therefore, this fact simplifies the interpretation of factors. The first factor is compounded mainly of the variables CR and QR, while the second factor is compounded mainly of the variables ROA and ROE. The first factor explains 23.5 percent out of the variance, while the second factor explains 20.93 percent out of the variance.

Hence, it is obtained the following form of the factor model:

- **Factor1** = -0.1913*DE - 0.6292*DTA - 0.2688*LEV - 0.0594*EPS + 0.0223*PER - 0.0591*ROS + 0.9434*CR + 0.9378*QR + 0.2254*ROA + 0.1335*ROE
- **Factor2** = -0.6142*DE - 0.3621*DTA - 0.1969*LEV + 0.5392*EPS + 0.2265*PER + 0.3382*ROS - 0.1036*CR - 0.1289*QR + 0.7031*ROA + 0.7541*ROE

For the first indicator variable (the debt to equity ratio), the communality is obtained as follows:

$$h_1^2 = a_{11}^2 + a_{12}^2 \rightarrow h_1^2 = (-0.1913)^2 + (-0.6142)^2 = 0.0366 + 0.3772 = 0.4138$$

Likewise, for the second indicator variable (the debt to total assets ratio), the communality is obtained as follows:

$$h_2^2 = a_{21}^2 + a_{22}^2 \rightarrow h_2^2 = (-0.6292)^2 + (-0.3621)^2 = 0.3959 + 0.1311 = 0.5270$$

The information regarding the specificity was determined by the difference between the variance of each variable and the communality related to both factors.

Thus, for the first measured variable, the specificity is determined as follows:

$$s_1^2 = \sigma_1^2 - h_1^2 = 1 - 0.4138 = 0.5862$$

Likewise, for the second measured variable, the specificity is determined as follows:

$$s_2^2 = \sigma_2^2 - h_2^2 = 1 - 0.5270 = 0.4730$$

5. Concluding Remarks

By employing the principal component analysis in order to evaluate a random sample consisting of 310 companies which belong to five European emerging countries, there resulted the possibility of their evaluation based on two principal components, also considering a minimum loss of information. Thus, by the instrumentality of the first two principal components there is recorded a covering of 80.01 percent of the variability out of the space of the ten selected variables. In fact, the informational loss registered is 20 percent. The utility of the principal component analysis with the aim of companies' valuation is remarkable because there is provided a decomposition of the total variability from the initial causal space expressed through a lower

number of components. Besides, the decomposition previously mentioned is not redundant. As well, by employing factor analysis there resulted two factors which explain 23.5 percent, respectively 20.93 percent out of the total variance.

However, both principal component analysis and factor analysis have the aim of reduction of the significant number of considered variables. This reduction is made in order to evaluate the selected companies through a lower number of principal components, respectively factors. In case of the principal component analysis the components are identified in order to take as much from the variance existing in the data, whereas in case of the factor analysis the lower number of factors is identified in order to explain why the measured variables are correlated between them.

References

Abdi, H., & Williams, L. J. (2010). Principal component analysis. *Wiley Interdisciplinary Reviews: Computational Statistics, 2*(4), 433-459. http://dx.doi.org/10.1002/wics.101

Ali, H. F., & Charbaji, A. (1994). Applying Factor Analysis to Financial Ratios of International Commercial Airlines. *International Journal of Commerce and Management, 4*(1/2), 25-37. http://dx.doi.org/10.1108/eb047285

Alter, O., Brown, P. O., & Botstein, D. (2000). Singular value decomposition for genome-wide expression data processing and modeling. *Proceedings of the National Academy of Sciences of the United States of America, 97*(18), 10101-10106. http://dx.doi.org/10.1073/pnas.97.18.10101

Altman, E. I. (1968). Financial ratios, discriminant analysis and the prediction of corporate bankruptcy. *The Journal of Finance, 23*(4), 589-609. http://dx.doi.org/10.1111/j.1540-6261.1968.tb00843.x

Cattell, R. B. (1966). The scree test for the number of factors. *Multivariate Behavioral Research, 1*(2), 245-276. http://dx.doi.org/10.1207/s15327906mbr0102_10

Conan, J., & Holder, M. (1979). *Variables explicatives de performances et controle de gestion dans les P.M.I.* These d'Etat, CERG, Université Paris Dauphine.

Conway, J. M., & Huffcutt, A. I. (2003). A review and evaluation of exploratory factor analysis practices in organizational research. *Organizational Research Methods, 6*(2), 147-168. http://dx.doi.org/10.1177/1094428103251541

De, A., Bandyopadhyay, G., & Chakraborty, B. N. (2011). Application of the factor analysis on the financialratios and validation of the results by the cluster analysis: An empirical study on the Indian cement industry. *Journal of Business Studies Quarterly, 2*(3), 13-31.

Delwiche, L. D., & Slaughter, S. J. (2008). *The Little SAS Book: A Primer* (4th ed.). SAS Institute.

Dray, S. (2008). On the number of principal components: A test of dimensionality based on measurements of similarity between matrices. *Computational Statistics & Data Analysis, 52*(4), 2228-2237. http://dx.doi.org/10.1016/j.csda.2007.07.015

Fabrigar, L. R., Wegener, D. T., MacCallum, R. C., & Strahan, E. J. (1999). Evaluating the use of exploratory factor analysis in psychological research. *Psychological Methods, 4*(3), 272-299. http://dx.doi.org/10.1037/1082-989X.4.3.272

Fernandez, G. (2010). *Statistical Data Mining Using SAS Applications* (2nd ed.). CRC Press.

Ford, J. K., MacCallum, R. C., & Tait, M. (1986). The application of exploratory factor analysis in applied psychology: A critical review and analysis. *Personnel Psychology, 39*(2), 291-314. http://dx.doi.org/10.1111/j.1744-6570.1986.tb00583.x

Hancock, P. J., Burton, A. M., & Bruce, V. (1996). Face processing: Human perception and principal components analysis. *Memory & Cognition, 24*(1), 26-40. http://dx.doi.org/10.3758/BF03197270

Hastie, T., Tibshirani, R., Eisen, M. B., Alizadeh, A., Levy, R., Staudt, L., … & Brown, P. (2000). 'Gene shaving' as a method for identifying distinct sets of genes with similar expression patterns. *Genome Biology*, *1*(2), 1-21. http://dx.doi.org/10.1186/gb-2000-1-2-research0003

Hastie, T., Tibshirani, R., & Friedman, J. (2009). *The elements of statistical learning. Data mining, inference, and prediction* (2nd ed.). Springer Series in Statistics.

Jackson, D. A. (1993). Stopping rules in principal components analysis: A comparison of heuristical and statistical approaches. *Ecology, 74*(8), 2204-2214. http://dx.doi.org/10.2307/1939574

Leger, L., & Leone, V. (2008). Changes in the risk structure of stock returns: Consumer confidence and the dotcom bubble. *Review of Financial Economics, 17*(3), 228-244. http://dx.doi.org/10.1016/j.rfe.2007.08.001

Meric, G., Leal, R. P. C., Ratner, M., & Meric, I. (2001). Co-movements of U.S and LatinAmerican equity markets before and after the 1987 crash. *International Review of Financial Analysis, 10*(3), 219-235. http://dx.doi.org/10.1016/S1057-5219(01)00053-9

O'Toole, A. J., Deffenbacher, K. A., Valentin, D., & Abdi, H. (1994). Structural aspects of face recognition and the other-race effect. *Memory & Cognition, 22*(2), 208-224. http://dx.doi.org/10.3758/BF03208892

Park, H. S., Dailey, R., & Lemus, D. (2002). The use of exploratory factor analysis and principal components analysis in communication research. *Human Communication Research, 28*(4), 562-577. http://dx.doi.org/10.1111/j.1468-2958.2002.tb00824.x

Pearson, K. (1901). On lines and planes of closest fit to systems of points in space. *Philosophical Magazine, 2*(11), 559-572. http://dx.doi.org/10.1080/14786440109462720

Peres-Neto, P. R., Jackson, D. A., & Somers, K. M. (2005). How many principal components? Stopping rules for determining the number of non-trivial axes revisited. *Computational Statistics & Data Analysis, 49*(4), 974-997. http://dx.doi.org/10.1016/j.csda.2004.06.015

Pinches, G. E., Mingo, K. A., & Caruthers, J. K. (1972). The stability of financial patterns in industrial organizations. *The Journal of Finance, 28*(2), 389-396. http://dx.doi.org/10.1111/j.1540-6261.1973.tb01782.x

Tan, P. M. S., Koh, H. C., & Low, L. C. (1997). Stability of financial ratios: A study of listed companies in Singapore. *Asian Review of Accounting, 5*(1), 19-39. http://dx.doi.org/10.1108/eb060680

Thurstone, L. L. (1931). Multiple factor analysis. *Psychological Review*, *38*(5), 406-427. http://dx.doi.org/10.1037/h0069792

Zou, H., Hastie, T., & Tibshirani, R. (2006). Sparse principal component analysis. *Journal of Computational and Graphical Statistics, 15*(2), 265-286. http://dx.doi.org/10.1198/106186006X113430

Apendix 1

Principal component analysis script employed in SAS 9.2

```
PROC IMPORT DATAFILE = 'E:\SAS\Database.xls' out = companies replace;
getnames = yes;
RUN;
PROC PRINT DATA = companies;
ID company;
RUN;
PROC SORT data = companies;
by company;
RUN;
ods html;
ods graphics on;
PROC CORR data = companies outp = out1;
var DE DTA LEV EPS PER ROS CR QR ROA ROE;
RUN;
PROC PRINCOMP data = companies cov out = Ratings n = 10 outstat = pca_results;
var DE DTA LEV EPS PER ROS CR QR ROA ROE;
title 'PCA Results';
RUN;
PROC PLOT data = Ratings;
plot prin2*prin1 = '+' $ company;
RUN;
DATA ratings_hq;
set ratings;
x = prin1;
y = prin2;
text = company;
size = 1;
xsys = '2';
ysys = '2';
label x = 'axis 1';
label y = 'axis 2';
keep x y xsys ysys text size;
RUN;
title 'The first two principal components area';
PROC GPLOT data = ratings_hq;
plot y*x=1/ annotate = ratings_hq href = 0 vref = 0;
RUN;
QUIT;
title 'Ratings matrix';
PROC PRINT data = ratings;
RUN;
title 'PCA Statistics';
PROC PRINT data = rez_ACP;
RUN;
ods graphics off;
ods html close;
```

Apendix 2

Factor analysis script employed in SAS 9.2

```
PROC IMPORT DATAFILE = 'E:\SAS\Database.xls' out = companies replace;
getnames = yes;
RUN;
ods html;
```

```
ods graphics on;
PROC FACTOR data = companies method = principal scree mineigen = 0 score priors = smc;
outstat = facto_results;
var DE DTA LEV EPS PER ROS CR QR ROA ROE;
RUN;
PROC FACTOR data = facto_results method = principal n = 2 rotate = varimax score outstat = facto_results_2f;
RUN;
PROC SCORE data = companies score = facto_results_2f out = ratings;
RUN;
PROC PLOT;
plot factor2*factor1;
RUN;
ods graphics off;
ods html close;
```

Modern Applied Science; Vol. 8, No. 3; 2014
ISSN 1913-1844 E-ISSN 1913-1852
Published by Canadian Center of Science and Education

The Online Temperature Measurement System for Substation Equipment Based on the Internet of Things (IOT)

Xiaoyan Ma[1], Hao Zou[2] & Tingting Xu[1]

[1] College of Information Engineering, TaiShan Medical University, Taian, Shandong, China

[2] Taian power supply company, Taian, Shandong, China

Correspondence: Ma Xiaoyan, College of Information Engineering, TaiShan Medical University, Taian, Shandong, China. Tel: 86-0538-622-9731. E-mail: maxiaoyan81@126.com

Received: March 18, 2014 Accepted: April 2, 2014 Online Published: May 29, 2014

doi:10.5539/mas.v8n3p217 URL: http://dx.doi.org/10.5539/mas.v8n3p217

Abstract

In order to realize the real-time monitoring of temperature, wireless temperature sensor network is put in the temperature-measuring point in the substation, and then it is transit to the base station through wireless transmission. Finally, by the base station, it is transmit to the management center through the electric power communication network. The temperature management software monitors the temperature timely, visually displays and alarm linkage etc.al. Indoor and outdoor experiments show that the system operates reliably and has good effects, which can accurately realize the online temperature monitoring in a substation.

Keywords: temperature monitoring, Internet of Things (IOT) technology, wireless temperature sensing system, visual display

1. Introduction

The safe operation of power systems is significant, it tightly related to economic development and economic stability. As the modern power system is developing quickly toward the direction of high voltage, large unit and large capacity, the requirements of reliability is much higher. The temperature characteristic of electrical equipment is the temperature varies slowly at most times, however, when there is an equipment failure (Jiansheng, Da, & Fan, 2004), a sudden change of temperature may occur. So it is important to perform online temperature monitoring to potential overheat parts. For the substation, Knife contact, cable connectors, copper connections, switch contacts, reactors, capacitors, arc-suppression coil and the equipments and cables within high voltage switchgear is easily overheat because of all kinds of reasons. So it is extremely important to find an online substation temperature monitoring program, which satisfies the requirements of low-priced, easily-conducted and well adapted. The development of the internet of things provides a new way for the substation equipments temperature online monitoring. The internet of thing is a network concept, according to the protocol it connects things to internet to perform intelligent recognition, track, locate, monitor and management.

When power equipment has no faults, the temperature mostly changes gradually and the change is slow (Huang, Li, Wang, & Fang, 2011); when it has faults, the temperature often changes suddenly. The contingency and emergency of equipment temperature faults decide the fatality of temperature faults. Once the fault appears, there will be heavy loss. The faults caused by overheating of electrical equipment or materials are mostly related to large current, so real-time online monitoring the temperature of large current in the points such as busbar junction (Hwang, Farris, Kompella, & Chandrasekar, 2003), contact and high voltage cable connector which are easy to overheat is very important.

The main difficulties in online monitoring the temperature anomaly for substation power equipment are: the hot spots of electrical equipment are often in the positions with high potential, making common temperature sensing method under restrictions; electrical equipment has a great number of hot spots to monitor, but because of the limits of sensor isolation, economy and equipment structure, it is impossible to install a great number of complex or expensive temperature sensors (Gao, Liu, & Zhan, 2011). Therefore, to find an online monitoring temperature solution which is also easy to realize equipment maintenance with low cost and short engineering construction period, as well as good adaptability and extensibility becomes particularly important.

In recent years, the rapid development of Internet of Things (IOT) technology has provided new path to online monitoring electrical equipment temperature for substation. The term Internet of Things is a concept of network, which connects objects to the internet for the exchange and communication of the information through such information sensing equipments as radio frequency identification, infrared sensor, global poisoning system, laser scanner and so on according to agreed protocol, so as to realize intelligent identification, track, positioning, monitoring and management. The aim of IOT is to connect all the objects to the internet so that the system can automatically real-time identify, locate, track, monitor and trigger corresponding events to the things (Xu & Nihong, 2005). The online temperature measurement system for substation based on the internet of things (IOT) is one of IOT's important applications in the development of smart grid, which mainly uses digital wireless temperature monitor installation to realize. It can meet the technological needs of online monitoring running temperature for main electrical equipment, power cable, connector, capacitor and electric reactor and provide basic data support for the informatization of total state overhaul (Gong, Yi, Wang, Yue, & Yu, 2006).

2. The Design of Online Monitoring Temperature System

2.1 System Configuration

Online monitoring temperature system configuration principle is shown in Figure 1. It is composed by management centre (host machine), data transmission base station and wireless temperature sensor.

Management centre is composed by a host machine based on Windows OS and configuration monitoring software. Host machine is a management platform which integrates various communication protocols and has perfect software functions, and has graphical human-computer interaction interface and complete and steady database. It is mainly used for receiving temperature anomaly alarms sent from thermometry workstation, as well as process, query, statistically analyzing all the data in the system. The management platform not only finishes the temperature management of all the cables, connectors and important equipment in a 220kV substation, but also implants other management and control functions so as to realize operating multiple management tasks in single platform, which effectively realizes multi-information integration and fusion and reduces users' total cost.

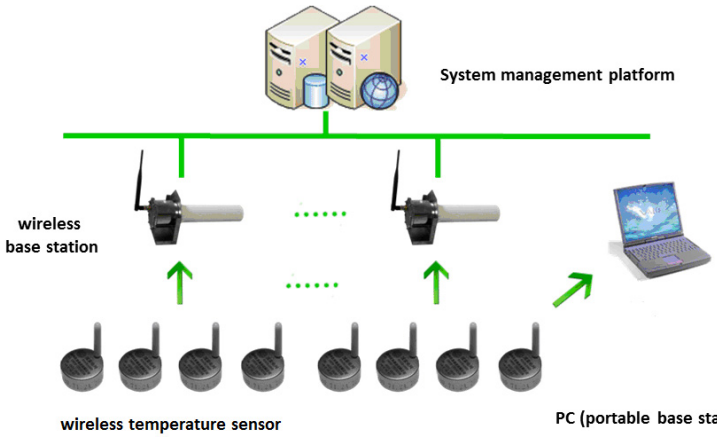

Figure 1. Online monitoring temperature system configuration principle

Data transmission base station automatically receives the data about temperature sent from wireless temperature sensor and uploads the data to thermometry workstation after receiving read command. Because of the limitation of the environment in the site, wireless sensing distance is several hundreds of meters theoretically, but in fact it is only dozens of meters. Each data transmission base station only manages a group of wireless temperature sensor, whose ID has to be configured and saved to terminal flash storage in advance.

Data transmission base station is composed by MCU/RS-485 connector, 2.45GHz digital RF transceiver, wide input DC/DC stabilized power supply, IP 68 ASA shell, high gain directional antenna and omni-directional antenna. Data transmission base station usually adopts RS-485 bus to communicate with host machine.

Install a wireless temperature sensor in each point of temperature monitor target. The sensor automatically measures the temperature in the position in every set time limit and outputs the data measured by wireless signal. Each wireless temperature sensor has unique 32 bits ID, which needs to be allocated and record the installation sites of each sensor in practice, and deposited into the configuration file of thermometry workstation.

Wireless temperature sensor is composed by micro power MCU, digital temperature sensor, 2.45 GHz digital RF transceiver, high-temperature lithium battery, IP168 stainless steel shell and antenna.

2.2 System Working Principle

Wireless temperature sensor measures the running temperature in the monitoring point at regular time. Environmental temperature sensor also automatically measures environmental temperature. The temperature data is transmitted to the base station by 2.45GHz wireless channel, and the base station saves and records the data.

Host machine polls each base station by RS-485 bus at regular time. Each base station transmits the temperature data received to the host machine. Host machine processes and saves the data.

Through comparisons of the relative temperature rise between equipment and environment, and the temperature rise between indoor and outdoor atmosphere, host machine can analyze possible situation of overheating and issues early warning signal in advance so as to remind manager. Host machine and centralized control station can communicate by Ethernet, or adopt custom temperature model to communicate with host machine in accordance with IEC 61850 Standard, or provide multiple warning signal for public measurement and control screen by relay.

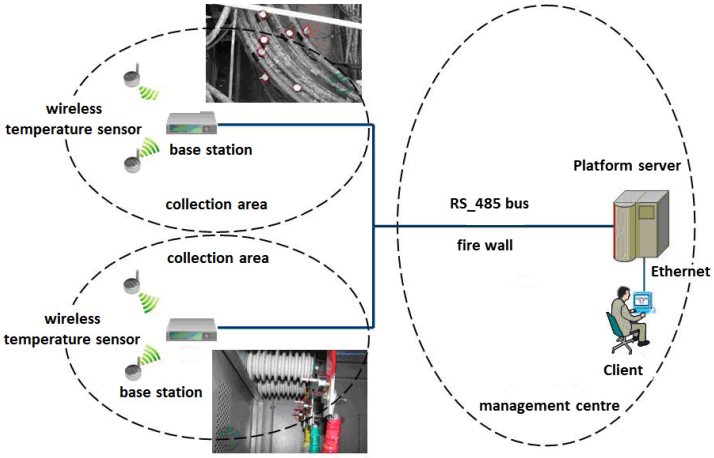

Figure 2. System principle chart

3. Temperature Monitoring System Software for Substation

Temperature monitoring system software for substation mainly includes two function modules: data collection server and hot spot monitoring system. Data collection system software obtains real-time data from I/O equipment in the site by I/O device driver and carries out necessary processing of the data. On the one hand, it is shown in the screen of computer visually in graphical form; on the other hand, according to configuration requirements and the commands of operators, it transmits the control data to I/O equipment, and has control of actuator or adjusts control parameter, so as to provide a perfect management function for sample data and the maintenance of database. Hot spot monitoring system is to collect the temperature data about some key equipment in substation and provide display, alarm and printing functions.

Monitoring point map information module shows the specific geographical information about the points monitored, which can realize 3D display, and select a specific point through “location” column; total regional map information module shows all the geographical information about the monitoring points in the substation, which is composed by each small point icon, able to select monitoring point by clicking the small icon in the module; monitoring point data information module shows the specific data information and diagnostic information about the point that is monitored, including ID, Point ID, Point name, Standard code, data, alarm type, alarm grade, area, alarm time and experts’ suggestion, whose display can be switchover by the options including alarm information and curve icon.

4. The Typical Configuration of Online Monitoring Temperature System

4.1 The Layout of Data Transmission Base Station

The first layer assigns seven data transmission base stations (two 10kV capacitors, four 10kV switch rooms, one grounding Peterson coil room). The second layer assigns nine data transmission base stations (four 110kV power distribution equipment rooms, two western walls, three eastern walls)

The sensor in 10kV switch room is installed in the switch cabinet or busbar bridge. Considering the characteristics of radio wave propagation, four data transmission base stations are lay out. 10kV capacitor lays out two data transmission base stations; there is no wall between Peterson coil room and switch room, but one data transmission base station.

110kV distribution equipment room is open and its equipment density is small, so only laying out 3-4 data transmission base stations reasonably can satisfy the system's requirements. The base station in eastern wall receives signal from main transformer sensors. In consideration of the influence of climate (for example, rain, snow) on communication distance, three base stations are assigned here to improve its reliability. The base station in western wall only receives signal from outside wall bushing sensors. The distance is short, in the premise of ensuring reliability, two data transmission base stations are assigned here.

Indoor installation: base station should select walls and columns far away high-voltage equipment and wire, where the coverage area is wide and the sight of electromagnetic wave is perfect. The height of installation position is usually between 2.5 and 3 meter, where it is convenient to install and maintain the equipment.

Outdoor installation: base station should select walls and towers far away high-voltage equipment and wire, where the coverage area is wide and the sight of electromagnetic wave is perfect. The height of installation position is usually between 2.5 and 3 meter, and on the centralized control room as possible as it can, convenient to lay out the line and shorten the signal line, as well as install and maintain the equipment.

4.2 The Layout of Wireless Temperature Sensor

SG-WT100 wireless temperature sensor adopts advanced integration, microminiaturization and equipotential packaging techniques. The project directly installs wireless temperature sensor in cable connector (ingoing and outgoing line of wall bushing, ingoing and outgoing line of current transformer, ingoing and outgoing line of switch, ingoing line of voltage transformer, ingoing and outgoing line of switch blade, outgoing line of switch cabinet, ingoing and outgoing line of transformer, ingoing and outgoing line of Petersen Coil, ingoing line of reactor), switch blade contact, switch contact, copper bar junction point, reactor, Petersen Coil, grounding, capacitor shell, power cable, ingoing and outgoing line of No. 1 & 2 transformers and so on so as to realize high-reliability real-time online monitoring temperature, temperature rise and differences. According to the principle that cable connector, switch blade contact, switch contact, copper bar junction point, reactor, Petersen Coil and capacitor shell lay out wireless temperature sensor, 268 points are assigned.

4.3 The Layout of Host Machine

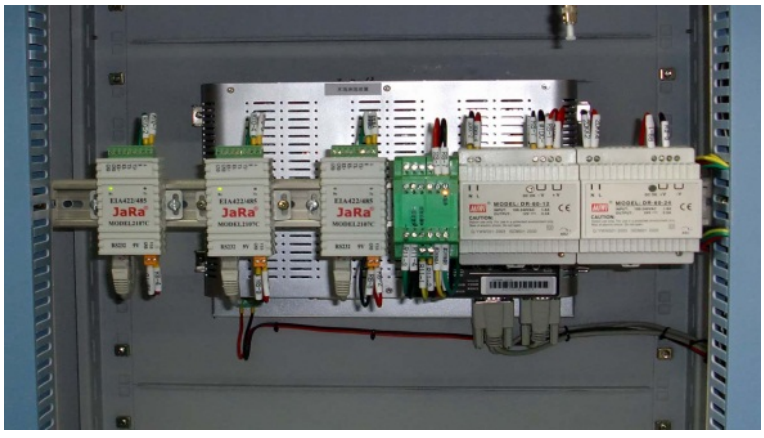

Figure 3. Installation system wiring diagram in the cabinet of industrial control computer

Temperature management software is able to smoothly run in the computer system with 32 bits Windows OS (desk, portable or embedded computer system). In consideration of future extensibility requirements of temperature management software, the project adopts ANOVO 2U complete industrial control computer, whose configuration is below: RPC-205case, /NOVO-7945mainboard/ BP-05V4 baseboard/ fully-welded 230 industrial power source/Intel dual-core E5300 2.6G CPU/1T hard disk/2G DDRII memory/512M separate video card/Xiba

RS-232PCI multiport serial card/DVD driver/ optoelectronic packages/AOC 19 inches of liquid crystal display, which satisfy the hardware requirements of current temperature management software and provide sufficient hardware redundancy for future system function extensions. The system wiring diagram in the cabinet of industrial control computer is shown in Figure3.

4.4 The Solution That Host Machine Polls Each Base Station

Wireless temperature sensor sends data to base station regularly. Wireless base station and wireless temperature sensor constitute wireless temperature sensing network through 2.4GHz WSN aerial wireless communication protocol and finish initial reception, storage and upload of the data. The data bearing network from wireless base station to main control room uses 485 bus. Host machine polls each base station by RS-485 bus regularly. Each base station transmits temperature data it receives to host machine. Host machine processes and saves the temperature data. After management centre receive the data, background software system finishes the receipt, storage and visual display, and has a deep mining of the data. Through various expert models, the function such as intelligent analysis and early warning of monitoring contents is realized, as well as the combination with other application system, so as to realize the sharing and mutual communication of the data between systems.

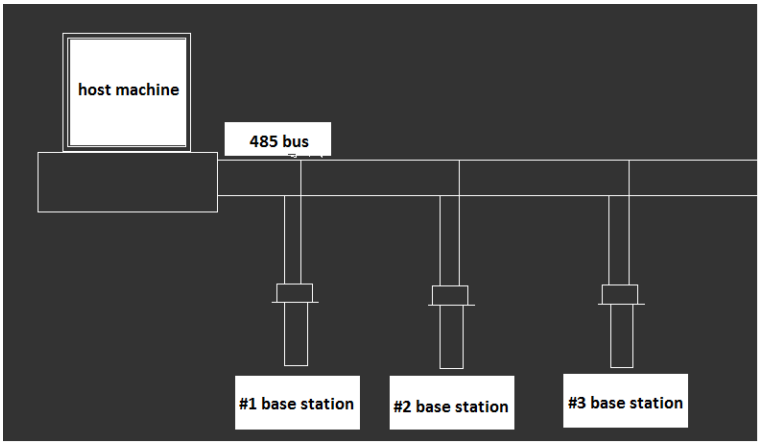

Figure 4. The diagram that host machine polls base station

That host machine polls each base station adopts unicast polling. No specific information is sent to host machine to realize polling. Uplink can allocate sufficient bandwidth that is used for the terminal sends request in mapping information. If the terminal does not need send request, the time slot corresponding to the allocation should be filled according to the protocol. If the terminal has an active UGS link and sufficient bandwidth, it should not be unicast polling, only when the terminal is set up in PM bit in the frame header of UGS link, which is able to avoid unicast polling all the terminal and thus save bandwidth. What needs to notice is that unicast polling for single terminal is usually realized by data authorization mechanism that allocates basic CiD aimed at the terminal.

5. Conclusion

The temperature monitoring system for substation based on IOT technology is a reform of power equipment temperature monitoring method. Compared with traditional thermometry methods such as wax sheet or infrared measurement, it not only saves a great deal of manpower and material resources, but also has the advantages such as high accuracy, rapid reaction speed, easy installation, small in size, all-weather, real-time, online, no failure to report and strong immunity from interference, so it is of great engineering significance.

The program of temperature online monitoring is to place wireless sensor networks at temperature monitoring point. Through the wireless network temperature data is transmitted to base station. Then the base station transmits data to management center and the temperature management software will realize online monitoring, visible display and linkage alarm. According to operation temperature, relative temperature and temperature difference the state of equipments can be judged.

This paper compares some different methods of substation temperature monitoring. Through the comparison the paper presents the temperature monitoring method based on the technique of the internet of things. In this paper, the method presented is studied and analyzed, research program, typical configuration and the function is given

too. The substation temperature online monitoring program is an important application in the smart grid. This program is basically realized by digital wireless temperature monitoring equipment, it is able to achieve online temperature monitoring on all major equipments of substation, and is also able to provide data support to condition-based maintenance information. The program presented in this paper is an evolution of electrical equipment temperature monitoring. Compared to traditional methods, it is low-priced, easily-conducted and well adapted, so it is of great engineering significance.

Acknowledgments

Supported by the Tai'an Science and Technology Bureau (Project: Research on intelligent substation data integration and visualization management) and China Society of Logistics (2014).

References

Gao, Z., Liu, X., & Zhan, T. (2011). The research of tempration control system based on type-k thermocouple. *Machinery Design & Manufacture, 4,* 5. Retrieved from http://en.cnki.com.cn/Article_en/CJFDTOTAL-JSYZ201104005.htm

Gong, X. F., Yi, H. G., Wang, C. S., Yue, S. F., & Yu, B. (2006). Research on Temperature Monitoring of Isolators in HV Switchgear. Paper presented at the Zhongguo Dianji Gongcheng Xuebao (Proceedings of the Chinese Society of Electrical Engineering). Retrieved from http://en.cnki.com.cn/Article_en/CJFDTOTAL-ZGDC200601029.htm

Huang, X., Li, X., Wang, Y., & Fang, S. (2011). An online temperature monitoring system of substation based on Zigbee wireless network. Paper presented at the Electrical and Control Engineering (ICECE), 2011 International Conference on. http://dx.doi.org/10.1109/ICECENG.2011.6057255

Hwang, J., Farris, T. N., Kompella, S., & Chandrasekar, S. (2003). Measurement of temperature field in surface grinding using infra-red (IR) imaging system. *Journal of Tribology, 125*(2), 377-383. http://dx.doi.org/10.1115/1.1537748

Jiansheng, L., Da, F., & Fan, Z. (2004). A novel method for remote on-live temperature detection of substation high-voltage contacts. *Automation of Electric Power Systems, 4,* 13. Retrieved from http://en.cnki.com.cn/Article_en/CJFDTOTAL-DLXT200404013.htm

Xu, Y., & Nihong, G. (2005). The on-line detector of temperature for the contact inside the H. V. Switchgear. *High Voltage Apparatus, 41*(2), 139-140. http://dx.doi.org/10.3969/j.issn.1001-1609.2005.02.019

Modern Applied Science; Vol. 8, No. 3; 2014
ISSN 1913-1844 E-ISSN 1913-1852
Published by Canadian Center of Science and Education

Reviewer Acknowledgements

Modern Applied Science wishes to acknowledge the following individuals for their assistance with peer review of manuscripts for this issue. Their help and contributions in maintaining the quality of the journal is greatly appreciated.

Modern Applied Science is recruiting reviewers for the journal. If you are interested in becoming a reviewer, we welcome you to join us. Please find the application form and details at http://www.ccsenet.org/reviewer and e-mail the completed application form to mas@ccsenet.org.

Reviewers for Volume 8, Number 3

Antonio Camarena-Ibarrola, Electrical Engineering School of UMSNH, Mexico

Antonio Comi, University of Rome Tor Vergata, Italy

Cristina Damian, University of Suceava, Romania

Daniela Popescu, Gheorghe Asachi Technical University of Iasi, Romania

Dinesh Sathyamoorthy, Science & Technology Research Institute for Defence (STRIDE), Malaysia

Kai Wei, University of Massachusetts, China

Lazaros MAVROMATIDIS, National School of Architecture of Lyon (ENSAL), France

Lim Hwee San, Universiti Sains Malaysia (USM), Malaysia

Marek Brabec, Academy of Sciences of the Czech republic, Czech Republic

Mohd Hafizi Ahmad, Universiti Teknologi Malaysia, Malaysia

Sevgihan Yildiz Bircan, Nagoya University, Belgium

Tuğba Özacar, Celal Bayar University, Turkey

Utku Kose, Usak University, Turkey

Valentina Valentina, Polytechnic University of Torino, Italy

Valter Aragao do Nascimento, Federal University of Mato Grosso do Sul, Brazil

Vítor Carvalho, University of Minho, Portugal

Yili Huo, Bentley Systems Inc., USA

Call for Manuscripts

Modern Applied Science (MAS) is an international, double-blind peer-reviewed, open-access journal, published by the Canadian Center of Science and Education. It publishes original research, applied, and educational articles in all areas of applied science. It provides an academic platform for professionals and researchers to contribute innovative work in the field. The scopes of the journal include, but are not limited to, the following fields: agricultural and biological engineering, applied mathematics and statistics, applied physics and engineering, chemistry and materials sciences, civil engineering and architecture, computer and information sciences, energy, environmental science and engineering, mechanics. The journal is published in both print and online versions. The online version is free access and download.

We are seeking submissions for forthcoming issues. All manuscripts should be written in English. Manuscripts from 3000–8000 words in length are preferred. All manuscripts should be prepared in MS-Word format, and submitted online, or sent to: mas@ccsenet.org

Paper Selection and Publishing Process

a) Upon receipt of a submission, the editor sends an e-mail of confirmation to the submission's author within one to three working days. If you fail to receive this confirmation, your submission e-mail may have been missed.

b) Peer review. We use a double-blind system for peer review; both reviewers' and authors' identities remain anonymous. The paper will be reviewed by at least two experts: one editorial staff member and at least one external reviewer. The review process may take two to four weeks.

c) Notification of the result of review by e-mail.

d) If the submission is accepted, the authors revise paper and pay the publication fee.

e) After publication, the corresponding author will receive two hard copies of the journal, free of charge. If you want to keep more copies, please contact the editor before making an order.

f) A PDF version of the journal is available for download on the journal's website, free of charge.

Requirements and Copyrights

Submission of an article implies that the work described has not been published previously (except in the form of an abstract or as part of a published lecture or academic thesis), that it is not under consideration for publication elsewhere, that its publication is approved by all authors and tacitly or explicitly by the authorities responsible where the work was carried out, and that, if accepted, the article will not be published elsewhere in the same form, in English or in any other language, without the written consent of the publisher. The editors reserve the right to edit or otherwise alter all contributions, but authors will receive proofs for approval before publication.

Copyrights for articles are retained by the authors, with first publication rights granted to the journal. The journal/publisher is not responsible for subsequent uses of the work. It is the author's responsibility to bring an infringement action if so desired by the author.

More Information

E-mail: mas@ccsenet.org

Website: www.ccsenet.org/mas

Paper Submission Guide: www.ccsenet.org/submission

Recruitment for Reviewers: www.ccsenet.org/reviewer

The journal is peer-reviewed
The journal is open-access to the full text
The journal is included in:

CABI
Chemical Abstracts database
DOAJ
EBSCOhost
ERA
Google Scholar
LOCKSS
Open J-Gate
Polish Scholarly Bibliography (PBN)
ProQuest
Scopus
Standard Periodical Directory
Ulrich's
Universe Digital Library

Modern Applied Science
Bimonthly

Publisher Canadian Center of Science and Education
Address 1120 Finch Avenue West, Suite 701-309, Toronto, ON., M3J 3H7, Canada
Telephone 1-416-642-2606
Fax 1-416-642-2608
E-mail mas@ccsenet.org
Website www.ccsenet.org/mas

ISSN 1913-1844